Spatial and Temporal Reconstructions of Surface and Deepwater Flow in the Subtropical NW Atlantic at Sharp Climatic Transitions

Helena Kay Evans

Submitted for the Degree of Doctor of Philosophy

Cardiff University

School of Earth, Ocean and Planetary Sciences

July 2007

ProQuest LLC
789 East Eisenhower Parkway
P.O. Box 1346
Ann Arbor, MI 48106-1346

Form: PGR_Submission_200701

NOTICE OF SUBMISSION OF THESIS FORM: POSTGRADUATE RESEARCH

APPENDIX 1:
Specimen layout for Thesis Summary and Declaration/Statements page to be included in a Thesis

DECLARATION

This work has not previously been accepted in substance for any degree and is not concurrently submitted in candidature for any degree.

Signed ..... H. Evans ..... (candidate) Date ... 16/07/07 .....

STATEMENT 1

This thesis is being submitted in partial fulfillment of the requirements for the degree of ..... PhD ..... (insert MCh, MD, MPhil, PhD etc, as appropriate)

Signed ..... H. Evans ..... (candidate) Date ... 16/07/07 .....

STATEMENT 2

This thesis is the result of my own independent work/investigation, except where otherwise stated. Other sources are acknowledged by explicit references.

Signed ..... H. Evans ..... (candidate) Date ... 16/07/07 .....

STATEMENT 3

I hereby give consent for my thesis, if accepted, to be available for photocopying and for inter-library loan, and for the title and summary to be made available to outside organisations.

Signed ..... H. Evans ..... (candidate) Date ... 16/07/07 .....

STATEMENT 4: PREVIOUSLY APPROVED BAR ON ACCESS

I hereby give consent for my thesis, if accepted, to be available for photocopying and for inter-library loans **after expiry of a bar on access previously approved by the Graduate Development Committee.**

Signed ..... (candidate) Date .....

Abstract

A suite of deep-marine sediment cores recovered from the Blake Outer Ridge (BOR) in the subtropical North West Atlantic (28-34°N, 75-71°W) provide material for centennial to millennial scale investigations of abyssal circulation and surface ocean conditions during selected intervals in the last 130 kyr. Particular focus is placed on reconstructing the position and strength of the Deep Western Boundary Current (DWBC) at a high temporal resolution.

Palaeocurrent dynamics are reconstructed using the 'sortable silt' (10-63 μm terrigeneous fraction) mean grain size sedimentological proxy. Paired Mg/Ca and $\delta^{18}O$ records from the planktonic foraminifera *G. ruber* (white) are used to reconstruct deglacial sea surface temperature (SST) and salinity variations, while benthic $\delta^{13}C$ data from *Cibicidoides spp.* document the interchange of northern- and southern source deepwater (NSW/SSW) in the subtropical Atlantic.

Comparison of Holocene sediments with modern physical hydrographic measurements reveals a DWBC high velocity core between 3,000-4,000 m water depth. A deep position for the DWBC core below 3,500 m was also observed during the peak of the last interglaciation, marine isotope stage (MIS) 5e. The benthic $\delta^{13}C$ during these interglacial intervals reveals little chemical stratification and a water column dominated by NSW. A shallow Labrador Sea Water (LSW)-sourced secondary fast flowing DWBC core is also apparent during the Holocene, however during MIS 5e palaeocurrent data at intermediate depths suggest a weaker and possibly shallower position for the LSW-sourced secondary DWBC limb.

The last glacial maximum and Younger Dryas reconstructions show similar hydrographic regimes with nutrient-depleted, vigorously flowing NSW above 2,500 m consistent with intermediate water formation. Northern sourced intermediate water was first apparent in the records presented at ~111 kyr BP and is suggested to have persisted throughout the last glacial. Benthic $\delta^{13}C$ data suggest the presence of a highly stratified water column with an increasing influence of SSW with depth.

Coupled suborbital oscillations in DWBC flow variability and palaeo-hydrography persist throughout the records. There is evidence for a broad-scale divergence in flow speed changes in the deep subtropical North Atlantic, with the presence of a vigorous, but poorly ventilated SSW mass below 4,200 m water depth during cold episodes of the last deglaciation and LGM, when shallower palaeocurrent and geochemical data suggest that NSW was suppressed. This is consistent with the operation of a bipolar see-saw effect.

This study suggests a hitherto unrecognised degree of linkage between oscillations in subtropical North Atlantic SST and DWBC flow. During the last deglaciation the SST record is dominated by the position/strength of the Gulf Stream, while the effects of tropical heat retention are restricted prior to Heinrich event 1. A combination of meridional overturning strength, meltwater inputs and hydrological changes control salinity variability.

Author's Note

Chapters 3, 5 and **6** of this thesis have been presented as papers in international publications and **Chapter 4** is in preparation for publication. The present status of these publications is summarised as follows:

Chapter 3 has been submitted to *Geochemistry, Geophysics, Geosystems* (G^3) as: Evans, H. K., and I. R. Hall, Time-slice reconstruction of deepwater circulation on the Blake Outer Ridge in the western subtropical North Atlantic: Holocene, Last Glacial Maximum and Younger Dryas.

Chapter 5 has been submitted to *Paleoceanography Currents* as: Evans, H. K., I. R. Hall, and L. D. Keigwin, Divergent deepwater flow speed changes in the subtropical North Atlantic during the last deglaciation.

Chapter 6 is in press in *Paleoceanography* as: Evans, H. K., I. R. Hall, G. G. Bianchi, and D. W. Oppo, Intermediate water links to Deep Western Boundary Current variability in the subtropical NW Atlantic during marine isotope stages 5 and 4.

As a consequence of chapters of this thesis being published as individual papers in scientific journals, some repetition of statement could not be avoided.

Declaration of co-author contributions

Chapter 3 **Time-slice reconstruction of deepwater circulation on the Blake Outer Ridge in the western subtropical North Atlantic: Holocene, Last Glacial Maximum and Younger Dryas.**

Hall, I.R.	Reviewed several versions of manuscript.

Chapter 5 **Divergent deepwater flow speed changes in the subtropical North Atlantic during the last deglaciation.**

Hall, I.R.	Reviewed several versions of manuscript.
Keigwin, L.D.	Provided the material for analysis and reviewed final version of the manuscript.

Chapter 6 **Intermediate water links to Deep Western Boundary Current variability in the subtropical NW Atlantic during marine isotope stages 5 and 4.**

Hall, I.R.	Reviewed several versions of manuscript.
Bianchi, G.G.	Reviewed several versions of manuscript.
Oppo, D.W.	Provided stable isotope analysis and reviewed the final manuscript.

Acknowledgements

Firstly I would like to thank my primary supervisor Ian Hall for his support, encouragement and patience. I would also like to express my gratitude to my co-supervisors Giancarlo Bianchi and Lloyd Keigwin for their expert guidance during my time in Cardiff.

I am also grateful to Karin Boessenkool who has provided an invaluable source of friendly advice and motivation throughout my PhD, while also providing the office supply of sweets. Her knowledge of IT has saved me many needless hours of work.

Special thanks go to the lab technicians in Cardiff, Cambridge and WHOI. In particular I would like to thank Helen Medley for expertly teaching me analytical techniques, Giancarlo Bianchi and Julia Becker for stable isotope analysis and Mervyn Greaves for enthusiastically sharing his expertise in Mg/Ca analysis. I would also like to thank one of my manuscript co-authors Delia Oppo for stable isotope analysis and insightful discussions on Chapter 7.

Thanks go to Steve Barker and Harry Elderfield for comments on early drafts of Chapter 5 and to Gregor Knorr for his encouragement and useful discussions concerning my work. The two anonymous reviewers of Evans *et al.* (in press)/Chapter 5 are also thanked for their constructive reviews.

Finally, a big thank you to all of my loved ones and close friends. To my mum, dad and Christian for their endless support, patience and unwavering belief in me, I am very grateful. My fantastic office mates for providing a friendly atmosphere to work in and all the other PhD students at Cardiff. In particular I would like to thank Lizzie Molyneux, Helen Medley and Rehanna Chaudhri for keeping me sane over the past 3+ years.

List of abbreviations

AABW	Antarctic Bottom Water
AAIW	Antarctic Intermediate Water
AII	*RV* Atlantis cores
AMS	Accelerator mass spectrometry
B/A	Bølling-Ållerød
BahOR	Bahama Outer Ridge
BFA	Benthic foraminifera abundance
BOR	Blake Outer Ridge
BR	Bermuda Rise
BW	Bottom Water
CHN	Carbon-Hydrogen-Nitrogen (%$CaCO_3$)
CLIMAP	Climate; Long-Range Investigation, Mapping and Prediction Project
D/O	Dansgaard-Oeschger
DWBC	Deep Western Boundary Current
E-P	Evaporation-precipitation balance
FWN	Freshwater experiment, North
GCM	General circulation model
GIN	Greenland-Norwegian-Iceland
GISP2	Greenland Ice Sheet Project 2
GNAIW	Glacial North Atlantic Intermediate Water
GOM	Gulf of Mexico
H	Heinrich
HAP	Hatteras Abyssal Plain
HCO	Holocene climatic optimum
HEBBLE	High Energy Benthic Boundary Layer Experiment
HL	High light
IRD	Ice rafted debris
ISOW	Iceland Scotland Overflow Water
ITCZ	Inter-tropical convergence zone
KNR	*RV* Knorr cores
kyr BP	Thousand years before present (calendar)
LDEO	Lamont Doherty Earth Observatory
LGM	Last Glacial Maximum
LIS	Laurentide ice sheet
LL	Low light
LNADW	Lower North Atlantic Deep Water
LSW	Labrador Sea Water
MAT	Modern analogue technique
MIS	Marine isotope stage
MOC	Meridional overturning circulation
MS	Magnetic susceptibility
MST	Multisensor track
MWP	Melt water pulse
Myr	Million years
NADW	North Atlantic Deep Water
NBS	National Bureau of Standards
NGRIP	North Greenland ice sheet project
NSW	Northern Source Water
ODP	Ocean Drilling Program
RC	*RV* Robert Conrad cores

PDB	Pee Dee Belemnite
RAPID	Rapid Climate Change scientific programme
SAP	Sohm Abyssal Plain
SLP	Sea level pressure
SLSW	Shallow Labrador Sea Water
SS	Sortable silt
$\overline{SS}$	Sortable silt mean grain size
SS%	Sortable silt weight %
SSS	Sea surface salinity
SST	Sea surface temperature
SSW	Southern Source Water
T1	Transect 1
T2	Transect 2
T3	Transect 3
THC	Thermohaline circulation
UHQ	Ultra High Quality
VM	*RV* Vema cores
VPDB	Vienna Pee Dee Belemnite
VSMOW	Vienna Standard Mean Ocean Water
WHOI	Woods Hole Oceanographic Institute
YD	Younger Dryas
Yr	Years

List of Contents

Chapter 3

Time-slice reconstruction of deepwater circulation on the Blake Outer Ridge in the western subtropical North Atlantic: Holocene, Last Glacial Maximum and Younger Dryas

Chapter 4

Rapid sea surface temperature and salinity oscillations during the last deglaciation in the subtropical NW Atlantic

Chapter 5

Divergent deepwater flow speed changes in the subtropical North Atlantic during the last deglaciation

Chapter 6

Intermediate water links to Deep Western Boundary Current variability in the subtropical NW Atlantic during marine isotope stages 5 and 4

Chapter 7

Summary and future work

References

Appendices

Chapter 1: Introduction

1.1 The Rapid Climate Change Project

The Rapid Climate Change Project ("*RAPID*") is a UK Natural Environmental Research Council thematic programme set up in 2001 to improve our understanding of the role played by the North Atlantic Meridional Overturning Circulation (MOC) and other processes in rapid climate change, along with the global and regional impacts of such change. The primary aim of the project is to enhance our ability to monitor and predict the probability and magnitude of future climatic change in the North Atlantic region. In order to achieve this aim the programme uses a novel combination of present day observations, palaeodata and a hierarchy of models (from local process models to global general circulation models).

Modelling studies of the present day heat transport in the North Atlantic have revealed that the MOC and its associated heat transport produces a substantially warmer climate in western Europe than would otherwise be the case (Manabe and Stouffer, 1988; Schiller *et al.*, 1997; Vellinga and Wood, 2002). The North Atlantic is therefore the focus of the RAPID programme as it is the centre of key oceanic processes which, apart from maintaining warm climates in NW Europe, provide a plausible mechanism for the large, abrupt and global climatic changes of past glacial and interglacial climates (Broecker and Denton, 1989; Dansgaard *et al.*, 1993; Broecker, 2000). Modelling work has suggested that significant reductions in the strength of the MOC might occur in the future as a result of human-induced increases in the atmospheric concentration of CO_2 and other greenhouse gases (e.g. Manabe and Stouffer, 1993; Wood *et al.*, 1999).

This thesis forms part of the RAPID project and utilises high resolution sediment cores from a large sediment drift in the western subtropical North Atlantic.

Sediment cores recovered from a number of cruises are used in this study and in many instances provide the temporal resolution necessary to resolve sub-millennial to millennial-scale fluctuations in environmental conditions. The study of suitable environmental analogues recorded within the palaeo deep sea sediment record will help to lead to a better understanding of the key role the oceans are likely to play in shaping the future climate.

1.2 Quaternary climate change and the role of the North Atlantic

The study of ocean sediment cores has made significant progress in understanding the climate system of the Quaternary (Imbrie and Imbrie, 1979). Quaternary climate change has been dominated by a number of large-scale climatic oscillations from glacial to interglacial conditions with a cyclicity of ~100 kyr, which have been recorded in a number of palaeoclimatic archives such as deep sea sediments (e.g. Shackleton, 2000), continental deposits of flora (e.g. Dynesius and Jansson, 2000), fauna (e.g. Lister, 2004), loess (e.g. Chlachula, 2003), and ice cores (e.g. Petit *et al.*, 1999). It is the surface of the North Atlantic that experiences the most dramatic temperature change of any of the world's oceans (CLIMAP Project Members, 1976) during these climate transitions. It is now widely accepted that these large-scale fluctuations in climate are driven by changes in the Earth's orbital parameters i.e. eccentricity, precession and obliquity (Figure 1.1), which control the seasonal distribution of insolation (Hays *et al.*, 1976; Imbrie *et al.*, 1993). However, the climate system does not respond linearly to these changes in insolation (Broecker and Denton, 1989), leading some authors to express concern over the validity of the Milankovitch climate link (e.g. Ridgewell *et al.*, 1999; Wunsch, 2004). Furthermore, the rapid transitions from full glacial to interglacial conditions and sub-millennial

scale climate variations during the last glacial cycle (Dansgaard *et al.*, 1989) are too short to be accounted for by the direct influence of the Earth's orbital parameters.

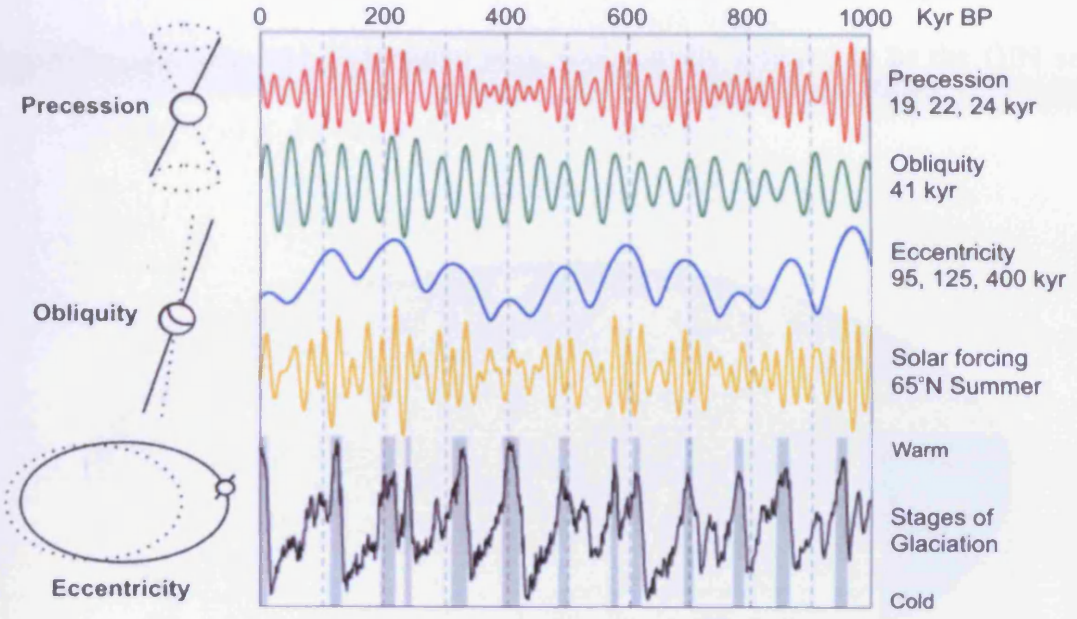

Figure 1.1: Three modes of variability in the Earth's orbital parameters, the amount of solar radiation at 65° N and the degree of glaciation.

Abrupt reorganisations in the thermohaline circulation (THC) or the 'global ocean conveyor' (Broecker, 1997) have been highlighted as the most plausible cause for both the rapid shifts in climate during the past million years (e.g. Sarnthein *et al.*, 1994; Bond *et al.*, 1997; Curry *et al.*, 1999; Ganopolski and Rahmstorf, 2001; Clark *et al.*, 2002) and the non-linear response to the Earth's orbital parameters, particularly in regions close to present day areas of deepwater formation. There are two key regions of deepwater formation i.e. the high latitude North Atlantic and the Weddell Sea, where water sinking from the surface to depth is responsible for the ventilation of the ocean basins (Broecker, 1997; Figure 1.2). Variations in the relative fluxes of these two primary deepwater masses have had climatic consequences on a global scale,

through changes in oceanic heat transport and atmospheric greenhouse gases (Weyl, 1968; Raymo *et al.*, 1990; Crowley, 1992). The North Atlantic MOC forms an important part of the THC, and is driven by the formation of deepwaters in the Greenland, Iceland, and Norwegian seas, (collectively referred to as the GIN seas) and Labrador Sea (e.g. Broecker *et al.*, 1990; Figure 1.2).

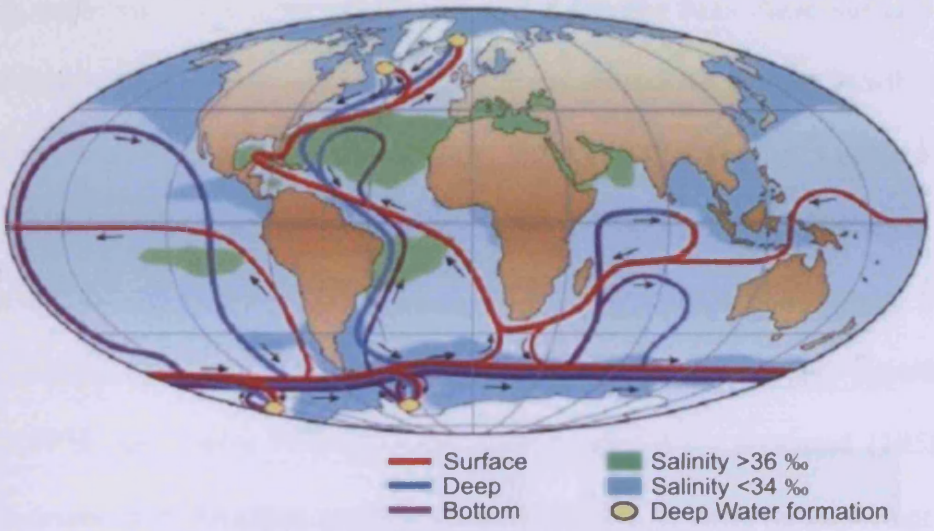

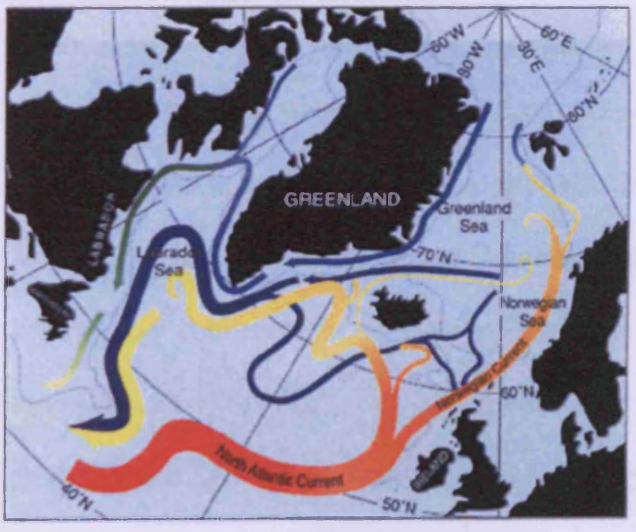

Figure 1.2: Global thermohaline circulation (Rahmstorf, 2002) and the northern component of the North Atlantic MOC (Mauritzen, 1996).

Hall and Bryden (1982) provide physical evidence that meridional overturning is occurring in the North Atlantic today, showing the tilt of the surfaces of equal density between the western and eastern sides of the Atlantic basin. Surface currents such as the Gulf Stream transport warm surface waters towards the high latitudes where they release their heat (~0.5×10^{15} W) to the atmosphere leading to a warming of ~4 °C compared with the northern North Pacific (Trenberth and Solomon, 1994). Following sufficient cooling in the Nordic and Labrador Seas these surface waters become dense enough to sink and collectively form southward flowing North Atlantic Deep Water (NADW) with an outflow of ~34 Sv (1 Sv =1×10^6 m^3 s^{-1}) south of 30 °N (McCartney, 1993; Schmitz and McCartney, 1993). These recently ventilated waters are carried southwards by a major component of the MOC, the Deep Western Boundary Current (DWBC). The North Atlantic DWBC was originally hypothesized by Wüst (1935) and Iselin (1936), analytically predicted by Stommel (1958), and originally observed by Swallow and Worthington (1961). It plays an important role in the climate system, prompting further investigations of the DWBC in an effort to understand its full nature (Fine, 1995). Past climate changes have been observed in the oscillating strength of the DWBC, suggesting that future climate change should also be observed and maybe even influenced by the strength of the DWBC. For example, the coupled ocean-atmosphere model of Manabe and Stouffer (1994) indicates that if the present day concentration of atmospheric carbon dioxide doubles, the DWBC may substantially slow (by a factor of more than two) in 150 yr.

Three main modes of the MOC have been identified from palaeoceanographic data and numerical palaeo-models (Stommel, 1961; Rahmstorf, 1994; Sarnthein *et al.*, 1994; refer also review of Rahmstorf, 2002 and references therein; Figure 1.3).

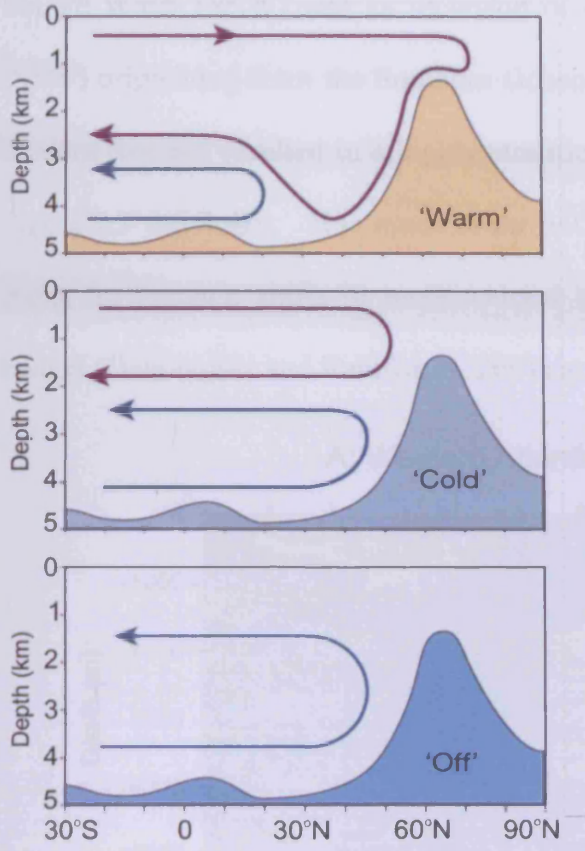

Figure 1.3: Schematic of the three modes of ocean circulation that prevailed during different times of the last glacial-interglacial period. Shown is a latitudinal section of the Atlantic; the rise in the bottom topography symbolises the shallow sill between Greenland and Scotland. North Atlantic overturning is shown by the red line, Antarctic Bottom Water by the blue line (Rahmstorf, 2002)

The first is a warm, "interglacial" mode with strong convection in the Nordic Seas and is characteristic of the modern day North Atlantic (Figure 1.3 and 1.4A). The second is a cold, "glacial" mode, with weaker convection south of the Greenland-Scotland sill in the open North Atlantic and/or Labrador Sea but not in the Nordic Seas. This mode is likely to have been caused by glacial advance approaching the Last Glacial Maximum (LGM, ~21 kyr BP) and migration of the polar front (Oppo and Lehman, 1993; Sarnthein *et al.,* 1994). During this mode of the MOC, overturning in the open North Atlantic is restricted to intermediate depths (~2,000-2,300 m water depth; Oppo and Lehman, 1993; Keigwin, 2004; Robinson *et al.,* 2005; Curry and Oppo, 2005). The intermediate water mass formed by this process is generally referred to as Glacial North Atlantic Intermediate Water (GNAIW) and was better oxygenated than modern NADW. Below this intermediate depth Northern

Source Water (NSW) was an incursion of oxygen-depleted Southern Source Water (SSW) originating from the Southern Ocean, which was less well ventilated than the modern day and resulted in a highly stratified water column (Curry and Oppo, 2005; Figure 1.3 and 1.4B). This mode of the MOC plausibly produces a metastable state, prone to dramatic shifts in mode caused by small perturbations in the freshwater budget (Ganopolski and Rahmstorf, 2001) and is thought to be representative of the

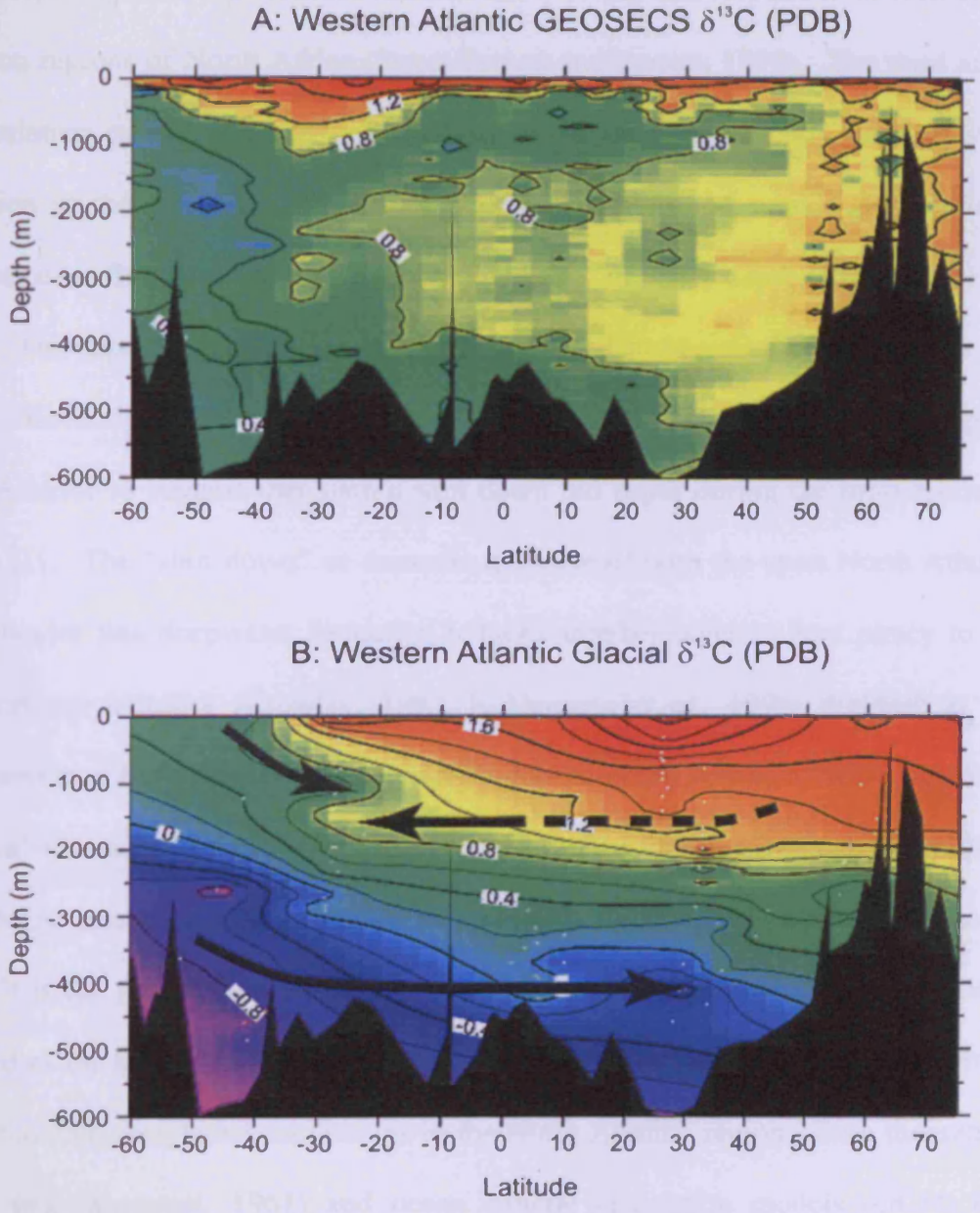

Figure 1.4: The distribution of $\delta^{13}C$ of ΣCO_2 in (A) the modern western Atlantic (Kroopnick, 1985) and, (B) a revised and updated glacial transect of western Atlantic (Curry and Oppo, 2005).

cold phase of Dansgaard-Oeschger (D/O) events and the LGM (Sarnthein *et al.*, 1994; Vidal *et al.*, 1997, 1998; Alley and Clark, 1999; Stocker and Marchal, 2000). In Northern Hemisphere ice core records, D/O events take the form of a rapid warming within a few decades, followed by a plateau phase with slow cooling lasting several centuries, then a more rapid drop back to cold stadial conditions (Dansgaard *et al.*, 1993). Shut down of the convective centre in the Nordic Seas has a strong effect on the atmosphere of the high latitude Atlantic and on areas that respond to it, such as the monsoon regions of North Africa (Street-Perrott and Perrott, 1990). The third mode of circulation is a "collapsed" or "meltwater" mode with virtually no deepwater formation in the North Atlantic and a poorly ventilated and weakly differentiated water mass of Southern Ocean origins below 2,000 m water depth (Sarnthein *et al.*, 1994). This mode of circulation has been suggested to prevail during Heinrich (H) events. Recently, McManus *et al.* (2004) used $^{231}Pa/^{230}Th$ ratios in the subtropical North Atlantic to suggest that such a shut down did occur during the most recent H event - H1. The "shut down" or dramatic decrease of both the open North Atlantic and Labrador Sea deepwater formation reduced interhemispheric heat piracy to the high northern latitudes (Crowley, 1992; Ruhlemann *et al.*, 1999; Weldeab *et al.*, 2006), and may have increased deepwater formation in the Southern Ocean as part of the so called bipolar see-saw (Crowley, 1992; Broecker, 1998). Although the splitting of the MOC into only three modes of circulation is somewhat simplistic (Rahmstorf, 2002), it is the progression between these end-member modes of circulation that is regarded as the key to understanding the abrupt climatic changes documented within the glacial and interglacial oscillations in the North Atlantic region. Both theoretical studies (e.g. Stommel, 1961) and ocean general circulation models (GCM; e.g. Manabe and Stouffer, 1988) have suggested that the MOC may have multiple

equilibria and that transitions between these equilibria may be triggered by sea surface anomalies in the freshwater flux (see Lynch-Stieglitz *et al.*, 2007).

In order to make a mechanistic connection between changes in deep ocean circulation and millennial- to centennial-scale climate events, well dated high resolution palaeo-proxy records are needed. Currently, there is widespread evidence from passive geochemical tracers from marine sediments showing that during the last glaciation the production of northern-source deepwaters was suppressed (Duplessy *et al.*, 1988; Curry *et al.*, 1988) and replaced to a varying extent by intermediate waters (Oppo and Lehman, 1993; Came *et al.*, 2003) probably fed by a Gulf Stream with different properties (Lynch-Stieglitz *et al.*, 1999). Millennial-scale fluctuations within the last glacial period are closely correlated to D/O events observed in the Northern Hemisphere ice core records (Keigwin and Boyle, 1999). Dansgaard-Oeschger events are suggested to occur with a pacing of 1.5 kyr, with further preferences at 3 and 4.5 kyr (Dansgaard *et al.*, 1993; Grootes *et al.*, 1993; Alley *et al.*, 2001) suggesting a stochastic resonance influence. During D/O stadial intervals the Northern Hemisphere climate was significantly cooler (5° to 10° C), and dryer (Johnsen *et al.*, 1992; Mayewski *et al.*, 1997; Cacho *et al.*, 1999; Sachs and Lehman, 1999; van Kreveld *et al.*, 2000). The resulting perturbations in NADW production are suggested to be caused by ocean-ice interactions leading to a freshening of the surface ocean (Bond and Lotti, 1995; Renssen *et al.*, 2002; Wiersma and Renssen, 2006). For example, over the last 80 kyr iceberg discharges in the North Atlantic have been correlated with D/O cycles (Bond and Lotti, 1995) showing that the ocean surface and atmosphere behaved as a coupled system, periodically undergoing massive reorganisations on the timescale of centuries or less.

A complex sequence of events is also evident during the last deglaciation (19 to 10 kyr BP; Figure 1.5), which is punctuated by a number of distinct millennial- (and centennial-) scale events (Alley *et al.*, 1993; McManus *et al.*, 2004; Schmidt *et al.*, 2004). One of the major goals of palaeoceanography is finding the mechanisms responsible for these changes. There is increasing evidence that the low-latitude climate system may have been an important catalyst of deglacial climate change, influencing both poleward heat and vapour transport (e.g., Broecker *et al.*, 1998; Cane and Clement, 1999), although some studies show that deglacial warming was asynchronous across the tropical band complicating the identification of causal mechanisms (e.g. Flower *et al.*, 2004, see **Chapter 4**).

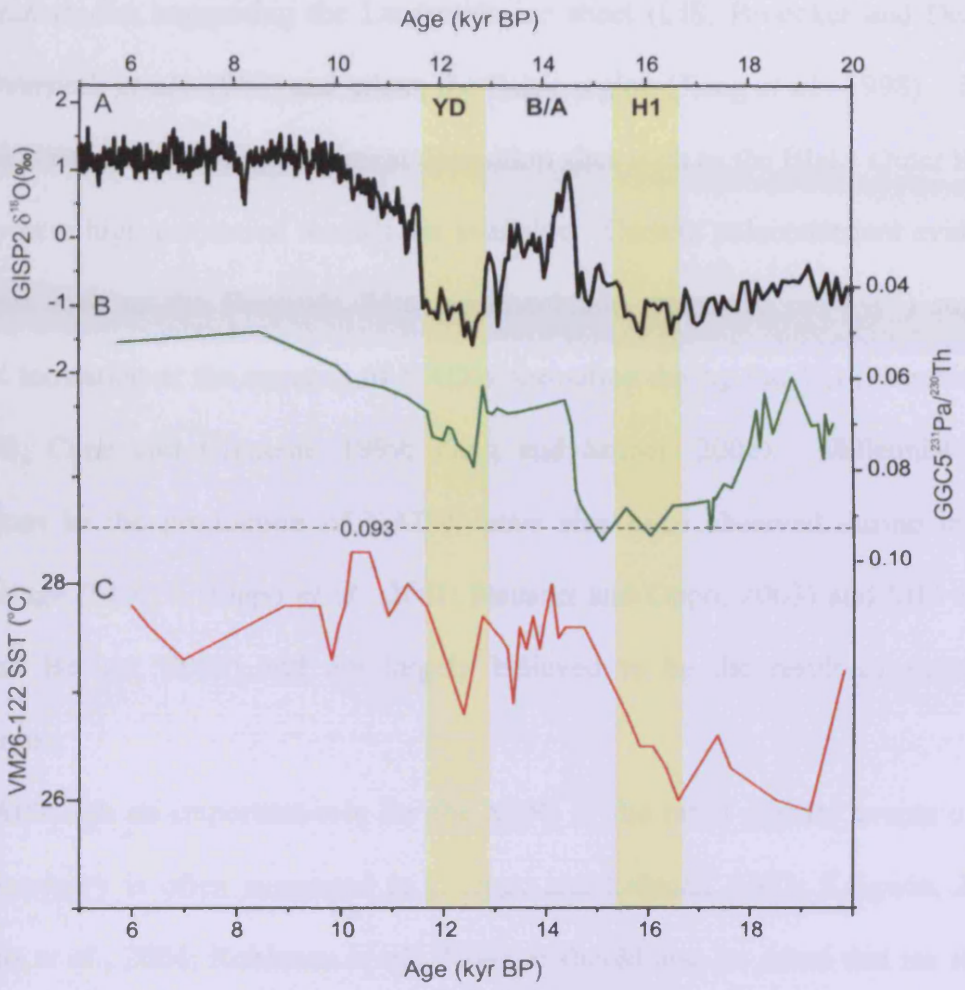

Figure 1.5: Various proxy records covering the last deglaciation. (A) GISP2 $\delta^{18}O$ (Grootes *et al.*, 1993). (B) $^{231}Pa/^{230}Th$ from the North Atlantic (a proxy for MOC) (McManus *et al.*, 2004). (C) Reconstructions of sea surface temperature (SST) from the tropical Atlantic (Schmidt *et al.*, 2004). Where H1 = Heinrich event 1, YD= Younger Dryas and B/A= Bølling-Ållerød.

One of the best documented events of the last glacial cycle is the Younger Dryas (YD) event (Figure 1.5), which is represented by a brief return to glacial temperatures ~13.5-11.5 kyr BP at the end of the last deglaciation. There is evidence of an ocean circulation involvement, with some studies suggesting a sudden disruption of NADW production caused by the rapid influx of freshwater to the surface of the North Atlantic from melting ice sheets (e.g. Lehman and Keigwin, 1992; Hughen *et al.*, 1998). The origin of this trigger mechanism remains uncertain,

with some studies suggesting the Laurentide ice sheet (LIS; Broecker and Denton, 1989; Overpeck *et al.*, 1989) and others the Baltic region (Jiang *et al.*, 1998). More evidence is needed from high sediment deposition sites such as the Blake Outer Ridge (BOR) where high resolution records are available. Current palaeonutrient evidence from sites such as the Bermuda Rise (sedimentation rates >10 cm kyr^{-1}) suggest GNAIW formation at the expense of NADW formation during the YD (Marchitto *et al.*, 1998; Cane and Clement, 1999; Zahn and Stüber, 2002). Millennial-scale fluctuations in the production of NADW have also been observed during marine isotope stage (MIS) 5 (Oppo *et al.*, 2001; Heusser and Oppo, 2003) and MIS 12/11 (Hall and Becker, 2007) and are largely believed to be the result of ocean-ice interactions.

Although an important role for the MOC in the rapid climate events of the Late Quaternary is often suggested (e.g. Oppo and Lehman, 1993; Keigwin, 2004, McManus *et al.*, 2004; Robinson *et al.*, 2004), it should also be noted that ice sheet-atmosphere interactions and amplifying mechanisms within the climate system may also play an important role. It has been suggested that ice-sheet–linked changes in freshwater delivery to the North Atlantic, and possibly free oscillations in the climate system, forced the millennial climate oscillations associated with changes in NADW flow (Alley and Clark, 1999 and references therein). The last deglaciation must therefore be understood as a superposition of these and other variations. Large land-ice fluctuations driving changes in ice albedo, sea level and possibly CO_2 have occurred in the north. These ice-albedo and CO_2 feedbacks caused changes in atmospheric and shallow oceanic circulation that further amplified rapid climate changes. For example, extratropical cooling increases the equator-to-pole temperature gradient and thus the wind strength. Stronger winds increase tropical upwelling and

other mixing processes, cool surface waters and reduce tropical water vapour causing additional cooling in and beyond the tropics (Alley and Clark, 1999). Cooling in the north tends to weaken the African and Asian monsoons, reducing tropical water vapour and cross-equatorial heat exchange. Furthermore several GCM investigations have revealed that during rapid climate deteriorations high ice sheets could result in the displacement of the jet stream, significant cooling over and downwind of the ice sheets, and reorganization and strengthening of storm tracks along the Laurentide ice sheet and extending across the North Atlantic (e.g. Manabe and Broccoli, 1985; Kutzbach *et al.*, 1996; Ganopolski *et al.*, 1998). Additionally, changes in atmospheric methane observed globally during rapid climate events, such as the Younger Dryas, implicate the low latitude hydrological cycle as a possible driving mechanism (Chappellaz *et al.*, 1993; refer **Chapter 4**).

The MOC is therefore a sensitive component of the climate system, capable of amplifying small environmental forcing mechanisms (Broecker, 1997). Despite the increasingly abundant palaeoceanographic evidence describing these changes in the MOC outlined above, there is still a notable paucity of detailed proxy records forming depth transects to study the flow of individual deepwater masses within the MOC at any one time. Most of the present evidence is inherently patchy as it focuses on the study of single sediment cores, thus providing a record of hydrographic events without a means of quantifying their extent due to the lack of further spatial coverage. Additionally, most research to date has also concentrated on the eastern basin of the North Atlantic (e.g. Sarnthein *et al.*, 1994) rather than the western basin where the most energetic and climatically important components of the ocean circulation occur. Using a depth transect of cores in the eastern basin Sarnthein *et al.* (1994) was able to map the shifts in the main convective centre of the NE Atlantic over the past 30 kyr

BP. The depth transect strategy successfully circumvented common problems linked to assessing the variable net fluxes of deepwater from a single core, being able to confidently distinguish simple vertical shifts in the mixing zone between SSW and NADW in addition to problems related to local peaks in the vertical flux of particulate organic carbon. Keigwin (2004) recently made the first concerted effort at a depth reconstruction of palaeo-proxy data in the western basin of the North Atlantic concentrating on $\delta^{13}C$ and $\Delta^{14}C$. Prior to this investigation the only data available in this region were upper ocean reconstructions in the Bahamas (Slowey and Curry, 1995) and in the Florida Straits (Lynch-Stieglitz *et al.*, 1999). There are few studies in the western basin of the North Atlantic that are on a comparable basis to the Sarnthein *et al.* (1994) reconstruction in the eastern basin.

This research focuses on sediment cores from the western subtropical North Atlantic and is aimed at reconstructing the hydrographic evolution of climatically significant water masses and the position and intensity of the DWBC through the rapid environmental changes of the last glacial cycle.

1.3 Palaeoceanographic proxies for deep circulation changes

A variety of palaeoceanographic proxies have been used to study deep palaeo-circulation changes. Benthic carbon isotopes ($\delta^{13}C$) and Cadmium-Calcium ratios (Cd/Ca) are the most widespread (e.g. Boyle and Keigwin, 1987; Curry *et al.*, 1988; Duplessy *et al.*, 1988; Sarnthein *et al.*, 1994; Marchitto *et al.*, 1998; Oppo and Lehman, 1993; Came *et al.*, 2003; Keigwin, 2004). These geochemical proxies allow inferences to be made about the extent of a water mass and can be used as non conservative tracers, since nutrient concentrations within the tests of benthic foraminifera are at least partially dependent on the nutrient concentration of the

waters they inhabited. However, inferences of circulation vigour can not be made from such proxies (LeGrand and Wunsch, 1995), although they may reveal changes in water mass distributions.

To date, little direct evidence has been presented to support the suggestion that there may have been perturbations in the vigour of deep sea circulation associated with climate oscillations and shifts in the location of deepwater formation. Measurements of the physical characteristics of deep sea sediments provide an additional, but very different proxy to geochemical methods, capable of recording relative changes in near-bottom flow speed vigour. The rationale behind this approach is that fluctuations in the rate of deepwater production affect both the geostrophic flow characteristics and possibly the density gradients of the resulting current and the relative changes in these variables can be measured (Bianchi *et al.*, 1999). One such physical proxy is the grain size distribution of the terrigenous sediment fraction. This approach is used extensively in this study in order to reconstruct the intensity and position of the DWBC in the western subtropical North Atlantic (**Chapters 3, 5 and 6**). The use and merits of both geochemical and physical proxies are discussed further in **Chapter 6**.

1.4 Aims and objectives

The primary aim of this thesis is to enhance our understanding of the role played by the MOC in climate change on both rapid and longer timescales over the last 130 kyr. Furthermore, a particular emphasis is placed on the reconstruction of the DWBC in the western subtropical North Atlantic during a variety of climatically significant time intervals of the last glacial cycle. In order to map both the vertical migration of the DWBC in the water column and changes in flow intensity, individual

sediment cores can not be used in isolation. Instead, depth transects of two or more sediment cores will be examined. The key steps followed to achieve these aims were as follows:

- To establish the present day relationship between the modern hydrography and environmental conditions in the western subtropical North Atlantic with measurements from palaeoceanographic proxies. A particular emphasis is placed on grain size, benthic $\delta^{13}C$ and $CaCO_3$ proxies from core top sediments in a vertical depth transect across the DWBC.
- To repeat the previous step for sediments deposited both at the peak of the last glaciation (during the LGM) and at selected times during the last deglaciation (e.g. Younger Dryas) when the position and strength of the DWBC should have been different to the modern, as the MOC was in its glacial mode.
- To obtain continuous, high-resolution (centennial-scale) reconstructions of the vigour and hydrography of the integrated outflow from the GIN seas and SSW during the last deglaciation when the climate was experiencing rapid reorganisations. These records are then integrated with previously published deepwater proxy records, e.g. $^{231}Pa/^{230}Th$ and benthic Cd/Ca.
- To construct high-resolution surface ocean hydrographic records for the western subtropical North Atlantic during the last deglaciation using stable isotopes and Mg/Ca palaeothermometry on paired samples of surface-dwelling planktonic foraminifera.
- To obtain continuous, high-resolution reconstructions of the vigour and hydrography of the integrated outflow from the GIN seas and shallower LSW during MIS 5 and the MIS 5/4 transition, utilising grain size, benthic $\delta^{13}C$ and $CaCO_3$ proxies. To combine these results with both other grain size and

benthic $\delta^{13}C$ studies from the region to create a convincing depth transect study, and with other Northern Hemisphere palaeoclimate records.

1.5 Thesis layout

Chapter 2 describes the study location, present hydrography and the background of the various methodological approaches used, from the initial core sampling to the final laboratory based analyses.

Chapter 3 presents records of DWBC flow vigour and hydrography for three depth transects during the Holocene, LGM and YD. This enables the proxies used in the Holocene section of this study to be 'ground-truthed' against detailed modern hydrographic measurements. The results are compared to an LGM and a YD reconstructions when, hydrographically, conditions should be very different to the present day. A slightly modified version of this chapter is currently submitted for publication

Chapter 4 presents a reconstruction of surface ocean conditions during the rapid climate transitions of the last deglaciation. Mg/Ca measurements on planktonic foraminifera are used for the first time at the Blake Outer Ridge (BOR) in the subtropical Atlantic to reconstruct sea surface temperatures (SST) and salinity (SSS) during the last deglaciation. This chapter highlights the complex combination of factors influencing both SST and SSS at the BOR including changes in the strength of the MOC, hydrological factors and regional meltwater inputs. A slightly modified version of this chapter is currently in preparation for publication.

Chapters 5 and 6 study change in the intensity and position of the DWBC during the last deglaciation and MIS 5/4. **Chapter 5** introduces two radiocarbon dated, high resolution grain size records that are used to document deepwater flow speed changes in the subtropical North Atlantic between NSW and SSW. A slightly modified version of this chapter is currently submitted for publication. **Chapter 6** considers intermediate water links to the DWBC variability during the interval 130-60 kyr BP using a combination of grain size and geochemical proxy data. The data collected from two sediment cores are compared and integrated with previously collected datasets allowing the reconstruction of the changing vertical position of the DWBC throughout this interval. A slightly modified version of this chapter has been accepted for publication (Evans *et al., in press*).

Chapter 7 draws together the key scientific findings, which are detailed in the discussions of **Chapters 3, 4, 5** and **6** and highlights their significance within the current field of knowledge on the role played by the MOC in modulating climate on both glacial to interglacial and shorter timescales.

Chapter 2: Methodology

2.1 Regional setting

The Blake Outer Ridge (BOR), in the western subtropical North Atlantic (28-34°N, 75-71°W) is a constructional sedimentary drift that protrudes out of the continental shelf south of Cape Hatteras. The ridge has been built progressively upwards since the early Tertiary (Ewing and Hollister, 1972) forming a continuous extension of the eastern continental margin of North America (Figure 2.1). The 700-km-long ridge slopes to the southeast between ~2,000 m (point of attachment to continental margin) and 5,000 m (Hatteras Abyssal Plain) water depth and has been moulded by deep contour-following bottom currents (Flood, 1979).

The orientation and formation is largely a direct response to the north eastward flowing Gulf Stream overriding the southward flowing DWBC (also known as the Western Boundary Undercurrent in the western North Atlantic), notably the interaction between the lower layer of the Gulf Stream as it detaches from the continental shelf and the uppermost DWBC (Bryan, 1970; Stahr and Sanford, 1999). The terrigenous sediment supply is dominated by material eroded from the continental margin to the north and transported to the BOR by the DWBC (Ewing *et al.*, 1966; Heezen *et al.*, 1966; Laine *et al.*, 1994) although, at shallower depths, the upper end of the ridge may additionally be influenced by a source of detrital carbonate derived from the scouring of the Blake Plateau further south by the Gulf Stream (Bryan, 1970; Markl *et al.* 1970; McCave and Tucholke, 1986). This interaction has resulted in the thickest Pleistocene sediments being located on the crest of the ridge where sedimentation rates reach up to ~60 cm kyr^{-1} (Keigwin, 2004). Furthermore, the crest

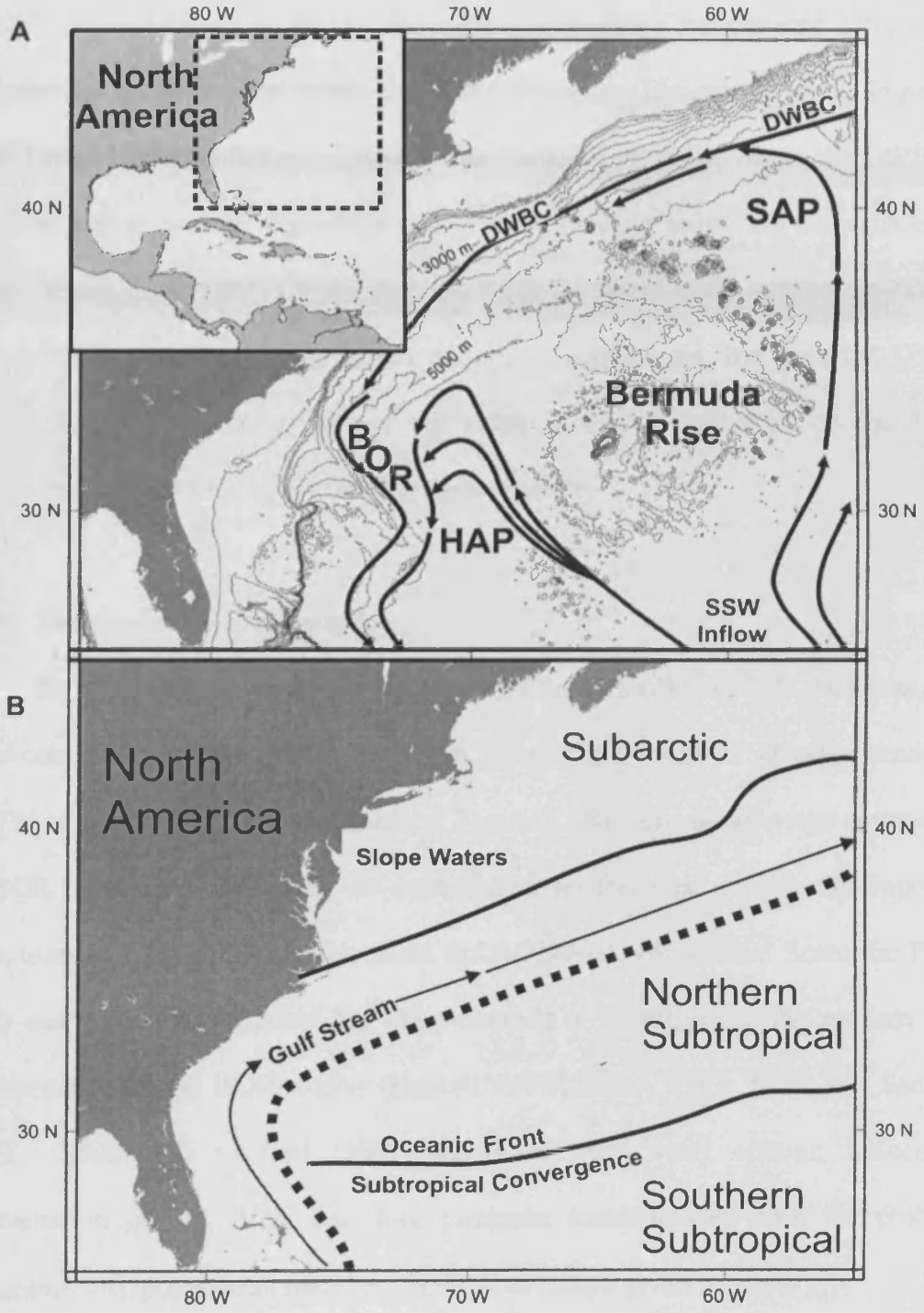

Figure 2.1: Maps of the western subtropical North Atlantic in the region of the Blake Outer Ridge (BOR). Map A shows the deep water hydrography of the area indicating the path of southwards flowing Deep Western Boundary Current (DWBC) and the recirculating Southern Source Water (SSW, thick black line; adapted from Weatherly and Kelley, 1984). The BOR, Bermuda Rise (BR), Hatteras Abyssal Plain (HAP) and Sohm Abyssal Plain (SAP) are shown. Map B shows the location of the modern surface water masses in the region (adapted from Bé *et al.*, 1971; Chaisson *et. al.*, 2002).

of the BOR is isolated from the continental slope by a bathymetric low, which precludes the occurrence of debris-flows and turbidites (Hoogakker *et al., in press*). Older Tertiary sediments are exposed on the flanks of the ridge where the DWBC is strong enough to prevent deposition and to erode existing sediments (Johnson *et al.*, 1988). Amos *et al.* (1971) found that the BOR topographically steered the DWBC towards the southeast and away from the continental margin, but once the DWBC rounded the southern most tip of the ridge it flowed westward to the Blake Escarpment, before once again flowing equatorwards.

2.1.2 The deepwater hydrography

The BOR provides a key region to study the variability of NADW where, as a major component of the MOC, the DWBC carries ~16-19 Sv of recently ventilated NADW equatorward (Stahr and Sanford; Figure 2.1A). The depth range spanned by the BOR means that sediments are deposited under the most climatically important water masses (Figure 2.2) which make up the DWBC (Shipboard Scientific Party, 1998) and considerable effort has been directed at investigating the modern flow characteristics in the BOR region (Haskell and Johnson, 1993; Stahr and Sanford, 1999). Stahr and Sanford (1999) subdivided the water column influencing sedimentation on the BOR into four principle water masses with the potential temperature (θ), potential density (σ_3), and depth ranges given in Table 2.1.

The uppermost of these is Shallow Labrador Sea Water (SLSW), located between 1,000 and 1,800 m water depth at the present day. This water mass has been previously located by its high CFC (specifically CFC-11) concentrations at the BOR (Johns *et al.*, 1997; Pickart and Smethie, 1993) and consists primarily of water from

the upper part of the Labrador Sea convected along the western boundary (Pickart *et al.*, 1997).

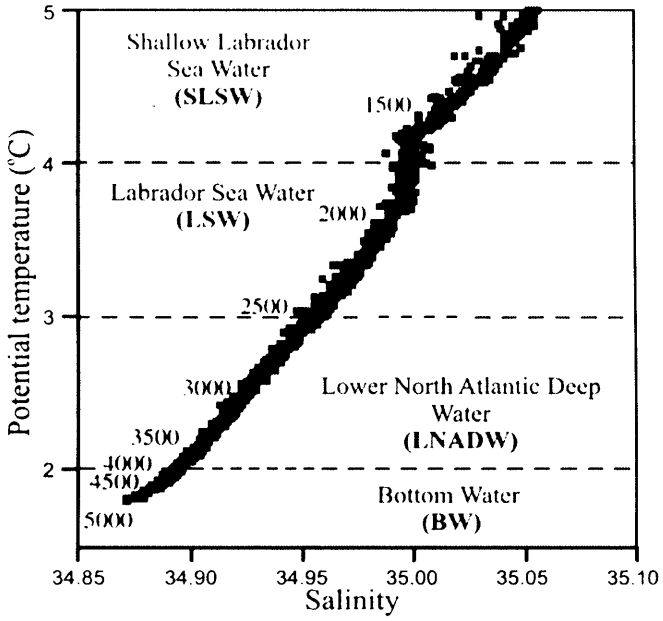

Figure 2.2: A hypothetical transect through the water column at the BOR showing the position and depth of the climatically important water masses (adapted from Shipboard Scientific Party, 1998).

Table 2.1: Limits and characteristics of DWBC water masses (taken from Stahr and Sanford, 1999)

Water Mass	Pot. temp. range	Approx. pot. density range	Approx. depth (m)
SLSW	$6°C > \theta \geq 4°C$	$41.00 < \sigma_3 \leq 41.27$ kg m^{-3}	1000-1800
LSW	$4°C > \theta \geq 2.8°C$	$41.27 < \sigma_3 \leq 41.44$ kg m^{-3}	1400-2800
LNADW	$2.8°C > \theta \geq 1.9°C$	$41.44 < \sigma_3 \leq 41.55$ kg m^{-3}	2500-4100
BW	$6°C > \theta \geq 4°C$	$\sigma_3 < 41.55$ kg m^{-3}	3400-bottom

The second water mass is Labrador Sea Water (LSW) that lies in the 1,400-2,800 m depth range. It is underlain, between 2,500 and 4,100 m water depth, by Lower North Atlantic Deep Water (LNADW) which originates from high latitude overflows such as the Denmark Strait and has the highest oxygen concentrations below the main thermocline (Stahr and Sanford, 1999). The deepest water mass is Bottom Water

(BW), which is below 3,400 m depth and consists of a varying mixture of Northern (84-90%) and Southern (10-16%) Source Waters indicated by its lower oxygen and higher silicate concentrations (Stahr and Sanford, 1999). This SSW has been recirculated in a cyclonic gyre north of the BOR (Amos *et al.*, 1971; Stahr and Sanford, 1999), and therefore has the same flow direction at the BOR as the overlying LNADW (Weatherly and Kelley, 1984; Figure 2.1A). The depth range of the BOR water masses given above overlap each other, reflecting the deepening of the DWBC flow along the ridge crest and the fact that these categories are partly based on an amalgamation of prior definitions (Stahr and Sanford, 1999).

Absolute velocity profiles along the eastern flank of the BOR (Stahr and Sanford, 1999) demonstrate that a high velocity core of the DWBC follows the bathymetric contours around the BOR. This high velocity core is located between 3,500 m near the upstream origin of the BOR (influencing depths as shallow as 3,000 m) and 4,100 m further downstream along the ridge. Speeds of 20-22 cm s^{-1} have been measured within this fast flowing core (Stahr and Sanford, 1999), although some studies suggest otherwise (e.g. Bulfinch *et al.*, 1982). Johns *et al.* (1997) also found a shallower, secondary core in the (S)LSW between 4° and 6°C (~1,000-1,800 m water depth) which is less constrained by topography than the deeper core and has velocity contours influencing depths down to ~2,500 m.

2.1.3 The surface water hydrography

The surface hydrography at the BOR (Figure 2.1B) is highly influenced by the warm northward flowing water of the Gulf Stream which at this latitude incorporates both the wind-driven subtropical gyre and the Atlantic MOC return flow (LeGrande and Lynch-Stieglitz, 2007) both of which presently flow directly over the BOR.

Volume transport estimates through the nearby Florida Straits suggest a northwards export of about 30 Sv by the Gulf Stream, of which 17 Sv is associated with the subtropical gyre circulation in the western North Atlantic while 13 Sv compensates for the southward deepwater flow (Baringer and Larsen, 2001). The core of the Gulf Stream current is about 100 km wide and has peak velocities of >2 m s^{-1} (Brown *et al.*, 2001). The BOR lies south of the relatively cold and fresh 'slope water' that presently lies between the western boundary currents and the continent (Bé *et al.*, 1971).

An appreciation of the modern annual variability in sea surface temperature (SST) and sea surface salinity (SSS) in the region of the BOR is crucial to provide a context for the interpretation of proxy records. Sea surface temperatures vary seasonally in the region, increasing from 20.8 °C in March to 27.8 °C in September (Levitus and Boyer, 1994), while HydroBase data shows an annual average of 25 °C (Curry, unpublished; Figure 2.3A). Similar variations are also apparent in the SSS profiles, with a seasonal salinity range at the surface of ± 0.30 ‰ (Levitus and Boyer, 1994) while the HydroBase data shows an average SSS of 36.3 ‰ (Curry, unpublished; Figure 2.3B).

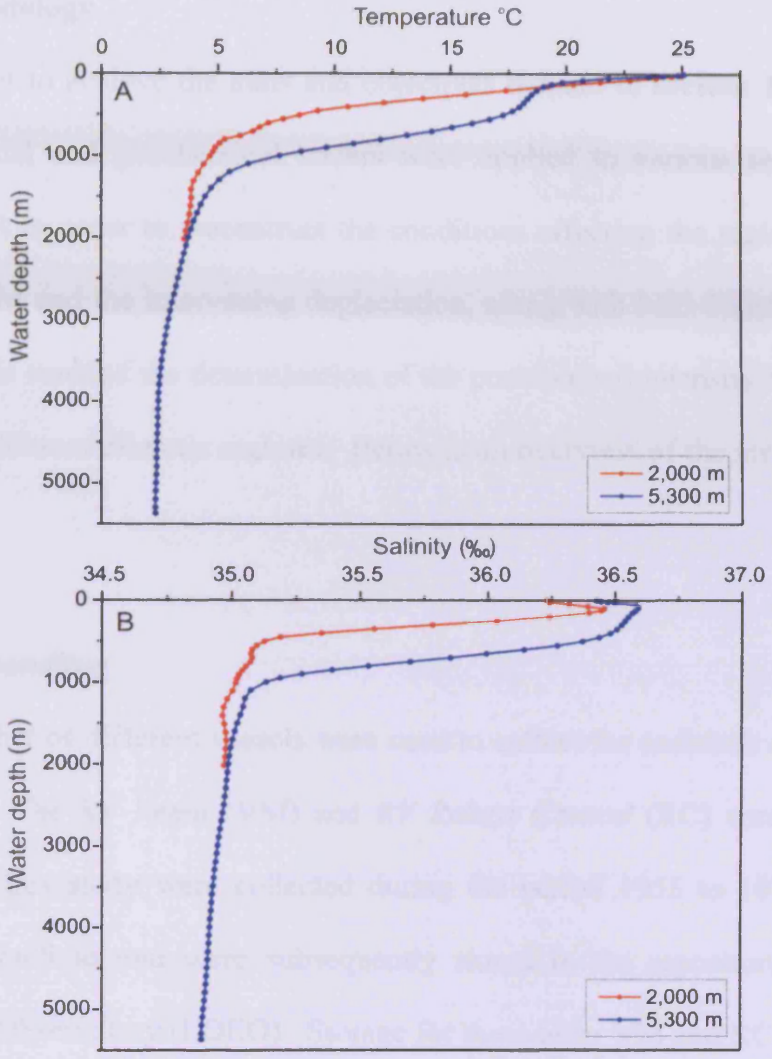

Figure 2.3: Temperature and salinity profiles down through the water column at two locations on the Blake Outer Ridge (Unpublished HydroBase data from Ruth Curry). The first location was where the water depth reached 2,000 m (red line) and the second location was further seaward along the ridge where the water depth reached 5,300 m (blue line). (A) The temperature profile, and (B) the salinity profile.

2.2 Methodology

In order to achieve the aims and objectives defined in **section 1.4** a range of sedimentological and geochemical tracers were applied to various sediment cores along the BOR in order to reconstruct the conditions affecting the region during the Holocene, LGM and the intervening deglaciation, along with MIS 5 and the MIS 5/4 transition. This enabled the determination of the position and intensity of the DWBC during these different climatic regimes. Below is an overview of the methods used in this thesis.

2.2.1 Core handling

A number of different vessels were used to collect the sediment cores utilised in this study. The *RV Vema* (VM) and *RV Robert Conrad* (RC) cores utilised in **Chapter 3** of this study were collected during the period 1955 to 1972 using the piston coring method and were subsequently stored in the repository at Lamont Doherty Earth Observatory (LDEO). Storage for these older VM and RC cores is dry, in 8-foot long galvanized steel trays. The *RV Atlantis* (AII) sediment cores (**Chapter 3**) were collected in 1972 and the sediment cores from the *RV Knorr* (KNR) cruise (**Chapters 3, 4, 5 and 6**) were collected in 1993. Core identification codes ending in 'GGC' were collected using the giant gravity corer, while those ending in 'JPC' were collected using the giant piston corer. The sediment cores from both of these cruises are stored under refrigerated conditions in the repository at Woods Hole Oceanographic Institute (WHOI). The KNR 140/2 cores were recovered as part of the site survey cruise for the subsequent Ocean Drilling Program (ODP) Leg 172 cores which were collected by the *RV Joides Resolution* during 1997 using the advanced

hydraulic piston corer and subsequently stored under refrigerated conditions in the Bremen Core Repository (**Chapter 6**).

The cores collected on board the AII, KNR and ODP vessels were extracted from the core barrel and cut into the standard 1.5 m length sections and labelled. High resolution measurements (2 cm resolution) of the bulk physical and acoustic properties of the sediment were undertaken on the most recent ODP and KNR cores using a Geotek Multisensor Track (MST) core logging system (this system is described in more detail in the *Initial Results* volume of ODP, Leg 172 (Shipboard Scientific Party, 1998)). Bulk measurements include compressional p-wave velocity, density and magnetic susceptibility. All sediment cores were split into a working half and an archive half, which were scraped and cleaned before the working half of the cores was photographed and then lithologically described.

Magnetic susceptibility measurements were made on the working halves of cores where no shipboard bulk magnetic susceptibility measurements were available. The objective was the construction of a preliminary stratigraphic framework, in order to select the most suitable cores for detailed palaeoceanographic work.

2.2.2 Magnetic susceptibility

The beginning of this section provides an introduction to the principles of magnetic susceptibility based on the study by Robinson (1990), where further comprehensive information can be found.

Minerals that are magnetisable in deep sea sediments include both those that can hold a remnant signal from the Earth's magnetic field, including detrital magnetic minerals such as magnetite, goethite and haematite (Lowrie and Hellier, 1982), and minerals that behave paramagnetically as they contain ions such as Fe^{2+}, Fe^{3+} and

Mn^{2+} e.g. clay. Biogenic components of deep sea sediments consisting of either calcium carbonate or silica are practically devoid of paramagnetic substances and therefore are only very weakly magnetised.

Magnetic susceptibility (K) is defined as the ratio of induced magnetization intensity (M) per unit volume of a substance to the strength of the applied magnetic field (H) inducing the magnetization ($K = M/H$; Thompson and Oldfield, 1986; Robinson, 1990). The magnetisation per unit volume intensity M is lost when H is removed. Therefore, measurement of the magnetic susceptibility of deep sea sediments provides a non-destructive method to assess relative oscillations in the biogenic/detrital ratio within the sediment that can directly be related to Pleistocene climate fluctuations (Robinson, 1986; Robinson *et al.*, 1995). In the BOR cores, calcium carbonate is by far the most abundant biogenic component with sediments consisting of climatically modulated cycles of marl (glacial/stadial horizons) and nanofossil chalk (interglacial/interstadial horizons). Therefore, glacial/stadial intervals correspond to high magnetic concentration when carbonate productivity was severely restricted and interglacial/interstadial horizons are characterised by low magnetic concentration and a high carbonate content of the sediment. However, it should be noted that changes in productivity and other factors may also affect carbonate content on the BOR. Most important of all was dilution of the calcium carbonate concentration by a changing supply of terrigenous material through the last glacial cycle on the BOR (Keigwin and Jones, 1989; Keigwin and Jones, 1994). Another important factor is calcium carbonate dissolution which again varies greatly in the intermediate to deepwater sediment on glacial-interglacial timescales (Keigwin and Jones, 1994). Importantly, the magnetic susceptibility measurement is a ratio and can therefore vary down core purely as a result of changes in the composition of the

carbonate fraction even though it is the lithic fraction which principally carries all the magentisable materials. This technique can therefore provide a record of changes in sediment properties that can be used as a correlation tool (Andrews *et al.*, 1995).

The magnetic susceptibility of 22 cores from the BOR region was measured at two core repositories –WHOI and LDEO. At WHOI measurements were made with the cores still in the plastic core liners/containers, however at LDEO cores were stored in metallic trays and therefore had to be removed and placed on a non metallic surface to be measured. At both locations measurements were generally made at 5 cm intervals on the unprocessed sediment. These bulk or whole core measurements were made using a Bartington MS2 magnetic susceptibility meter fitted with a hand-held probe, as described in detail by Robinson (1990). The sediment surface was covered by a thin layer of plastic film to prevent contamination of the probe when it was applied to the surface of the sediment. At the start of each new core and between individual measurements a blank air reading was taken, allowing corrections to be made for instrumental drift. Sediments stored in the repository at WHOI are kept refrigerated and it was noted that initial measurements experienced considerable drift making them less reliable when held against the refrigerated sediment. In order to overcome this problem the probe was left in contact with the sediment for approximately a minute to allow the sensor of the probe to equilibrate with the temperature of the sediment and therefore stabilise the reading. After this initial step, alternating between blank and magnetic susceptibility measurements was sufficient to stabilise instrumental drift.

It was assumed that the sediment thickness was constant throughout and, therefore, equal volumes of sediment were being analysed. On the working halves of the cores where this assumption could not be made due to heavy sampling, the more

complete archive halves were measured. Additionally, it should be noted that bulk magnetic susceptibility measured using this technique is not only a function of the carbonate/non-carbonate ratio but is also controlled by the water content, which affects the concentration of all sediment components within a given volume. The cores measured at LDEO had not been stored under optimum conditions and had been allowed to dry out. Variations due to water content changes in these cores are not expected.

2.2.3 Sample preparation

The sediment for all the cores used in this study was dominated by a silty-clay texture, with the finest grey-green material found within the most recent sediments and previous interglacial sediments, while the last glacial sediments had a more reddish colour. Some cores from the WHOI repository had an oxidised layer at the top of the core suggesting the presence of relatively modern sediments and a probable age zero core top.

The working halves of the AII and KNR cores were sampled at WHOI, the VM and RC cores were sampled at LDEO, while the ODP cores were sampled at the Bremen Core Repository. Samples were taken in 1 cm thick sub-sections and avoided the material closest to the core lining to remove the potential mixing effects caused by 'smearing' along the core lining. With the exception of the VM and RC cores all the other sediment cores were sampled using a small spatula. Due to the dry storage of the VM and RC cores, sampling required cutting with a scroll saw fitted with a diamond coated musical wire. This procedure produced a clean cut with almost no loss of material. All the samples collected were then processed at Cardiff University. Samples were gently disaggregated in deionised water on a rotating carousel for 24 hr

before the 'coarse' and 'fine' fractions were separated by wet sieving through a 63 μm mesh using deionised water. Both the coarse (>63 μm) and fine (<63 μm) fractions were left to settle before the excess water was siphoned off and the samples were placed in the oven at 50°C until completely dry. When the samples were dry both the fine and coarse size fractions were weighed. The coarse fraction was then dry sieved through a 150 μm and a 250 μm mesh to produce the coarse fractions suitable to pick foraminifera for stable isotope and geochemical analyses. The mass of the coarse fraction was typically, <1 g (see **Appendix C**) and visual inspection with a binocular microscope found that it was dominantly comprised of planktonic foraminifera, few benthic foraminifera and traces of siliceous 'fluff.' There was minimal evidence for the presence of any ice rafted debris (IRD; lithic grains larger than 150 μm are assumed to be IRD) in the samples. The only lithic (potential IRD) grains noted in this study were in the 150-250 μm fraction of two glacial sediment samples, one in core RC9-10 and one in core KNR140/2-43GGC. The foraminifera present generally displayed good preservation. When dry, the fine fraction was bagged and stored awaiting preparation for sortable silt grain size analysis (**section 2.2.7**).

2.2.4 Stable isotope work

Planktonic stable isotope studies have been extensively used throughout the Quaternary often providing the basis of stratigraphic correlations and the MIS subdivisions (Shackleton and Opdyke, 1973; Shackleton and Kennett, 1975; Imbrie and Imbrie, 1979). Planktonic foraminifera are free-floating, single cell protozoa and the foraminifera used for stable isotope analyses are largely composed of calcium carbonate ($CaCO_3$). The accumulation of planktonic foraminifera and coccoliths on the sea floor accounts for in excess of 80% of modern carbonate deposition in the

oceans (Brasier, 1980). Presently sediments at the BOR are mainly composed of carbonates therefore providing an ideal location for the use of planktonic foraminifera in palaeoceanographic reconstructions. The oxygen isotopic ratio ($\delta^{18}O$) varies as a function of changes in the relative abundance (ratio) of ^{16}O and ^{18}O within the calcium carbonate of the foraminiferal test. The $\delta^{18}O$ of foraminifera is dependent upon the temperature of the water from which the calcium carbonate precipitates (e.g. Urey, 1947), local salinity variations (e.g. Flower *et al.*, 2004) and continental ice volume (e.g. Duplessy *et al.*, 1986). All isotope ratios measured ($\delta^{18}O$ per mil) are referenced to the VPDB (Vienna Pee Dee Belemnite) scale through repeat analysis of the National Bureau of Standards NBS-19 international carbonate standard.

$$\delta^{18}O = 1000 \times \frac{^{18}O/^{16}O\text{sample} - ^{18}O/^{16}O\text{ standard}}{^{18}O/^{16}O\text{ standard}} \qquad (1)$$

Expansion of the polar ice masses during glacial intervals trap ^{16}O, leaving the oceans relatively enriched in ^{18}O, while during the interglacial periods the polar ice melts releasing ^{16}O into the ocean giving lighter $\delta^{18}O$ ratios (Shackleton and Opdyke, 1973).

For planktonic stable isotope analysis yielding results for both $\delta^{18}O$ and $\delta^{13}C$, 25 to 30 foraminifera specimens were picked from the 150-250 μm fraction using a binocular microscope. It should be noted that for core KNR140/2-39GGC paired samples were picked for stable isotope and Mg/Ca analysis and this procedure is described in detail in **section 2.2.6**. Stable isotope analyses were carried out on the planktonic species *Globigerinoides ruber* (white), in accordance with the methods of Keigwin and Schlegel (2002), which are representative of sea surface conditions as this species generally lives in the top 50 m of the water column (Anand *et al.*, 2003). Only well preserved and relatively clean specimens were selected where possible.

Tests of the planktonic foraminifer *G. ruber* (white) have become a standard tool for reconstructing past oceanic environments. However, it should be noted that *G. ruber* (white) has two recognised morphotypes: *G. ruber* sensu stricto (s.s.) living in the upper 30 m of the water column and *G. ruber* sensu lato (s.l.) living at depths below 30 m (Wang, 2000; Figure 2.4).

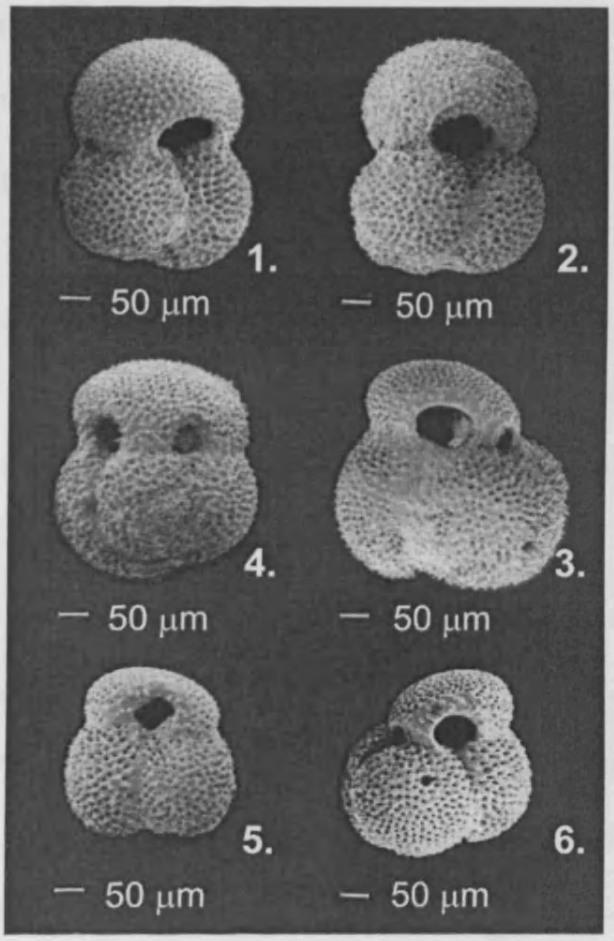

Figure 2.4: Representatives of the two morphotypes of Globigerinoides ruber (white) used to distinguish between the morphotypes in this investigation: 1–2, Globigerinoides ruber sensu stricto (s.s.); 3–6, Globigerinoides ruber sensu lato (s.l.) (Steinke *et al.*, 2005).

Stable isotope analysis of both *G. ruber* (s.l.) and *G. ruber* (s.s.) from the same sample has revealed statistically significant differences of about 0.21 ± 0.21 ‰ and −0.28 ± 0.29 ‰ for $\delta^{18}O$ and $\delta^{13}C$, respectively (Wang, 2000). Additionally, *G. ruber* (s.s.)

generally shows higher Mg/Ca than *G. ruber* (s.l.), suggesting that *G. ruber* (s.l.) precipitate their shells in slightly colder (presumably deeper) waters (Steinke *et al.*, 2005). During this study, in order to avoid problems posed by the presence of different morphotypes of a species, only *G. ruber* (s.s) were picked unless too few were available. Specimens of *G. ruber* (s.s) tended to be the easiest to recognise consistently as they are specimens with spherical chambers sitting symmetrically over previous sutures with a wide, high arched aperture, whereas G. ruber (s.l.) refers to a more compact test with a diminutive final chamber and small aperture.

Benthic oxygen isotopes are derived from the ratio of $^{18}O/^{16}O$ in the fossil carbonate shells of bottom-dwelling, single-celled foraminifera. This ratio reflects both the temperature and the $^{18}O/^{16}O$ ratio of the seawater (which generally covaries with salinity in the upper ocean) in which the foraminifera calcify (Emiliani, 1955). Benthic foraminifera proved scarce in the samples at the BOR but, wherever present, 1-4 specimens of *Cibicidoides wuellerstorfi* or *Cibicidoides spp.* were selected from the >150 μm fraction. Keigwin (2004) has previously shown that benthic foraminifera are discontinuously present at the BOR.

Specimens (both planktonic and benthic) were lightly crushed using a glass plate just enough to break open all of the chambers prior to cleaning. Before analysis the tests were immersed in 3% hydrogen peroxide (H_2O_2) for 30 minutes in order to remove any organic matter present. A drop of 3% Analar Acetone was added and the samples were ultrasonicated at a low frequency for 10 seconds to remove any adhering debris from the test walls. The dirty residue and excess liquid was quickly removed and the tests then dried at 50 °C. All stable isotope measurements for **Chapters 3, 4 and 5** were made at Cardiff University using the ThermoFinnigan MAT 252 mass spectrometer coupled to a Kiel II carbonate device for automated

carbonate preparation. The long-term reproducibility of the system is ≤0.08 ‰ for $\delta^{18}O$ and 0.03 ‰ for $\delta^{13}C$. Stable isotope measurements in **Chapter 6** were made at WHOI with a long-term analytical precision of ±0.07 ‰ for the $\delta^{18}O$ data and ±0.03 ‰ for the $\delta^{13}C$ measurements, based on over 2000 analysis of NBS-19 (Ostermann and Curry, 2000).

2.2.4.1 Bottom water ventilation

The carbon isotope ($\delta^{13}C$ of ΣCO_2) values recorded in the calcite tests of benthic foraminifera vary systematically with bottom water mass chemistry (e.g. Duplessy *et al.*, 1984; Curry *et al.*, 1988). Primary producers in the surface ocean take up both nutrients and carbon, discriminating against the heavy isotope of carbon, resulting in high $^{13}C/^{12}C$ ratios in surface waters and in low nutrient water masses such as NADW that have had recent contact with the atmosphere. Higher nutrient concentrations and lower $^{13}C/^{12}C$ in SSW reflect the longer time these waters have spent away from the surface, acquiring nutrients and carbon from the decay of organic matter transported to depth by particulates and dissolved minerals.

The benthic, epifaunal species *Cibicidoides wuellerstorfi* and *Cibicidoides spp.* have been shown to faithfully record the $\delta^{13}C$ of dissolved inorganic carbon in ambient bottom water (Belanger *et al.*, 1981; Graham *et al.*, 1981; Curry and Lohman, 1982; Duplessy *et al.*, 1984). On the BOR, Holocene sediments shallower than 4,000 m show $\delta^{13}C$ values ~1 ‰ VPDB (refer **Chapter 3**), which is similar to previous core top values in the region (Keigwin, 2004) and compare well with the $\delta^{13}C$ of ambient seawater total CO_2 in the GEOSECS profile (Kroopnick, 1985). This nutrient proxy has been used successfully by previous studies to reconstruct deep ocean palaeocirculation from sediment cores in both the eastern and western North Atlantic

basins (e.g. Boyle and Keigwin, 1987; Oppo and Lehman, 1993; Sarnthein *et al.*, 1994; Zahn *et al.*, 1997; Elliot *et al.*, 2002; Keigwin, 2004).

It has been suggested that the $\delta^{13}C$ of the marine carbon reservoir has undergone changes in the past. For example, a secular change in the $\delta^{13}C$ of ΣCO_2 of ~0.3 ‰ has been observed in the eastern tropical Pacific between the LGM and the Holocene, (e.g. Duplessy *et al.*, 1984; Boyle *et al.*, 1988). Currently, the robust constraints needed on the mean ocean $\delta^{13}C$ variations across both the glacial and deglacial periods at high temporal resolution to correct for the influence of carbon reservoir changes on epibenthic $\delta^{13}C$ are unavailable. However, mean-ocean $\delta^{13}C$ changes will have affected $\delta^{13}C$ records from different core sites on the BOR equally (Keigwin, 2004). Therefore, this factor is not considered an obstacle in the regional comparison of epibenthic $\delta^{13}C$ gradients presented in **Chapters 3 and 6**. A further discussion of the pros and cons of the $\delta^{13}C$ proxy can be found in **Chapter 6, section 6.1.**

2.2.5 Radiocarbon dating

Accelerator mass spectrometer (AMS) ^{14}C dating was carried out at the NERC radiocarbon laboratory. A typical sample consisted of up to 1500 individual (>10 mg) planktonic foraminifera from the >150 μm fraction. Where sufficient specimens were available, particularly in the more recent sediments, monospecific samples of *G. ruber* were picked for analysis. Occasionally, when this species was not abundant enough, particularly during the cold glacial periods, a mixed assemblage had to be picked. Where larger sediment sub-samples were needed in order to achieve sufficient foraminifera for ^{14}C analysis, estimates were made of the additional mass of sediment required (Figure 2.5) in order to prevent needless destruction of the core.

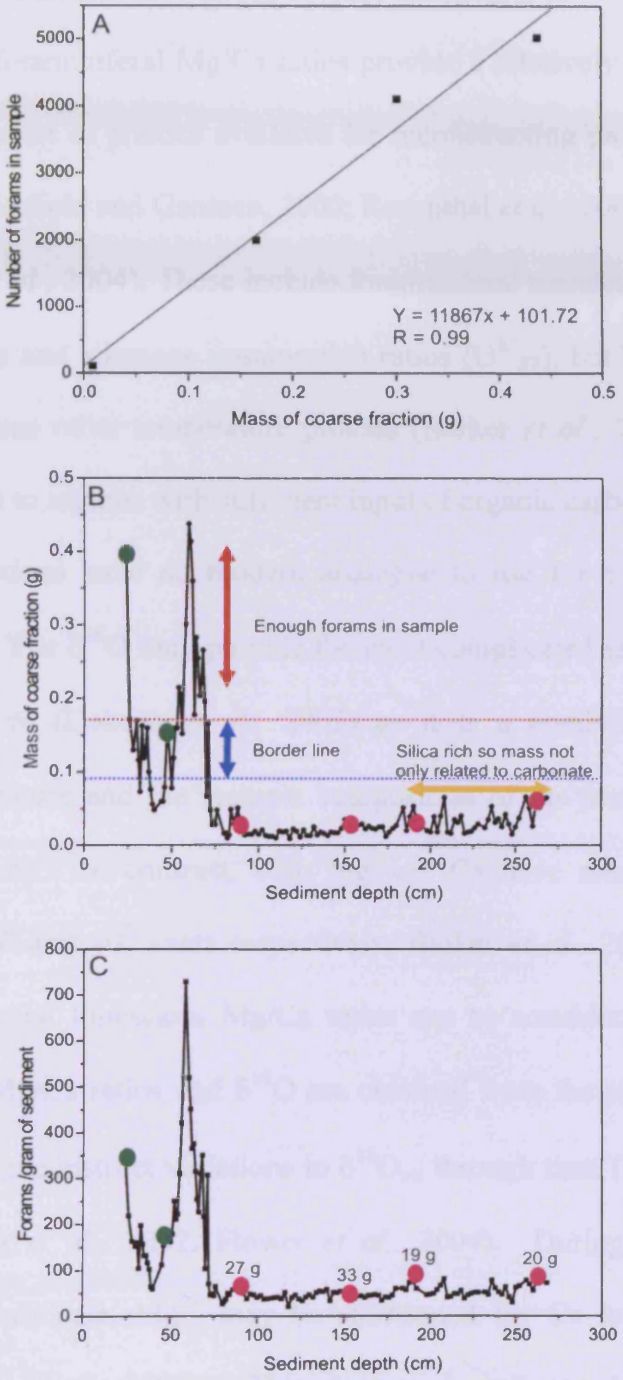

Figure 2.5: Coarse fraction mass data for core KNR140/2-28GGC. (A) Correlation plot showing a strong positive correlation between the numbers of foraminifera and the mass of the coarse fraction in a sample. This relationship was then used to estimate the mass of coarse fraction required to obtain enough specimens for ^{14}C-AMS dating. (B) Changing coarse fraction mass with sediment depth in core KNR140/2-28GGC. Green circles show the location of ^{14}C-AMS dates where there are ample specimens in the sample. Pink dots show the location where additional sediment was required in order to achieve sufficient specimens for analysis. (C) The estimated number of foraminifera per gram of sediment in core KNR140/2-28GGC is shown to change with depth. The mass of additional sediment required to obtain the ~1000 foraminifera needed for ^{14}C-AMS dating is shown.

2.2.6 Magnesium Calcium derived sea surface temperatures

Planktonic foraminiferal Mg/Ca ratios provide a relatively new, but routinely used addition to the set of proxies available for reconstructing past SST (e.g. Lea *et al.*, 2000, 2002; Elderfield and Ganssen, 2000; Rosenthal *et al.*, 2000, 2003; Pahnke *et al.*, 2003; Flower *et al.*, 2004). These include foraminiferal transfer functions, $\delta^{18}O$ of foraminiferal calcite and alkenone unsaturation ratios ($U^{K'}_{37}$), but Mg/Ca has distinct advantages over these other temperature proxies (Barker *et al.*, 2005). The use of alkenones is limited to regions with sufficient input of organic carbon (Herbert, 2001), while transfer functions have no modern analogue to use for calibration purposes (Mix *et al.*, 1999). The $\delta^{18}O$ may provide the most complicated signal to interpret in terms of temperature (Dekens *et al.*, 2002) as it is a combination of both the calcification temperature and the isotopic composition of the seawater ($\delta^{18}O_{sw}$) the calcite precipitated in. In contrast, both Mg and Ca have relatively long ocean residence times (10^6 and 10^7 years respectively, Barker *et al.*, 2005) and therefore over glacial-interglacial timescales Mg/Ca ratios can be considered to be constant. However, as both Mg/Ca ratios and $\delta^{18}O$ are obtained from the same medium, they can be combined to reconstruct variations in $\delta^{18}O_{sw}$ through time (e.g. Elderfield and Ganssen, 2000; Lea *et al.*, 2002; Flower *et al.*, 2004). During the formation of biogenic calcium carbonate, Mg^{2+} may be substituted for Ca in the foraminiferal calcite lattice (Lea *et al.*, 1999). This process is influenced by the seawater temperature surrounding the test during growth such that Mg/Ca ratios increase with increasing seawater temperature (e.g., Chave, 1954; Nürnberg, 1995; Lea *et al.*, 1999; Anand *et al.*, 2003), with secondary factors such as salinity and pH exerting minor influences on shell Mg (Nürnberg *et al.*, 1996; Lea *et al.*, 1999). Although the uptake of Mg/Ca is a thermodynamic effect, it is biologically mediated and therefore requires

calibration based on biogenic calcite (Rosenthal *et al.*, 1997). Therefore, Mg/Ca provides an appropriate proxy for the estimation of palaeoceanographic seawater temperature changes through time.

In this investigation Mg/Ca was determined on the planktonic species *G. ruber* (white). Unlike other planktonic foraminifera species which suffer from heterogeneity of Mg/Ca ratios within their tests due to vertical migration in the water column, *G. ruber* appears to give relatively constant Mg/Ca ratios (Eggins *et al.*, 2003), showing little evidence of gametogenic calcite (Caron *et al.*, 1990) and is representative of the surface and mixed layer temperatures (Barker *et al.*, 2005). A total of 100-130 specimens were picked from each sample in the 150-250 μm fraction and prepared for "paired" Mg/Ca and $\delta^{18}O$ analysis.

The following cleaning strategy is based on the methods described in Boyle and Keigwin (1985) with modifications from this method described both here and in more detail in Barker *et al.* (2003).

Step 1: Crushing

Prior to cleaning the foraminifera, tests were gently crushed between two clean glass plates in order to crack open all the test chambers and allow debris to escape during the subsequent cleaning, while avoiding over-crushing which could lead to excessive sample loss. It was noted at this stage that the samples in this investigation appeared to contain reasonably large particles of pyrite and some mica that would need to be removed manually later in the procedure. Once the samples had been crushed they were homogenized and divided into 75 and 25 % portions for Mg/Ca and $\delta^{18}O$ (see **section 2.2.4**) cleaning, respectively. The portion of the sample

allocated for Mg/Ca cleaning was transferred to an acid-cleaned 500 ml microcentrifuge tube.

Step 2: Silicate Removal

Clay minerals such as illite, kaolinite, montmorillonite and chlorite make up a significant proportions of marine sediments and, as they may contain on average 1-10% Mg by weight (though insignificant amounts of Sr), their removal from samples for Mg/Ca analysis is crucial (Deer *et al.*, 1992). Only 1 μg of clay would be needed to cause significant uncertainty in the measured Mg/Ca ratio (Barker *et al.*, 2003). Fortunately, high Mg/Ca ratios (>3 mmol/mol) and a lack of IRD make the samples analysed in this study typically less prone to contamination than those from colder regions.

In order to remove the silicates, the following procedure was followed in batches of 10-15 samples:

1. Initially, 500 μl of ultra high quality water (UHQ H_2O) was added to the crushed samples.
2. The samples were allowed to settle for 30 seconds or so. The overlying solution (supernatant) was then removed until all tubes contained about 10-20 μl of H_2O.
3. The sample rack was placed in an ultrasonic bath for 1 minute so that suspended clays appeared as a milky residue in the liquid above the samples.
4. The sample rack was rapped on the bench top to agitate the samples and bring loose clays into suspension.
5. The samples were allowed to briefly settle (long enough for the distinct carbonate grains to reach the bottom).

6. The overlying solution was removed and the above process was repeated a further 4 times.

7. After the water cleaning steps, methanol was used for further clay removal as the lower viscosity of this reagent helped to dislodge material still attached to the carbonate tests. Aristar methanol was squirted into each tube.

8. The tubes were then ultrasonicated for 1 minute.

9. The sample rack was rapped on the bench before being allowed to settle for a few seconds before the methanol was removed.

11. The methanol step was carried out twice.

12. Steps (2) to (5) were repeated twice in order to remove any remaining methanol and silicate grains.

Step 3: Removal of organic matter

The presence of organic matter in foraminiferal samples may produce higher Mg/Ca ratios (Hastings *et al.*, 1996; Rathburn and De Decker, 1997; Barker *et al.*, 2003). Initial visual inspection of the samples under the microscope revealed that, particularly in Holocene specimens, significant organic matter was present and it was therefore decided to repeat this stage twice. The organic matter was removed by adding a 250 µl of alkali buffered 0.3 % H_2O_2 solution to each tube and then heating to 80-90 °C. Samples were subjected to the oxidative treatment for 10 minutes and rapped on the bench top and briefly ultrasonicated to release any gaseous build-up at 5 minutes. Once removed from the water bath the samples were washed with UHQ H_2O multiple times to remove any suspended impurities and traces of reagent.

Step 4: Removal of coarse-grained silicates

As silicates and pyrite were often observed in the samples after crushing, these were transferred onto a glass plate and examined under the microscope using a light coloured background. Unwanted particles were removed and the sample transferred back into a clean microcentifuge tube. Strongly discoloured carbonate was also removed during this step.

Step 5: Dilute acid leach

A dilute acid (~0.001M HNO_3) was used prior to dissolution and analysis. The purpose of this leach was to remove any adsorbed contaminants from the surface of the test fragments (Boyle and Keigwin, 1985; Barker *et al.*, 2003). A 250 µl solution of 0.001M HNO_3 was added to each sample before being ultrasonicated for 30 seconds. The acid was removed from each sample and UHQ H_2O was used to wash the samples. The acid leach was only used very briefly in order to prevent excess dissolution. The acid leach step was repeated 4 times for all of the samples. At the end of this process any liquid was carefully removed from each sample so that they could be stored awaiting dissolution on the day they were run.

Step 6: Dissolution

After 330 µl of 0.075 M HNO_3 was added to each sample, they were ultrasonicated to aid dissolution. As soon as the production of carbon dioxide ceased and particles of carbonate were no longer visible, the samples were shaken to mix. The samples were then centrifuged (5000 rpm for 5 minutes) in batches of 18 to settle any remaining small silicate particles. A 300 µl sub-sample of the solution was immediately transferred to a clean sample tube, leaving any particles to be discarded

in the residual 30 µl. The dissolution acid is left on a sample only as long as necessary to dissolve the foraminifera calcite in the sample. This approach minimises the high risk of contamination by elemental leaching.

Step 7: Dilution

The samples were analysed for Mg/Ca and Sr/Ca on the Varian Vista ICP-AES (Atomic Emission Spectrometry) (e.g. de Villiers *et al.*, 2002). The method requires, for best precision and accuracy, solutions containing known Ca concentrations of typically 60 ppm to minimise the matrix effect and uses ~250 µl solution per analysis. Two runs of each sample were required; an initial concentration determination followed by a second run at optimum (60 ppm) Ca concentration for Mg/Ca and Sr/Ca determinations.

Therefore, a 5 fold dilution was carried out for the initial concentration determination, followed by dilution of the remaining concentrate as required. A 200 µl solution of 0.075M HNO_3 was added to a clean tube followed by the addition of 50 µl of sample to give a 5 fold dilution.

The dilutions required to give optimum Ca for the intensity calibration of Mg/Ca & Sr/Ca ratios were then calculated. The remaining 250 µl of sample concentrates were diluted as calculated and run on the Vista using the intensity ratio calibration at the appropriate Ca concentration. Measurements of a standard solution of Mg/Ca (5.13 mmol/mol) Sr/Ca (2.088 mmol/mol) at 60 ppm were run in parallel with the samples and had an analytical error of <0.015 mmol/mol and <0.004 mmol/mol (1σ), respectively.

2.2.6.1 The omission of a reduction step

A Mn-oxide (or Mn-Fe-Oxide) coating is often observed on foraminiferal shells usually due to Mn^{2+} being mobilized during the breakdown of organic matter deep in the sediment column (Boyle, 1983; Barker *et al.*, 2003). This oxide coating can be removed by reductive cleaning using a buffered solution of hydrous hydrazine (Boyle and Keigwin, 1985). Although this procedure is a vital part of the cleaning process for Cd/Ca and Ba/Ca isotopes (Boyle, 1991; Boyle and Keigwin, 1985; Lea and Boyle, 1991) it is unclear whether such a procedure is needed in the analysis of Mg/Ca. It has been shown that samples cleaned by the Cd/Ca method of Boyle and Keigwin (1985) gave consistently lower values of Mg/Ca (~15%) than those cleaned by the Elderfield and Ganssen (2000) method. However, the reductive step is corrosive to carbonate and causes partial dissolution of the sample which is known to lower the Mg/Ca ratios (Brown and Elderfield, 1996; Rosenthal *et al.*, 2000). Furthermore, Barker *et al.* (2003) suggest that the contribution of Mg from a Mn-oxide coating to the corresponding Mg/Ca ratio of a typical sample is only ~1%. Sr/Ca ratios remain unaffected by the reductive cleaning method.

It was chosen not to carry out the reductive steps on the samples as, particularly during the later stages of the deglaciation, foraminiferal specimens were sparse, smaller and delicate. Excessive dissolution caused by the procedure may have resulted in some of the samples being lost. Importantly, Barker *et al.* (2003) convincingly demonstrate that the silicate removal step has by far the greatest influence on Mg/Ca values (Barker *et al.*, 2003) rather than the reductive cleaning issue.

Chapter 4 describes the results and discussion of the Mg/Ca record. The core used for the study is KNR140/2-39GGC recovered from ~2,985 m water depth on the

BOR. The location of this core is described in more detail in both **section 2.1** and in **Chapter 4**.

2.2.6.2 Possible sources of contamination of the Mg/Ca signal

The removal of silicate contamination is the most important step for the accurate measurement of Mg/Ca ratios; elevated Mg/Ca in association with high Al/Ca (and Fe/Ca) may give an indication of the presence of clay or other authogenic contaminants (Skinner and Elderfield, 2003; Figure 2.6 and 2.7). Only a very slight positive correlation between Al/Ca and Mg/Ca is apparent in this study (Figure 2.6A) and generally Al/Ca values are very low (<0.2 mmol/mol) and are not considered problematic. Further evidence that there is no significant contamination from silicate material is shown by a lack of covariance between down core records of Mg/Ca and Al/Ca (Figure 2.6B). A negative correlation ($y = -0.1114x + 0.5404$, $R^2 = 0.49$) is present between Fe/Ca and Mg/Ca (Figure 2.7A) suggesting that in this instance Fe/Ca is not acting as an indicator of silicate contamination. However, the positive correlation ($y = 0.5127x - 0.0366$, $R^2 = 0.45$) between Fe/Ca and Mn/Ca (Figure 2.7B) suggests the presence of authigenic ferromanganese carbonate overgrowths (Boyle, 1983). The plot of the down core records (Figure 2.7C) reveals a pattern of increasing Mg/Fe ratios throughout the last deglaciation and into the Holocene similar, but not identical, to that seen in the Mg/Ca dataset. This trend is likely to be the result of changing redox conditions within the sediment column, as Mn^{2+} has been mobilised during anoxic breakdown of organic matter deeper in the sediment column. An increase in organic matter delivery to the sediments during colder intervals could be the driving force for most of the primary diagenetic redox-reactions (Haese, 2000).

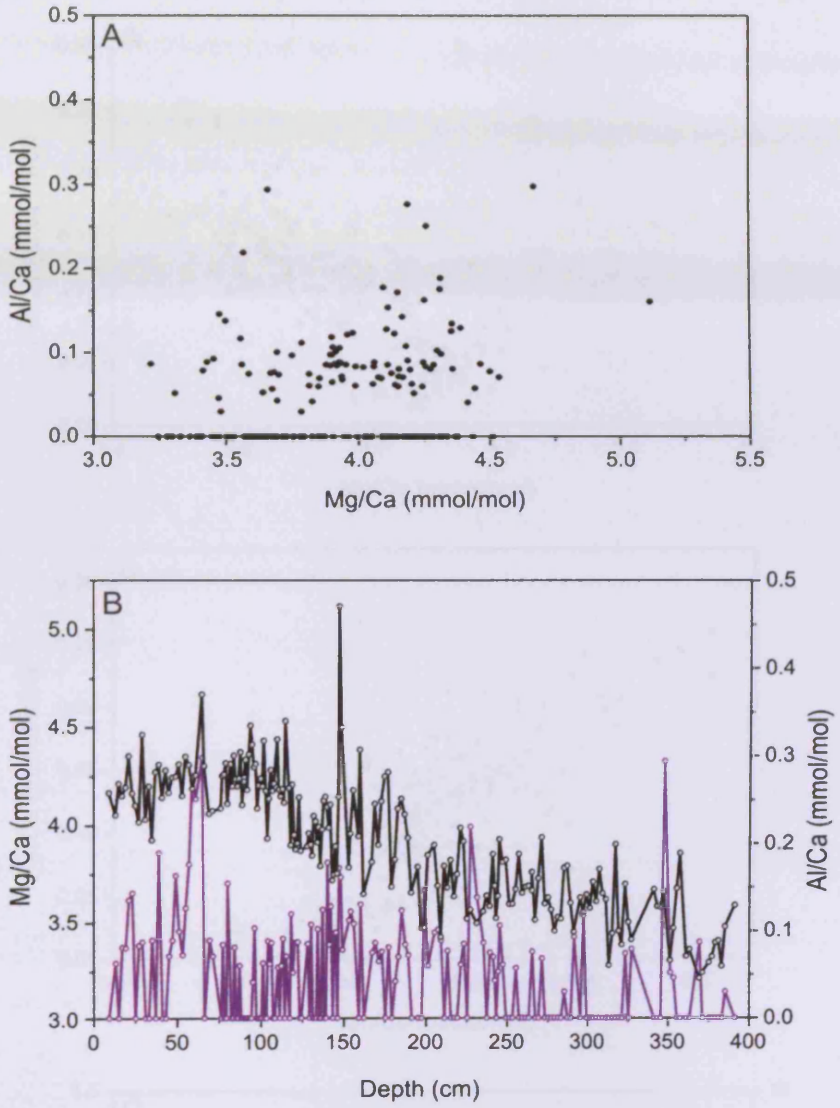

Figure 2.6: (A) Mg/Ca plotted against Al/Ca data for *G. ruber* from core KNR140/2-39GGC during the last deglaciation. The presence of Al is generally below detection for determination on the ICP-AES and is represented by an arbitrary value of zero on the graph. (B) Down core Mg/Ca (black line) and Al/Ca (purple line) data demonstrating that an efficient clay removal technique was employed.

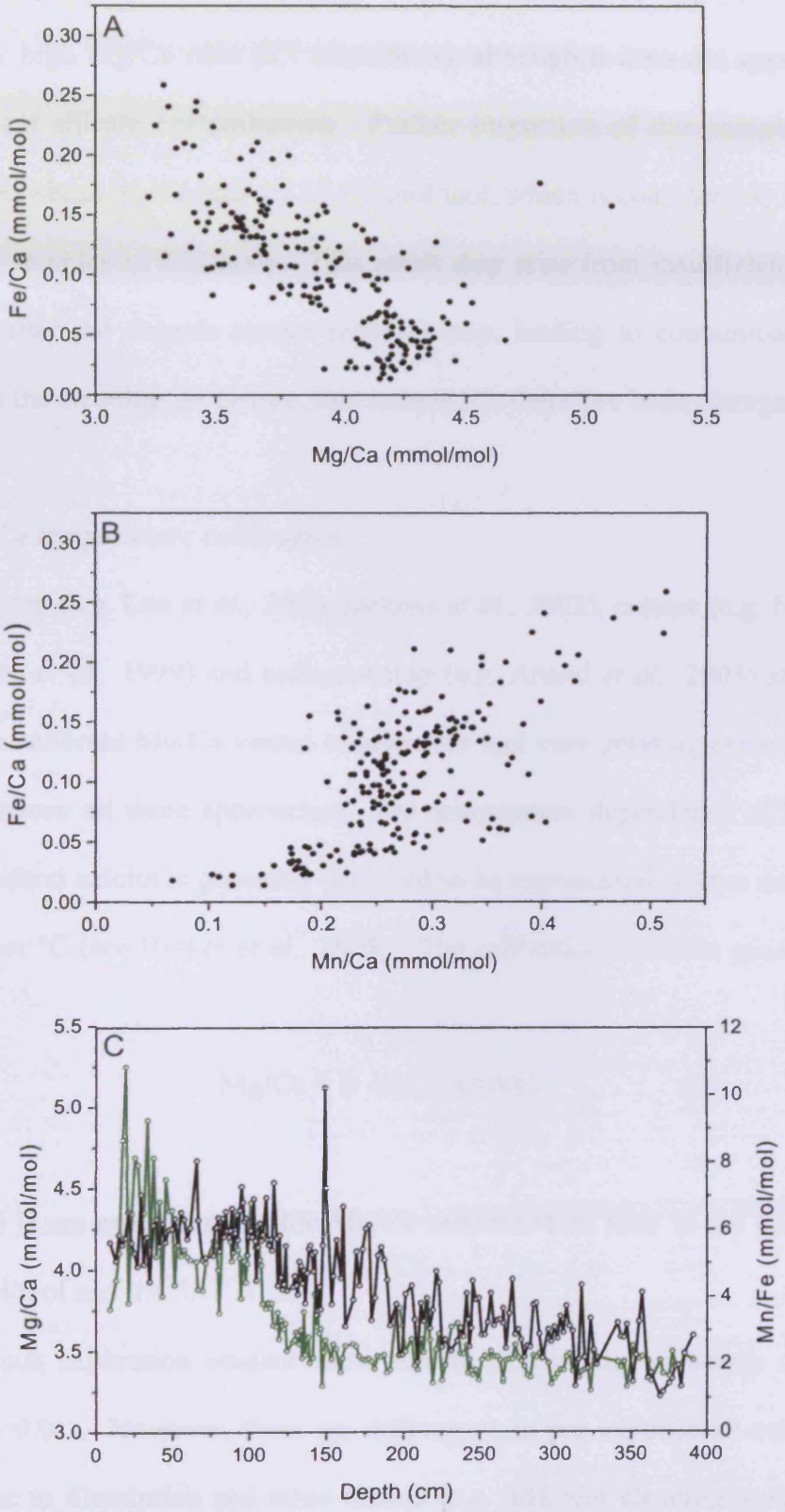

Figure 2.7: (A) Mg/Ca plotted against Fe/Ca, indicating that contamination has not controlled Mg/Ca variability. (B) Mn/Ca plotted against Fe/Ca reveals the presence of Mn-Fe-oxide coatings on the foraminifera. (C) Down core Mg/Ca (black line) and Mn/Fe (green line) data. Mn/Fe ratios increase after ~150 cm due to changes in redox conditions within the sediment column.

A sample at 148-149 cm (Figure 2.6 B and 2.7C) appears to have an anomalously high Mg/Ca ratio (5.1 mmol/mol), although it does not appear to have any significant silicate contamination. Further inspection of this sample however, revealed a very high Na/Ca ratio of 11.1 mmol/mol, which is considerably higher than all the other samples in this study. This result may arise from insufficient rinsing of the sample after the organic matter removal step, leading to contamination of the sample from the cleaning procedure, this sample has therefore been disregarded.

2.2.6.3 Mg/Ca temperature calibration

Core top (e.g. Lea *et al.*, 2000; Dekens *et al.*, 2002), culture (e.g. Nürnberg *et al.*, 1996; Lea *et al.*, 1999) and sediment trap (e.g. Anand *et al.*, 2003) studies have been used to calibrate Mg/Ca versus temperature and very good agreement has been achieved between all three approaches. The temperature dependence of Mg uptake into foraminiferal calcite is generally accepted to be exponential, with a sensitivity of about 10% per °C (see Barker *et al.*, 2005). The calibration equation generally takes the form:

$$Mg/Ca = B \exp(A \times SST) \qquad (2)$$

where A and B are constants and the Mg/Ca concentration ratio in the foraminiferal tests in mmol/mol and the SST is in °C.

Previous calibration studies show similar exponential constants (A) within error (0.09 ± 0.01). However, there are differences in pre-exponential constant (B), which are due to dissolution and other factors (e.g. different cleaning methods, inter laboratory differences, etc.). As no previous studies have been undertaken to calibrate the Mg/Ca versus temperature relationship at the BOR or proximal to the site, a range

of previously used calibrations in the North Atlantic have been assessed for suitability (Table 2.2).

Table 2.2: Summary of previously published calibration for single and multiple species

SPECIES	SOURCE	TEMP	EQUATION	REFERENCE
G. ruber (w)	Sed. trap	Annual SST	SST= [Ln (Mg/Ca)-Ln(0.34)]/0.102	Anand *et al.* (2003)
Mixed	Core top	$\delta^{18}O$ derived	SST= [Ln (Mg/Ca)-Ln(0.52)]/0.10	Elderfield and Ganssen (2000)
G. ruber (w)	Core top	Annual SST	SST= [Ln (Mg/Ca)-Ln(0.30)]/0.089	Lea *et al.* (2000)
G. ruber (w)	Core top	Annual SST	SST= {[Ln (Mg/Ca)-Ln(0.38)]/0.09}+ 0.61(depth km)	Dekens *et al.* (2002)

The 6 youngest samples from core KNR140/2-39GGC (< 3 kyr BP) were converted from Mg/Ca ratios into SST using each of the equations in Table 2.2 (Figure 2.8). The Lea *et al.* (2000) and Dekens *et al.* (2002) equations yield temperature estimates of 26.5–30°C for the Holocene which are 1.5–5.5 °C warmer than the present day annual average temperature (~24.5 – 25 °C) at Site 39GGC (Levitus and Boyer, 1994; Curry, unpublished). More worryingly these calibrations would fail to display temperatures lower than the modern day during the early deglaciation (~18 kyr BP) giving temperatures of 24.5-28.5 °C. In contrast, the Elderfield and Ganssen (2000) equation yields SST estimates for the Holocene which are ~2 °C below the present day temperature at the BOR. However, both the Elderfield and Ganssen (2000) and Dekens *et al.* (2002) calibration equations have been used previously at the BOR in studies of the MIS 12/11 transition (Healey and Thunell, 2004) and MIS 3 (Schmidt *et al.*, 2006). On the basis of our observations the calibration of Anand *et al.* (2003) for *G. ruber* (white) lies closest to the present day temperature at the BOR of ~24.5 °C (dashed line, Figure 2.8; Levitus and Boyer, 1994). This calibration was derived from sediment trap data for the size range 250-

350 μm which is larger than the samples used in this study but still appears to provide a good approximation. Although a modern core top calibration was unavailable at this site, the Mg/Ca value of 4.168 ± 0.001 mmol/mol at 9 cm (~1.7 kyr BP) in core KNR140/2-39GGC gives a SST of 24.51 °C ± 0.003 °C. The average precision for all the data is ± 0.005 mmol/mol (~ ± 0.132 °C).

2.2.6.4 Dissolution

One important consideration is the effect of dissolution at Site 39GGC. Several studies have shown that foraminiferal Mg/Ca decreases due to post depositional dissolution under the influence of under-saturated bottom water or pore-water (Brown and Elderfield, 1996; Hastings *et al.*, 1998; Rosenthal *et al.*, 2000), with preferential dissolution of the Mg rich parts of the test, i.e. those formed in warmer waters. Dissolution generally increases with water depth, but can affect cores significantly shallower than the lysocline (Brown and Elderfield, 1996; Lea *et al.*, 2000).

Dekens *et al.* (2002) have included a depth correction to account for the effects of dissolution on cores below 2,800 m (see Table 2.2). Inclusion of this correction in the calibration at the BOR increases the temperature estimates by ~2°C (Figure 2.8) and therefore significantly overestimates the SST at this site. Site 39GGC is only slightly deeper than the 2.8 km boundary where dissolution is thought to have a significant effect and *G. ruber* have been consistently shown to be more resistant to Mg loss due to dissolution than many other species (Dekens *et al.*, 2002; Fehrenbacher *et al.*, 2006). Furthermore, no evidence of dissolution has been found in the Mg/Ca ratios at other subtropical sites in the South Atlantic (Jones *et al.*, 1984) where cores are similarly located above the lysocline.

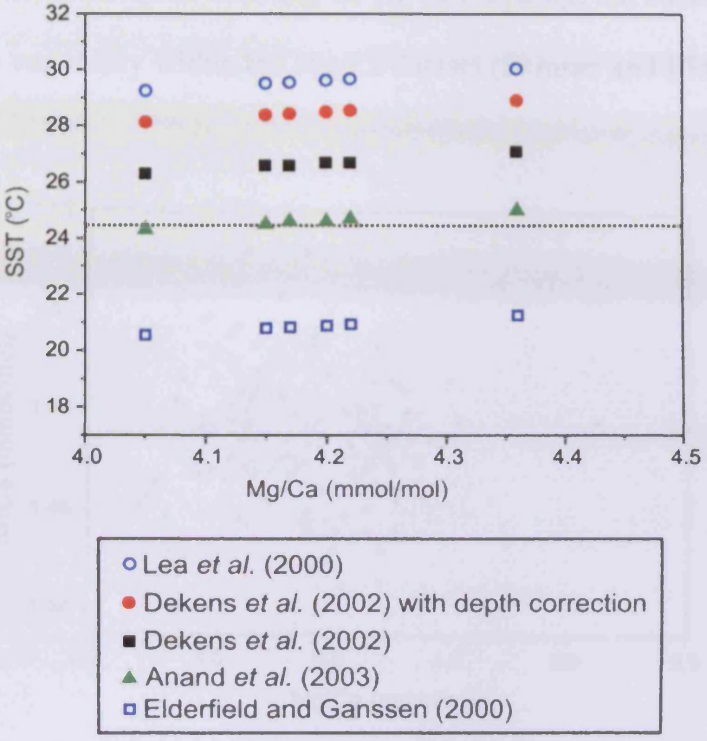

Figure 2.8: Temperature estimates as calculated by the Elderfield and Ganssen (2000), Lea *et al.* (2000), Dekens *et al.* (2002), and Anand *et al.* (2003) equations plotted versus Mg/Ca for Site 39GGC. The Dekens equation was calculated both with (red circle) and without (black square) the depth correction (see **Table 2.2**). The dashed line indicates the modern annual SST in this region of the Atlantic (Levitus and Boyer, 1994; Curry,unpublished).

A possible test of whether dissolution has significantly affected 39GGC is by consideration of the Mg/Ca – Sr/Ca relationship in *G. ruber* shell material. Partial dissolution has been shown to reduce both Mg/Ca and Sr/Ca ratios in planktonic foraminifera (Brown and Elderfield, 1996) and should therefore result in a positive covariance between the two ratios (Skinner and Elderfield, 2003). However, the lack of a positive correlation shown in Figure 2.9 and by regression analysis ($y = -0.0055x + 1.4958$, $R^2 = 0.022$) shows that there is no statistically significant relationship between Mg and Sr in our data, suggesting that partial dissolution has not appreciably affected the primary Mg/Ca record. It does not however rule out a consistent Mg/Ca

offset due to partial dissolution affecting all the data equally, but such an offset would not contribute to variability within the Mg/Ca dataset (Skinner and Elderfield, 2003).

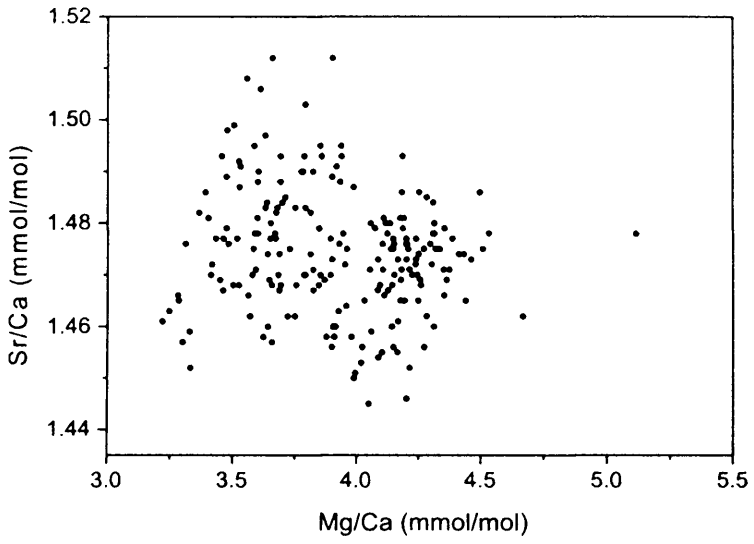

Figure 2.9: Mg/Ca plotted against Sr/Ca for core KNR140/2-39GGC during the last deglaciation, eliminating dissolution as a control on Mg/Ca variability.

2.2.7 Grain size analysis

The wet sieving of the samples described above in **section 2.2.3** allowed a subdivision of the sediment into a 'fine' and 'coarse' fraction and it is the fine fraction (<63 μm) which is the focus of this section. An important aspect of this study is to accurately measure grain size variations in deep ocean sediments and relate this to current speed at the time of deposition in order to reconstruct past ocean circulation, in particular the strength and position of the DWBC. In recent years the development and application of such physical proxies has been recognised as a key aspect of understanding ocean dynamics.

Most deep sea currents are predominantly only capable of moving sediments below the sand size range (i.e. <63 μm; Masson *et al.*, 2004), with sediment sorting

occurring principally due to resuspension and deposition as a result of aggregate break-up, particle selection according to settling velocity and stress (McCave *et al.*, 1995; McCave and Hall, 2006). The different rates of sediment transport allow sorting to occur, converting originally unsorted sediments into narrower distributions downstream. The controlling variables are the critical erosion stress (τ_e), the critical suspension stress (τ_s) and the critical deposition stress (τ_d). Generally, for a non cohesive material $\tau_d<\tau_e<\tau_s$ (McCave *et al.*, 1995). Early grain size measurements were carried out on the bulk silt fraction, i.e. the 4-63 μm fraction (e.g. Ledbetter, 1986; Johnson *et al.*, 1988; Haskell *et al.*, 1991), but following McCave *et al.* (1995) this size fraction was refined to include only the 10-63 μm fraction, known as the sortable silt (SS). McCave *et al.* (1995) argued that the fine end of the silt fraction (2-10 μm) which is dominated by clay minerals, should also be disregarded as it behaves cohesively because of charge imbalances (Weaver, 1989) and adhesion by van der Waals forces (Russel, 1980). Therefore, these sediments are mainly deposited as aggregates and their disaggregated size (i.e. what is measured) can not be related to the hydrodynamic processes of sorting (Figure 2.10). Particle aggregation below 10 μm often results in a pronounced minimum in size frequency between 8-10 μm (e.g. Chang *et al.*, 2005).

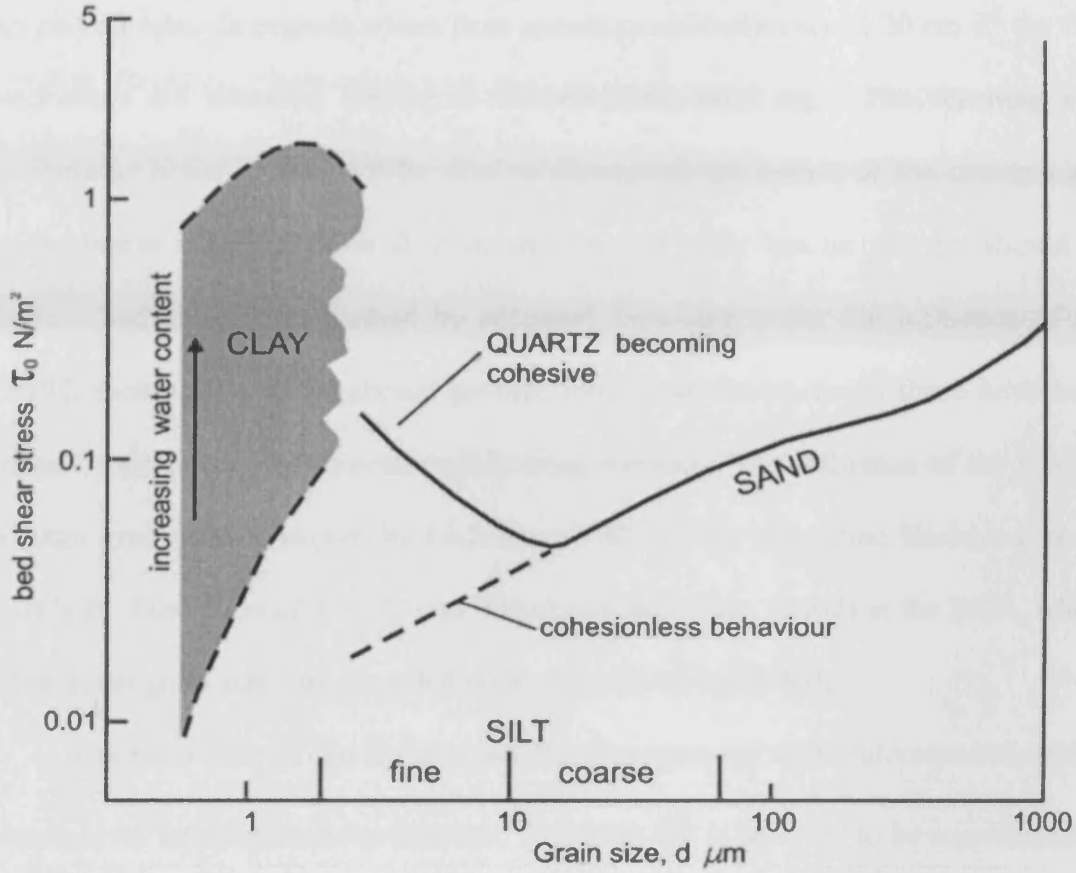

Figure 2.10: Critical erosion flow shear stress versus grain size showing non cohesive behaviour down to about 10 μm, and cohesive behaviour below that with a strong dependence on water content (after McCave *et al.*, 1995).

The mean size of the 'sortable silt' fraction ($\overline{SS}$) has been proposed as the most sensitive indicator of the flow speed of the depositing current and has been related to flow speed experimentally (e.g. HEBBLE (High Energy Benthic Boundary Layer Experiment); Hollister and McCave, 1984; Driscoll *et al.*, 1985; McCave, 1985). It has since been used successfully in numerous palaeocurrent studies (Bianchi and McCave, 1999; Bianchi *et al.*, 2001; Hall and McCave, 2000; Yokokawa and Franz, 2002; Ellison *et al.*, 2006; also see review of McCave and Hall, 2006). Selective deposition is primarily responsible for the sorting of sediment in the SS range, however at speeds above 10-15 cm s^{-1} removal of finer material by winnowing

also plays a role. In regions where flow speeds persistently exceed 20 cm s^{-1} the fine components are removed leaving a (foraminiferal) sand lag. The resulting size distributions however, can not be used to distinguish the nature of the currents and regions where a strong mean flow resides i.e. low eddy kinetic energy, should be chosen. Sediment drifts formed by sediment focussing under the influence of the DWBC, such as the BOR, should provide ideal study locations as these have been formed by persistent, deep, contour-following currents. The influence of the DWBC on mean grain size is shown by Ledbetter (1986) in the Argentine Basin and more recently by Bianchi *et al.* (2001) and Yokokawa and Franz (2002) at the BOR, where higher mean grain sizes are recorded under the path of the DWBC.

The behaviour of the sortable silt fraction must be well understood to enable palaeocurrent interpretations to be made. A higher $\overline{SS}$ is believed to be representative of current sorted sediment that has experienced on average a stronger current than a site with a lower $\overline{SS}$. The $\overline{SS}$ proxy can be used where the source sediment is characterized by a broad range of grain sizes and the distance to the core site is sufficient for a sorted signal to develop. The BOR fits these criteria, as its supply of terrigenous sediment to the area is principally from transport by the DWBC (Heezen *et al.*, 1966) and there are no known significant sediment inputs from IRD or turbidity currents (Bianchi *et al.*, 2001).

2.2.7.1 The influence of source

The assertion that sediment source changes interfere with flow speed interpretations from grain size measurements (e.g. Corliss *et al.*, 1986) is erroneous as the $\overline{SS}$ parameter varies independently of sediment supply in current-sorted and deposited muds. The influence of source is less of a problem for these fine sediments

than it is for sands where an influence of source rock on size and size on mineralogy can be found. Generally sediment is delivered to the deep ocean through gravitational processes (e.g. turbidity currents or debris flows) and has undergone sufficient mixing to eliminate any systematic effects associated with source on short timescales (less than 100 kyr-1 Myr; Embley and Jacobi, 1977; Weaver and Thomson, 1993). Source is only problematic at these short timescales when a sediment with a distinct sorted size spectrum (e.g. loess, beach sand) is delivered to the deep ocean, however as mud (clay plus some silt) comprises over 50% of all the sediment on Earth, few sources would fail to provide some sediment in this range (McCave and Hall, 2006).

A full overview of the theory behind and use of the grain size parameter for inferences of palaeo-flow speed can be found in the review of McCave and Hall (2006).

2.2.7.2 Sortable silt measurement techniques

To determine the particle size distribution in the fine fraction mechanical methods (e.g. sieving and pipette method) would not have been practical because of the small amount of sample available for analysis, the time consuming nature of these techniques and the degree of accuracy required. Instead, two alternative analytical instruments were used: (i) the Coulter Counter Multisizer III, (ii) the Sedigraph 5100.

The Coulter Multisizer III is a resistance pulse counter that measures the voltage change caused by a particle passing through an electric field maintained within an electrolyte (Isoton) which is proportional to its volume. These pulses are related to the spherical particle volume by calibration experiments (Krank and

Milligan, 1979; Milligan and Krank, 1991). The Coulter Multisizer III assumes a grain density equal to quartz and that all particles are spherical to convert to volume.

The Sedigraph 5100 uses a settling technique in accordance with Stokes Law to estimate grain size distributions. Stokes Law states that a particle of equivalent spherical diameter D will settle a distance h in a time t, according to the expression $D = K(h/t)^{0.5}$, where K is the liquid viscosity. The Sedigraph uses the attenuation of an X-ray beam scanning a settling tube to measure the changing concentration of fine sediments settling in the suspension, and therefore, the size distribution of the settling particles. Numerous measurements are made at varying heights over a 3-5 minute period, progressively approaching the top of the suspension, minimising the analytical time required (Coakley and Syvitski, 1991). Similarly to the Coulter Multisizer III the Sedigraph 5100 assumes a grain density equivalent to quartz to convert settling velocity to size. Some samples did experience flocculation problems such as those discussed by Stein (1985), which was attributed to the presence of montmorillonite/smectite in the sample.

Bianchi *et al.* (1999) have shown that both the Coulter Multisizer III and the Sedigraph 5100 are capable of producing both precise and accurate measurements of the $\overline{SS}$ and weight %, with an analytical precision of ~1-6% when $\overline{SS}$ concentrations are >5% of the total sample. The $\overline{SS}$ concentrations in this study occasionally fall below 5% and the associated error estimates on the Sedigraph analyses increase significantly (Bianchi *et al.*, 1999). Bianchi *et al.* (1999) show that the Coulter Counter provides a viable alternative to the Sedigraph particularly where $\overline{SS}$ concentrations are low. Since the Coulter Counter is as accurate as the Sedigraph at low SS component concentrations but, significantly, more precise, it is used to estimate the $\overline{SS}$ in the following studies. The principal drawback of the Coulter

Counter is its relatively narrow sensing zone that disregards particles outside a given size window (depending on the size of the aperture employed for the analyses, e.g. 2.80-70 μm using an aperture of 140 μm) when compared to the Sedigraph (0-63 μm). Therefore, the Sedigraph is used to obtain a measure of the SS% and the ratio of silt/clay, which cannot be obtained from the Coulter Counter as all of the clay fraction (sedimentologically the boundary between clay and silt lies at 2 μm) is below the detection window.

2.2.7.3 Carbonate carbon determinations

Indirect estimates of the biogenic carbonate content of the samples were made following the thermal method described in King *et al.* (1998, lab F), which aims to separate organic carbon from inorganic carbon by selecting a temperature for combustion at which organic carbon is totally converted to carbon dioxide while carbonate is completely stable. The method then involves determination of carbonate carbon by instrumental CHN analysis. A similar procedure to that described in Bianchi *et al.* (2001) was utilised, with the analyses conducted on the <63 μm (fine) fraction rather than the bulk sediment allowing determination of the weight of sediment required for the sedimentological measurements of the $\overline{SS}$, which were undertaken on a carbonate free basis (equations 2 and 3). When the coarse fraction abundance is low, as is the case for cores from the BOR, Bianchi *et al.* (2001) have already demonstrated that the carbonate record derived from the fine fraction is deemed similar to the bulk carbonate record.

The steps involved in this process are as follows:

1) A 7-10 mg sub-sample of dry, homogenised sediment was weighed using a Mettler MT5 balance and placed in a silver capsule.
2) The capsules were left open and batches of weighed samples were placed in a furnace at a temperature of 400°C for 3 hours in order to remove the organic carbon by combustion (King *et al.*, 1998).
3) Once cooled the capsules were closed and stored in a dessicator until analysed.
4) Indirect estimates of the carbonate content of the samples were obtained using a Perkin Elmer 2400 elemental CHN analyzer to measure the inorganic carbon content. The machine was calibrated before each batch of samples was run using standard additions of acetanilide ($CH_3CONHC_5H_6$) of the widest possible sample weights in order to achieve the most reliable correlation line.

Carbonate weight percentage (wt%) estimates were then calculated from the inorganic carbon data assuming that the remainder of the sample was carbonate carbon after the removal of the organic carbon.

Carbonate weight percent = (Carbon content x 100)/12 (3)

Min mass required for SS work = (100/(100-previous equation result)) × 2.5 (4)

2.2.7.4 Carbonate and Silica Removal

The $\overline{SS}$ used to infer flow speed is generally derived from only the terrigenous fraction because biogenic material often carries specific size modes characteristic of the species involved and confuses the signal by adding noise.

Appropriate sub-samples of the fine fraction were weighed out following the discussion in **section 2.2.7.3** and decarbonised with two room temperature acid

digestions using 2M acetic acid. Each acid digestion lasted 24 hours and most of the liquid solution was removed when all the sediment had settled and rinsed twice with deionised water. Reliable analysis of the silt fraction requires the removal of not only the biogenic carbonate but also the biogenic opal when this exceeds 5% of the coarse sediment fraction (McCave *et al.*, 1995). Visual inspection of the coarse fraction revealed that the majority of samples in **Chapter 3 and 5** consisted of >5% of siliceous material and therefore it was judged necessary to use the desilication method. For the samples in **Chapter 6** it was not judged necessary to use the desilication method as the siliceous material in the samples was deemed negligible. Desilication was carried out using a 2M solution of Sodium Carbonate (Na_2CO_3) mixed with the sediment and heated in a water bath at 85 °C for 5 hours. The samples were further stirred every two hours in order to re-suspend the sediment. Samples were then rinsed twice with deionised water and transferred to 60 ml bottles, filled to the neck with 0.2 % calgon solution and placed on the carousel.

Samples were sonified for 1 minute and vigorously shaken immediately before analysis. This homogenised sample was sub-sampled using a 300 µl pipette for analysis on the Coulter Counter and diluted with a particle-free electrolyte (Isoton) to concentrations <5 mg L^{-1} in order to minimize coincidence in the aperture (Wales and Wilson, 1961, 1962; Bianchi *et al.*, 1999) and run to a preset particle count of 70,000. A 140 µm aperture was used, allowing a data window of 2.80-70 µm. The data are expressed as the diameter of a sphere with the same volume as the measured particle (volume equivalent spherical diameter, ESD). Following the Coulter Counter analysis, samples were once again homogenised on a rotating carousel for 24hr and sonified for 1 minute immediately before analysis on the Sedigraph. Samples were

run on the Sedigraph at a constant temperature of 35 °C with a 1.54-63 μm analysis range, therefore covering both the SS range and the silt/clay transition at 2 μm.

Chapter 3: Time-slice reconstruction of deepwater circulation on the Blake Outer Ridge in the western subtropical North Atlantic: Holocene, Last Glacial Maximum and Younger Dryas[1]

Abstract

Three depth transects containing a total of thirty three sediment cores were investigated along the Blake Outer Ridge in the western subtropical North Atlantic. Sortable silt mean ($\overline{SS}$) grain size, stable isotope and calcium carbonate records were used to assess the position and intensity of the Deep Western Boundary Current (DWBC) during the Holocene, the Last Glacial Maximum (LGM) and the Younger Dryas (YD) intervals. The Holocene reconstruction is consistent with modern physical and chemical hydrographic measurements in the area suggesting a deep position for the fast flowing core of the DWBC (3,000-4,000 m, deepening to ~4,500 m water depth on the ridge flanks) and a water column dominated by North Atlantic Deep Water. The LGM and YD reconstructions show that a comparable hydrographic regime was present during both these intervals suggesting that the mode of circulation was similar, but appreciably different to the Holocene reconstruction. The DWBC during these intervals is suggested to have shoaled above 2,500 m water depth, consistent with nutrient depleted Glacial North Atlantic Intermediate Water formation with an increasing influence of Southern Source Water (SSW) below. Below 4,000 m water depth, $\overline{SS}$ results hint at increased SSW flow vigour during both the LGM and YD with higher flow speeds than during the Holocene. This study provides a framework for aiding the interpretation of time-series records of palaeocurrent flow speed changes in the region of the DWBC.

[1]Submitted to *Geochemistry Geophysics and Geosystems* as
Evans H. K., and I. R. Hall, Time-slice reconstruction of deepwater circulation on the Blake Outer Ridge in the western North Atlantic: Holocene, Last Glacial Maximum and Younger Dryas

3.1. Introduction

The Deep Western Boundary Current (DWBC) transports recently ventilated North Atlantic Deep Water (NADW) along the Northeast American continental margin towards the Blake Outer Ridge (BOR), a 700 km long sediment drift in the subtropical Atlantic Ocean (Figure 3.1). For the most part, NADW flow is strongly constrained by bottom topography, with the most recently ventilated waters being located adjacent to the steepest parts of the continental margin (Johns *et al.*, 1997). Deep Western Boundary Current volume transports of between 16-19 Sv have been recorded for water flowing equatorward below a potential temperature of 6°C at the BOR (Stahr and Sanford, 1999) with current speeds of 10-30 cm s^{-1} - both measured and estimated from geostrophic calculations (e.g. Amos *et al.*, 1971; Hogg, 1983; Stahr and Sanford, 1999). It has been suggested from both observations (e.g. Mix and Fairbanks, 1985; Lea and Boyle, 1991; Haskell *et al.*, 1991; Alley *et al.*, 1993) and numerical models (e.g. Manabe and Stouffer, 1997) that changes in the DWBC are indicative of changes in the climate as this current is an important component of the global thermohaline circulation system.

Grain size analysis potentially provides a direct measure of relative circulation intensity and can provide an important palaeoceanographic tool in regions of drift deposits such as the BOR, giving insights into deepwater circulation patterns and complementing information gained from geochemical tracers. As such, it is necessary to understand the relationship between sediment properties and circulation patterns when interpreting sedimentological proxies in the palaeoceanographic record (Haskell and Johnson, 1993).

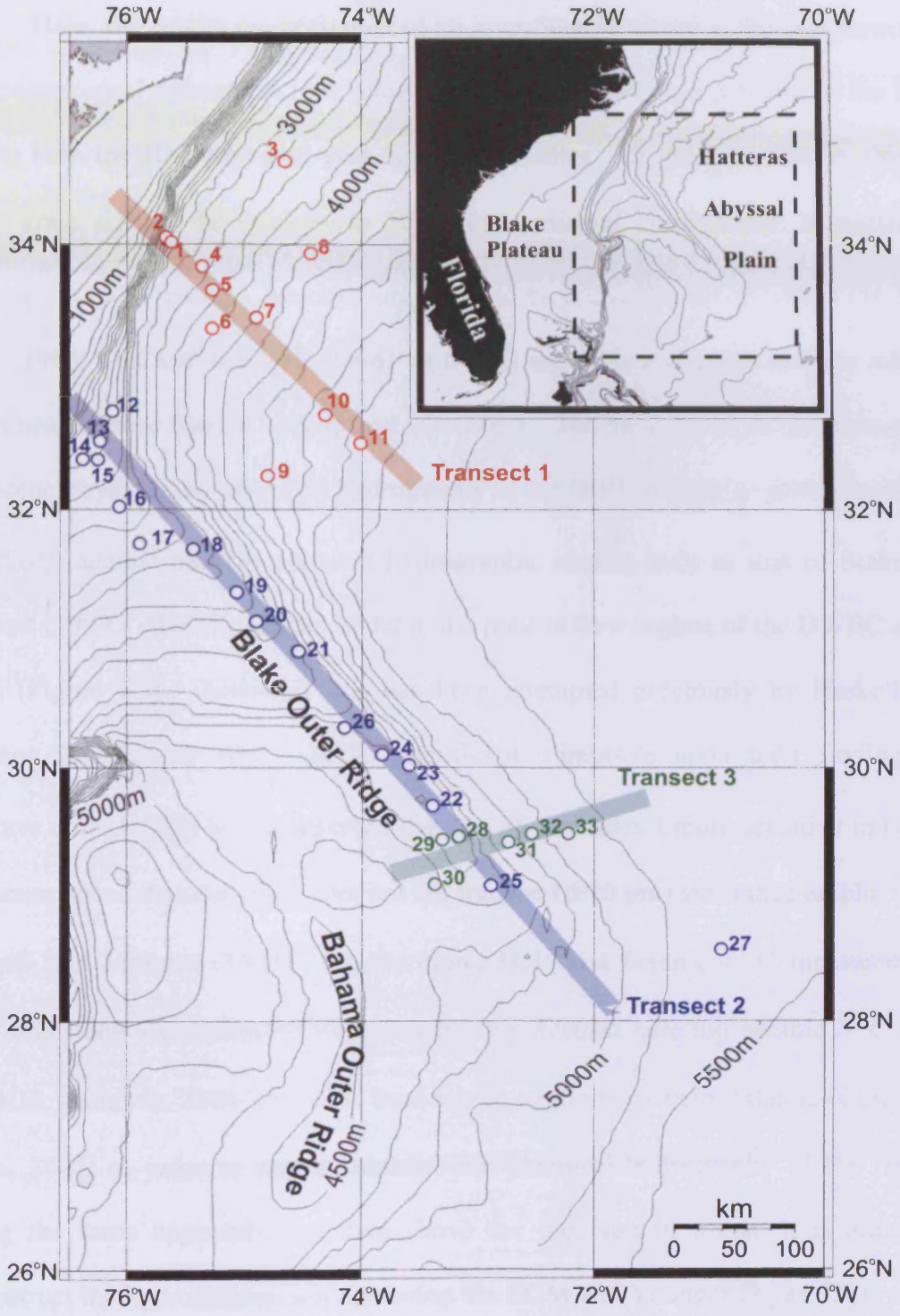

Figure 3.1: Bathymetric map of the study area showing the locations of the three transects used in this study. Transect 1 and its core sites are labelled in red. Transect 2 and its core sites are labelled in blue, while transect 3 and its core sites are labelled in green. The core sites are numbered following the Map ID column in **Table 3.1** (p. 3-8).

Here, the results are presented of an investigation aimed at the comparison of sedimentological parameters in relation to deepwater circulation patterns on the BOR during both the Holocene and past climatic extremes. In order to achieve this the mean grain size of the terrigenous 10-63 μm sediment is employed, hereafter the sortable silt ($\overline{SS}$) fraction, which is suggested to be primarily current sorted (McCave *et al.*, 1995; McCave and Hall, 2006) with high values representing stronger relative mean near-bottom current speeds and *vice versa*. The first aim is to reconstruct the Holocene physical and chemical hydrography at the BOR in order to ground truth the $\overline{SS}$ proxy against modern physical hydrographic studies such as that of Stahr and Sanford (1999), which describes in detail the present flow regime of the DWBC at the BOR (Figure 3.2). Although this has been attempted previously by Haskell and Johnson (1993), our study should significantly improve upon their findings as McCave *et al.* (1995) have suggested that the $\overline{SS}$ provides a more sensitive indicator of current speed than the 'total' detrital silt fraction (6-70 μm) size range employed by Haskell and Johnson (1993). Furthermore, Holocene benthic $\delta^{13}C$ measurements from this study are compared with previously published core top benthic $\delta^{13}C$ from the BOR (*Keigwin*, 2004) and $\delta^{13}C$ transects through the western Atlantic (Curry and Oppo, 2005) in order to firmly establish the chemical hydrography of the region. Using the same approach described above for the modern ocean, it is aimed to reconstruct the hydrographic setting during the LGM and Younger Dryas (YD, where the age control is sufficiently well constrained) when, climatically (e.g. freshwater budgets and atmospheric circulation in the Northern and Southern high latitudes (Lynch-Stieglitz *et al.*, 2007)), conditions should have been most different from the Holocene. A comparison of these three time intervals will enable determination of the

extent of any vertical migrations of the fast flowing core of the DWBC and the benthic front between Northern- and Southern Source Water (NSW/SSW).

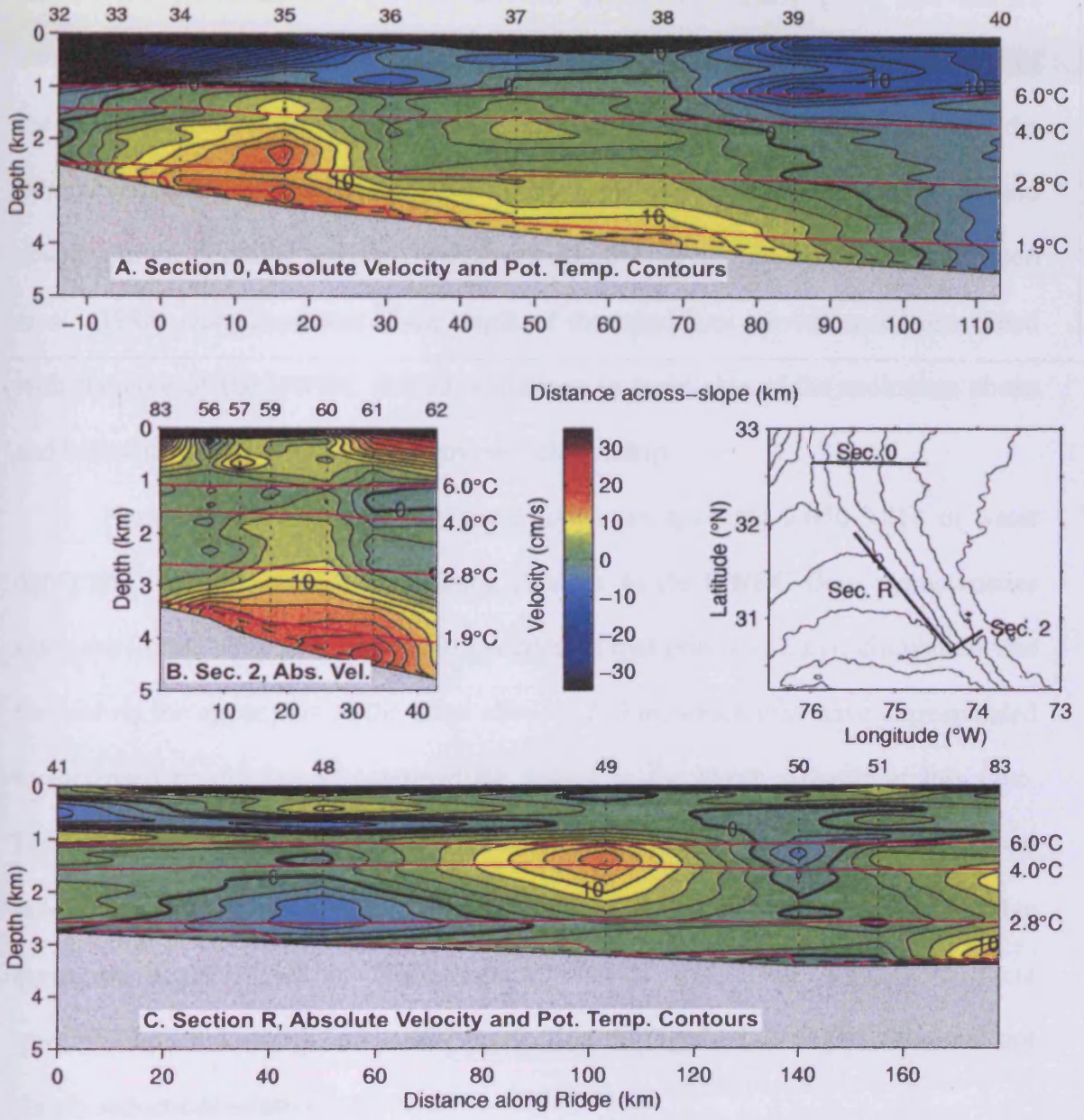

Figure 3.2: Contours of the absolute velocity component normal to the sections and the potential temperature at the Blake Outer Ridge, July 1992. Contour intervals are every 5 cm s^{-1}. The coordinate system is along-stream with positive flow equatorward. Potential temperature contours that divide transport categories are labelled to the right of each panel. The height of the bottom mixed layer is indicated by the dashed line near the bottom. Panel (A) is Section 0, (B) is Section 2, and (C) is Section R. A map clarifying section locations is also shown (adapted from Stahr and Sanford, 1999).

3.1.1 Past palaeocurrent reconstructions from the BOR

Several investigations have utilised sedimentary grain size measurements at the BOR with the intention of reconstructing the strength and flow characteristics of the DWBC on millennial- to Milankovitch timescales. Early grain size studies attempted to reconstruct the palaeocurrent intensity of the DWBC along the crest of the BOR (Johnson *et al.*, 1988), where variations in grain size at one location on the ridge crest could be a response to both fluctuations in the strength of the DWBC and changes in the depth of the fast flowing core (Ledbetter and Balsam, 1985). Johnson *et al.* (1988) recognised that if the depth of the maximum current speed associated with the core of the DWBC shifted, variations in grain size of the sediments above and below the core should have an inverse relationship.

Haskell *et al.* (1991) investigated four sites spanning 2,650-3,818 m water depth and concentrated on determining changes in the DWBC flow characteristics since the LGM. Haskell *et al.* (1991) suggested that prior to 12 kyr, circulation was focused on the upper part of the ridge above 2,700 m, which may have corresponded to increased production of intermediate waters in the North Atlantic at this time. Furthermore, opposing trends in the shallow and deep cores suggest that two independent circulation patterns were in operation at the top and bottom of the ridge during the deglacial period. The results of Haskell *et al.* (1991) suggest that there were absolute reductions in NADW production during the last deglaciation and not simply reductions relative to SSW.

The first attempt at reconciling the modern hydrography at the BOR with grain size measurements from core top samples was made by Haskell and Johnson (1993). This study, using the mean size of the detrital silt fraction (6-63μm), suggested that modern sediment texture and composition on the flanks of the BOR was influenced by

the DWBC, but proximity to the continental slope and distance from the upstream sediment source areas dominated the grain size signal down the crest of the ridge. There was no direct indication of DWBC influence recorded in the sediment properties on the crest of the ridge, even where the DWBC fast flowing core crosses the ridge above 4,200 m water depth, which Haskell and Johnson (1993) use as evidence to suggest that the DWBC crossed the ridge crest in an oblique manner rather than as a discrete jet closely following the bathymetric contours.

Several recent palaeocurrent studies followed Ocean Drilling Program (ODP) Leg 172. Bianchi *et al.* (2001) used ODP Sites 1060 (3,481 m water depth) and 1062 (4,763 m water depth) from Leg 172 to reconstruct both the physical and hydrographic conditions during marine isotope stage (MIS) 6-5d (~130-110 kyr). A combination of sedimentological parameters i.e. the $\overline{SS}$, and benthic $\delta^{13}C$ were used to reconstruct the intensity and position of the fast flowing core of the DWBC during MIS 5e (~4,000 m) and suggested that changes in the lower (L)NADW/SSW ratio were accompanied by vertical migrations of the DWBC flow axis, which appeared to shoal in response to a reduced presence of LNADW. Yokokawa and Franz (2002) focused on the time interval from 350-250 kyr BP (MIS 10.2-8.3) at Sites 1055-1062 (1,800 m to 4,760 m water depths), using a combination of grain size measurements and magnetic properties (anisotropy of the magnetic susceptibility). They suggest that the core of the DWBC was located at ~2,200 m water depth during the glacial periods (MIS 10.2 and 8.4-8.3), deepening to >3,000 m water depth during the warm intervals (MIS 9.3 and 8.5). Finally, sedimentological properties have also been combined with stable isotope data during the MIS 12-10 interval at Site 1061 (4,047 m water depth; (Hall and Becker, 2007)) revealing that the DWBC had three modes of operation during this interval. Glacial MIS 12 was associated with reduced LNADW

production, increased advection of SSW and a shallow fast flowing DWBC. During peak interglacial conditions (MIS 11.3) there was evidence for a deep flowing DWBC and an increased production of LNADW, while a variable intensity and position for the DWBC is recorded after 397 kyr BP.

3.2 Materials and methods

Thirty three sediment cores were sampled along three transects at the BOR in order to study how circulation patterns on different parts of the ridge affect surface sediment properties (Figure 3.1 and Table 3.1). The cores were collated from several different research cruises. Cores recovered during *RV Knorr* (KNR) and *RV Atlantis* II (AII) cruises were sampled at the repository at Woods Hole Oceanographic Institution (WHOI), USA, while those cores from the *RV Vema* (VM) and *RV Robert Conrad* (RC) cruises were sampled at Lamont-Doherty Earth Observatory (LDEO), at Columbia University, USA. The first transect (hereafter T1) was positioned across the mouth of the ridge with the purpose of capturing the entire width of the DWBC as it enters the region of the BOR. This transect is located close to 'Section 0' of Stahr and Sanford (1999) (Figure 3.2A). The second location (hereafter T2) forms a depth transect running along the crest of the ridge, similar to the ridge crest transect of Haskell and Johnson (1993) and hydrographic 'Section R' of Stahr and Sanford (1999) (Figure 3.2C). Previous studies utilising sediment cores from the crest of the BOR (e.g. Haskell and Johnson, 1993; Bianchi *et al.*, 2001; Keigwin and Schlegel, 2002; Keigwin, 2004) have highlighted the presence of high sedimentation rates (up to ~60 cm kyr^{-1}) providing an opportunity to obtain millennial-scale, or better, resolution records suggesting the potential for further palaeoceanographic work, including investigations of rapid climate change. Transect 3 (hereafter T3) is a small

Table 3.1: Locations, water depths and sampling intervals for Blake Outer Ridge cores.

	Store	Core ID	Lat.	Long.	Depth (m)	Holo (cm)	Glacial (LGM) (cm)	YD (cm)	Stratigraphy	Ref	Map ID
Tr. 1	WHOI	AII72-21PC	34.1	-75.7	2202	0-15	120-160	-	MS/δ18O	a	1
	WHOI	AII72-22PC	34.0	-75.6	2942	0-15	70-100	-	MS/δ18O	a	2
	LDEO	VM30-5	34.6	-74.7	3203	0-25	-	-	MS/δ18O	a	3
	WHOI	AII72-23PC	33.8	-75.3	3204	0-25	60-90	-	MS/δ18O	a	4
	LDEO	RC9-4	33.4	-75.3	3552	0-15	130-170	-	MS/δ18O	a	5
	WHOI	AII72-24PC	33.4	-74.9	3824	0-15	70-120	-	MS/δ18O	a	6
	LDEO	VM26-175	33.9	-74.4	3995	0-25	120-170	-	MS/δ18O	a	7
	LDEO	RC7-2	32.3	-74.8	4398	0-10	240-260	-	MS/δ18O	a	8
	LDEO	VM30-7	32.7	-74.4	4702	0-10	-	-	MS/δ18O	a	9
	LDEO	RC1-10	32.5	-74.0	4892	0-10	110-130	-	MS/δ18O	a	10
	WHOI	AII72-16PC	32.5	-73.5	5058	-	120-160	-	MS/δ18O	a	11
Tr. 2	WHOI	KNR140/2-50GGC	32.7	-76.2	2155	0-170	240-280	180-200	δ18O/BFA	b	12
	WHOI	KNR140/2-66GGC	32.5	-76.3	2155	0-50	120-160	77-87	δ18O/BFA	b	13
	WHOI	KNR140/2-1JPC	32.3	-76.4	2243	0-73	130-165	91-96	δ18O/BFA	b	14
	WHOI	KNR140/2-46GGC	32.3	-76.3	2320	0-78	218-238	-	δ18OBFA	b	15
	WHOI	KNR140/2-43GGC	32.0	-76.1	2590	0-35	167-215	59-67	δ18OBFA	b	16
	WHOI	KNR140/2-42GGC	31.7	-75.9	2710	0-10	130-170	-	MS/δ18O	a	17
	WHOI	KNR140/2-39GGC	31.7	-75.4	2975	0-100	300-450	125-130	$\Delta^{14}C$ /δ18O	c	18
	WHOI	KNR140/2-36JPC	31.4	-75.1	3007	0-15	200-300	-	MS/δ18O	a	19
	WHOI	KNR140/2-33JPC	31.1	-74.9	3315	-	200-300	-	MS/δ18O	a	20
	WHOI	KNR140/2-31GGC	30.9	-74.5	3410	0-50	300-400	105-125	δ18O/BFA	b	21
	WHOI	KNR140/2-26GGC	29.7	-73.4	3845	0-40	320-400	-	δ18O/BFA	b	22
	WHOI	KNR140/2-29GGC	30.0	-73.6	3978	0-30	400-450	39-63	δ18O/BFA	b	23
	WHOI	KNR140/2-28GGC	30.1	-73.8	4211	0-24	260-360	53-60	δ18O/BFA	b	24
	WHOI	KNR140/2-12JPC	29.1	-72.9	4250	-	200-270	73-85	δ18O/BFA	b	25
	LDEO	RC16-7	30.3	-74.1	4893	-	50-70	-	MS/δ18O	a	26
	LDEO	VM25-2	28.6	-71.1	5409	0-10	50-75	-	MS/δ18O	a	27
Tr. 3	WHOI	KNR140/2-25PC	29.6	-73.2	3865	0-10	25-40	-	MS/δ18O	a	28
	LDEO	RC9-10	29.4	-73.3	4277	0-10	30-60	-	MS/δ18O	a	29
	LDEO	VM22-6	29.1	-73.3	4499	0-15	50-80	-	MS/δ18O	a	30
	LDEO	RC9-13	29.4	-72.7	4735	0-10	80-90	-	MS/δ18O	a	31
	LDEO	RC9-12	29.5	-72.5	4958	0-10	40-70	-	MS/δ18O	a	32
	LDEO	RC9-11	29.5	-72.2	5212	-	20-40	-	MS/δ18O	a	33

The stratigraphy column gives an indication of the methods used to locate the time interval of interest, where, MS magnetic susceptibility measurements, $\delta^{18}O$ planktonic oxygen isotope stratigraphy, BFA benthic foraminifera abundance peaks, ^{14}C existing AMS radiocarbon dates. Reference a this study, b Keigwin (2004) and c Keigwin and Schlegel (2002). The location of the cores can be found on **Figure 3.1** using the MAP ID in the final column of the table

transect traversing the northeast side of the BOR and is at a similar location to the across-ridge transect of Haskell and Johnson (1993) and hydrographic 'Section 2' of Stahr and Sanford (1999) (Figure 3.2B). The northeast side of the BOR was chosen as previous studies have shown the presence of a strong DWBC with no indication of a recirculation gyre (Haskell and Johnson, 1993; Johns *et al.*, 1997), which can prove difficult to separate from the equatorward flow of the DWBC where both are present (McCartney, 1993). The nearest reported gyre is to the south in the Blake Abyssal Basin at 26.5°N (Lee *et al.*, 1996; Johns *et al.*, 1997; Leaman and Vertes, 1996).

All the core sites were investigated (core log records, cruise reports and previous publications) to check, where possible, that the sediment had not been disturbed by recent slumps or debris flows. The presence of specimens of *Globorotalia menardii*, a warm water indicator, in LGM sediments was noted. Keigwin (2004) has suggested that instances of this species in LGM sediments at the BOR may indicate downslope transport, as *G. menardii* were introduced to glacial sediments via sediment transport from interglacial outcrops up-slope.

On average 3-5 sub-samples were taken, where possible, from each core during the Holocene, LGM and YD time intervals in order to obtain an average grain size measurement covering a range of water depths for each time period under investigation. All of the sediment sub-samples collected were wet sieved through 63 μm sieves and both the 'fine' and 'coarse' fractions were preserved, dried and

weighed following the sample preparation procedures described by *Bianchi et al.* (2001) and in **Chapter 2**. Grain size measurements on the SS fraction were initially carried out on the Coulter Counter Multisizer III, in order to obtain a measure of the $\overline{SS}$. Additional grain size measurements were then undertaken using the Sedigraph 5100 in order to determine the sortable silt abundance (SS%) and silt/clay ratio. The SS% was found to vary in the range of 5-15% enabling the determination of the $\overline{SS}$ with an analytical error of 2-3% (Bianchi *et al.*, 1999).

Stable isotope ($\delta^{18}O$ and $\delta^{13}C$) analyses were carried out on both planktonic and benthic foraminifera in order to reconstruct water mass properties and provide additional chronological support (see below). For planktonic isotopic measurements ~30 specimens of the species *Globigerinoides ruber* (white) were picked from the 150-250 μm size fraction. Additionally, when abundant benthic foraminifera were available, 2-3 specimens of *Cibicidoides spp.* were selected from the >150 μm fraction for analysis. In contrast to the $\overline{SS}$ record which is continuous since terrigenous silts are ubiquitous, the benthic foraminiferal stable isotope records are patchy as suitable benthic foraminifera are not found in all samples due to the small sample size available, dissolution of the calcareous shells (particularly at the deeper sites below ~3,000 m water depth) and dilution due to high sedimentation rates (particularly along the ridge crest).

3.3 Chronology

Several techniques were used to develop preliminary chronologies for each of the core sites. Previously published planktonic isotope stratigraphies and ^{14}C AMS dates (Keigwin and Schlegel, 2002; Keigwin, 2004) were used to constrain the

location and duration of the Holocene (last 10 kyr BP), LGM (interval centred on 21 kyr BP with a duration of a few millennia (Lynch-Stieglitz *et al.*, 2007)) and YD (13-11.5 kyr BP) in the KNR cores. Additionally, benthic foraminifera abundance peaks have been previously observed in many instances (but not exclusively) to correspond with maxima in the planktonic $\delta^{18}O$ record consistent with YD cooling and to a lesser extent the LGM at the BOR (Keigwin and Schlegel, 2002; Keigwin, 2004; Figure 3.3) providing a further stratigraphic marker. The cause of these benthic foraminifera abundance peaks is unclear, although Keigwin (2004) speculated that temporal changes in surface ocean productivity documented elsewhere in the ocean may be related (e.g. Zahn *et al.*, 1986; Loubere, 1991, 2000; Keigwin *et al.*, 1992).

For the remaining core sites, without existing isotope stratigraphies, only the Holocene and LGM were sampled, as locating the YD proved too speculative. A combination of magnetic susceptibility and colour variations of the sediment were used to locate the Holocene and the LGM in the remaining cores (Figure 3.4). Sediments from the LGM are generally clay-rich and show higher magnetic susceptibility, whereas carbonate-rich sediments dominate in the interglacial periods and show low magnetic susceptibility. Sediments deposited at the BOR at the time of the LGM are condensed and oxidized resulting in a reddish sediment colour, compared with the more reducing, finer, green-brown over-lying Holocene sediments. This colour transition between glacial and interglacial periods is typical of other cores in the region (Keigwin *et al.*, 1998) and can be used to distinguish between cold and warm periods. The colour change from the LGM to the Holocene has been attributed to a possible provenance change in the early Holocene with a reduced influx of material from upstream originating in the Canadian maritime provinces (Heezen *et al.*, 1966; Barranco *et al.*, 1989).

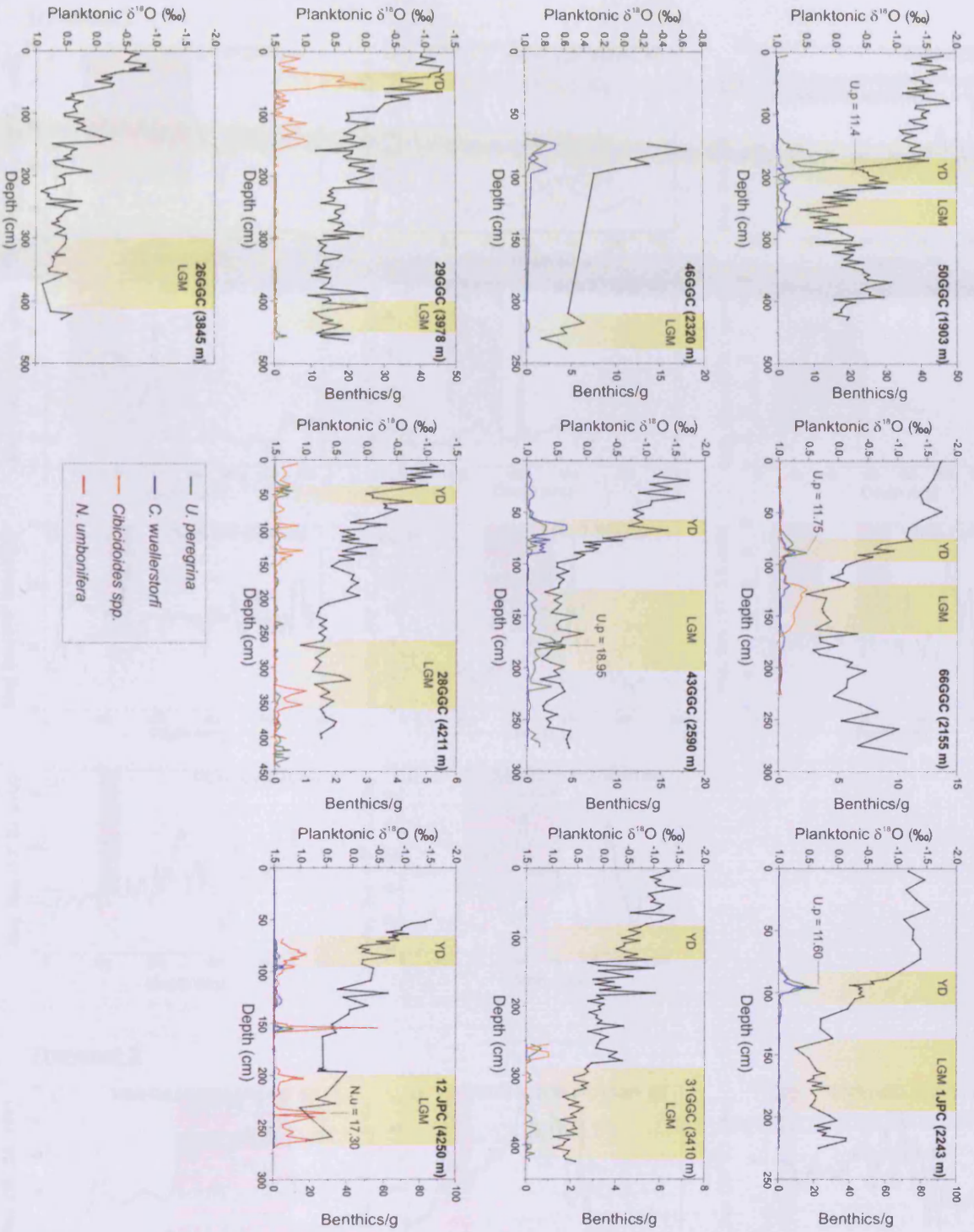

Figure 3.3: Oxygen isotope stratigraphies and benthic foraminifera abundance data (taken from Keigwin, 2004) for transect 2. The $\delta^{18}O$ stratigraphy is based on the surface-dwelling planktonic foraminifera *G. ruber* (black line). Benthic foraminiferal abundance data are as follows: green line, *U. peregrina*; blue line, *C. wuellerstorfi*; orange line, *Cibicidoides spp.*; red line, *N. umbonifera.* The shaded panels mark the probable locations of the Younger Dryas (YD) and the Last glacial Maximum (LGM).

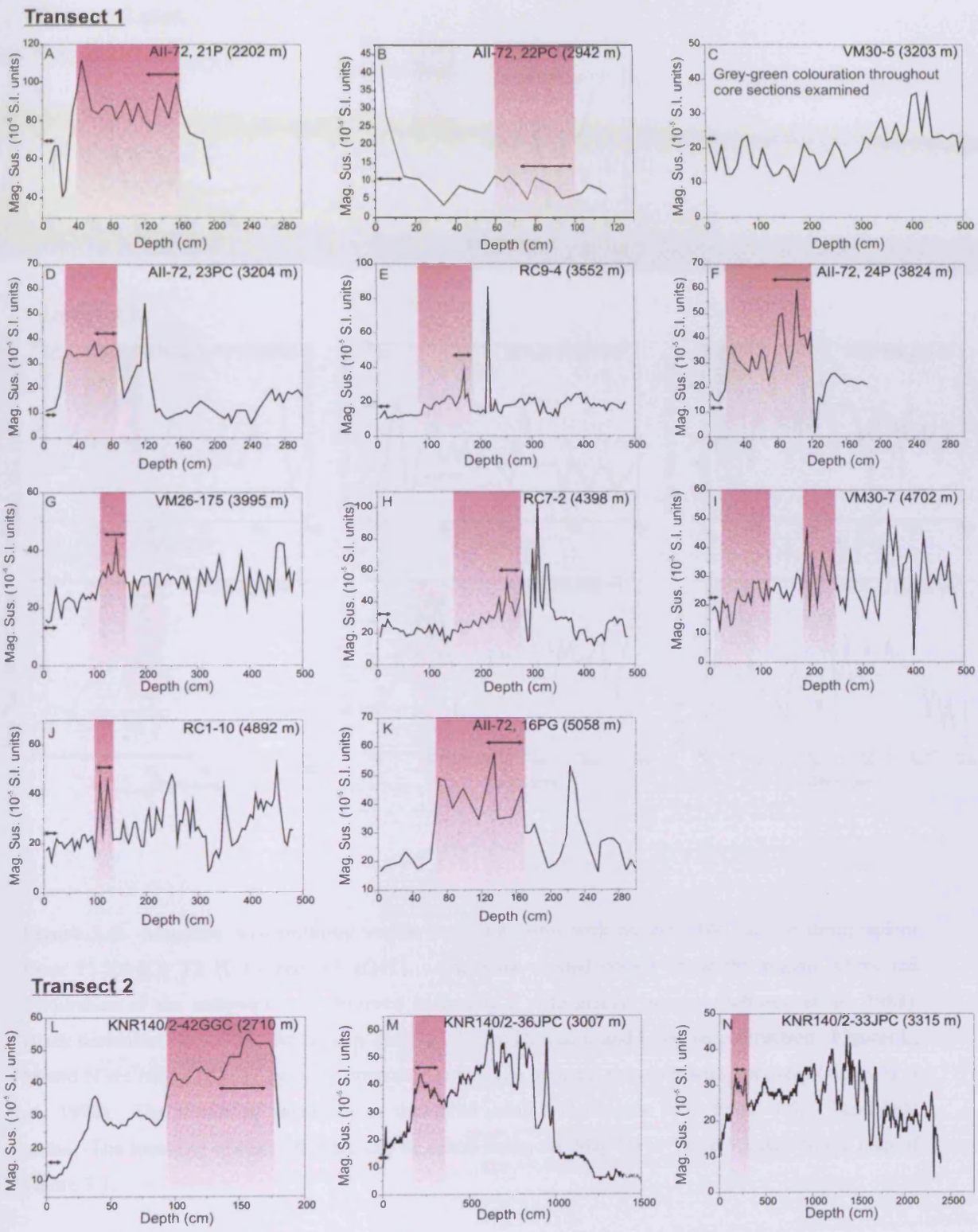

Figure 3.4 (continued below).

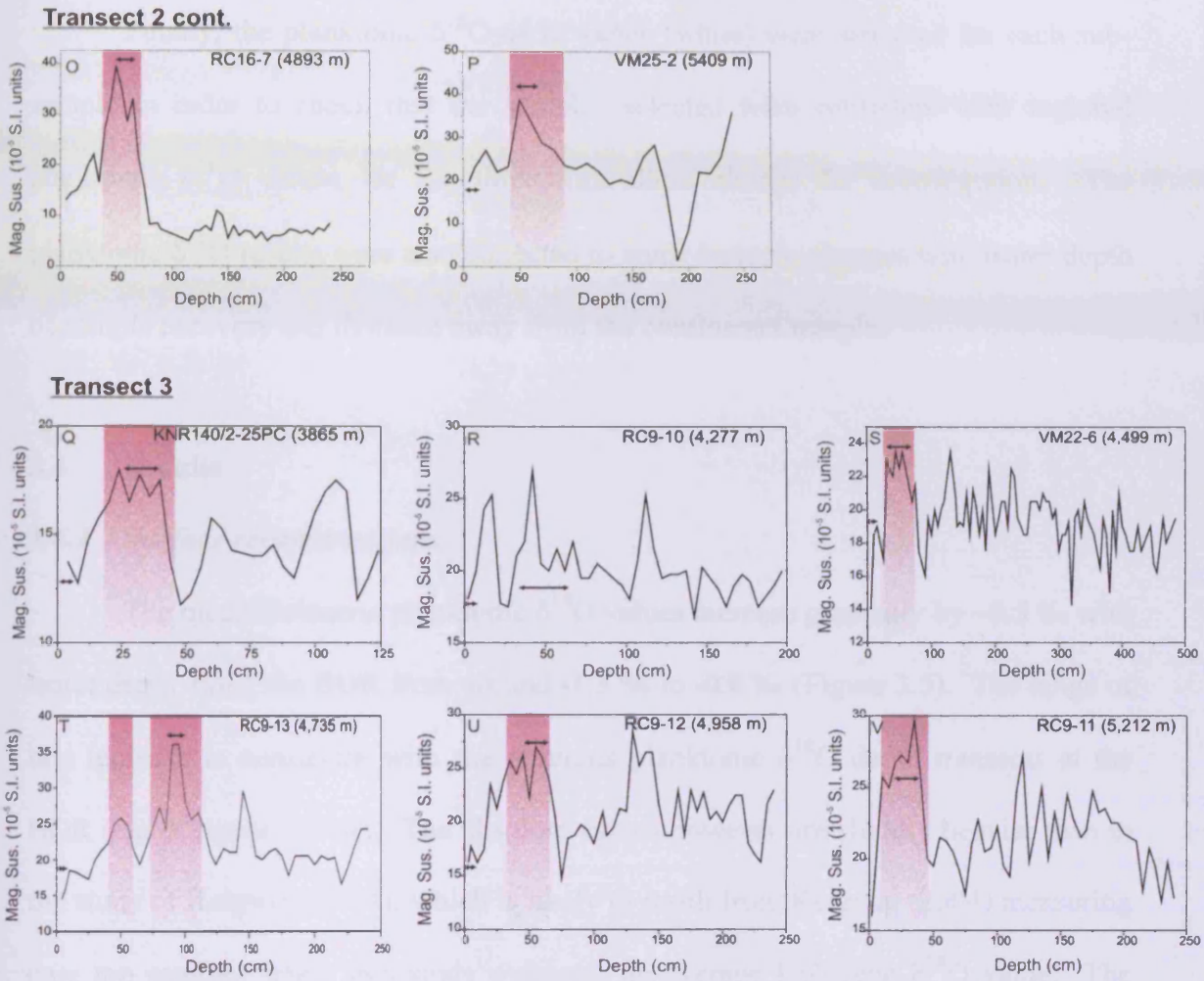

Figure 3.4: Magnetic Susceptibility versus depth for cores with no available isotope stratigraphies from T1 (A-K), T2 (L-P) and T3 (Q-V). The pink shaded panels show the region where red colouration of the sediment was observed indicating a cold glacial interval (Johnson *et al.*, 1988). Black horizontal lines show the regions sampled for the Holocene and LGM reconstruction. Figures L, M and N are magnetic susceptibility measurements made onboard ship following recovery (Keigwin *et al.*, 1998). The remaining figures were measured using a Bartington MS2 fitted with a hand held probe. The locations of the core sites can be found using the Map ID in Table 3.1 and on the map of Figure 3.1.

Finally, the planktonic $\delta^{18}O$ of *G. ruber* (white) were analysed for each sub-sample in order to check that the samples selected were consistent with regional planktonic $\delta^{18}O$ values for the three time-slices chosen for investigation. The planktonic $\delta^{18}O$ results were also collected to study isotopic changes with water depth of sample recovery and distance away from the continental margin.

3.4 Results

3.4.1 Surface reconstructions

The mean Holocene planktonic $\delta^{18}O$ values increase gradually by ~0.5 ‰ with water depth along the BOR from around -1.3 ‰ to -0.8 ‰ (Figure 3.5). The range of this increase is consistent with the previous planktonic $\delta^{18}O$ depth transects at the BOR (e.g. Keigwin, 2004). The absolute values however are slightly heavier than in the study of Keigwin (2004), which is likely to result from Keigwin (2004) measuring core top samples while this study estimates an average Holocene $\delta^{18}O$ value. The mean Holocene $\delta^{18}O$ values at the shallow sites close to the continental margin on the BOR are ~1 ‰ lower than the previously published Bermuda Rise data (Keigwin, 1996; McManus *et al.*, 2004), which is consistent with the 4°C temperature difference between these locations today (Keigwin, 2004). The mean LGM planktonic $\delta^{18}O$ values also show a small increase seaward similar to the Holocene data, but values are typically ~1.8 ‰ heavier than during the Holocene. This is comparable to the ~2 ‰ difference between these time periods suggested by Keigwin (2004). Keigwin (2004) further noted that LGM $\delta^{18}O$ values are similar on the BOR to the Bermuda Rise suggesting that during the LGM the western Sargasso Sea was more uniformly cool than it is today. The mean YD planktonic $\delta^{18}O$ values are intermediate between the

3.4.2 The Deep hydrography

3.4.2.1 Grain size

All three transects during the three time intervals under investigation reveal a changing pattern of $\overline{SS}$ with depth (Figure 3.6). The bars in Figure 3.6 are based on the 1σ standard deviations of the averaged $\overline{SS}$ data for each core site. The Holocene reconstruction shows a region of coarse $\overline{SS}$ at both T1 and T2 between ~3,000 m and 4,000 m water depth, suggesting a region of fast flow speeds at this depth, consistent with modern hydrographic reconstructions of the fast flowing core of the DWBC (e.g. Stahr and Sanford, 1999; Figure 3.6A and 3.6B). It is this coarsening in the $\overline{SS}$ that dominates the grain size signal at T1 suggesting that this transect is relatively unaffected by any proximity effect to the continental margin. At T2 the Holocene $\overline{SS}$ average over the depth range of the present day fast flowing core of the DWBC, although high, has lower $\overline{SS}$ values than at T1 (~16.5 at T2 compared with ~18.5 at T1). This is suggestive of a possible slowing of the DWBC between T1 and T2. An increase in $\overline{SS}$ is also apparent at T2 at shallower depths <2,300 m, consistent with the location of the modern shallow secondary core of the DWBC which is presently (S)LSW-sourced (Johns *et al.*, 1997). As there is only a single data point shallower than 2,300 m water depth at T1 it is unclear as to whether this transect is also influenced by the shallow secondary core of the DWBC. Below 4,000 m water depth, the Holocene $\overline{SS}$ shows a decreasing trend at both T1 and T2 consistent with a decreasing influence of the deep fast flowing core of the DWBC. T1 reaches a minimum value of ~14.25 μm at 4,750 m water depth, while T2 reaches a minimum of 15.25 μm at 4,211 m water depth. The higher value at T2 is likely to be a reflection of the lack of suitable Holocene samples between 4,211 m and 5,400 m

water depth. T3 was designed to study the deepest component of the flow regime on the BOR and is a much shorter transect than T1 and T2, consisting of only 6 data points covering a depth range of 3,865-5,212 m (Figure 3.6C). However, this is sufficient to resolve the main flow characteristics at depth. Similarly to T1 and T2, the Holocene T3 also suggests coarser $\overline{SS}$ values consistent with the position of the fast flowing core of the DWBC, but with coarse values reaching a greater depth of 4,500 m.

The LGM reconstruction suggests that an appreciably different hydrographic setting was present at this time compared with the Holocene and this is further highlighted by the deviation (Holocene-LGM) graphs in the right panel of Figure 3.6. In all 3 transects the ~3,000-4,000 m depth range of the Holocene $\overline{SS}$ maximum shows a minimum in grain size for the LGM, with $\overline{SS}$ values 1.5-2.5 μm finer than during the Holocene. The decrease in $\overline{SS}$ is greater than the 1σ variance on the Holocene and LGM samples suggesting that these data are statistically different from one another. All three transects suggest that below 4,000 m $\overline{SS}$ values increase to higher values than those associated with the Holocene reconstruction, suggesting that faster flow speeds were present below ~4,000 m water depth in the LGM than during the Holocene. The T1 and T2 depth reconstructions further suggest that shallower depths (<2,500 m) also experienced coarser grain sizes during the LGM, with $\overline{SS}$ values reaching 19.35 μm at 2,202 m water depth and 20.29 μm at 2,155 m water depth, respectively (Figure 3.6A and 3.6B), consistent with more vigorous intermediate depth flow speeds during the last glacial than the Holocene.

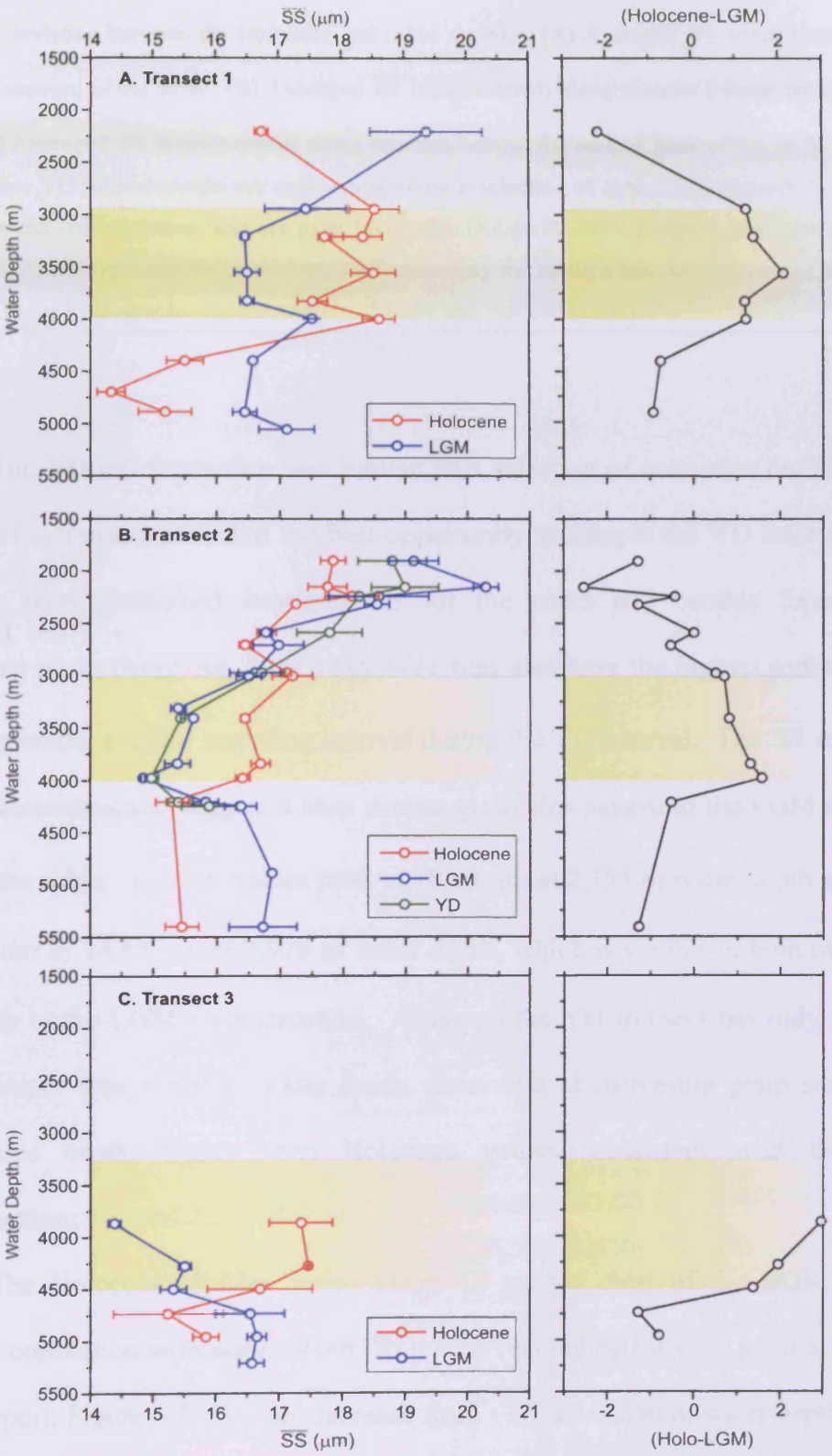

Figure 3.6: The left panel shows the sortable silt mean ($\overline{SS}$) measured on Holocene (red), LGM (blue) and YD (green) samples where available. Each point represents an average value of 3-5 $\overline{SS}$ measurements with horizontal bars showing the 1σ standard deviations at each depth. The right panel

shows the deviation between the Holocene and LGM samples. (A) Averaged $\overline{SS}$ measurements along transect 1 seaward of the BOR. (B) Averaged $\overline{SS}$ measurements along transect 2 down the crest of the BOR. (C) Averaged $\overline{SS}$ measurements along transect 3 down the eastern flank of the BOR. It should be noted that YD measurements are only available on a selection of cores from transect 2, where age constraints and sedimentation rates are most favourable (Keigwin, 2004; Keigwin and Schlegel, 2002). The shaded panels represent the depth range influenced by the modern fast flowing core of the DWBC according to the hydrographic measurements of Stahr and Sanford (1999).

The YD reconstruction was limited to a selection of core sites on T2 (Figure 3.6B). This transect provided the best opportunity to sample the YD interval as not only are there published stratigraphies for the cores and benthic foraminiferal abundance peaks (Keigwin, 2004), but these sites also have the highest sedimentation rates, presenting a larger sampling interval during the YD interval. The $\overline{SS}$ results for the YD reconstruction suggest a very similar grain size pattern to the LGM along the crest of the ridge. The $\overline{SS}$ values peak at 18.99 μm at 2,155 m water depth and reach a minimum of 14.97 μm at 3,978 m water depth, which is similar in both magnitude and depth to the LGM reconstruction. Although the YD transect has only two data points deeper than 4,000 m water depth, these hint at increasing grain size values below this depth, higher than Holocene values, consistent with the LGM reconstruction.

The Holocene silt/clay ratios along T2 on the crest of the BOR, show a negative correlation with water depth ($R^2 = 0.36$ (excluding the data point at 5,409 m water depth); Figure 3.7). Values decrease from ~1.1 at ~2,250 m water depth to ~0.4 at ~4,250 m water depth. These data highlight the previously reported (Haskell and Johnson, 1993) general trend of increasing clay and decreasing silt abundances with water depth.

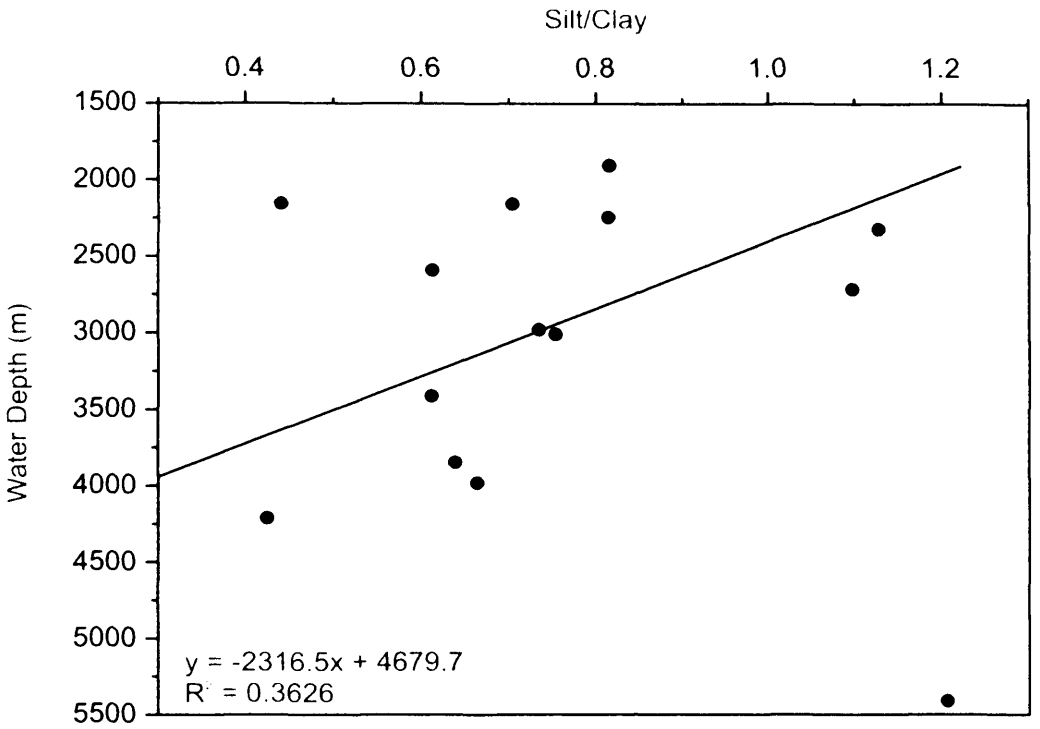

Figure 3.7: The relationship between the silt/clay ratio of the sediment with depth along the crest of the ridge during the Holocene. Each point represents an average of 3-5 measurements.

A selection of the volume % versus particle diameter curves for samples derived from the Coulter Counter analyses covering a range of depths along T2 are shown in Figure 3.8. These cropped distributions of particle size are inconsistent with previous suggestions of a simple pattern of fining away from the continental margin dominating the $\overline{SS}$ signal along the crest of the BOR (Haskell and Johnson, 1993).

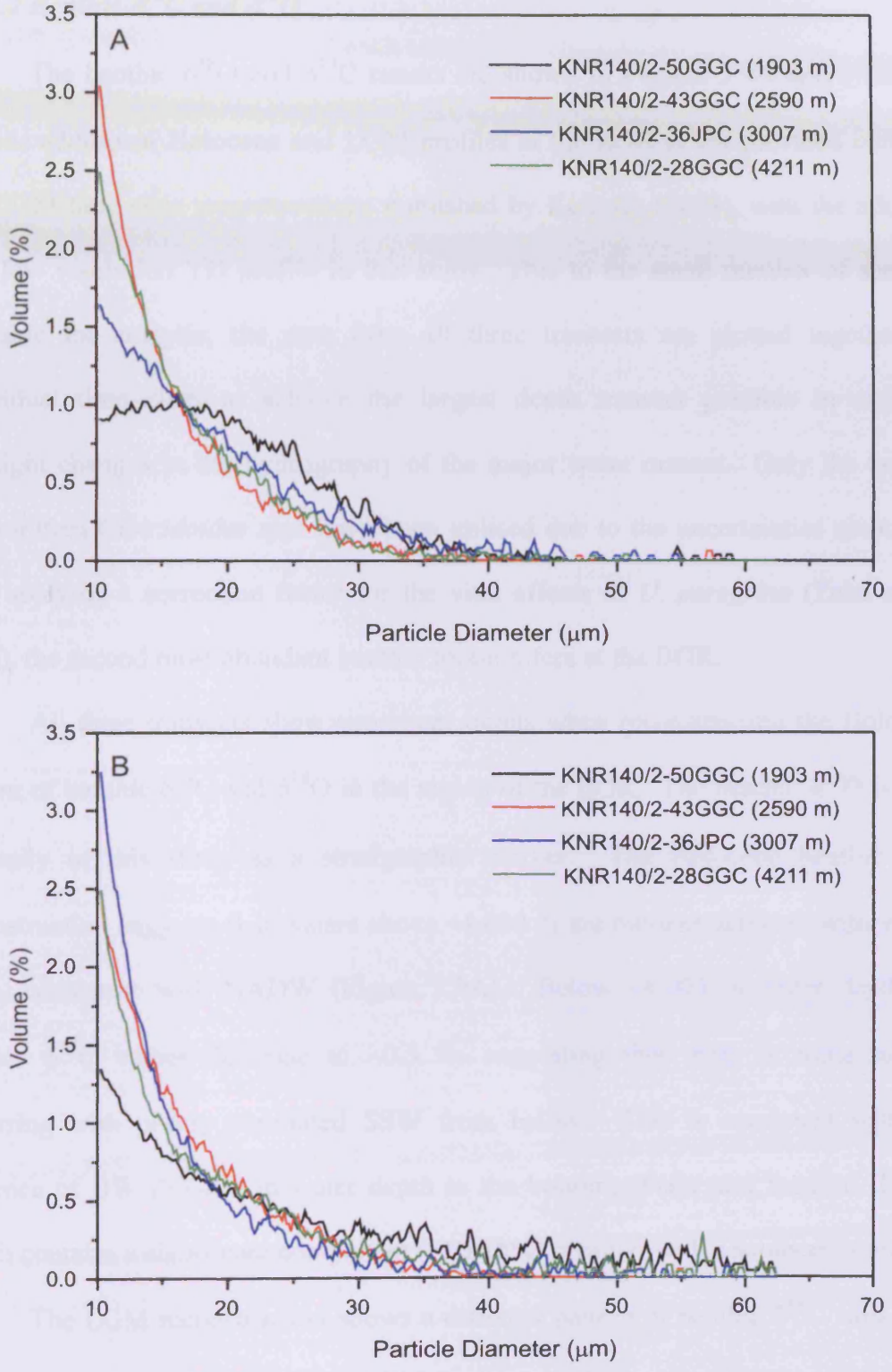

Figure 3.8: A selection of grain size distributions of the sortable silt fraction calculated by the Coulter Counter, covering a depth transect along the crest of the BOR during (A) the Holocene, and (B) the LGM. The distributions have been smoothed using a 3 point moving average.

3.4.2.2 Benthic $\delta^{13}C$ and $\delta^{18}O$

The benthic $\delta^{18}O$ and $\delta^{13}C$ results are shown in Figures 3.9A and 3.9B and provide additional Holocene and LGM profiles at the BOR to the previous core top and LGM time-slice reconstructions published by Keigwin (2004), with the addition of a low resolution YD profile in this study. Due to the small number of samples available for analysis, the data from all three transects are plotted together for individual time-slices to achieve the largest depth transect possible in order to highlight changes in the hydrography of the major water masses. Only the benthic foraminifera *Cibicidoides spp.* have been utilised due to the uncertainties associated with applying a correction factor for the vital effects of *U. peregrina* (Zahn *et al.*, 1986), the second most abundant benthic foraminifera at the BOR.

All three transects show consistent trends when reconstructing the Holocene pattern of benthic $\delta^{13}C$ and $\delta^{18}O$ in the region of the BOR. The benthic $\delta^{18}O$ is used primarily in this study as a stratigraphic marker. The Holocene benthic $\delta^{13}C$ reconstruction suggests that waters above ~4,000 m are nutrient-depleted with values ~1‰, consistent with NADW (Figure 3.9A). Below ~4,000 m water depth the benthic $\delta^{13}C$ values decrease to ~0.5 ‰ suggesting that there is some mixing occurring with poorly ventilated SSW from below. This is consistent with the presence of BW (>3,400 m water depth to the bottom; (Stahr and Sanford, 1999)) which contains a significant component (~10-16%) of water with a southern source.

The LGM reconstruction shows a different pattern of benthic $\delta^{13}C$ variability with depth (Figure 3.9A). The LGM is dominated by a decreasing trend in the benthic $\delta^{13}C$ with depth, suggesting a shoaling of nutrient-depleted NSW and an increased penetration of nutrient-enriched SSW below. At intermediate water depths (<2,500 m), the LGM experiences benthic $\delta^{13}C$ values 0.1-0.2 ‰ greater than during

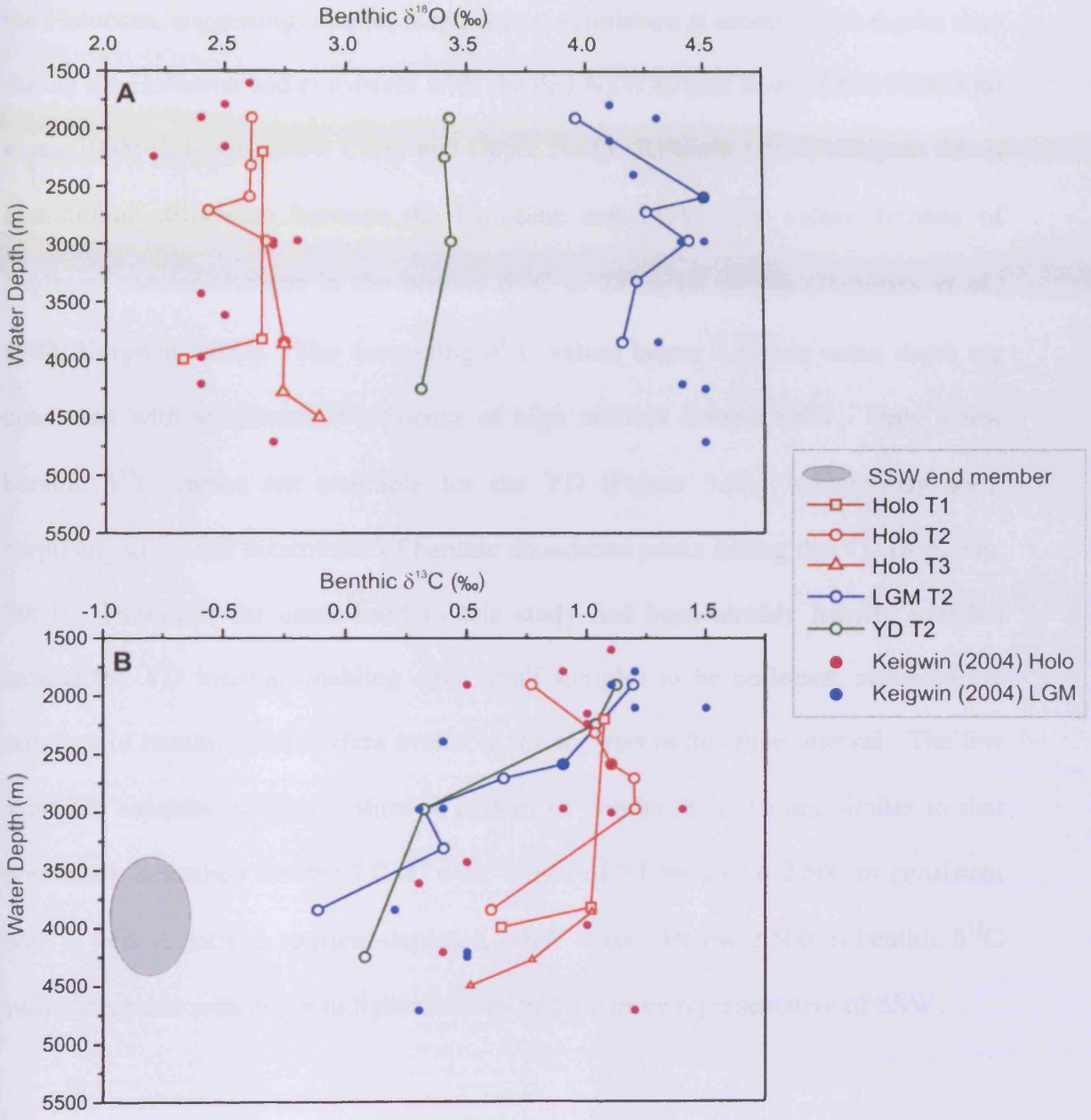

Figure 3.9: Summary of benthic (A) $\delta^{13}C$, and (B) $\delta^{18}O$ data from the Holocene (red), the LGM (blue) and YD (green) time-slices. Measurements were made on *Cibicidoides spp.* Squares represent the data from transect 1, circles the data from transect 2 and triangles the data from transect 3. Solid pink and blue circles show previous benthic stable isotope measurements from the area during the Holocene and LGM respectively (Keigwin, 2004). The grey circle represents the southern source end member (Curry and Oppo, 2005).

the Holocene, suggesting similar, if not better, ventilation at intermediate depths than during the Holocene and consistent with shoaled NSW (Came *et al.*, 2003; Marchitto *et al.*, 1998; Keigwin, 2004; Curry and Oppo, 2005). Keigwin (2004) suggests this is a minimum difference between the Holocene and LGM $\delta^{13}C$ values because of deglacial secular changes in the benthic $\delta^{13}C$ of ΣCO_2 of ~0.3‰ (Duplessy *et al.*, 1988; Keigwin, 2004). The decreasing $\delta^{13}C$ values below 2,500 m water depth are consistent with an increased influence of high nutrient content SSW. Only a few benthic $\delta^{13}C$ values are available for the YD (Figure 3.9A), which may seem surprising given the occurrence of benthic abundance peaks during the YD (Keigwin, 2004). However, the cores used in this study had been already heavily sampled around the YD interval enabling only small samples to be collected, reducing the numbers of benthic foraminifera available for analysis in this time interval. The few available samples, however, show a pattern of benthic $\delta^{13}C$ values similar to that previously described for the LGM, with values of >1 ‰ above 2,500 m consistent with a well ventilated, nutrient-depleted, NSW mass. Below 2,500 m benthic $\delta^{13}C$ values decrease with depth to lighter values that are more representative of SSW.

3.4.2.3 Calcium Carbonate

As sufficient foraminifera to produce continuous benthic $\delta^{13}C$ records are sparse, an additional proxy, the $CaCO_3$ (wt %), is used to infer the relative influence of NSW and SSW masses along the ridge crest (Figure 3.10). Previous studies (e.g. Keigwin and Jones, 1994; Keigwin *et al.*, 1994) suggest that $CaCO_3$ fluctuations in the western subtropical North Atlantic vary mainly in response to changes in dissolution caused by changes in the relative influence of SSW. Keigwin *et al.* (1994)

suggest that $CaCO_3$ (wt%) in cores from the western subtropical North Atlantic provides an additional proxy to benthic $\delta^{13}C$ for monitoring changes in deepwater ventilation. North Atlantic Deep Water (^{13}C-enriched) is less corrosive to $CaCO_3$ than SSW (^{13}C-depleted) and therefore replacement of NADW by SSW drives down the $CaCO_3$ (wt%). The $CaCO_3$ is also controlled by changes in terrigenous dilution and productivity.

The $CaCO_3$ values during the Holocene decrease with increasing water depth and distance along the ridge (Figure 3.10). $CaCO_3$ values decrease rapidly between ~2,320-3,000 m water depth from 56-38 wt% and then remain at 38-42 wt% from 3,007-4,211 m water depth, before decreasing to 27 wt% at 5,409 m water depth. This second drop in $CaCO_3$ values below 4,211 m water depth probably corresponds to the depth of the regional lysocline (Balsam, 1983). The maximum $CaCO_3$ values at the shallower sites reach a similar peak (at ~2,300 m) to that observed in the record of Haskell and Johnson (1993) with values of ~55 wt%, which is suggested to be related to increased productivity near the continental slope or to the transport of detrital carbonate from the Blake plateau by the Gulf Stream. The Holocene $CaCO_3$ values along the crest of the ridge are not clearly modified by the presence of the fast flowing and well ventilated core of DWBC.

The LGM $CaCO_3$ profile displays lower abundances throughout the depth transect than during the Holocene, with values decreasing with increasing depth from 38-27 wt% (Figure 3.10). Both the Holocene and LGM records reach similar values at 5,409 m water depth of ~27 wt%. The main difference between the Holocene and LGM records is that during the LGM the $CaCO_3$ content remains low and relatively unchanged below 3,000 m water depth, while $CaCO_3$ levels still decrease significantly below this depth in the Holocene. Despite generally lower LGM values, the highest

LGM values are associated with the shallowest depths above 2,500 m. This is consistent with a greater influence of more corrosive SSW below this depth reducing the $CaCO_3$ values during the LGM. The YD shows a similar pattern to the LGM suggesting increasing SSW influence with depth.

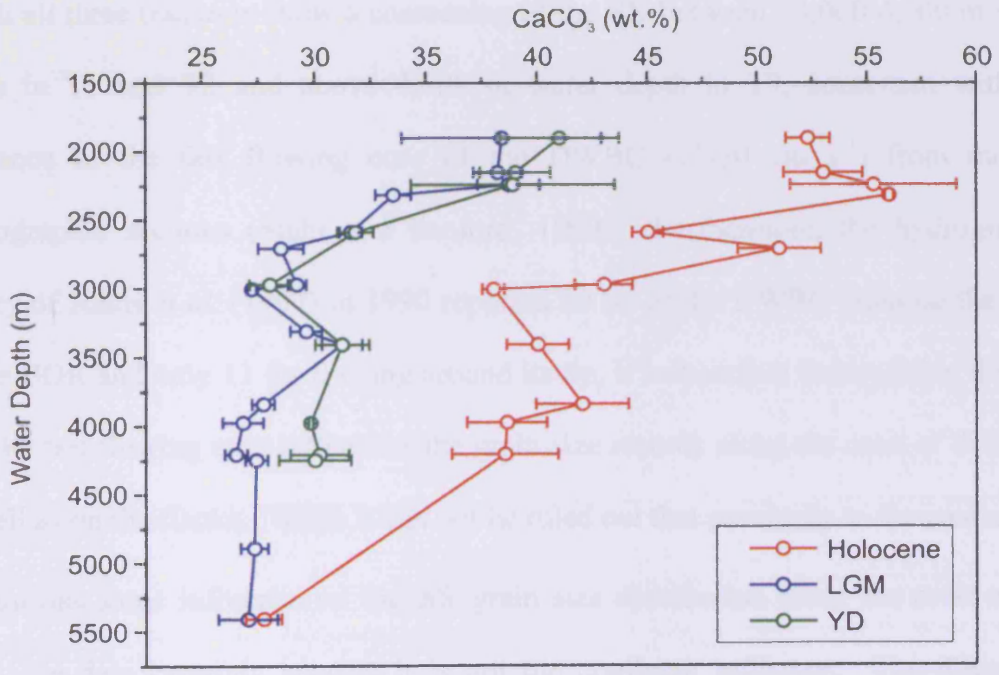

Figure 3.10: Comparison of the $CaCO_3$ (wt.%) profiles during the Holocene (red), LGM (blue) and YD (green) along transect 2 down the crest of the ridge. Each point represents an average value of 3-5 measurements with bars showing the 1σ standard deviation at each depth.

3.5. Discussion

3.5.1. The Holocene

Previous studies on the BOR which attempted to reconcile physical hydrographic measurements with grain size proxy data have suggested that during the Holocene sediment texture and composition were only influenced by the intensity and migrations of the DWBC on the flanks of the ridge (Haskell and Johnson, 1993),

while the sediment texture on the crest of the ridge was dominated by fining in the grain size with proximity to the continental margin and the sediment source areas (Figure 3.11B). Haskell and Johnson (1993) found no direct indication of the DWBC influence on the ridge crest even where the major axis of the DWBC crossed the crest above 4,200 m water depth. This differs markedly to the results presented here in which all three transects show a coarsening of the $\overline{SS}$ between ~3,000-4,000 m water depth in T1 and T2 and above 4,500 m water depth in T3, consistent with the influence of the fast flowing core of the DWBC (15-30 cm s^{-1}) from modern hydrographic sections (Stahr and Sanford, 1999). Furthermore, the hydrographic survey of Johns *et al.* (1997) in 1990 reported 20 Sv of the DWBC crossing the crest of the BOR and only 11 Sv flowing around its tip, it is therefore unsurprising that the DWBC fast flowing core influences the grain size records along the crest of the ridge as well as on the flanks. While it can not be ruled out that proximity to the continental margin has some influence on the $\overline{SS}$ grain size distribution along the crest of the ridge, the data certainly suggest it is not the dominant influence. The difference between the results presented and those of Haskell and Johnson (1993) is most likely the result of the different grain size fractions used in the two studies. The 6-70 μm fraction used by Haskell and Johnson (1993) includes part of the 'very fine' silt fraction, which tends not to be primarily current sorted by settling velocity as individual particles but is rather deposited as aggregates (McCave *et al.*, 1995; McCave and Hall, 2006). In comparison, the $\overline{SS}$ fraction varies independently of sediment supply in areas of current-sorted muds, allowing it to become an established proxy for flow speed in many locations (see review by McCave and Hall (2006)). The fining in the mean grain size record of Haskell and Johnson (1993) along the crest of the ridge is likely to result from an increased abundance of fine fraction which is

not current sorted. This is consistent with the silt/clay ratios in Figure 3.7 showing increasing clay and decreasing silt content with depth along the crest of ridge, while the SS fraction is shown to vary independently of depth (Figure 3.6). This supports the use of the $\overline{SS}$ fraction in order to study changes in the near bottom flow in which the influence of smaller cohesive size fractions that are not current sorted are removed (McCave *et al.*, 1995; McCave and Hall., 2006).

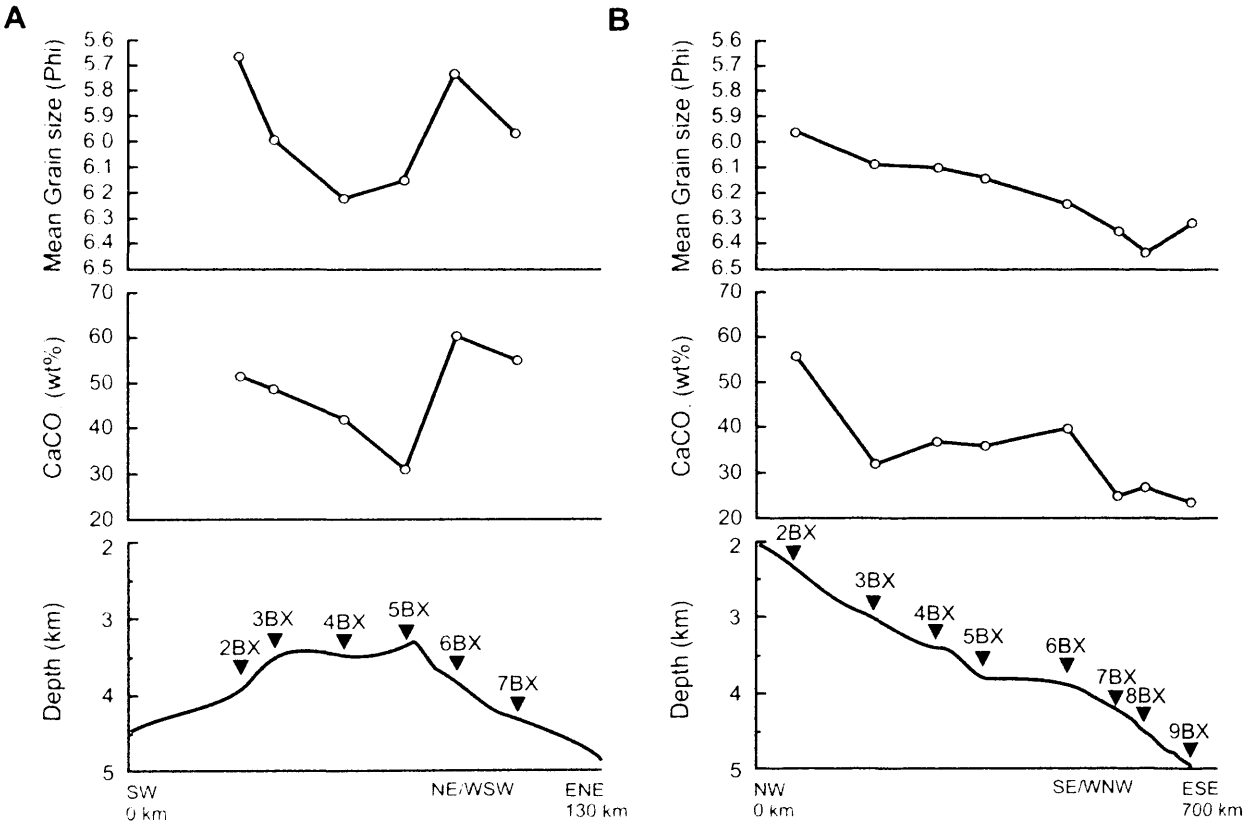

Figure 3.11: Compositional and textural parameters measured in surface sediment from box cores from (A) the transect across the middle of the Blake Outer Ridge in 1989. Both grain size and carbonate reflect the presence of strong circulation along the flanks of the ridge, and (B) from the transect down the crest of the Blake Outer Ridge in 1988. Note the fining in mean grain size down the crest of the ridge (figure adapted from Haskell and Johnson, 1993).

The Holocene $\overline{SS}$ grain size reconstruction suggests a similar physical hydrography to that based on the measurements of Stahr and Sanford (1999) (see

shaded panels on Figure 3.6). Stahr and Sanford (1999) record a high velocity core of the DWBC that flows along the bathymetric contours deepening from ~3,500 m at its upstream origin to 4,100 m further downstream along the eastern flank of the ridge which is consistent with the increase in current intensity between ~3,000 m and 4,000 m water depth in T1 and along the crest of the ridge, extending as deep as ~4,500 m in T3 on the eastern flank of the ridge. Previous reconstructions at the BOR at Sites 1060 (3,481 m water depth) and 1062 (4,763 m water depth) during the time interval 130-110 kyr BP (MIS 5d-5e) have also suggested a deepening of the DWBC fast flowing core to ~4,000 m water depth during the last interglacial (MIS 5e; Bianchi *et al.*, 2001). However, the coarser $\overline{SS}$ values at T1 compared to T2 (difference of ~2 μm) are suggestive of a slowing of the fast flowing DWBC core between these two transects. A possible explanation for this is that T1 is located close to where the DWBC is topographically steered by the BOR and forced to separate from the continental margin. As the current is steered it also accelerates producing the higher $\overline{SS}$ values at T1, in agreement with previous observations of Stahr and Sanford (1999) showing higher velocities further up-slope at the BOR. As the ridge slopes progressively deeper towards the abyssal plain, water is transported across the ridge crest. This water is no longer steered and constrained by the topography and may therefore slow down. Transect 2 also reveals fast flow speeds at depths shallower than 2,500 m which are likely to reflect the influence of the secondary fast flowing core of the DWBC along the crest of the ridge which is mainly composed of (S)LSW at these depths today (Johns *et al.*, 1997). Its influence extends from 1,000 m to 2,500 m water depth, consistent with the $\overline{SS}$ data presented in this study, and reaches current speeds of ~15 cm s^{-1} (Stahr and Sanford, 1999).

Below 4,200 m water depth at T1 and T2 and 4,500 m water depth at T3 flow speeds are low during the Holocene (Figure 3.6), suggesting little current activity at these abyssal depths, consistent with the physical hydrographic measurements (Stahr and Sanford, 1999). Haskell and Johnson (1993) observed a small increase in mean grain size values at ~5,000 m water depth in their ridge crest reconstruction (Figure 3.11B) and attributed it to either the presence of a vigorous deeper circulation system or the influence of a distal turbidity from the Hatteras Abyssal Plain. No evidence is found for a deeper circulation system during the Holocene and the hydrographic measurements of Stahr and Sanford (1999) show no evidence in support of a vigorous deeper circulation during the Holocene. Furthermore, previous grain size reconstructions at the BOR have suggested that the DWBC fast flowing core did not influence the depth of Site 1062 (4,763 m) during previous warm interglacial/interstadial intervals (Bianchi *et al.*, 2001; Yokokawa and Franz, 2002). It is suggested that the increase in grain size recorded by Haskell and Johnson (1993) is therefore likely to be the result of a recent event which is not recorded in the averaged Holocene records.

Overall, these data suggest that the $\overline{SS}$ grain size proxy can provide a reliable reconstruction of averaged spatial flow speed variability at the BOR during the Holocene that appear consistent with modern hydrographic observation. This allows increased confidence when using this proxy to interpret flow speed changes throughout the last glacial cycle in this region.

The Holocene bathymetric profiles of benthic $\delta^{13}C$ and $CaCO_3$ are consistent with the modern configuration of water masses intersecting the BOR and correlate well with the GEOSECS $\delta^{13}C$ profile from the western North Atlantic (Kroopnick, 1985; Curry and Oppo, 2005; Figure 3.12) and are also consistent with the Holocene

western Atlantic Cd/Ca transect (Marchitto and Broecker, 2006). The benthic $\delta^{13}C$ maximum associated with nutrient-depleted NADW (~1 ‰) dominates the region above 4,000 m water depth, consistent with the modern position of the DWBC as shown by both the $\overline{SS}$ reconstruction and the hydrographic profiles (Hogg, 1983; Stahr and Sanford, 1999). The slightly lower benthic $\delta^{13}C$ (0.75-0.5 ‰) and lower $CaCO_3$ wt% (<30 %) values are found at depths below 4,000 m consistent with the increased influence of nutrient-enriched, corrosive SSW (Hogg, 1983).

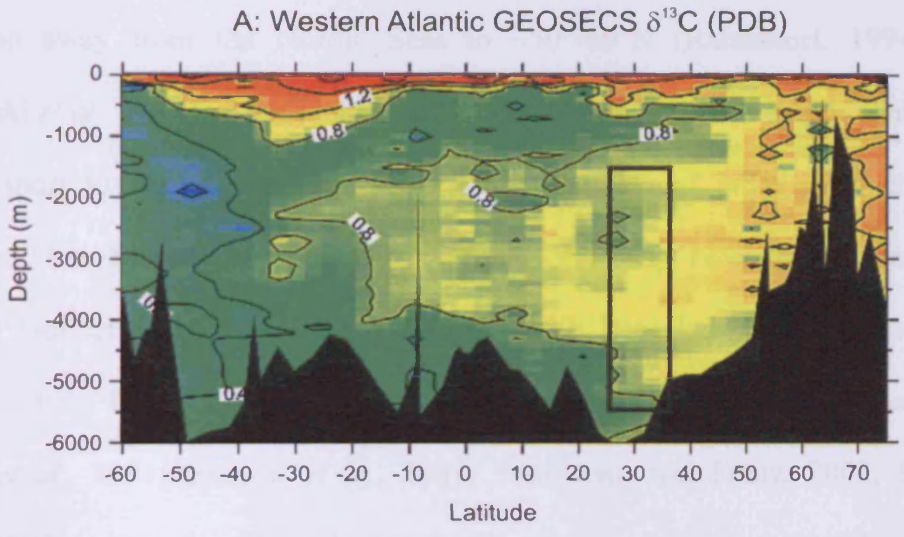

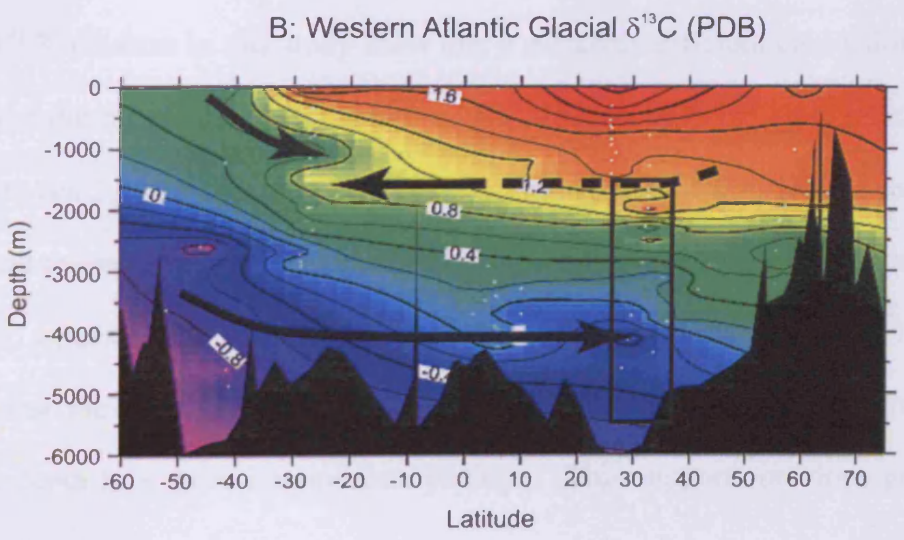

Figure 3.12: Adapted from Curry and Oppo (2005). (A) The distribution of $\delta^{13}C$ of ΣCO_2 in the modern western Atlantic (Kroopnick, 1985) and, (B) a revised and updated glacial transect of $\delta^{13}C$ of ΣCO_2 for the western Atlantic Ocean basins. The black boxes represent the depth interval and latitudes considered in this study.

3.5.2. The LGM

During the LGM (23-18 kyr BP) surface waters in the North Atlantic were less dense than their modern day analogue, which resulted in a reduced rate of formation and/or depth penetration of NSW (e.g. Broecker *et al.*, 1985; Lynch-Steiglitz *et al.*, 2007). Furthermore, ocean models suggest there not only existed a shallower mode of deepwater production during the LGM, but there was also a southward shift in production away from the Nordic Seas to ~50°-60°N (Rahmstorf, 1994, 2002; Ganopolski *et al.*, 1998). This change in the deep convection sites could reduce ocean heat transport to the higher latitudes, even if the rate of NSW production was unchanged, but decreased production in the North may have been balanced by increased production of SSW (e.g. Crowley, 1992; Broecker, 1998). The vertical migration of the DWBC documented by previous studies (e.g. Johnson *et al.*, 1988; Haskell *et al.*, 1991; Bianchi *et al.*, 2001; Yokokawa and Franz, 2002; Hall and Becker, 2007) is thought to be linked to the changes in production of NSW described above. All 3 transects in this study show that a markedly different circulation pattern was present during the LGM compared with Holocene, with the slow relative flow speeds between 3,000-4,000 m water depth suggesting that the fast flowing core of the DWBC had migrated and/or weakened. The substantial increase in flow speed above 2,500 m to values higher than those associated with the Holocene in both T1 and T2 suggests that the DWBC fast flowing core had most likely shoaled relative to its Holocene depth to a more intermediate position. This supports previous grain size work on the BOR, which suggests that as a result of increased production of intermediate depth waters prior to 12 kyr and post LGM, circulation was focused on

the upper part of the ridge above 2,700 m (Haskell *et al.*, 1991), while during the glacial intervals within MIS 10-8 the DWBC shoaled to around ~2,200 m (Yokokawa and Franz, 2002).

The shoaling of the DWBC fast flowing core is consistent with the benthic $\delta^{13}C$ and $CaCO_3$ records presented here and in previous studies, suggesting a decrease in the production of NADW during the LGM and its replacement with shallower, nutrient-depleted GNAIW (e.g. Boyle and Keigwin, 1987; Oppo and Fairbanks, 1987; Curry *et al.*, 1988; Duplessy *et al.*, 1988; Oppo and Lehman, 1993; Slowey and Curry, 1995; Marchitto *et al.*, 1998; Keigwin and Schlegel, 2002; Keigwin, 2004; Curry and Oppo, 2005; Marchitto and Broecker, 2006)). Marchitto *et al.* (1998) suggest that an inverse relationship exists between the formation of these deep and intermediate water masses (when NADW production is strong, GNAIW is absent and *vice versa*) both on orbital and millennial timescales. Previous DWBC shoaling events documented during MIS 5e and 5d (130-110 kyr BP) at the BOR have also been associated with reductions in NADW formation (e.g. Bianchi *et al.*, 2001) and it is therefore suggested the shoaling revealed by the $\overline{SS}$ records during the LGM is the result of reduced NADW formation and its replacement by vigorous but shallow GNAIW. The reconstructed benthic $\delta^{13}C$ and $CaCO_3$ profiles for the BOR region, show that this vigorous intermediate depth circulation is indeed associated with the presence of nutrient-depleted NSW, consistent with GNAIW (end-member value of 1.5‰ (Curry and Oppo, 2005)), with a significant northward expansion of SSW (end-member value of -0.2‰ (Curry and Oppo, 2005)) below. This high nutrient SSW below 2,500 m water depth in the North Atlantic has been shown to have high zinc concentrations, supporting the notion that this water mass originated in the Southern Ocean (Marchitto *et al.*, 2000). However, the deep benthic $\delta^{13}C$ values in the subtropical

North Atlantic are heavier than records from the deep South Atlantic (Curry and Oppo, 2005), suggesting that waters originating in the North Atlantic also contributed to the water mass below 2,500 m. During the LGM, the large differences in water mass properties of GNAIW and SSW produce a steep vertical gradient, which has been previously highlighted in a transect of the western Atlantic by Curry and Oppo (2005) resulting in the decrease in the benthic $\delta^{13}C$ and $CaCO_3$ observed in the water column below ~2,300 m. Oppo and Lehman (1993) and Raymo *et al.* (2004) have previously suggested that this transition between GNAIW and SSW was very abrupt in the subpolar North Atlantic with a 1 ‰ decrease in $\delta^{13}C$ across a 500 m depth interval, centred on ~2,000 m. However, Keigwin (2004) has suggested that this is not the case in the subtropical western North Atlantic, in agreement with this study, as the $\delta^{13}C$ decreases continually with depth suggesting a large mixing zone between the two water masses (Figure 3.9). In the modern North Atlantic the range of ocean hydrographic properties is small as NADW dominates the water column and therefore mixing produces only weak gradients (Mauritzen *et al.*, 2002). In the glacial ocean the range of hydrographic properties is much larger as the deep ocean is flooded with nutrient-enriched SSW. The strength of glacial intermediate water has been disputed in previous studies, with some suggesting vigorous renewal of GNAIW (Gherardi *et al.*, 2005; Hall *et al.*, 2006), with a reduction in deepwater export from the North Atlantic of only 30-50% during the LGM (LeGrand and Wunsch, 1995; Seidov *et al.*, 1996; Marchal *et al.*, 2000; McManus *et al.*, 2004), while other proxy and modelling studies suggest similar (or possibly stronger) NADW production rates to the present day (e.g. Yu *et al.*, 1996; Kitoh *et al.*, 2001; Hewitt *et al.*, 2003). This study supports the presence of vigorous intermediate waters during the LGM at the expense of NADW formation. It is well documented that a large range of factors (e.g. air-sea

exchange, carbonate saturation state, oxidation of organic matter in sediments) can contribute to the $\delta^{13}C$ of benthic foraminiferal shells and potentially decouple $\delta^{13}C$ regionally from global nutrient stoichiometry (e.g. Broecker and Maier-Reimer, 1992; Lynch-Stieglitz, 2003). However, the consistent results between the $\overline{SS}$ and benthic $\delta^{13}C$ proxies gives increased confidence in their combined use as circulation tracers in this region, providing consistent hydrographic and dynamical reconstructions.

Despite the vigorous flow speeds at intermediate depths during the LGM, consistent with a shoaling of the DWBC and GNAIW formation, the $CaCO_3$ record shows lowered values at these depths during the LGM than the Holocene by ~10% (Figure 3.10) even though it is influenced by GNAIW. This low $CaCO_3$ signature is likely to partially reflect increased terrigenous supply and dilution because of lower sea levels and increased continental erosion, which may drive down values in the bulk $CaCO_3$ record (Keigwin and Jones, 1994).

Decreased rates of production in the northern deepwater source areas may have been compensated for by an increased rate of production of SSW in the Southern Ocean so that overall rates of deep ocean circulation may have been as strong as the present day (Broecker *et al.*, 1998; Wunsch, 2003). The higher flow speeds below 4,000 m water depth during the LGM compared with the Holocene (most obvious in T2) suggests the possibility of a vigorously flowing abyssal circulation at this time, although it can not be concluded with certainty that this is related to increased production of SSW. Even though few cores were available for analysis below 4,000 m water depth with both their LGM and Holocene sediments preserved, the higher $\overline{SS}$ values during the LGM are a consistent feature of all cores sampled. This suggests that the increase in flow speeds at depths greater than 4,000 m is a robust feature of the DWBC system at the BOR. The benthic $\delta^{13}C$ and $CaCO_3$ signatures suggest that

the water mass feeding this vigorous circulation is of a southern origin, with a benthic $\delta^{13}C$ of <0.5 ‰ and a $CaCO_3$ at < 28 wt% below 4,000 m water depth. Furthermore, Robinson *et al.* (2005) found that the pattern of deep sea $\Delta^{14}C$ during the LGM varied synchronously with the atmosphere and suggested that this could result from either vigorous SSW circulation (Reimer *et al.*, 2004) or the occurrence of extensive sea-ice coverage in the Southern Ocean which reduced the air-sea carbon exchange. Combined with the $\overline{SS}$ results it is suggested that the results of Robinson *et al.* (2005) are consistent with vigorous SSW flow during the LGM. However, there has been some evidence based on coupled deep-sea coral $\Delta^{14}C$ and Cd/Ca measurements, which suggested a very different situation with the presence of a relatively stagnant deep water mass (Adkins *et al.*, 1998). These measurements were however made at 15.4 kyr BP and may therefore not be representative of the LGM.

3.5.3. The Younger Dryas

The Younger Dryas is characterised by a return to near glacial temperatures in most of the Northern Hemisphere (Grootes and Stuiver, 1997) between 13-11.5 kyr BP. At present the role of the MOC and the DWBC during the YD remains partially understood (Lehman and Keigwin, 1992; Keigwin, 2004). Some early studies suggest that Late Holocene-style deepwater production was established before and during most of the YD (Sarnthein *et al.*, 1994), but most palaeodata now shows that this was not the case (e.g. Marchitto *et al.*, 1998; Zahn and Stüber, 2002); despite this the actual degree of change in the MOC remains controversial. Recent evidence based on $\Delta^{14}C$ ventilation ages (Schlegel and Keigwin, 2002; Keigwin, 2004) suggests the replacement of NADW by GNAIW with older SSW at depth was similar during both the LGM and YD.

The combined $\overline{SS}$, benthic $\delta^{13}C$ and $CaCO_3$ data presented in this study (Figures 3.6, 3.9 and 3.10) strongly suggest that both the physical and chemical hydrography in the western subtropical North Atlantic were similar at the time of the YD and the LGM, with a shoaled DWBC fast flowing core above 2,500 m consistent with nutrient-depleted GNAIW formation (Boyle and Keigwin, 1987; Oppo and Lehman, 1993). This is in support of previous observations from the BOR made from $\Delta^{14}C$ ventilation ages (Keigwin, 2004). The results of Keigwin (2004) revealed similar ventilation ages of ~1,000 years below 2,300 m during both the LGM and YD consistent with the modelling results of Stocker and Wright (1998) indicating an increasing influence of SSW. Although no LGM benthic and planktonic foraminifera pairs were available above 2,300 m water depth, YD pairs reveal ventilation ages similar to the present day (<500 years) consistent with the production of well ventilated GNAIW. This is supported by both the grain size and benthic $\delta^{13}C$ data presented in this study (Figures 3.6 and 3.9) which show that there was vigorous, well ventilated circulation above 2,500 m on the BOR during the YD similar to that previously described for the LGM reconstruction. Previous grain size studies at the BOR have hinted at an increased vigour of a shallow circulation above 2,700 m water depth during the YD (e.g. Haskell *et al.*, 1991), which is consistent with nutrient-depleted GNAIW formation (Boyle and Keigwin, 1987; Marchitto *et al.*, 1998). The data also hint at an increase in SSW vigour at depths below 4,000 m during the YD although there are too few records below this depth to draw any firm conclusions.

3.6. Conclusions

This study demonstrates that changes in $\overline{SS}$ can be used successfully as a proxy to reconstruct changes in deepwater circulation patterns, providing the

capability to map shifts in both the position and strength of the DWBC when utilised in the form of a depth transect. Contrary to the grain size results of previous studies which utilized the 6-63 μm sediment fraction, the $\overline{SS}$ results in this study suggest that the fast flowing core of the DWBC can be observed along the crest of the BOR between ~3,000-4,000 m water depth, which is consistent with previous hydrographic studies in the area (Stahr and Sanford, 1999). The LGM reconstruction suggests a very different hydrographic pattern was present during this interval compared with the Holocene, with a shoaling of the DWBC from its Holocene position (3,000-4,000 m water depth) to <2,500 m water depth, consistent with reduced NADW and increased GNAIW production. This is in agreement with both previously published (e.g. Keigwin, 2004; Curry and Oppo, 2005) and new geochemical data from the region. The deep cores selected for this study further suggest an increase in flow speed below 4,000 m water depth hinting at an increase in SSW flow speeds during the LGM. Furthermore, similarly to the results of Keigwin (2004), both the $\overline{SS}$ and benthic $\delta^{13}C$ records suggest that a similar pattern of circulation was present during the YD as during the LGM.

It also appears that the cores on the crest of the ridge provide the greatest potential for further grain size work due to their good preservation; they have the largest numbers of foraminifera suitable for stable isotope work and high sedimentation rates. This study supports the use of more than one core when studying time-series records in order to track the vertical movement of the DWBC, which is suggested to be occurring in response to changes in NADW production. The position of the DWBC reconstructed in this study during the extremes of the Holocene and LGM should aid the interpretation of further down core time-series records.

Chapter 4: Rapid sea surface temperature and salinity oscillations during the last deglaciation in the subtropical NW Atlantic

4.1 Introduction

Many studies have focused on understanding the role of changes in the North Atlantic Meridional Overturning Circulation (MOC) in promoting abrupt shifts in climate (e.g. Bond *et al.*, 1993). While most of these investigations have concentrated on the subpolar regions near the source of North Atlantic Deep Water (NADW; e.g. Oppo *et al.*, 1998; McManus, 1999), far less effort has been spent understanding the role of the MOC in the low- to middle-latitude Atlantic Ocean (Healey and Thunell, 2004). However, it is the warm-surface water reservoir in the low-latitude western (sub)tropical Atlantic that provides the source of the warm surface waters that transport heat to the subpolar North Atlantic, through the North Atlantic Current, to compensate for the southward flow of NADW (Broecker, 1991). Therefore, changes in surface water hydrography at the Blake Ridge are intricately associated with variability in high-latitude circum-North Atlantic climates and, in particular, the convective formation of deepwaters.

The warming trend in the high latitude North Atlantic during the last deglaciation was punctuated by several returns to near-glacial temperatures (Keigwin and Lehman, 1994; Dansgaard *et al.*, 1993; Bond *et al.*, 1993; Alley and Clark, 1999; Alley, 2000). The most prominent was the Younger Dryas (YD) cold event (~13-11.5 kyr BP, e.g. Broecker *et al.*, 1989; Keigwin *et al.*, 1991) towards the end of the last deglaciation. Previous modelling experiments of the YD suggest a freshwater induced slowdown of NADW production (Broecker *et al.*, 1988), resulting in a decrease in the northward heat transport and a warming in the western tropical

Atlantic and throughout most of the Southern Hemisphere (Manabe and Stouffer, 1997). Previous studies have shown increasing sea surface temperature (SST) trends during the YD in the Tobago Basin (Rühlemann *et al.*, 1999; Hüls and Zahn, 2000), the Caribbean Sea (Schmidt *et al.*, 2004), off the coast of Brazil (Weldeab *et al.*, 2006) and in the Gulf of Mexico (Flower *et al.*, 2004). Significant differences exist however, with respect to the timing and magnitude of these SST changes. For example, a study in the Gulf of Mexico (hereafter referred to as GOM; core EN32-PC6; 26°56.8'N, 91°20.0'W; Flower *et al.*, 2004) recorded a SST anomaly consistent with the YD event that can be divided into a warming early phase (12.9-12.2 kyr BP) and cooler late phase (12.2-11.5 kyr BP).

A similar asynchronous pattern between cooling SST at northern latitudes and the warming tropics is also observed at a range of locations during Heinrich Event 1 (H1; e.g. Rühlemann *et al.*, 1999; Hüls and Zahn, 2000; Schmidt *et al.*, 2004; Flower *et al.*, 2004; Weldeab *et al.*, 2006). In the GOM (Flower *et al.*, 2004), SST exhibited an early deglacial warming (17.2-15.5 kyr BP), that occurred prior to the peak meltwater incursion associated with Laurentide ice sheet (LIS) decay during H1 and >2 kyr before the Bølling-Ållerød (B/A) interval. This suggests that heat was retained in the (sub)tropical Atlantic during H1, consistent with modulation of deglacial climate by the MOC (Flower *et al.*, 2004). This asynchrony with northern latitudes provides further evidence that at least some of the (sub)tropical western Atlantic experienced warming and cooling that was asynchronous with Greenland air temperatures (e.g. GISP2; Grootes and Stuiver, 1997) and has been attributed to the 'bipolar see-saw' model of deglacial climate change (Crowley, 1992; Broecker, 1998). There is, however, considerable disagreement on the exact timing and spatial pattern of SST variability in the (sub)tropics, which could have important implications

on our understanding of climate change induced by variability in the MOC (e.g. Lea *et al.*, 2003).

Freshwater input to the North Atlantic is a major component capable of modulating the strength of the MOC. It has been demonstrated by dynamical ocean models that freshwater perturbations on the order of 0.1 Sv are sufficient to impact North Atlantic overturning (Stocker and Wright, 1991; Manabe and Stouffer, 1997; Aharon, 2003). A theoretical model has been proposed (Clark *et al.*, 2001) to account for the changes in the MOC (and hence regional and global climate) caused by switches in the drainage pathway of meltwater, controlled by the retreat and advance of the LIS margins during the last deglaciation. During the last deglaciation eastward meltwater discharge through the Hudson and St. Lawrence Rivers (Figure 4.1, see drainage pathways 2, 3, and 4) may have inhibited deep convection and NADW formation in the northern North Atlantic (Licciardi *et al.*, 1999; Clark *et al.*, 2001), while meltwater inputs via the southern drainage pathway i.e. the Mississippi River (Figure 4.1, see drainage pathway 1), may have little impact on NADW production, coinciding with warming SST in the northern latitudes. This is supported by the presence of a large meltwater input to the GOM via the Mississippi River during the B/A warm event (15.2-13 ky BP) which is suggested to have had little, if any effect on the MOC (Keigwin *et al.*, 1991; Flower *et al.*, 2004; McManus *et al.*, 2004). Although the timing and magnitude of deglacial meltwater events in the GOM are now well constrained (16.1-15.6 kyr BP and 15.2-13 ky BP), it remains unclear how these events influence the open North Atlantic and the Gulf Stream palaeohydrography and dynamics.

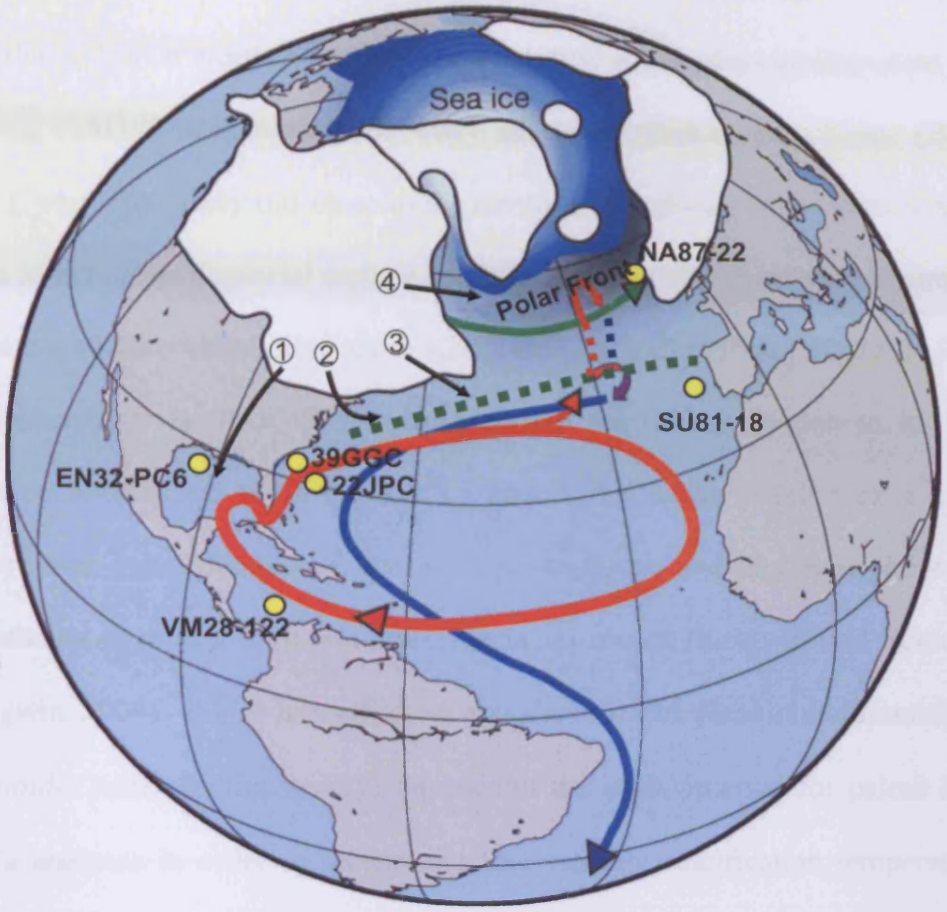

Figure 4.1: Schematic of the North Atlantic (based on Schmidt *et al.*, 2006). Idealised North Atlantic surface (red arrows) and deepwater (blue arrows) circulation during the last deglaciation. During cold events, such as the Younger Dryas, the overturning circulation migrated south of the present day polar front. During warm events, such as the Bølling-Ållerød, convection of the surface waters moved north of Iceland. The location of cores KNR140/2-39GGC (this study) at the Blake Outer Ridge, KNR140/2-22JPC (LeGrande and Lynch-Stieglitz, 2007) at the Bahama Outer Ridge, EN32-PC6 (Flower *et al.*, 2004) in the Gulf of Mexico, SU81-18 (Bard *et al.*, 1987; Duplessy *et al.*, 1992) on the Iberian Margin and NA87-22 (Duplessy *et al.*, 1992) on the Rockall Plateau are shown. The more southerly location of the polar front during Heinrich event 1 and the Younger Dryas is represented by the dashed green line. The continental ice sheets and sea ice extent is shown at its maximum during the LGM. The four main routes of continental runoff during the last deglaciation (after Clarke *et al.*, 2001) are shown and numbered: 1, Mississippi River; 2, Hudson River; 3, St. Lawrence River; 4, Hudson Strait.

This study will be aimed at establishing the influence the open subtropical western Atlantic has on North Atlantic surface salinity, which plays an important part in regulating NADW formation. The study site is the Blake Outer Ridge (BOR; Figure 4.1), which presently lies close to the northwards pathway of the Gulf Stream. The aim is to assess the deglacial surface conditions at the BOR in relation to circum-North Atlantic climate variability. Core KNR140/2-39GGC (31°40.1'N, 75°24.9'W; hereafter referred to as 39GGC) has been chosen for this study due to its high sedimentation rates of up to 70 cm kyr^{-1}. This is due to its position on a small sedimentary drift superimposed on the main Blake Ridge and has been shown by previous studies to give a high resolution deglacial record (Keigwin and Schlegel, 2002; Keigwin, 2004). It also has sufficient abundance of the planktonic foraminifera *Globigerinoides ruber* (white variety) throughout the study interval for paired $\delta^{18}O$ and Mg/Ca analyses in order to reconstruct SST (strictly calcification temperature) and salinity variations at the BOR. A detailed overview of all the methods used can be found in **Chapter 2** and a brief summary of the methodology is also given in the following section.

4.2 Sampling strategy and the age model

Sediment core 39GGC was recovered from the crest of the BOR in a water depth of 2,975 m and is ideally located to monitor Gulf Stream variability. Samples were obtained every 2 cm in the 1.5 to 19.5 kyr BP (7-429 cm) interval employing the methods described in **Chapter 2**. The YD interval was precisely identified from a previously published lower resolution planktonic $\delta^{18}O$ record (Keigwin and Schlegel, 2002) and sampled at an increased resolution of 1 cm. Sea surface temperatures were determined through paired Mg/Ca and $\delta^{18}O$ analyses of near-surface dwelling (Lin *et*

al., 1997; Deusser 1987; Anand *et al.*, 2003) *G. ruber* (white). Samples of 100 specimens in the 150 to 250 μm size fraction, where available, were lightly crushed, homogenised and split. The method for this process is described in detail in **Chapter 2**. Keigwin and Schlegel (2002) have previously demonstrated the potential for foraminiferal work at the site of 39GGC by convincingly showing that the palaeoceanographic signal is not compromised by lateral sediment transport.

The chronology employed for 39GGC is based on 11 previously published ^{14}C-AMS dates (Keigwin and Schlegel, 2002). The two samples from the top 100 cm are composed of mixed planktonic foraminifera while the nine deeper samples are composed of *G. ruber*. Radiocarbon ages have been (re)calibrated to calendar years before present (yr BP) using the CALIB programme (v. 5.0.1 with the MARINE 04 dataset; Stuiver *et al.*, 2005), incorporating a 400 yr correction for marine reservoir age (Table 4.1).

Table 4.1: Radio carbon ^{14}C-AMS dating results from core KNR140/2-39GGC with a marine reservoir correction of -400 yr. The old calibrated calendar ages of Keigwin and Schlegel (2002) are shown along with the new calibrated calendar ages obtained from CALIB v5.0.1 programme (Stuiver *et al.*, 2005).

Laboratory Number	Material	Depth (cm)	^{14}C Age yr BP	Error Age ±1σ yr BP	Old Calendar Age yr	New Calendar Age yr
39GGC						
NOSAM-7139	mixed	6-8	1980	35	1527	1543
NOSAM-7129	mixed	62-64	6620	40	7158	7167
NOSAM-7141	G. ruber	126-128	11350	50	12906	12889
NOSAM-16368	G. ruber	174-176	13250	70	15393	15353
NOSAM-26405	G. ruber	206-208	13900	80	16099	16035
NOSAM-26406	G. ruber	234-236	14500	100	16789	16810
NOSAM-26407	G. ruber	262-264	15150	130	17537	17836
NOSAM-26408	G. ruber	294-296	15000	80	17365	17677
NOSAM-26409	G. ruber	358-360	15550	80	17998	18593
NOSAM-26410	G. ruber	390-392	15700	90	18170	18688
NOSAM-26432	G. ruber	429-432	16900	75	19551	19731

The age model and resulting sedimentation rates (Figure 4.2 and Table 4.1) show that the ^{14}C-AMS date at 263 cm appears anomalously old in comparison to the ^{14}C-AMS dates either side of it, hinting that this sample has undergone mixing with forams from a greater depth in the sediment, and is therefore excluded from the age model calculations. Further ^{14}C-AMS dates at 391 cm and 359 cm have 1 sigma error bars that overlap suggesting that they are statistically indistinguishable from each other. Based on consideration of the resulting sedimentation rate curve the age control at 391 cm has been removed.

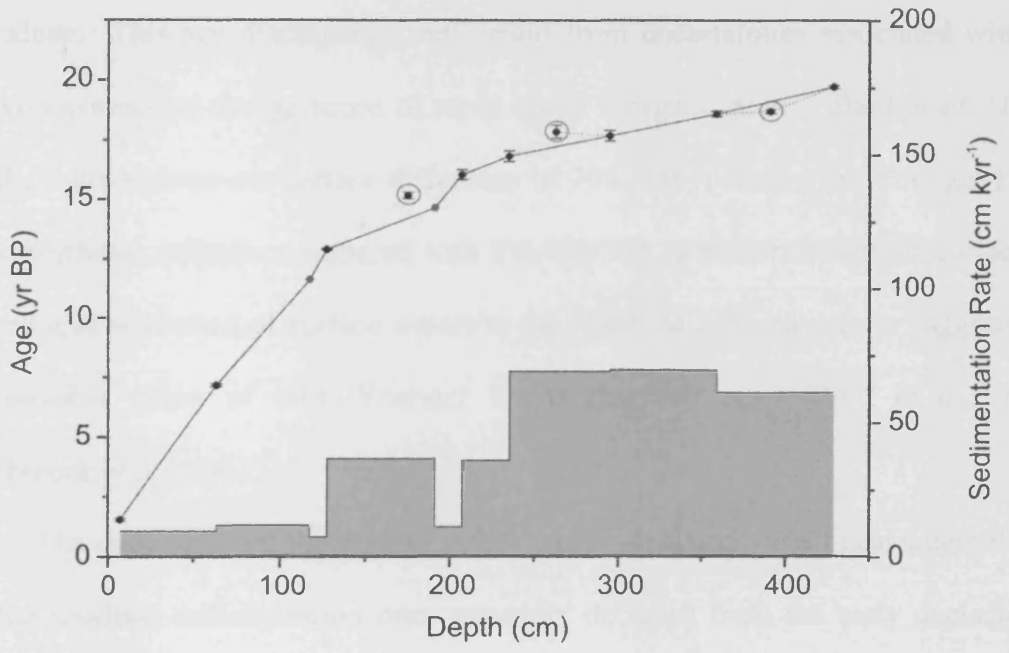

Figure 4.2: Age model for core KNR140/2-39GGC from the Blake Outer Ridge in the western subtropical North Atlantic. The black circles represent the positions of previously published ^{14}C-AMS dates (Keigwin and Schlegel, 2002) and the pink circles indicate where the sea surface temperature (SST) record of core 39GGC has been tied to GISP2. Error bars are shown for the ^{14}C-AMS dates. A linear interpolation was employed in between the age control points. The black line represents the age model used in this study, while the dashed line shows how the age model would differ if it were based only on the ^{14}C-AMS dates. The ^{14}C-AMS dates circled in red are not included in the age model. The youngest of these is an age reversal while the older date is statistically indistinguishable from the AMS date preceding it. See text for more details. The shaded region represents the sedimentation rate at the core site.

Two additional control points were then added at 117 cm and 191 cm that were derived from graphical correlation of the SST record at 39GGC to the GISP2 ice core $\delta^{18}O$ record (Grootes and Stuiver, 1997; shown by pink circles in Figure 4.2 and based on the correlation shown in Figure 4.3 by the dashed blue lines). The additional age control point at 117 cm is tied at the mid-point of the Younger Dryas-Holocene transition while the control point at 191 cm is tied at the mid point of the transition into the Bølling warm period from deglacial conditions. The addition of these two extra control points leads to the removal of the ^{14}C-AMS date at 175 cm making the age of the core younger (~1 kyr) during this interval than suggested by the ^{14}C-AMS ages alone. This age discrepancy may result from uncertainties associated with the reservoir correction during times of rapid ocean reorganisations. Bard *et al.* (1994) found an atmosphere-sea surface difference of 700-800 yr during the Younger Dryas in the northeast Atlantic, compared with the 400-500 yr modern reservoir correction. The reduced advection of surface waters to the North Atlantic have been suggested as one possible cause of high Younger Dryas reservoir ages (Bard *et al.*, 1994; Waelbroeck *et al.*, 2001).

The ages between the control points were calculated via a linear interpolation and the resulting sedimentation rates generally decrease from the early deglaciation into the Holocene, ranging between 70 and 8 cm kyr^{-1}. This is consistent with other observations of low Holocene sedimentation rates on the North American continental margin (Keigwin and Jones, 1989) and has been suggested to reflect reduced shelf bypassing and decreased proximity to the sediment sources during higher sea level (Haskell *et al.*, 1991).

4.3 Results

4.3.1 Planktonic $\delta^{18}O$ and Mg/Ca

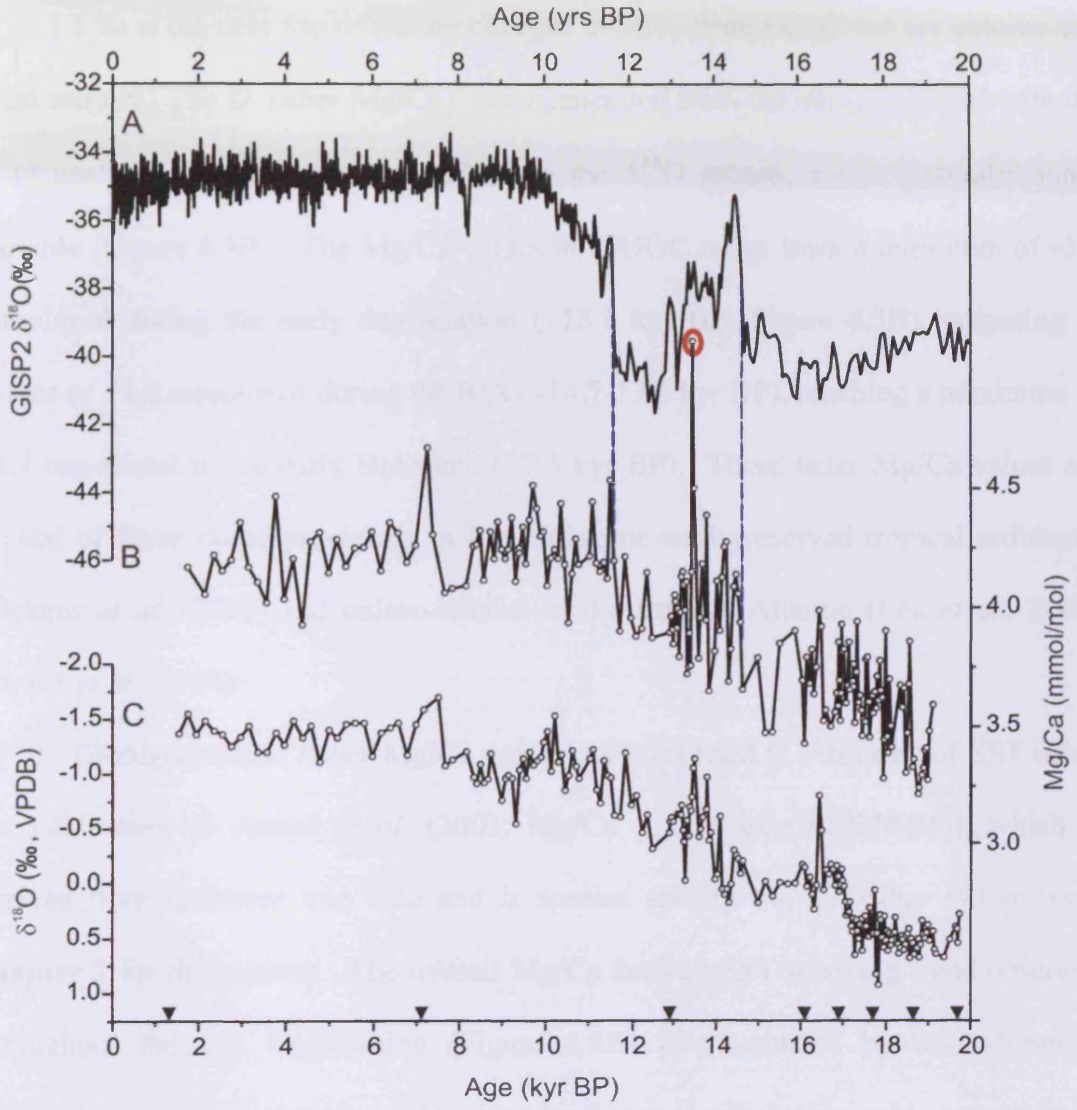

Figure 4.3: (A) Oxygen isotope record giving an indication of Greenland air temperature from the Greenland Ice Sheet Project 2 (GISP2; Grootes and Stuiver, 1997). Paired (B) Mg/Ca and (C) planktonic $\delta^{18}O$ records from the Blake Outer Ridge core KNR140/2-39GGC versus calendar age. Note that the $\delta^{18}O$ record extends further than the Mg/Ca record as there were insufficient specimens in these oldest samples for Mg/Ca analysis. Also shown are the depths of the 8 ^{14}C-AMS dates used to construct the age model (Keigwin and Schlegel, 2002; solid inverted triangles) in conjunction with tie points to the ice core record (GISP2; blue dashed lines; see text). The sample circled in red is thought to be anomalous (refer **Chapter 2, section 2.2.6.2** pg. 2-31) and is removed from the data set. VPDB-Vienna Pee Dee Belemnite.

The *G. ruber* $\delta^{18}O$ record is dominated by a long-term trend (Figure 4.3C) with values decreasing from ~ 0.5 ‰ at the end of the Last Glacial Maximum (LGM) to ~ -1.5 ‰ at the core top reflecting changes in SST, changing global ice volume and local salinity. The *G. ruber* Mg/Ca record generated from the samples paired with the $\delta^{18}O$ analyses shows many similarities to the $\delta^{18}O$ record, but is generally more variable (Figure 4.3B). The Mg/Ca values at 39GGC range from a minimum of ~3.2 mmol/mol during the early deglaciation (~18.8 kyr BP, Figure 4.3B) increasing to values of ~4.0 mmol/mol during the B/A (~14.7-13.5 kyr BP), reaching a maximum of ~4.7 mmol/mol in the early Holocene (~7.3 kyr BP). These latter Mg/Ca values are typical of those found previously in late Holocene well-preserved tropical sediments (Dekens *et al.*, 2002) and palaeo-studies in the tropical Atlantic (Lea *et al.*, 2003; Flower *et al.*, 2004).

Globigerinoides ruber Mg/Ca values are converted to estimates of SST using the calibration of Anand *et al.* (2003; Mg/Ca = 0.34 exp(0.102*SST)), which is derived from sediment trap data and is species specific for *G. ruber* (white) (**see chapter 2** for discussion). The overall Mg/Ca derived SST warming trend observed throughout the last deglaciation (Figure 4.4B) is punctuated by several multi-centennial to millennial-scale colder episodes that generally have a cold counterpart in the GISP2 ice core record (e.g. H1 and YD in Figure 4.4A). Precision and accuracy determined from replicate runs of a standard solution of Mg/Ca was found to be <0.3 % (1σ). Anand *et al.* (2003) suggest that due to uncertainties which derive from the Mg/Ca calibration used and errors in the method, a temperature estimate of ±0.5 °C should be place on all Mg/Ca-derived temperature estimates.

Figure 4.4 (next page): Deglacial multi-proxy comparison of records spanning the 20-0 kyr BP interval. (A) Oxygen isotope record giving an indication of Greenland air temperature from the Greenland Ice Sheet Project 2 (GISP2; Grootes and Stuiver, 1997). (B) Blake Outer Ridge sea surface temperatures (SST) based on Mg/Ca ratios from *G. ruber* (white) at site 39GGC. (C) Planktonic $\delta^{18}O$ record for site 39GGC based on G. ruber (white). (D) Calculated $\delta^{18}O_{sw}$ values based on paired $\delta^{18}O$ values and Mg/Ca ratios. (E) Calculated $\delta^{18}O_{sw}$ with the ice volume component removed, utilising the ice volume record of Lea *et al.* (2002). (F) Salinity estimates based on the ice volume corrected $\delta^{18}O_{sw}$ values using the modern subtropical gyre relationship and two possible Laurentide end-member compositions (see text). The ages of the ^{14}C-AMS dates (Keigwin and Schlegel, 2002) are shown as triangles and the additional tie points between 39GGC and GISP2 are shown as stars. Heinrich event 1 (H1) from 16.9-15.4 kyr BP is shaded along with the Younger Dryas (YD) from 13-11.6 kyr BP. The Bølling Ållerød (B/A) is also indicated from 15.4-13 kyr BP. VSMOW - Vienna Standard Mean Ocean Water. A 3 point running mean is shown by the bold line for each record.

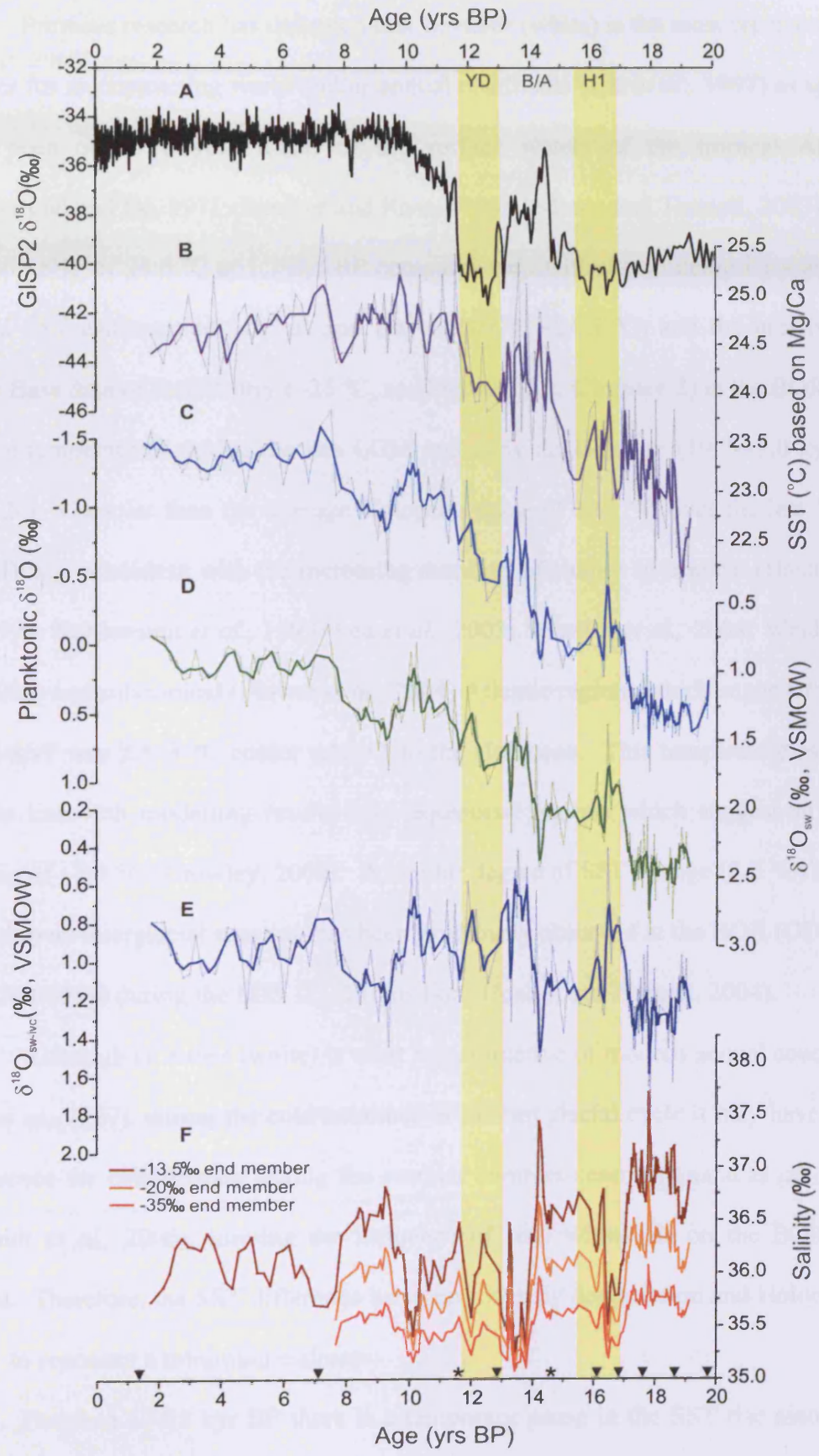

Figure 4.4 (continued above).

Previous research has indicated that *G. ruber* (white) is the most representative species for reconstructing warm and/or annual conditions (Lin *et al.*, 1997) as species have been observed year round in the surface waters of the tropical Atlantic (Tolderlund and Bé, 1971; Deusser and Ross, 1989; Tedesco and Thunell, 2003). The core top SST of 24.6 °C at 1.7 kyr BP compares well with the contemporary average annual SST estimates of Levitus and Boyer, (1994; ~24.5 °C) and the unpublished HydroBase data of Ruth Curry (~25 °C, see Figure 2.3A, **Chapter 2**) at the BOR. Sea surface temperatures during the late LGM and early deglaciation (19.7-17.0 kyr BP) were 2-3 °C cooler than the average Holocene value of 24.7 °C over the last 10 kyr BP. This is consistent with the increasing numbers of studies in tropical (Hastings *et al.*, 1998; Rühlemann *et al.*, 1999; Lea *et al.*, 2003; Schmidt *et al.*, 2004; Weldeab *et al.*, 2006) and subtropical (Flower *et al.*, 2004) Atlantic regions which suggest that the LGM SST was 2.5–3 °C cooler relative to the Holocene. This temperature range is also in line with modelling results from equatorial regions which suggest an LGM cooling of ~2.5 °C (Crowley, 2000). A similar degree of SST change (2-3 °C) from a glacial to an interglacial scenario has been previously observed at the BOR (ODP Leg 172, Site 1059) during the MIS 12/11 transition (Healey and Thunell, 2004).

Although *G. ruber* (white) is most representative of modern annual conditions (Lin *et al.*, 1997), during the cold extremes of the last glacial cycle it may have had a preference for calcification during the warmer summer season (Anand *et al.*, 2003; Schmidt *et al.*, 2006), limiting the influence of cold winter air on the BOR SST record. Therefore, the SST difference between the early deglaciation and Holocene is likely to represent a minimum estimate.

Between 17-15 kyr BP there is a temporary pause in the SST rise associated with the deglacial warming trend at the BOR. A 3-point running mean applied to the

data set reveals a transient cooling at the start (16.8-16.5 kyr BP) and end (15.1-15.8 kyr BP) of this interval of >0.5 °C (Figure 4.4B). This halt in the general warming trend at the BOR is thought to encompass the H1 ice rafting event and its associated meltwater surge at northerly latitudes (e.g. Bond *et al.*, 1992; Bard *et al.*, 2000; Hemming, 2004; The ^{14}C-AMS dates during and either side of the suspected H1 event allow confidence in the age model of core 39GGC during this time interval). The small cooling associated with start and end of H1, are similar in magnitude to previous records from the Cariaco Basin (Lea *et al.*, 2003), with a much larger counterpart in the subtropical NE Atlantic (Bard *et al.*, 2000). This supports previous modelling studies (e.g. Lohmann, 2003) that show the strongest temperature decrease occurred in sea ice covered regions and downstream along the eastern side of the subtropical gyre. Between the two cooling events at the ends of the H1 interval (16.5-15.8 kyr BP) is a SST warming of 1-0.5 °C, which appears to have a warm counterpart in the ice core record of GISP 2. This cold-warm-cold structure is in contrast to many other western tropical sites that have recorded increasing surface temperatures and asynchrony with the Greenland ice core records during H1 (Rühlemann *et al.*, 1999; Hüls and Zahn, 2000; Schmidt *et al.*, 2004; Flower *et al.*, 2004; Weldeab *et al.*, 2006).

The B/A is represented by a distinct warm, but variable SST regime at the BOR, again in contrast to many previous studies from the tropical western basin (Rühlemann *et al.*, 1999; Hüls and Zahn, 2000; Weldeab *et al.*, 2006; Schmidt *et al.*, 2004; Flower *et al.*, 2004). The B/A warming is rapidly followed by the YD (13.2-11.5 kyr BP), which is represented by a return to glacial temperatures in the northern North Atlantic (GISP2; Grootes and Stuiver, 1997). The 39GGC SST record suggests cooling also occurred above the BOR during the YD (Figure 4.4B), although

temperatures remain some 1-1.5 °C higher than those during the LGM and H1 intervals suggesting that the YD was not as severe in the subtropical North Atlantic as it was at northerly latitudes.

Sea surface temperatures reached peak values in the early Holocene of ≥24.5 °C at ~9.5 kyr BP i.e. the Holocene climatic optimum (HCO), which has previously been observed in the northern North Atlantic (de Vernal and Hillaire-Marcel, 2006; Andersen *et al.*, 2004) and the adjacent Western European mainland (Mangerud *et al.*, 1974), although the timing between different sites does not appear to be synchronous (e.g. Kaufman *et al.*, 2004). The sites that record maximum early Holocene temperatures are located along the axis of the Gulf Stream, as is core 39GGC, and may indicate a strong or warmer Gulf Stream during the early Holocene (de Vernal and Hillaire-Marcel, 2006). The HCO was followed by millennial-scale cooling (Marchal *et al.*, 2002; Andersen *et al.*, 2004; Moros *et al.*, 2004; Rimbu *et al.*, 2004), which coincides with a trend towards long-term cooling from the mid Holocene at the BOR. Furthermore, this cooling has been shown in the Nordic Seas to be instep with the decreasing Northern Hemisphere high latitude insolation since the early Holocene, indicating that Holocene climate evolution may indeed be largely orbitally driven (Bradley, 1990; Koç and Jansen, 1992, 1994; Andrews *et al.*, 1997; Andersen *et al.*, 2004). Embedded within this post HCO cooling is a significant increase in the planktonic $\delta^{18}O$ between 9.6-7.4 kyr BP, accompanied by a SST decrease of >0.5 °C (Figure 4.4B and 4.4C). This distinct cooling punctuating the Holocene may be consistent with a broad millennial-scale cooling previously documented in the northern North Atlantic, which encompasses the short duration 8.2 kyr Event (Rohling and Pälike, 2005; Ellison *et al.*, 2006).

Overall, core 39GGC exhibits SST changes (within the errors of our age model) that appear largely synchronous with the changes exhibited by GISP2 (Grootes and Stuiver, 1997) and the Cariaco Basin (Lea *et al.*, (2003) and are asynchronous to trends observed in most of the western (sub)tropical Atlantic (Rühlemann *et al.*, 1999; Hüls and Zahn, 2000; Schmidt *et al.*, 2004; Flower *et al.*, 2004; Weldeab *et al.*, 2006). It is only prior to H1 (19-16.8 kyr BP) that there is considerable asynchrony between the SST record from core 39GGC and the GISP2 ice core record, as SST at the BOR appear to be increasing during this interval, while the ice core record suggests slightly decreasing atmospheric temperatures.

4.3.2 The $\delta^{18}O$ of seawater

In order to reconstruct salinity variations, the $\delta^{18}O$ of the sea water ($\delta^{18}O_{sw}$) was isolated from the $\delta^{18}O$ of the planktonic (*G. ruber*, white) carbonate ($\delta^{18}O_c$), which reflects a combination of ice volume, SST and salinity variations. To achieve this, the temperature component of the $\delta^{18}O_c$ was removed using the Mg/Ca derived SST record. Importantly both $\delta^{18}O_c$ and Mg/Ca are measured on the same population of *G. ruber*, eliminating any temporal or spatial ambiguity in the controlling factors allowing us to compute $\delta^{18}O_{sw}$ directly (Schmidt *et al.*, 2006). Similarly to the work of Flower *et al.* (2004) on core EN32-PC6 in the GOM, the $\delta^{18}O_{sw}$ was calculated using a palaeotemperature equation based on cultured planktonic foraminifera *Orbulina universa* grown under high light (HL) conditions (Bemis *et al.*, 1998), which has also been shown to be appropriate for *G. ruber* (Thunell *et al.*, 1999):

$$SST = 14.9 - 4.8\ (\delta^{18}O_c - \delta^{18}O_{sw}) \qquad (1)$$

Where SST is in °C. The equation was rearranged to make $\delta^{18}O_{sw}$ the subject and 0.27 ‰ was added to convert the PDB scale to the Vienna Standard Mean Ocean

Water (VSMOW) scale. The HL rather than the low light (LL) equation was chosen in order to be consistent with the published record of Flower *et al.* (2004). It should be noted that the slope of both the HL and the LL *O. universa* equations is the same and only the y-intercept changes. The resulting $\delta^{18}O_{sw}$ record reflects a combination of global ice volume–controlled $\delta^{18}O_{sw}$ changes and salinity variations (Figure 4.4D). The global $\delta^{18}O_{sw}$ ice volume component was removed from the 39GGC $\delta^{18}O_{sw}$ dataset using the Cocos Ridge, eastern equatorial Pacific, $\delta^{18}O_{sw}$ record of Lea *et al.* (2002). Variation in the resultant $\delta^{18}O_{sw\text{-}ivc}$ record is thus directly attributable to variations in local salinity due to variations in the evaporation-precipitation (E-P) balance, meltwater input and advection (Flower *et al.*, 2004; Schmidt *et al.*, 2004). The deglacial $\delta^{18}O_{sw\text{-}ivc}$ record for core 39GGC (Figure 4.4E) reveals a number of low anomalies which can only readily be explained by a significant freshening of the surface ocean and most likely indicate advected meltwater signals from the various outlets surrounding the western Atlantic. Changes in the E-P balance may lead to salinity anomalies due to the southward migration of the Inter Tropical Convergence Zone (ITCZ) during the cool periods of the last deglaciation. Incorporating the analytical error of the Mg/Ca and the $\delta^{18}O_c$ analysis along with the error on the ice volume correction from the Cocos Ridge, the error on the $\delta^{18}O_{sw\text{-}ivc}$ estimates is in the region of 0.21 ‰. This is similar to previous error estimates made in the Gulf of Mexico (Flower *et al.*, 2004)

The residual $\delta^{18}O_{sw\text{-}ivc}$ is transformed to an estimate of the actual salinity (Figure 4.4F) using the modern $\delta^{18}O$-surface salinity relationship for the southwestern North Atlantic gyre for the last deglaciation (Schmidt *et al.*, 1999; Schmidt *et al.*, 2006), where:

$$\delta^{18}O_{sw\text{-}ivc} = 0.4 \times (\text{surface salinity}) - 13.5 \qquad (2)$$

As previously outlined by Schmidt *et al.* (2006), the conversion of the $\delta^{18}O_{sw}$ proxy to an estimate of salinity is difficult to constrain accurately as the slope of these two variables in the past is uncertain. During glacial times it is likely that a steeper slope was present due to the input of significant quantities of meltwater, which had a light but poorly constrained $\delta^{18}O$ signature. Therefore, two additional $\delta^{18}O_{sw\text{-}ivc}$ versus salinity relationships were derived for BOR surface waters, based on two possible Laurentide meltwater end-member compositions of -20 ‰ and -35 ‰ (Maslin *et al.*, 1995).

$$\delta^{18}O_{sw\text{-}ivc} = 0.58571 \times (\text{surface salinity}) - 20 \quad (3)$$

$$\delta^{18}O_{sw\text{-}ivc} = 1.01429 \times (\text{surface salinity}) - 35 \quad (4)$$

Modern day surface salinity at the BOR is 36.4-36.2 ‰ (Curry, unpublished HydroData, see Figure 2.3B, **Chapter 2**), which compares well with the computed average late Holocene (last 7 kyr) salinity of 36.1 ‰. There is a general decrease in salinity throughout the last deglaciation at the BOR equivalent to a maximum change of ~1.0-1.5 ‰ (Figure 4.4E and 4.4F), although it must be noted that *G. ruber* may sink to the subsurface to avoid the lowest salinities (Spero and Williams, 1991). The first significant salinity excursion in the record occurs at ~17-16.4 kyr BP, and is represented by a decrease in $\delta^{18}O_{sw\text{-}ivc}$ of > 0.8 ‰ (a salinity decrease of ~1.5 ‰). This low salinity event is not seen in the other (sub)tropical Atlantic records (Flower *et al.*, 2004; Schmidt *et al.*, 2004; Weldeab *et al.*, 2006) and is likely to be coincident with the onset of H1 in the North Atlantic. This is followed by increased salinity values that last throughout the later stages of H1 and into the B/A. A second salinity decrease (>2 ‰) is observed during the late B/A ~14 kyr BP, some 1.5 kyr later than the initiation of the large salinity minimum in the record of core EN32-PC6 (Flower *et*

al., 2004), which is suggested to result from increased meltwater delivery to the GOM via the Mississippi. Following the B/A, the salinity and $\delta^{18}O_{sw\text{-}ivc}$ records at core 39GGC are similar to the Caribbean $\delta^{18}O_{sw\text{-}ivc}$ record of VM28-122 (11°34'N, 78°25'W; 3,623 m; Schmidt *et al.*, 2004). The YD is represented by a small salinity increase, which is similar in both structure and timing to a YD $\delta^{18}O_{sw\text{-}ivc}$ record from core JPC26 in the Florida Straits (Schmidt *et al. in prep*) followed by a short-lived decrease in salinity, which is similar in both timing and magnitude to the salinity changes recorded in VM28-122 (Schmidt *et al.*, 2004) in the Caribbean. A further millennial-scale increase in salinity is noted during the early Holocene between 9.6-7.7 kyr BP that coincides with a positive planktonic $\delta^{18}O_c$ excursion.

4.4 Discussion

4.4.1 Deglacial sea surface temperature changes on the BOR

Modelling experiments have revealed that an increased flux of freshwater to the sites of NADW formation causes a decrease in deepwater formation, resulting in a disrupted MOC and reduced meridional heat transport with cooling in the northern North Atlantic and warming in the southern South Atlantic (e.g. Ganopolski and Rahmstorf, 2001; Knutti *et al.*, 2004). During H1 and the YD, proxy evidence from the northern North Atlantic (GISP2; Grootes and Stuiver, 1997), the Iberian Margin (Bard et al., 2000) and regions such as the Cariaco Basin (Lea *et al.*, 2003) have revealed a dramatically cooler climate compared with the present day and there is considerable proxy evidence linking this cooling to a substantial slowing down of the MOC (e.g. Duplessy *et al.*, 1988; Curry *et al.*, 1988; Elliot *et al.*, 2002; McManus *et al.*, 2004; Gherardi *et al.*, 2005; Robinson *et al.*, 2005; Hall *et al.*, 2006 see also, **Chapter 5**). In turn, this MOC slow down has been linked to heat retention and a

resultant warming at tropical and subtropical latitudes (Rühlemann *et al.*, 1999; Huls and Zahn, 2000; Flower *et al.*, 2004; Schmidt *et al.*, 2004; Weldeab *et al.*, 2006; Figure 4.5B and 4.5C). Periods of rapid tropical warming during the last deglaciation have been presented as evidence of the modulation of climate on millennial timescales by the MOC (Flower *et al.*, 2004). The results from this study, however, are complex, suggesting a general synchronicity between the surface waters at the subtropical BOR and Greenland air temperatures following the initiation of H1 (Figure 4.4A and 4.4B). Prior to H1 (19-16.8 kyr BP) however, there is a slight warming (~1.5°C) at the BOR coincident with a cooling of Greenland air temperatures (Grootes and Stuiver, 1997) and a slowing down of the MOC (McManus *et al.*, 2004; Hall *et al.*, 2006; see **Chapter 5**). Although still in the subtropics, core 39GGC is further north than any of the other previously studied deglacial core sections from (sub)tropical sites (Rühlemann *et al.*, 1999; Hüls and Zahn, 2000; Schmidt *et al.*, 2004; Flower *et al.*, 2004; Weldeab *et al.*, 2006) and lies on the boundary of the expected northwards extent of heat retention in the North Atlantic during MOC reductions. The data suggest that the influence of increased heat storage as a result of a weaker MOC was largely confined to more southerly latitudes, having a smaller influence on the BOR (Figure 4.4). Recent evidence indicates that the Gulf Stream flow was largely confined within the Florida Straits during glacial times (LeGrande and Lynch-Stieglitz, 2007) and its transport was about two-thirds lower during the LGM (15-18 Sv) than the present day (30-32 Sv; Lynch-Stieglitz *et al.*, 1999) and as such would have trapped heat in the (sub)tropics and transported less heat northwards. The possible effects of such heat retention at the BOR are seen during the early deglacial (19-16.8 kyr BP) warming at 39GGC. This warming trend occurs earlier (~2 kyr) than that previously observed in the (sub)tropical Atlantic (Figure 4.5; Flower *et al.*,

2004; Schmidt *et al.*, 2004) and may result from heat retention in the (sub)tropics earlier than previously recorded in the lower resolution records of core EN32-PC6 (Flower *et al.*, 2004) and core VM28-122 (Schmidt *et al.*, 2004) influencing as far north as the BOR until the onset of H1. It can not be ruled out however, that the early deglacial rise in SST is a reflection of increased Gulf Stream influence at the BOR, feeding enhanced intermediate-depth NADW convection (see **Chapter 5**).

An additional factor at the BOR is the fact that the study site at the present day lies under the flow path of the Gulf Stream. Shifts in the position or disappearance of the Gulf Stream during the last deglaciation could also result in significant changes in SST at the BOR, which would be superimposed on the small effects of heat retention in the region. The Gulf Stream contains significant horizontal gradients in both temperature and salinity, although shifts in these lateral gradients are suggested to have a minimal effect on the palaeo records from core 39GGC. This is because a sediment record under such an energetic surface, intermediate and deepwater circulation must receive a population of foraminifera tests that represents an average of a reasonably large surface area and not just the water lying directly overhead, reducing the influence of lateral gradients in the proxy records. Figure 3.5 (**Chapter 3**) shows that the average planktonic $\delta^{18}O$ values along the Blake Ridge crest are very similar in the cores spanning a depth range of ~1,000 m either side of core 39GGC during both the Holocene and the LGM, suggesting that the effect of latitudinal gradients within the Gulf Stream on the proxy records was small. Even the largest planktonic $\delta^{18}O$ gradient during the Holocene of ~0.5 ‰ along the BOR crest covering a depth transect of ~4,000 m (Figure 3.5) is relatively small in comparison to the large planktonic $\delta^{18}O$ changes recorded in core 39GGC with time (Figure 4.4C). LeGrande and Lynch-Stieglitz (2007) have suggested that core KNR140/2-22JPC

(28°15.0'N, 74°24.0'W; 4,712 m water depth) located south east of the BOR (Figure 4.1), was outside the Gulf Stream recirculation cell during the LGM, but inside the recirculation cell at present, implying both a shift in glacial wind patterns and a potential northward migration of the recirculation cell, which could also have occurred during H1 and the YD, lowering SST above the BOR. However, core 39GGC is unlikely to be sufficiently offshore (unlike 22JPC) to lie outside the influence of the Gulf Stream at any one time in the last glacial-interglacial cycle. Low SST during H1 and the YD are likely to result from a significant decrease in the strength/heat transport of the Gulf Stream. It is likely that the warming at the initiation of the B/A (~14.7 kyr BP) results from a reinvigoration of the Gulf Stream transporting warm water from the tropics, raising SST at core 39GGC on its journey north.

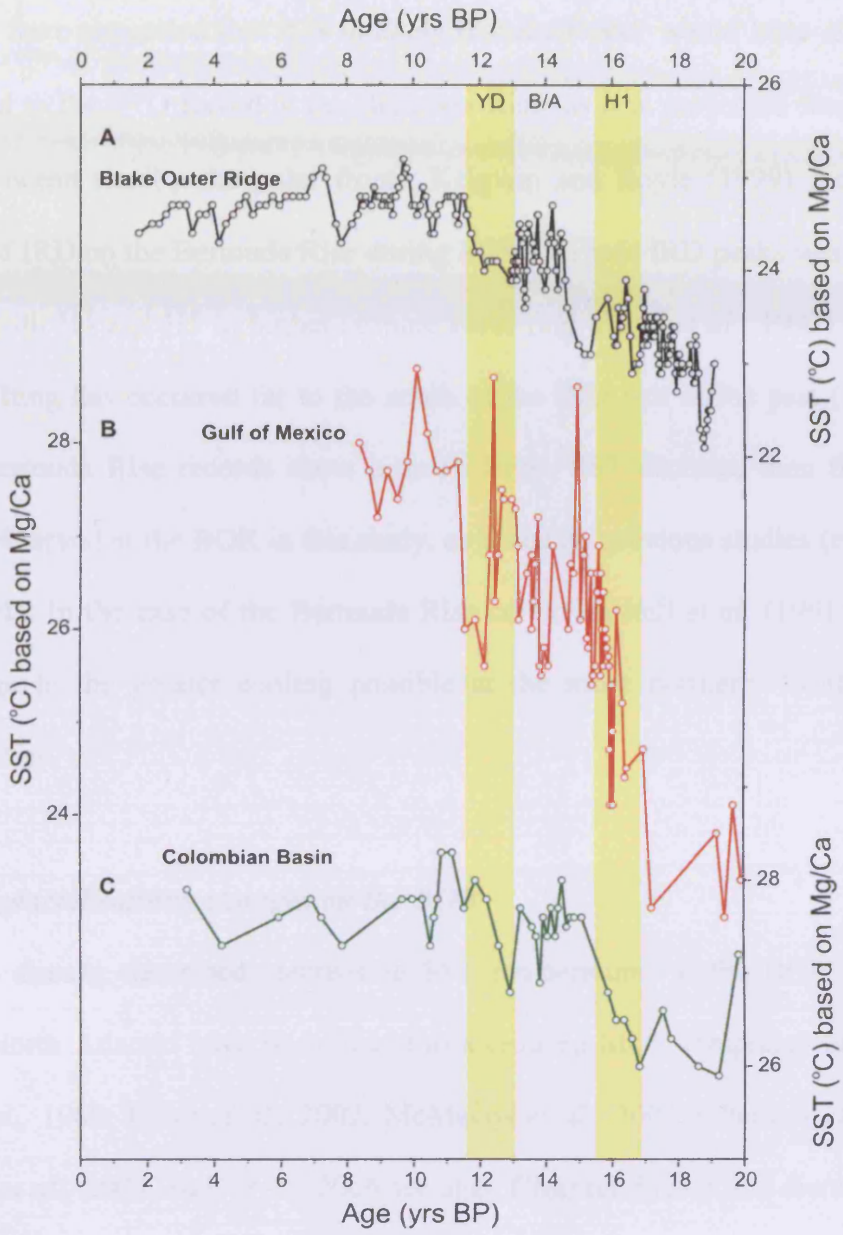

Figure 4.5: (A) Mg/Ca derived sea surface temperature record from core KNR140/2-39GGC on the Blake Outer Ridge; (B) Mg/Ca derived sea surface temperature record from core EN32-PC6 in the Gulf of Mexico (Flower *et al.*, 2004); (C) Mg/Ca derived sea surface temperature record from core VM28-122 in the Columbian Basin in the Caribbean (Schmidt *et al.*, 2004). The areas shaded yellow represent Heinrich Event 1 (H1) and the Younger Dryas (YD) cooling.

Nearby planktonic $\delta^{18}O$ records from the Bermuda Rise (McManus *et al.*, 2004) also show increasing values coinciding with the initiation of H1 (and the YD), suggesting a SST decrease of up to 4 °C from the LGM to H1. Although Keigwin *et*

al. (1991) have suggested that it is unlikely that meltwater would have significantly contributed to the $\delta^{18}O$ record at the Bermuda Rise (as it is prevented from reaching this open ocean site by the polar front). Keigwin and Boyle (1999) recorded two intervals of IRD on the Bermuda Rise during MIS 3. These IRD peaks were shown to correlate with H4 and H5 in higher latitude cores (e.g. Bond *et al.*, 1993) suggesting that ice rafting has occurred far to the south of the IRD belt in the past (Ruddiman, 1977). Bermuda Rise records show a much larger SST decrease than the ~0.5 °C decrease observed at the BOR in this study, as noted by previous studies (e.g. Haskell *et al.*, 1991). In the case of the Bermuda Rise cores, Haskell *et al.* (1991) attributed this change to the greater cooling possible at the more northerly location of the Bermuda Rise.

4.4.2 Deglacial salinity changes on the BOR

As already described, decreasing SST temperatures at the BOR and in the northern North Atlantic have been linked to a reduced MOC (Duplessy *et al.*, 1988; Curry *et al.*, 1988; Elliot *et al.*, 2002; McManus *et al.*, 2004; Gherardi *et al.*, 2005; Robinson *et al.*, 2005; Hall *et al.*, 2006 see also, **Chapter 5**) and this disrupted MOC may have been caused by varying meltwater inputs into the North Atlantic (Broecker *et al.*, 1988; Maslin *et al.*, 1995) leading to the abrupt climate changes that punctuated the last glacial to interglacial cycle. Duplessy *et al.* (1992) have shown the complex nature of delineating such changes in the subtropical North Atlantic. Here, changes in salinity can also result from changes in the hydrological cycle, in addition to the potential influence of meltwater inputs and variations in the strength of the MOC throughout the deglaciation. Previous Mg/Ca-derived salinity investigations have used sediment cores from the Caribbean (VM28-122; Schmidt *et al.*, 2004; Figure

4.5C) to investigate the combined effect of hydrological changes in the western tropical Atlantic and changes in the rate of the MOC. The net E-P balance during a reduced MOC regime is significantly larger at VM28-122 than at core 39GGC according to modelling experiments (Zhang and Delworth, 2005; Figure 4.6) and therefore salinity changes due to hydrological changes in the Caribbean core VM28-122 represent the maximum that could be experienced at core 39GGC. Core VM28-122 is also far removed from any North Atlantic meltwater sources and therefore comparison of core 39GGC with core VM28-122 should allow the delineation of what is likely to be meltwater influence at our site. Further comparison of core 39GGC with core EN32-PC6 from the GOM (Figure 4.5B), which has been previously used to map the meltwater outflow from the Mississippi River (Flower *et al.*, 2004) may give an indication of the source of meltwater pulses at core 39GGC.

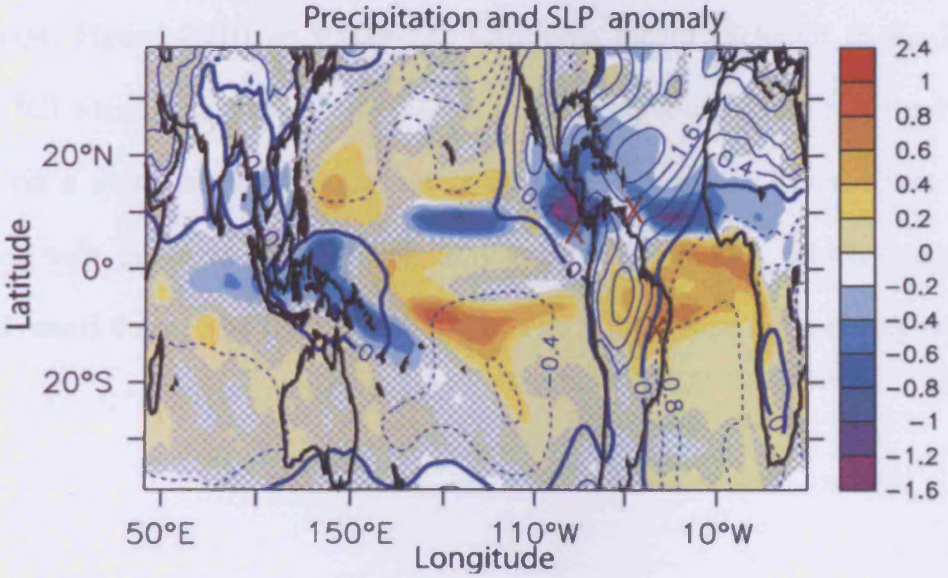

Figure 4.6: Results from the coupled model using the OGCM (Zhang and Delworth, 2005) during an MOC shutdown simulation showing the annual mean precipitation anomaly (m yr^{-1}). The blue contour is the annual mean sea level pressure (SLP) anomaly with an interval of 0.4 hPa.

During H1 freshwater released by melting icebergs, caused a reduction in surface salinities in the northern North Atlantic which resulted in lower surface densities leading to a decrease in deepwater production via convection (Maslin *et al.*, 1995; Vidal *et al.*, 1997; Zahn *et al.*, 1997; Broecker, 2000) and a disrupted MOC (Boyle and Keigwin, 1987; McManus *et al.*, 2004; Hall *et al.*, 2006, **Chapter 5**). The major source of the icebergs and resulting meltwater pulse responsible for H1 is the LIS (Andrews and Tedesco, 1992; Bond *et al.*, 1992; Bond and Lotti, 1995). The freshening of the ocean surface recorded at core 39GGC, which starts at ~17 kyr BP and lasts until ~16.3 kyr BP (Figure 4.4F and Figure 4.7), corresponds with the inception of H1, i.e. 16.8 kyr BP (Bond *et al.*, 1992; Bard *et al.*, 2000; Hemming *et al.*, 2004). All three cores in Figure 4.7 have well constrained age models around the H1 interval. This allows confidence in the conclusion that the low salinity event at core 39GGC on the BOR has no counterpart in the EN32-PC6 GOM record (Flower *et al.*, 2004; Figure 4.7B) or VM28-122 Caribbean record (Schmidt et al., 2004; Figure 4.7C) suggesting that it represents a meltwater pulse delivered to the North Atlantic via a more northerly outlet rather than the Mississippi River. This is in agreement with previous studies such as Clarke *et al.* (2001), which suggested increased runoff through both the Hudson River and St Lawrence River during H1.

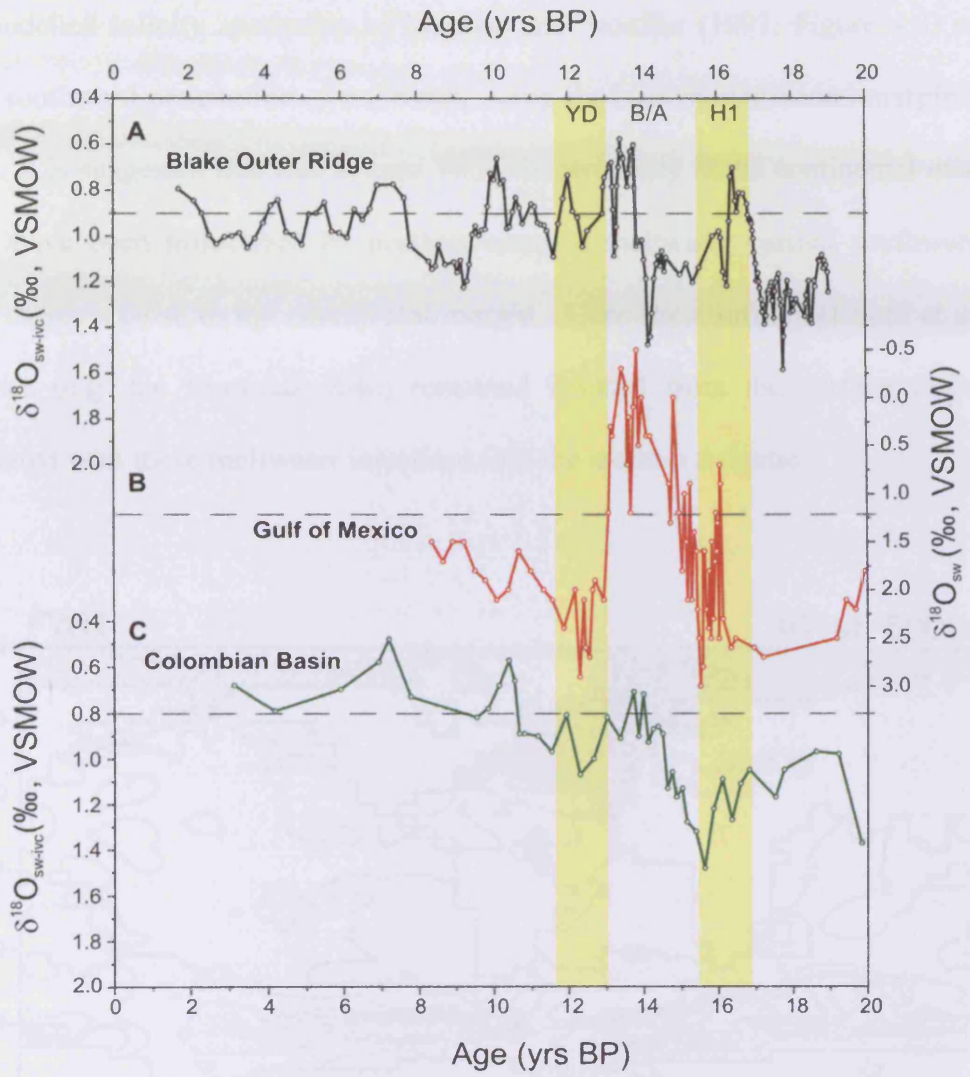

Figure 4.7: (A) Ice volume corrected $\delta^{18}O_{sw}$ record from the Blake Outer Ridge. (B) $\delta^{18}O_{sw}$ record from the Gulf of Mexico (Flower *et al.*, 2004). (C) Ice volume corrected $\delta^{18}O_{sw}$ record from the Columbian Basin in the Caribbean (Schmidt *et al.*, 2004). The areas shaded yellow represent Heinrich Event 1 (H1) and the Younger Dryas (YD) cooling. Dashed lines represent the modern day $\delta^{18}O_{sw}$ at the sites. Note the Gulf of Mexico record is not on the same scale.

Some previous work in the western North Atlantic has suggested that the input of large amounts of freshwater at northerly latitudes did not spread to subtropical latitudes, being restricted by the southerly position of the polar front (Ruddiman and McIntyre, 1981; Keigwin *et al.*, 1991). However, close inspection of

the modelled salinity anomalies of Manabe and Stouffer (1997; Figure 4.8) reveals some southward penetration of meltwater along the eastern continental margin of the USA. It is suggested that due to core 39GGCs proximity to the continental margin it could have been influenced by northern-sourced meltwater carried southwards by slope currents close to the continental margin. Core sites further offshore at similar latitudes (e.g. the Bermuda Rise) remained isolated from the surface freshening associated with these meltwater injections into the western Atlantic.

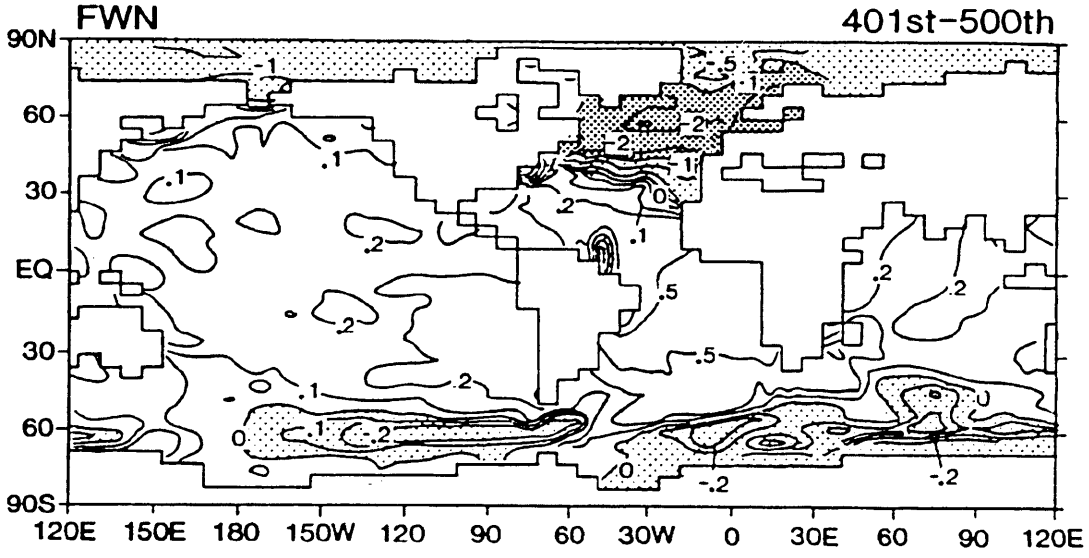

Figure 4.8: From Manabe and Stouffer (1997). The geographical distribution of the sea surface salinity (SSS) anomalies (psu) averaged over the 401st-500th year of the Fresh Water Experiment, North (FWN). Here the anomaly represents the difference between the FWN and the control experiment (simulated modern state of the coupled ocean-atmopshere system). Contours are drawn in logarithmic intervals for values of 0, ±0.1, ±0.2, ±0.5, ±1, ±2.

Meltwater input during H1 is responsible for stabilising the water column in the regions of deepwater formation and reducing the MOC leading to salinity and temperature build up in many tropical regions (Rühlemann *et al.*, 1999; Hüls and

Zahn, 2000; Schmidt *et al.*, 2004, Weldeab *et al.*, 2006; Flower *et al.*, 2004). The reinvigoration of the MOC at the start of B/A is represented in the tropics by a decrease in salinity as the highly saline water is exported northwards (Schmidt *et al.*, 2004; Figure 4.7C). A similar salinity and associated $\delta^{18}O_{sw\text{-}ivc}$ increase is recorded at core 39GGC following the initial meltwater pulse of H1 (~15.9 kyr BP), and lasted until the latter stages of the B/A (~14 kyr BP). This increase in salinity was the likely effect of (i) the removal of the influence of the meltwater pulse at the BOR associated with H1 and (ii) changes in the hydrological cycle which accompany the transition from a significantly reduced to an increasingly active MOC. Modelling studies have revealed the presence of a small evaporation excess in the region of the BOR during a potential MOC shut down (Zhang and Delworth, 2005, Figure 4.6). The evaporation excess is the likely result of a southwards migration of the ITCZ during the cold intervals of H1 and the YD (Peterson *et al.*, 2000; Lea *et al.*, 2003; Wang *et al.*, 2004), triggered by reduced northward heat transport that altered the tropical Atlantic SST field (Lund *et al.*, 2006). Speleothem records from a currently semi-arid region of the tropical northeastern Brazil record wetter conditions during Heinrich intervals consistent with a southwards shift in the ITCZ (Figure 4.9). This migration of the ITCZ caused a southward shift in the Hadley cell and may have accentuated the net evaporation compared with the modern North Atlantic. The associated reduction in precipitation has also been linked to salinity enrichments of 0.7-1.5 ‰ at nearby Site 1060 at the BOR during MIS 3 stadials (Schmidt *et al.*, 2006), suggesting that hydrological changes have had a significant influence in the region throughout the last glacial cycle. The salinity build up apparent above the BOR during the latter stages of H1 is not as large as that recorded by core VM28-122 in the tropical Caribbean (Schmidt *et al.*, 2004; Figure 4.7) where the net E-P change was expected to be much

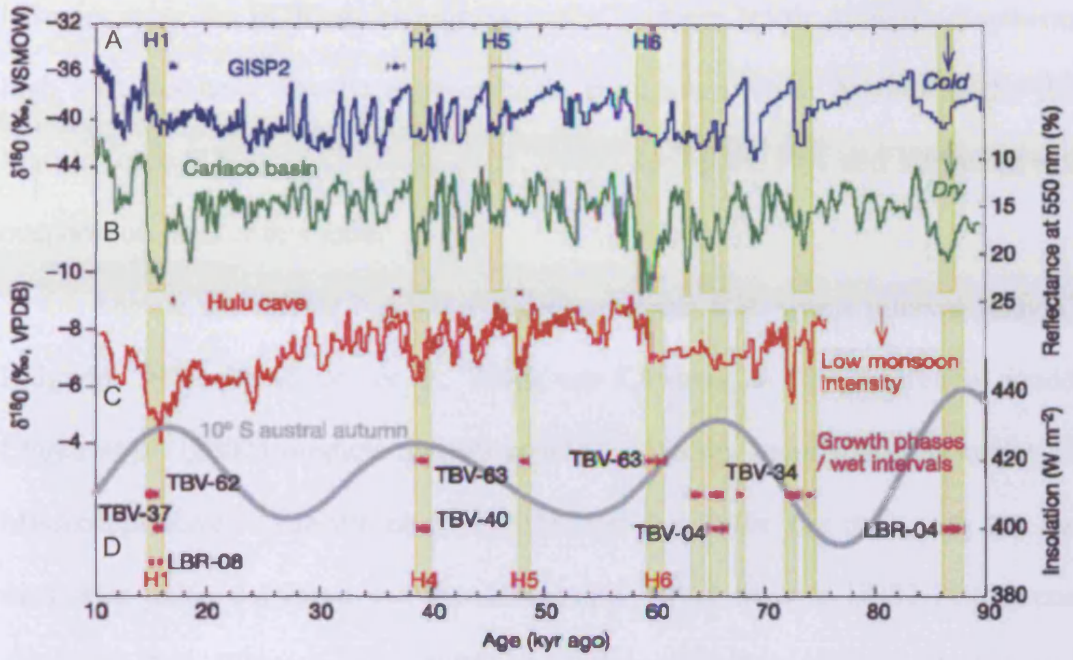

Figure 4.9: Comparison of the growth patterns of speleothems from northeastern Brazil with events recorded in several Northern Hemisphere palaeoclimate archives (taken from Wang *et al.*, 2004). (A) $\delta^{18}O$ values of Greenland ice (Grootes and Stuiver, 1997). (B) Light colour reflectance (greyscale) of the Cariaco basin sediments from ODP Hole 1002C (Peterson *et al.*, 2000). (C) $\delta^{18}O$ values of Hulu cave stalagmites (Wang *et al.*, 2001). (D) Speleothem growth patterns in northeastern Brazil. Growth intervals are shown by separated pink dots or connections between dots if they are within the same phase (Wang *et al.*, 2004). 2σ dating errors (error bars) are typically 0.5–1%. Yellow vertical bars indicate possible correlations between four records. Also shown are dating errors for the GISP2 ice core (blue bars; Meese *et al.*, 1997) and Hulu cave speleothems (red bars; Wang *et al.*, 2001), and 10 °S austral autumn insolation (grey line; Berger and Loutre, 1991). VSMOW, Vienna standard mean ocean water. VPDB, Vienna PeeDee Belemnite. H1, H4, H5, H6, Heinrich events.

larger (Zhang and Delworth, 2005). A similar, although less extreme, situation is also apparent during the YD when there is a slow down in the MOC coincident with a small salinity increase at core 39GGC.

This salinity excess at the end of H1 is likely to have been maintained and maybe even accentuated in the early B/A by the reinvigoration of the MOC. This led to decreasing salinity in the Caribbean (Schmidt *et al.*, 2004; Figure 4.7C), and enabled the Gulf Stream to transport high salinity waters, originating from the low

latitudes, over the BOR on its journey to the northern North Atlantic. Furthermore, high salinities have also been observed in the eastern North Atlantic at the Iberian Margin (core SU81-18; Duplessy *et al.*, 1992) during the B/A and attributed to high evaporation rates at this time.

During the strong NADW formation of the B/A warm interval (Boyle and Keigwin, 1987; McManus *et al.*, 2004; see **Chapter 5**), the theoretical model of Clarke *et al.* (2002) predicts meltwater routing via the more southerly outlet of the Mississippi River. Flower *et al.* (2004) find this to be the case with the largest meltwater pulse delivered via the Mississippi River to core EN32-PC6 occurring during the B/A (Flower *et al.*, 2004) and is represented by increasingly low surface salinity values throughout the B/A. Initially during the early B/A, this meltwater pulse has no counterpart at the BOR, suggesting that it is unlikely that it reached the open ocean as an intact low salinity pulse. This meltwater is believed to have entered the GOM in a hyperpycnal manner (Aharon, 2006), and the resultant strong mixing with seawater would have reduced its influence on the salinity profile at the BOR and ultimately therefore on NADW formation (Tarasov and Peltier, 2005; Aharon, 2006). It was only when the discharge into the GOM reached its maximum did a low salinity/low $\delta^{18}O_{sw\text{-}ivc}$ signal register at the BOR ~13.9 kyr BP. This event has lower $\delta^{18}O_{sw\text{-}ivc}$ (0.7-0.4 ‰) values than the modern day $\delta^{18}O_{sw}$ (1.0-0.8 ‰; Schmidt *et al.*, 1999) at the BOR, suggesting that it results from a considerable injection of relatively freshwater at the site. The timing of the meltwater anomaly at the BOR is similar (within the constraints of the age model) to the recent timing for MWP-1a (14.1-13.6 kyr BP) proposed by Stanford *et al.* (2006). There has been considerable debate surrounding the origin of MWP-1a with some studies ruling out a Northern Hemisphere source, advocating instead an Antarctic origin (Clarke *et al.*, 2002;

Weaver *et al.*, 2003). This is derived from the notion that the addition of meltwater to the surface of the Southern Ocean would have caused the process of Antarctic Deep water (AABW) and Antarctic Intermediate Water (AAIW) production to decrease, resulting in an intensification of NADW formation, warming the Northern Hemisphere. However, Peltier (2005) has recently shown that observations of sea level rise at Barbados (Fairbanks, 1989; Bard *et al.*, 1990) and the Sunda Shelf (Hanebuth *et al.*, 2000) at the time of MWP-1a can be recreated in the Ice-4G model using a Northern Hemisphere origin for MWP-1a. Furthermore MWP-1a occurred during the summer seasonal insolation maximum in the Northern Hemisphere and minimum in the Southern Hemisphere (Peltier, 2005), which is more conducive to increased ice ablation and instability in the Northern Hemisphere. The data presented in this study suggest that MWP-1a had, at least in part, a Northern Hemisphere origin, as a low salinity pulse is detected at core 39GGC coincident with the lowest salinities recorded in core EN32-PC6 (Figure 4.7B). This further suggests that at least part of the Northern Hemisphere component of MWP-1a originated from meltwaters routed via the Mississippi River into the GOM. Stanford *et al.* (2006) also suggest a brief slow down in circulation in the northern North Atlantic associated with MWP-1a, although previous lower resolution records from the Rockall Trough (core site NA87-22) near to the sites of LNADW formation show no meltwater influence at this time (Duplessy *et al.*, 1992). Irrespective of whether it caused a brief slow down in the MOC, it is likely that meltwater discharged via the Mississippi River was responsible for 'priming' the North Atlantic ready for the smaller pulses of meltwater delivered via the eastern outlets, thought to be responsible for the YD cooling (Keigwin *et al.*, 1991).

The onset of the YD cold interval at 13.0 kyr BP coincided with the diversion of drainage from the Mississippi River to the St. Lawrence River as the ice margin retreated out of the Lake Superior basin (Broecker *et al.*, 1989). This coincided with an increase in the $\delta^{18}O_{sw\text{-}ivc}$ and resultant salinity at the BOR along with a depression of SST, in contrast to the highly saline and warm tropics (Rühlemann *et al.*, 1999; Hüls and Zahn, 2000; Schmidt *et al.*, 2004; Flower *et al.*, 2004; Weldeab *et al.*, 2006) during the YD. As described above the apparent warming in the western tropical basin coincident with northern North Atlantic cooling (Grootes and Stuiver, 1997) suggests heat and salt retention in the low latitudes. The small increase in the $\delta^{18}O_{sw\text{-}ivc}$ and salinity at the BOR to values similar to the late Holocene suggests that this increase is largely a result of the removal of meltwater input to the area combined with a small increase in evaporation caused by changes in the tropical hydrological cycle. Previous studies have shown that the reduction in the MOC may not have been as great during the YD as during H1, with a vigorous but shallow overturning (<2,300 m water depth; Keigwin, 2004; McManus *et al.*, 2004) and therefore changes in the hydrological cycle may have been more subdued.

The early Holocene is marked by a significant salinity/$\delta^{18}O_{sw\text{-}ivc}$ increase between 9.5-7.5 kyr BP (Figure 4.4 and 4.7) indicating this period may have been unstable with continued rearrangements of the surface hydrography. This period also spans the brief 8.2 kyr event that has been previously documented in the northern North Atlantic (O'Brien *et al.*, 1995; Risebrobakken *et al.*, 2003; Moros *et al.*, 2004; Rohling and Pälike, 2005; Ellison *et al.*, 2006). The long duration of the event in core 39GGC results from a lack of firm age control during the earliest Holocene. However, recent evidence suggests that the more sudden climate anomaly around 8.2 kyr BP appears superimposed on a longer-term cooling (Rohling and Pälike, 2005;

Ellison *et al.*, 2006) and it is this broader anomaly that is likely to be controlling the salinity signal observed at the BOR. Rohling and Pälike (2005) demonstrate the season-specific nature of these two anomalies, identifying the sharp 8.2 kyr event anomaly as a winter phenomenon and the broader anomaly as a summer phenomenon. The planktonic foraminifera, *G. ruber*, used to reconstruct SST and $\delta^{18}O_{sw\text{-}ivc}$ at the BOR, as discussed previously in this chapter, reflect annual/warm conditions and are therefore more likely to be representative of the broad anomaly, which is characteristic of summer conditions. The suggestion that core 39GGC is recording the broad anomaly rather than a poorly constrained 8.2 kyr event is supported by a similar duration increase in salinity in the Caribbean core VM28-122 at this time (Schmidt *et al.*, 2004; Figure 4.4C). This broad anomaly is part of a repeating pattern of climate deteriorations during the Holocene, which seem to be related to solar output fluctuations (Bond *et al.*, 2001). There is also a broad multi-peak low in Ti percentages between 8.4 and 7.75 kyr BP in the Cariaco basin, which reflects increased aridity due to reduced northward migration of the ITCZ in summer (Haug *et al.*, 2001). A southerly position of the ITCZ has already been shown to lead to enhanced evaporation in the region of the BOR resulting in increased salinity due to changes in the hydrological cycle.

4.5 Conclusions

It is clear that the (sub)tropical oceans have played a key role in the last glacial–interglacial climate transition with core 39GGC, on the BOR located on the northern boundary of heat and salt retention in the (sub)tropics. Sea surface temperatures at the BOR were primarily affected by the strength of the Gulf Stream during the last deglaciation, in addition to the effects of heat retention in the tropical

Atlantic prior to H1. Salinity reconstructions at the BOR reflect a combination of meltwater inputs, hydrological changes and variations in the MOC. Comparison with other core sites has allowed the separation of these different influences at the BOR to be attempted. The salinity reconstruction at core 39GGC shows the presence of a number of meltwater signals that can be traced to both the southern and eastern outlets of the LIS. A low salinity anomaly during H1 suggests meltwater from the eastern outlets can reach as far south as the BOR probably as a result of its proximity to the coast. It is shown that during the latter stages of the B/A a meltwater signal influences the BOR from the GOM consistent with a Northern Hemisphere origin for at least part of MWP-1a which may have 'primed' the North Atlantic ready for the YD. The results suggest that both the tropical hydrological cycle and meltwater inputs to the North Atlantic play a direct role in regulating rapid climate change.

Chapter 5: Divergent deepwater flow speed changes in the subtropical North Atlantic during the last deglaciation[1]

Abstract

Climate fluctuations during the last deglaciation have been linked to changes in North Atlantic Meridional Overturning Circulation (MOC) through its modulation of northward marine heat transport. Consequently, much research into the causes of rapid climate change has focused on the northern North Atlantic as the presumed primary driver of global ocean circulation. The production of cold, deep waters in the Southern Ocean is an important factor in the Earth's heat budget, but the involvement of deep Southern Source Water (SSW) in deglacial climate change has yet to be fully established. Here, the terrigenous silt grain size data from two ocean sediment cores retrieved from the western subtropical North Atlantic are used to reconstruct past changes in the speed of deepwater flow. The first core site is located under the influence of Lower North Atlantic Deep Water (LNADW), and is representative of changes in the MOC. The second core site is close to the modern boundary between LNADW/SSW and is therefore ideally positioned to detect changes in SSW delivery to the North Atlantic. There is evidence for a broad-scale divergence in flow speed changes at the two sites, with the presence of a vigorous, but poorly ventilated SSW mass at ~4,200 m water depth during the cold episodes of the last deglaciation when shallower (2,975 m water depth) grain size and geochemical data suggest that Northern Source Water was suppressed. This supports the notion of a bipolar see-saw.

[1]Submitted to *Paleoceaography Currents* as
Evans, H. K., I. R. Hall and L. D. Keigwin, Divergent deepwater flow speed changes in the subtropical North Atlantic during the last deglaciation

5.1 Introduction

Records from Greenland ice cores have revealed that the last deglaciation was punctuated by several millennial-scale climate events (Alley *et al.*, 1993; Chappellaz *et al.*, 1993; Blunier and Brook 2001), but the role of the deep ocean in these events remains uncertain (e.g. McManus *et al.*, 2004; Robinson *et al.*, 2005). As the deep ocean is one of the largest reservoirs of heat and carbon in the climate system, changes in the Meridional Overturning Circulation (MOC) are likely to have played a central role in controlling rapid climatic variations (Broecker *et al.* 1985; Clark *et al.*, 2002 and references therein). The MOC is characterized by the sinking of oxygenated and nutrient-depleted North Atlantic Deep Water (NADW), formed when northwardly advected surface waters release their heat in the Norwegian-Greenland (Mauritzen, 1996) and Labrador (Dickson and Brown, 1994) Seas. These waters are entrained by the southwards flowing Deep Western Boundary Current (DWBC) with an outflow of about 20 Sv (10^6 m^3 s^{-1}) (Schmitz and McCartney, 1993), which is progressively undercut by nutrient enriched Southern Source Water (SSW) inflowing via the southwest Atlantic. In the modern western North Atlantic NADW is mainly confined above the 4,000 m isobaths (Stahr and Sanford, 1999), while a greater proportion of re-circulated SSW resides at depth (Hogg, 1983; Figure 5.1). The behaviour of NADW during the last glacial cycle has been investigated at many sites (e.g. Boyle and Keigwin, 1985; Marchitto *et al.*, 1998; Raymo *et al.* 2002), but the history of SSW in the North Atlantic remains relatively unstudied. During the Last Glacial Maximum (LGM) geochemical tracers from marine sediments have revealed that the boundary between Northern Source Water (NSW) and SSW shoaled to ~2,000 m in the western North Atlantic (Oppo and Lehman, 1993; Keigwin, 2004, Curry and Oppo, 2005) and the transition from the LGM to the modern state was marked by a

series of changes in the deep-ocean circulation (Boyle and Keigwin, 1987; Marchitto *et al.*, 1998). The palaeohydrography of SSW has yet to be fully established with recent suggestions of a more saline SSW mass during the LGM compared with its modern equivalent (Adkins *et al.*, 2002; Adkins and Schrag, 2003). The dynamics of this SSW also remain poorly understood with some evidence hinting at vigorous flow during cool periods (e.g. Masse *et al.*, 1994).

Here, the terrigenous silt grain size data obtained from two high-accumulation rate sediment cores recovered from the crest of the Blake Outer Ridge (BOR) in the western subtropical North Atlantic (Figure 5.1) is used to reconstruct changes in near bottom flow speeds associated with both NSW and SSW throughout the last deglacial period.

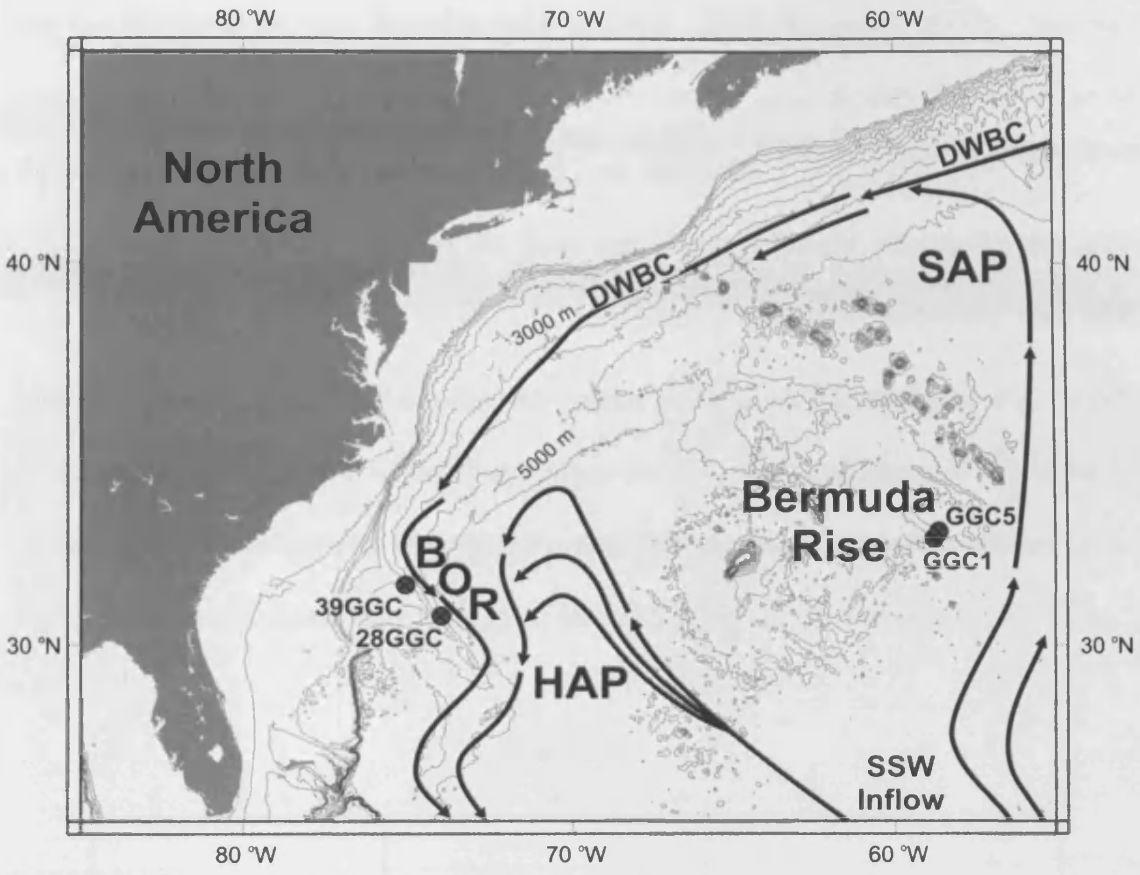

Figure 5.1: Map showing the pathway of recirculating Southern Source Water (SSW, thick black line) in the western North Atlantic (adapted from Weatherly and Kelley, 1984). The locations of sediment cores KNR140/2-39GGC and KNR140/2-28GGC are highlighted. The Blake Outer Ridge (BOR), Bermuda Rise (BR), Hatteras Abyssal Plain (HAP), Sohm Abyssal Plain (SAP) and position of the Deep Western Boundary Current (DWBC) are shown.

5.2 Material and methods

Sediment core KNR140/2-39GGC (31°40.1'N, 75°24.9'W; 2,975 m water depth, hereafter 39GGC) lies in modern lower (L)NADW, while core KNR140/2-28GGC (30°05.9'N, 73°50.2'W; 4,211 m water depth, hereafter 28GGC) presently lies on the boundary between LNADW and SSW (Stahr and Sanford, 1999) and is thus ideally located to record changes in SSW delivery to the North Atlantic (Figure 5.1). These sediment cores provide high resolution palaeoceanographic records spanning

the last deglaciation (e.g. Keigwin and Schlegel, 2002; Keigwin, 2004). Samples were collected every 2 cm throughout the 5-20 kyr BP interval with the exception of the Younger Dryas which was sampled at 1 cm intervals.

To examine variability in the deep ocean flow intensity we employ the grain size distribution within the 10-63 μm terrigenous (biogenic carbonate and opal removed) sub-fraction, the "sortable silt" mean grain size ($\overline{SS}$; McCave *et al.*, 1995; McCave and Hall, 2006), where fluctuations reflect *relative* changes in the intensity of the near-bottom current through selective deposition, with coarser mean values representing more vigorous near-bottom current speeds and *vice versa* (Figure 5.2).

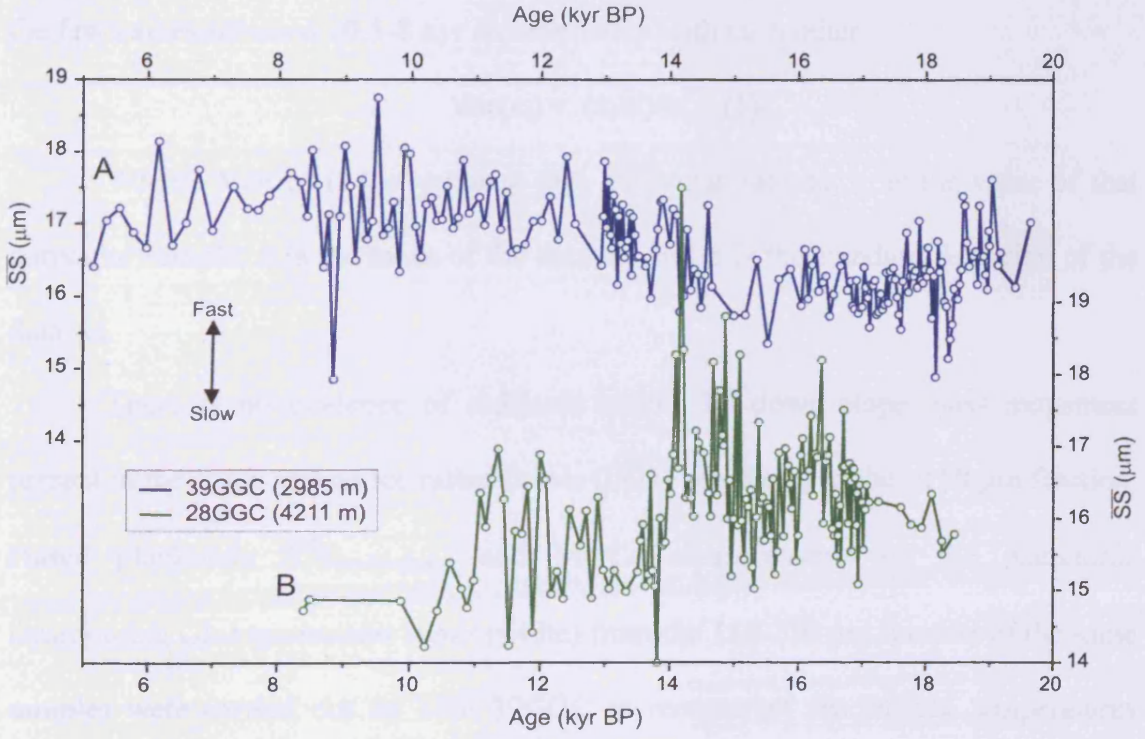

Figure 5.2: The original $\overline{SS}$ records for cores (A) KNR140/2-39GGC (blue line) and (B) KNR140/2-28GGC (green line).

Measurements were undertaken using a Coulter Counter Multisizer III as outlined in Bianchi *et al.* (1999). The SS% varies in the range of 5-10% enabling the determination of the $\overline{SS}$ with an analytical error of 2-3% (Bianchi *et al.*, 1999). In order to highlight the magnitude of the variability in the $\overline{SS}$ data against the background signal and enable a comparison of the two records against a common baseline, the grain size values were normalised (Haskell *et al.*, 1991) about a common mean set equal to zero (see equation 1; Figure 5.3E, 5.3F). To achieve this it was assumed that each site exhibits full glacial to interglacial variability. Despite having a record starting from the late Holocene, core 28GGC is assumed to have values representative of the Holocene interval which does not seem unreasonable given that the few values between 10.5-8 kyr are consistent with each other.

$$Var(x_i) = (x_i - x)/\sigma \quad (1)$$

Where: $Var(x_i)$ is the variance of a particular sample, x_i is the value of that particular sample, x is the mean of the data set and σ is the standard deviation of the data set.

There is no evidence of sediment supply by down slope mass movement present in the cores and no ice rafted debris (IRD) was found in the >150 μm fraction. Paired planktonic $\delta^{18}O_{carbonate(c)}$ and Mg/Ca measurements on the planktonic foraminifera *Globigerinoides ruber* (white) from the 150-250 μm fraction of the same samples were carried out on core 39GGC to reconstruct sea surface temperatures (SST) and isolate the seawater component of $\delta^{18}O$ ($\delta^{18}O_{sw\text{-}ivc}$) with an ice volume correction (Lea *et al.*, 2002; Figure 5.3C and 5.3D; described in detail in **Chapter 4**). Variations in the resultant $\delta^{18}O_{sw\text{-}ivc}$ are thus directly attributable to variations in local salinity or the salinity/$\delta^{18}O$ relationship, reflecting changes in the evaporation-precipitation balance, advection and mixing. The planktonic $\delta^{18}O$ data are generally

similar to the previously published record for *G. ruber* (white) in core 39GGC (Keigwin and Schlegel, 2002; see Figure 5.5C).

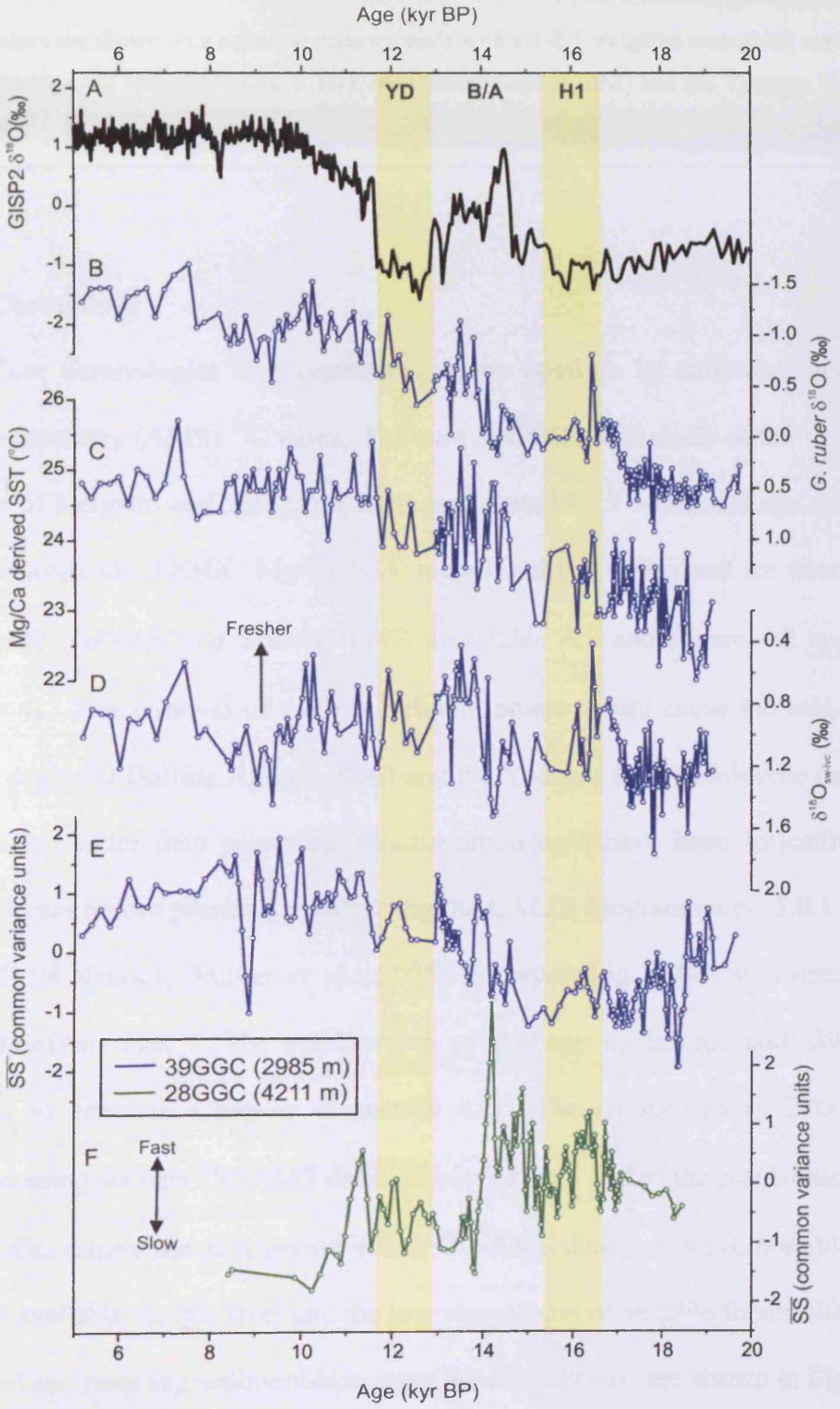

Figure 5.3: Surface and deep ocean proxy records from core KNR140/2-39GGC (2,975 m water depth) and KNR140/2-28GGC (4,211 m water depth) spanning the interval 5-20 kyr BP. (A) GISP2 $\delta^{18}O$ (Grootes and Stuiver., 1997). (B) Planktonic $\delta^{18}O$ for core 39GGC measured on the foraminifera

G. ruber. (C) Sea surface temperature (SST) record derived from Mg/Ca ratios on *G. ruber* in core 39GGC. (D) The derived ice volume corrected $\delta^{18}O$ of seawater ($\delta^{18}O_{sw\text{-}ivc}$) for 39GGC representative of local surface salinity changes at the BOR. (E) $\overline{SS}$ for core 39GGC, and (F) $\overline{SS}$ for core 28GGC. The $\overline{SS}$ values are shown on a common variance scale with a 1-2-1 weighted smoothing applied to the records. Positions of Heinrich Event 1 (H1), the Bølling/Ållerød (B/A) and the Younger Dryas (YD) are indicated.

5.3 Chronology

Core chronologies are constrained where possible by calibrated accelerator mass spectrometry (AMS) ^{14}C dates. For core 39GGC use is made of the ^{14}C derived age scale of Keigwin and Schlegel (2002) augmented by 2 additional age correlation points between the 39GGC Mg/Ca SST record and the Greenland ice core, GISP2 $\delta^{18}O$ record (Grootes and Stuiver, 1997; see Table 4.1 and Figure 4.2 and 4.3 in **Chapter 4**). The removal of these correlation points would cause the mid-point of both the deglacial-Bølling Ållerød (B/A) and the Younger Dryas-Holocene transitions to be ~1 kyr older than presented. Radiocarbon ages have been (re)calibrated to calendar years before present (yr BP) using the CALIB programme (v. 5.0.1 with the MARINE 04 dataset; Stuiver *et al.*, 2005), incorporating a 400 yr correction for marine reservoir age. The construction of the age model for core 39GGC is described in detail in **Chapter 4, section 4.2**. The chronology of 28GGC was generated using six new ^{14}C-AMS dates (Table 5.1) and tied to the planktonic $\delta^{18}O$ of core 39GGC during the B/A period where ^{14}C-AMS dating was not possible due to the small available sample sizes and the low abundances of suitable foraminifera. The age model and resulting sedimentation rates for core 28GGC are shown in Figure 5.4, with ages between the control points calculated via a linear interpolation. Similarly to core 39GGC and previous observations from the North American continental margin

(Keigwin and Jones, 1989), sedimentation rates are high, reflecting the focussing of sediments by the interaction of the DWBC with seabed topography. Sedimentation rates decrease from ~175 cm kyr^{-1} during the early deglaciation to ~15 cm kyr^{-1} in the early Holocene.

Table 5.1: Radio carbon ^{14}C-AMS dating results from core KNR 140/2-28GGC, with a marine reservoir correction of -400 yr. Obtained from CALIB v5.0.1 programme (Stuiver *et al.*, 2005).

Laboratory Number	Material	Depth (cm)	^{14}C Age yr BP	Error Age ±1σ yr BP	Calendar Age yr
28GGC					
SUERC-7701	G. ruber	24-25	9405	29	10324
SUERC-7702	G. ruber	48-49	10924	11.6	12439
SUERC-7703	mixed	88-89	12891	11.4	14596
SUERC-7704	mixed	152-157	13613	45	15633
SUERC-7705	mixed	207.5-209	14303	48	16558
SUERC-7707	mixed	261-263	14664	51	17037

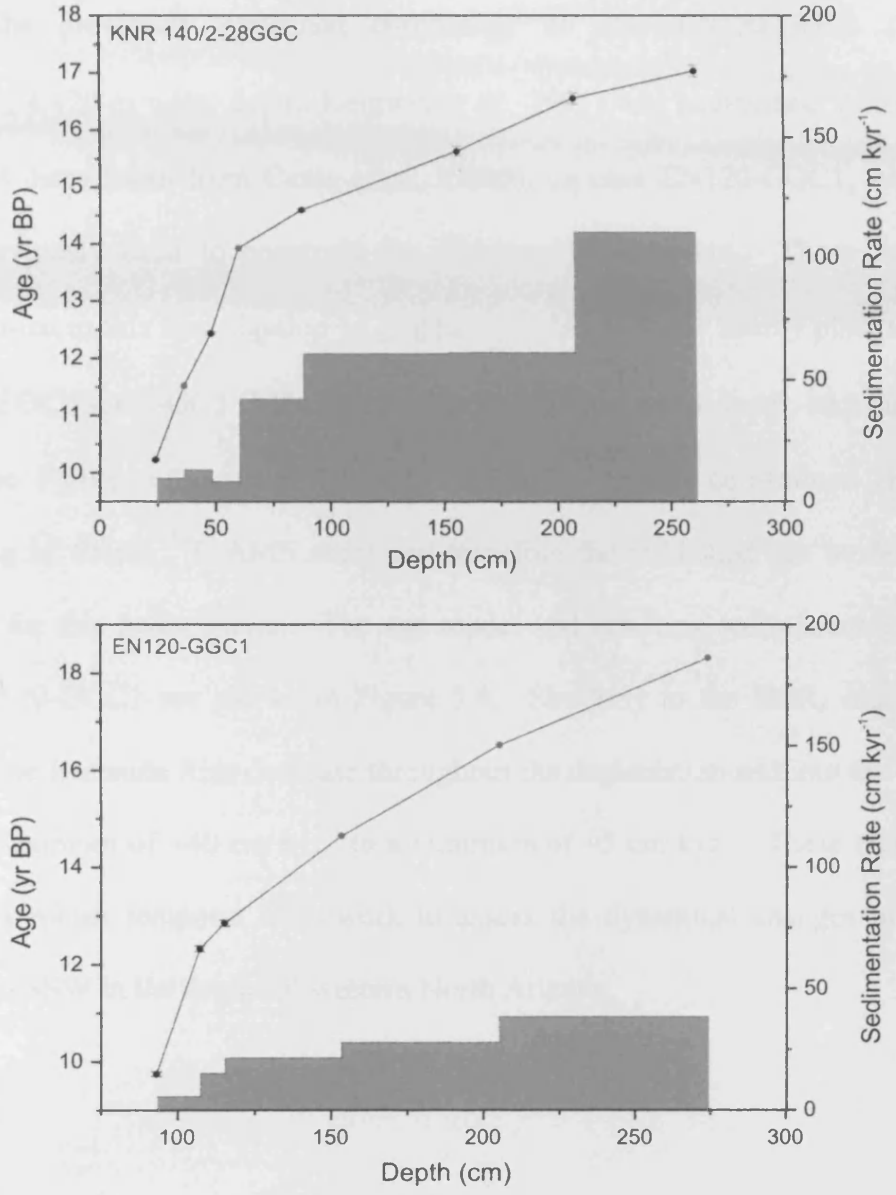

Figure 5.4: Age models for cores KNR140/2-28GGC on the Blake Outer Ridge and EN120-GGC1 on the Bermuda Rise. The black circles represent the positions of ^{14}C-AMS dates and the pink circles indicate where the planktonic δ^{18}O record has been tied to the chronology of an existing planktonic δ^{18}O record (see Figure 5.5 and the text further details). Core 28GGC has been tied to the chronology of 39GGC (refer **Chapter 4**), while core EN120-GGC1 has been tied to the chronology of core OCE326-GGC5 (McManus *et al.*, 2004; see Figure 5.4). The 1σ error bars are shown for the ^{14}C-AMS dates. The shaded region represents the sedimentation rates at the core sites.

The previously published chronology of core EN120-GGC1 (33°40'N; 57°37'W; 4,420 m water depth; Keigwin *et al.*, 1991) was augmented, utilising three ^{14}C-AMS dates taken from Came *et al.*, (2003), on core EN120-GGC1, which have been previously used to constrain the Younger Dryas event. These dates were accompanied in this investigation by graphic correlation to the nearby planktonic $\delta^{18}O$ record of OCE326-GGC5 (33°42'N, 57°35'W; 4,550 m water depth; McManus *et al.*, 2004; see Figure 5.5). Core OCE326-GGC5 has a well constrained chronology consisting of fifteen ^{14}C-AMS dates and therefore the published age model was not adjusted for this investigation. The age model and resulting sedimentation rates for core EN120-GGC1 are shown in Figure 5.4. Similarly to the BOR, sedimentation rates on the Bermuda Rise decrease throughout the deglaciation and into the Holocene from a maximum of ~40 cm kyr^{-1} to a minimum of ~5 cm kyr^{-1}. These chronologies provide a robust temporal framework to assess the dynamical changes in both the MOC and SSW in the deglacial western North Atlantic.

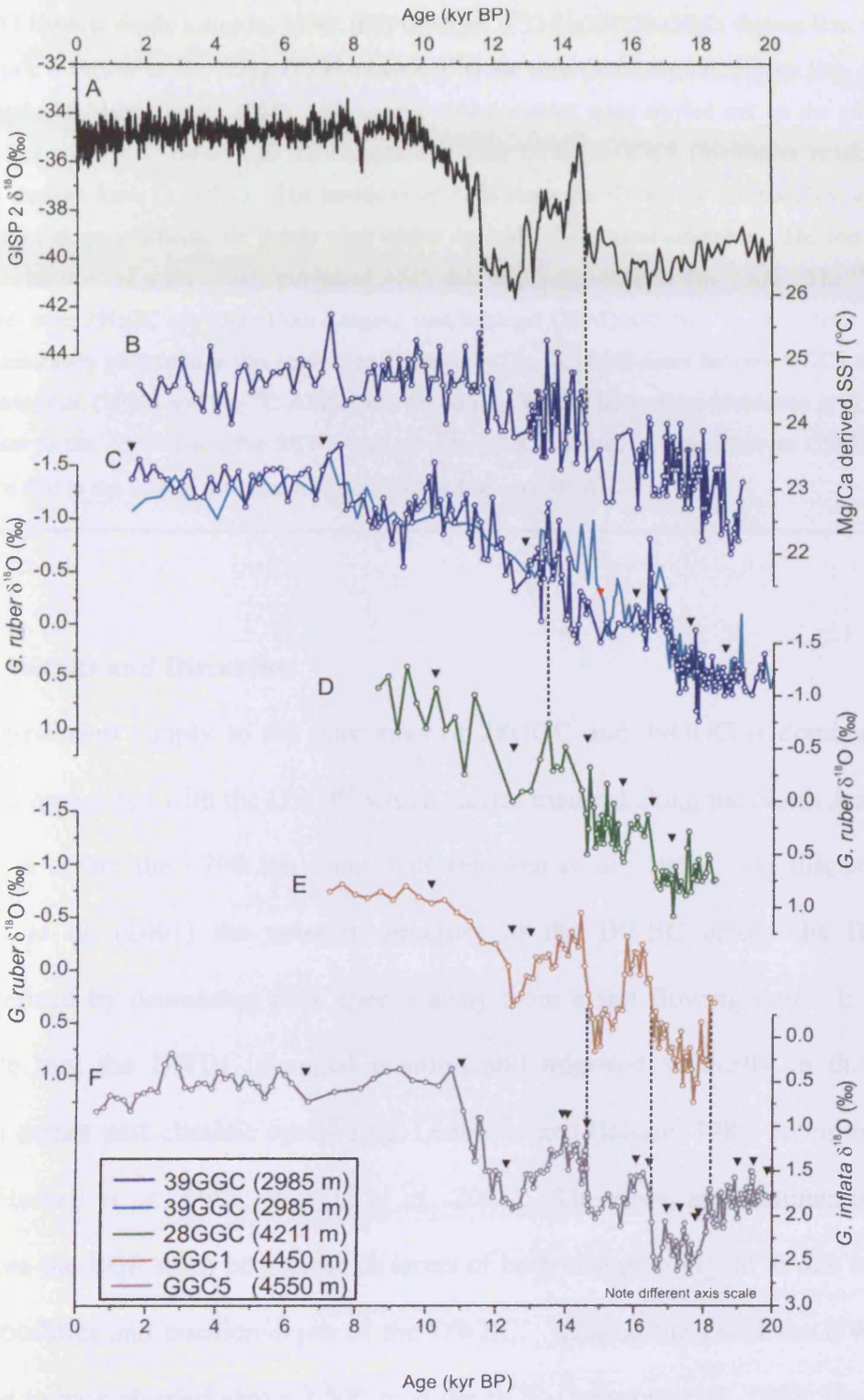

Figure 5.5: Core chronology. Various isotope records are shown versus age. (A) GISP2 $\delta^{18}O$ (black line; Grootes and Stuiver, 1997). (B) Sea surface temperature record for core KNR140/2-39GGC derived from Mg/Ca measurements. (C) Planktonic $\delta^{18}O$ record for core KNR140/2-39GGC (dark blue line, 2,985 m water depth) overlies the previously published lower resolution $\delta^{18}O$ record of Keigwin and Schlegel (2002) at the site (light blue line). (D) Planktonic $\delta^{18}O$ for core KNR140/2-28GGC (green

line, 4,211 m water depth; Keigwin, 2004). (E) Planktonic $\delta^{18}O$ for EN120-GGC1 (brown line, 4,450 m water depth; Keigwin *et al.*, 1991). (F) Planktonic $\delta^{18}O$ for core OCE326-GGC5 (grey line, 4,550 m water depth; McManus *et al.*, 2004). All isotope measurements were carried out on the planktonic foraminifera species *G. ruber* with the exception of core OCE326-GGC5 (McManus *et al.*, 2004), which is derived from *G. inflata*. The positions of AMS dates are shown by the triangles, while the dashed lines show additional tie points used where no AMS dates were available. The red triangle shows the location of a previously published AMS date that is not used in this study. The ^{14}C-AMS dates from core 39GGC are taken from Keigwin and Schlegel (2002) and the ^{14}C-AMS dates for core 28GGC are newly presented in this study (see Table 5.1). The ^{14}C-AMS dates for core GGC1 are taken from Came *et al.* (2003) and the ^{14}C-AMS dates for core GGC5 are taken from McManus *et al.* (2004). In addition to the AMS dates, the SST record of core 39GGC is tied at two points to GISP2. Core 28GGC is tied at the B/A to the planktonic $\delta^{18}O$ record of core 39GGC.

5.4 Results and Discussion

Sediment supply to the core sites of 28GGC and 39GGC is dominated by transport associated with the DWBC which carries material along the North American margin to create the ~700 km long BOR (Heezen *et al.*, 1966). As discussed by Bianchi *et al.* (2001) the velocity structure of the DWBC across the BOR is characterized by decreasing flow speeds away from a fast flowing core. It is also probable that the DWBC changed position and migrated vertically in the water column during past climatic cycles (e.g. Ledbetter and Balsam, 1985; Johnson *et al.*, 1988; Haskell *et al.*, 1991; Bianchi *et al.*, 2001). Therefore, any sedimentological data from the BOR must be viewed in terms of both changing vigour at one or more given localities and position/depth of the DWBC. During the LGM the DWBC is believed to have shoaled above 2,500 m at the BOR (Johnson *et al.*, 1988; Haskell *et al.*, 1991), consistent with shallower and reduced NSW formation. The general coarsening trend throughout the deglaciation in the site 39GGC $\overline{SS}$ record is therefore consistent with a deepening and/or strengthening DWBC proximal to 39GGC. This coincides with a general trend towards increasing SST at the BOR (Figure 5.3). An

important observation is the close correspondence, apparent throughout the deglaciation and into the Holocene, between flow speeds changes inferred from the $\overline{SS}$ at the shallower site 39GGC and the $^{231}Pa/^{230}Th$ record from core OCE326-GGC5 (hereafter GGC5 Figure 5.6B; McManus *et al.*, 2004) located on the plateau of the Bermuda Rise at 4,550 m water depth (Figure 5.1). The changes in deepwater export traced by $^{231}Pa/^{230}Th$ have been suggested as a kinematic proxy for meridional overturning that demonstrates a significant slow-down, or even total cessation, of MOC coincident with the catastrophic iceberg discharge of Heinrich Event (H) 1, and a transient sharp decline in MOC during the Younger Dryas cold event. The close similarities between the two proxy records suggests that the near-bottom flow speed changes of the NSW component of the DWBC monitored by the 39GGC $\overline{SS}$ record are closely related to MOC activity (Figure 5.6B). These deglacial variations in the North Atlantic MOC are also well traced in the benthic Cd/Ca palaeonutrient record of core EN120-GGC1 (hereafter GGC1; Figure 5.6C) on the Bermuda Rise at 4,450 m water depth (Boyle and Keigwin, 1987) and at other deepwater sites (e.g. Curry *et al.*, 1988; Duplessy *et al.*, 1998; Keigwin, 2004). These records suggest that reduced NSW flux and/or shoaling of the DWBC revealed by the $\overline{SS}$ records allowed nutrient-enriched SSW to shoal and spread northwards in the North Atlantic Ocean. A notable feature of the $\overline{SS}$ data presented here is the broad-scale divergent relative flow speeds apparent between changes in northern-source DWBC flow speed recorded in core 39GGC and the deeper, SSW influenced core, 28GGC (Figure 5.3E and 5.3F). The increase in the relative SSW contribution to the deep North Atlantic during the cold events of the last deglaciation (e.g. Boyle and Keigwin, 1987; Marchitto *et al.*, 1998)

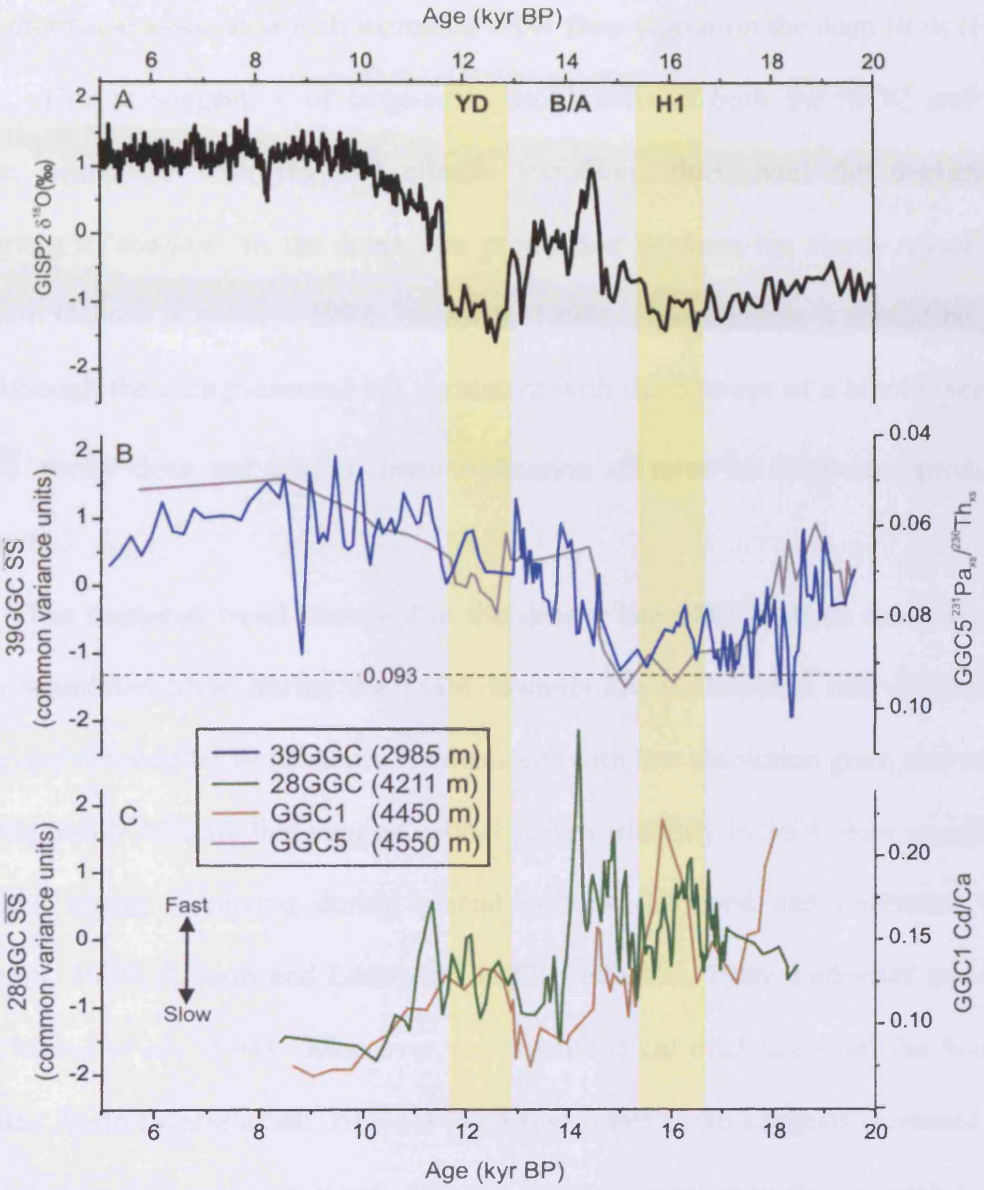

Figure 5.6: Comparison of sedimentary records from the subtropical western North Atlantic with trace metal and polar ice core records spanning the interval 20-5 kyr BP. (A) GISP2 $\delta^{18}O$ (Grootes and Stuiver., 1997). (B) $\overline{SS}$ for core KNR140/2-39GGC (black line, 2,975 m water depth) from the BOR and the $^{231}Pa/^{230}Th$ for core OCE326-GGC5 (grey line, 4,550 m water depth; McManus *et al.*, 2004) from the Bermuda Rise. (C) $\overline{SS}$ for core KNR140/2-28GGC (black line, 4,211 m water depth) from the BOR and the Cd/Ca for core EN120-1GGC (grey line, note revered scale; Boyle and Keigwin, 1987). The $\overline{SS}$ values are shown on a common variance scale with a 1-2-1 weighted smoothing applied to the records and the records for each site are normalized about a common mean set equal to zero. Positions of Heinrich Event 1 (H1), the Bølling/Ållerød (B/A) and the Younger Dryas (YD) are indicated.

is therefore also associated with increased SSW flow vigour on the deep BOR (Figure 5.6C). This is suggestive of large-scale oscillations in both the MOC and SSW vigour, coincident with regional climate variations throughout the deglaciation, supporting a 'see-saw' in the deepwater production between the North Atlantic and Southern Oceans (Crowley, 1992; Broecker, 1998). Nonetheless it should be noted that although the data presented are consistent with the concept of a bipolar see-saw, the $\overline{SS}$ proxy does not give a direct indication of rates of deepwater production upstream.

The deglacial trend observed at the deeper site 28GGC from more vigorous poorly ventilated SSW during the LGM towards lower Holocene near-bottom flow vigour and reduced SSW influence is consistent with low resolution grain size records from the South Atlantic that suggest orbital scale variability in SSW flow speeds with increased vigour occurring during glacial periods (Ellwood and Ledbetter, 1977; Ledbetter, 1979; Allison and Ledbetter, 1982; Ledbetter, 1986; Ledbetter and Bork, 1993; Masse *et al.*, 1994). Moreover, sedimentological evidence from the Southern Brazilian Basin (Masse *et al.*, 1994) at >4,200 m water depth suggests increased SSW vigour during cold northern North Atlantic intervals, similar to the increase in SSW flow speeds observed during both the H1 and Younger Dryas intervals at 28GGC.

The contrasting behaviour in the $\overline{SS}$ records is most clearly evident in the 18.5-15 kyr BP interval (Figure 5.3E, 5.3F). This interval incorporates H1 at ~16.8 kyr BP, characterized by a large flux of IRD-bearing icebergs in the North Atlantic (Bond *et al.*, 1992; Bard *et al.*, 2000; Hemming, 2004) that reduced the density of the surface waters and has been associated with substantially reduced NSW production (e.g. Keigwin and Lehman, 1994; Vidal *et al.*, 1997, 1998; Zahn *et al.*, 1997; Willamowski and Zahn, 2000; Elliot *et al.*, 2002; Zahn and Stüber, 2002; Rickaby and

Elderfield, 2005; Robinson *et al.*, 2005). Freshening of the surface ocean recorded at core 39GGC, ~17-16.3 kyr BP (Figure 5.3D), corresponds to the timing associated with H1, suggesting that some meltwater from the eastern outlets of the Laurentide ice sheet (Bond *et al.*, 1992) reached as far south as the BOR. The decreased flow speeds suggested at the shallower site, 39GGC, occur at a similar time as the slowdown/cessation in the MOC inferred from the GGC5 $^{231}Pa/^{230}Th$ records (McManus *et al.*, 2004; Figure 5.6B) and also coincides with the initiation of surface ocean heat being retained in the tropical (Schmidt *et al.*, 2004) and subtropical (Flower *et al.*, 2004) Atlantic (Figure 5.7; also see **Chapter 4**). During the initial decrease in the MOC from ~18.5-17 kyr BP, SST at core 39GGC increases by approximately 1°C, demonstrating a linkage between the Atlantic MOC and local surface hydrography. We can not rule out the possibility that this SST increase reflects an increased Gulf Stream influence at the BOR, perhaps feeding enhanced intermediate-depth convection, as overall MOC diminished. We suggest however, as have authors working at lower latitudes (Schmidt *et al.*, 2004; Flower *et al.*, 2004), that this early warming prior to H1, is likely to reflect regional heat retention at the BOR as the MOC slowed down. Coincident with the onset of the meltwater anomaly at ~17 kyr BP (Figure 5.3D), minimum MOC rates and 39GGC flow speeds (Figure 5.6B), there is a pause in the general warming SST trend above the BOR which persists for the ~2,000 year (Figure 5.3C) of this weakened circulation interval. While the reduction in flow speed at ~3,000 m during H1 (Figure 5.3E) suggests a shallower and/or weaker DWBC driven by decreased NSW production, the $\overline{SS}$ record also shows small-scale variability within the H1 interval suggesting that the MOC was subdued at this time rather than totally absent.

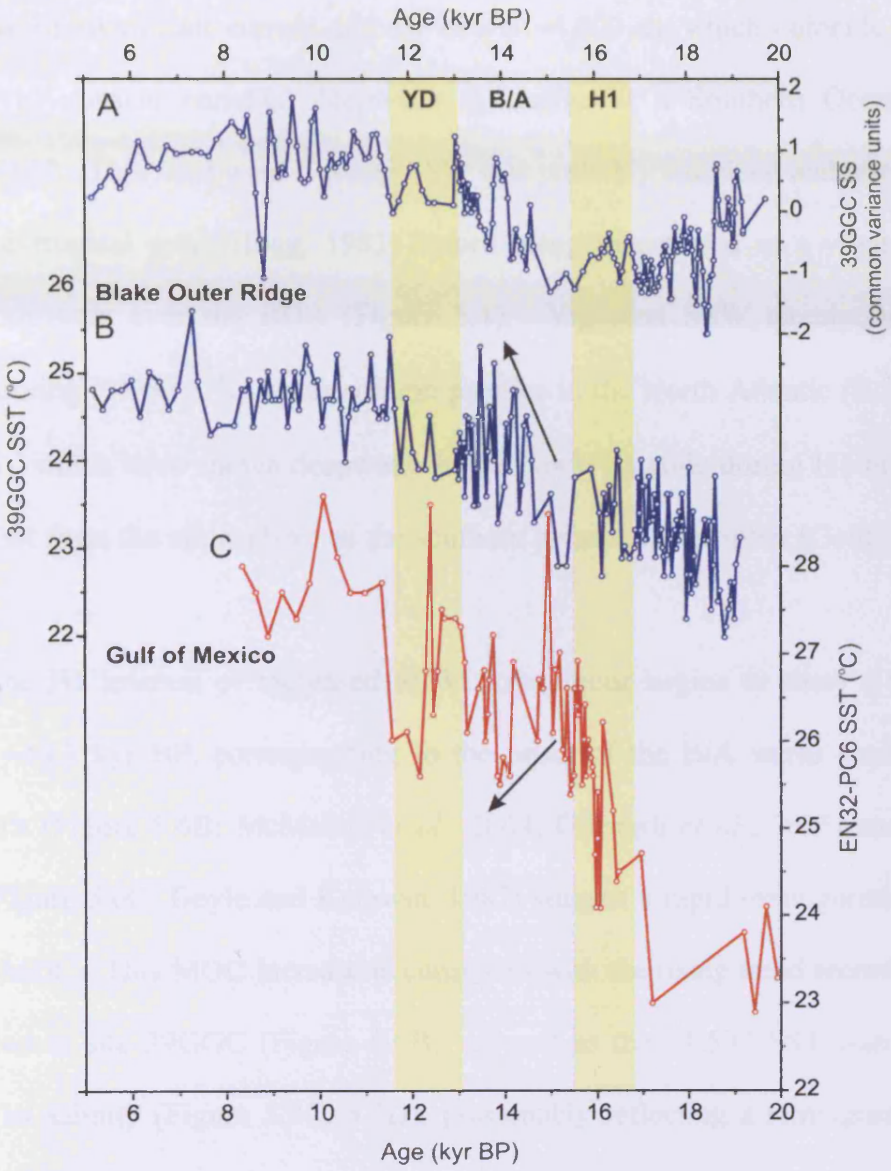

Figure 5.7: (A) $\overline{SS}$ record with a 1-2-1 weighted smoothing applied for core KNR140/2-39GGC (2,975 m water depth) on the BOR. (B) Blake Outer Ridge sea surface temperatures (SST) based on Mg/Ca ratios from *G. ruber* in core 39GGC. (C) Gulf of Mexico SST based on Mg/Ca ratios from *G. ruber* in core EN32-PC6. Positions of Heinrich Event 1 (H1), the Bølling/Ållerød (B/A) and the Younger Dryas (YD) are indicated.

During the interval 18.5-15 kyr BP the deepest core, 28GGC, was distant from the influence of the shoaled northern-source DWBC, but coarse $\overline{SS}$ values are

suggestive of significant current activity below ~4,000 m, which coincide with the presence of nutrient enriched deepwater indicative of a Southern Ocean source (Figure 5.6C). This northward flowing SSW was probably entrained and re-circulated in the sub-tropical gyre (Hogg, 1983) before being transported as a vigorous flow back southwards over the BOR (Figure 5.1). Vigorous SSW circulation is also implied during H1 by $\Delta^{14}C$ water column profiles in the North Atlantic (Robinson *et al.*, 2005), which have shown deepwater in the North Atlantic during H1 to have the same offset from the atmosphere as the southern source end member (Goldstein *et al.* 2001).

The H1 interval of increased SSW flow vigour begins to show a reversing trend at ~14.7 kyr BP, corresponding to the onset of the B/A warm period, when $^{231}Pa/^{230}Th$ (Figure 5.6B; McManus *et al.*, 2004; Gherardi *et al.*, 2005) and benthic Cd/Ca (Figure 5.6C; Boyle and Keigwin, 1987) suggest a rapid reinvigoration of the Atlantic MOC. This MOC increase is consistent with the rising trend recorded in the flow speed at site 39GGC (Figure 5.6B), as well as the ~1.5°C SST warming and increase in salinity (Figure 5.3C, 5.3D), presumably reflecting a reinvigorated Gulf Stream transport of warm and saline water northwards from the tropics over the study site. This northward transport of warm water is supported by a synchronous cooling observed in the tropical Gulf of Mexico core EN32-PC6 (26°56.8'N, 91°20.0'W; Flower *et al.*, 2004; Figure 5.7). These changes support the suggestion that B/A warming resulted primarily from reinvigoration of the oceanic heat transport as MOC increased (Schmidt *et al.*, 2004). As highlighted by McManus *et al.* (2004) the timing of the MOC reinvigoration occurred shortly before meltwater pulse 1a (MWP-1a), the most extreme rapid deglacial rise in global sea level (~25 m) and reduction of continental ice volume, which has been dated at ~14.0 kyr BP (Fairbanks, 1989,

Peltier, 2005; Stanford *et al.*, 2006). A low salinity anomaly is recorded at the BOR ~13.9 kyr BP consistent with the recent timing (within dating error) proposed for MWP-1a and coincident with the maximum meltwater discharge from the Mississippi River into the Gulf of Mexico (Flower *et al.*, 2004; Figure 5.3D). This suggests that MWP-1a had, at least in part, a Northern Hemisphere origin. Furthermore, the increased oceanic heat transport indicated by our data is consistent with the suggestion that this supply of warmth to the high latitudes, as well as increasing insolation, may have played a role in promoting the ablation of the Laurentide ice sheet, resulting in MWP-1a (McManus *et al.* 2004). Previous studies have also traced meltwater discharges from the Gulf of Mexico into the open subtropical Atlantic and suggested that this meltwater was advected to the sites of deepwater formation leading to a decreased NADW flux (Keigwin *et al.*, 1991). A transient reduction in the DWBC flow speeds indicated by a decrease in 39GGC $\overline{SS}$ values centred at ~13.6 kyr BP (Figure 5.3E) may correspond to the small reduction in the NADW formation previously associated with MWP-1a (Keigwin *et al.*, 1991; Stanford *et al.*, 2006).

Increased $^{231}Pa/^{230}Th$ (McManus *et al.*, 2004; Gherardi *et al.*, 2004), Cd/Ca (Boyle and Keigwin, 1987) and decreased $\Delta^{14}C$ (Robinson *et al.*, 2005) have been used to infer a reduction in the MOC and increased penetration of SSW into the North Atlantic during the Younger Dryas. This is consistent with our palaeocurrent records (Figure 5.3E) that show that the flow speeds associated with the rate and/or position of the DWBC decreased at ~13 kyr BP, at the same time SST's show a slight (~0.5°C) cooling at the BOR (Figure 5.3D), indicative of reduced surface heat transport as a result of a weaker MOC. The slight salinity increase at this time is likely to be a reflection of a reduction in regional meltwater input and changes in the hydrological

cycle (Schmidt *et al.*, 2004). During this interval SSW at the deeper site again shows generally contrasting flow speeds to the shallower site (Figure 5.3E, 5.3F), indicating increased vigour. As also suggested in the GGC5 $^{231}Pa/^{230}Th$ record (Figure 5.6B), the flow speed changes recorded during the Younger Dryas are substantially less marked than those observed during H1. Indeed it is reassuring that the relative magnitudes of each of the recorded circulation changes are so similar.

As zero age samples are not available from either core 39GGC or core 28GGC, we are unable to fully assess how representative the general Holocene $\overline{SS}$ pattern is of the modern flow regime. During the early Holocene, at about ~9.5 kyr BP, the $\overline{SS}$ records show a maximum at the shallower site 39GGC (Figure 5.3E) and a minimum at the deeper site 28GGC (Figure 5.3F), coincident with high ventilation rates and vigorous NADW export in the deep North Atlantic (Boyle and Keigwin., 1987; McManus *et al.*, 2004). This difference suggests that the fast flowing core of the DWBC was likely to be close to its present day position, influencing depths from 3,000 m down to 4,100 m (Stahr and Sanford, 1999), from that time onwards.

5.4.1 Implications for $^{231}Pa/^{230}Th$ interpretations

Previous research has suggested the operation of a bipolar see-saw between the Hemispheres for the largest Antarctic warmings (Blunier *et al.*, 1998; Blunier and Brook, 2001; Stocker and Johnsen, 2003), with recent research suggesting a one-to-one coupling between the Hemispheres (EPICA Community Members, 2006) throughout the last glacial period. The EPICA Community Members (2006) suggest the amplitude of the Antarctic warm events is linearly dependent on the duration of the concurrent stadial in the North, suggesting that they each result from a similar reduction in the MOC. As deepwater formation warms the atmosphere, Northern

Hemispheric cooling would lead to Southern Hemisphere warming and *vice versa*, with vigorous SSW inflow to the North Atlantic during the Greenland deglacial cold episodes, coincident with reduced NSW export. The broad contrast between our flow speed records, with decreasing NSW vigour and/or a shoaling DWBC coinciding with increasing SSW flow speeds, supports the notion of a bipolar see-saw and it is therefore not totally unexpected that relative flow speeds at 28GGC resemble the inverted $^{231}Pa/^{230}Th$ and Cd/Ca records (Figure 5.6B, 5.6C). However, the presence of a vigorous, poorly ventilated water mass in the western North Atlantic below ~4,000 m, at times of high $^{231}Pa/^{230}Th$ may have implications for our understanding of sedimentary $^{231}Pa/^{230}Th$. Generally, it is assumed that sedimentary $^{231}Pa/^{230}Th$ is controlled by the whole water column and an increase towards the production ratio (0.093) in the North Atlantic is indicative of reduced MOC, as the rate of MOC directly affects the lateral advection export of ^{231}Pa (Yu *et al.*, 1996; Marchal *et al.*, 2000; Siddall *et al*, 2007). However, it is possible that $^{231}Pa/^{230}Th$ may not represent average flow in regions of complex hydrography but may instead more clearly reflect changes from the bottom ~1,000 m of the water column (Thomas *et al.*, 2006). The Bermuda Rise GGC5 record is located at 4,550 m water depth well within the depth range that would be likely to experience the inflow of vigorous poorly ventilated SSW during the cold intervals of the last deglaciation. Indeed, sedimentation rates as high as 200 cm kyr^{-1} recorded on the Bermuda Rise during the last glacial have been suggested as indicative of vigorous activity of the recirculation gyres (Keigwin and Jones, 1989). Water masses from the Southern Ocean are likely to have high $^{231}Pa/^{230}Th$ signatures due to long transport distances allowing time to reach equilibrium, leading to values exported to the underlying sediments close to the production ratio (Thomas *et al.*, 2006). It might therefore be that during the cold

periods of the last deglaciation the GGC5 $^{231}Pa/^{230}Th$ record more faithfully records increased export and flow from the Southern Ocean rather than strictly MOC reduction.

5.5 Conclusions

This study demonstrates that a $\overline{SS}$ near-bottom flow record from ~3,000 m (core 39GGC) on the BOR provides a good proxy for MOC activity, as it correlates well to the $^{231}Pa/^{230}Th$ circulation tracer from the Bermuda Rise irrespective of climate state. The data suggest the presence of a vigorous, poorly ventilated deep water mass (SSW) below ~4,000 m in the North Atlantic during the cold episodes of the last deglaciation when intermediate depth flow speeds and $^{231}Pa/^{230}Th$ suggest substantially weaker NSW export (Keigwin and Schlegel, 2002; Keigwin, 2004; McManus *et al.*, 2004). This study highlights the divergent flow speed behaviour between ~3,000 m and >4,000 m water depth in the subtropical North Atlantic and is consistent with the notion of a bipolar see-saw.

Chapter 6: Intermediate Water links to Deep Western Boundary Current variability in the subtropical NW Atlantic during Marine Isotope Stages 5 and 4[1]

Abstract

Records from Ocean Drilling Program (ODP) Sites 1057 and 1059 (2,584 m and 2,985 m water depth respectively) have been used to reconstruct the behaviour of the DWBC on the Blake Outer Ridge from 130 to 60 kyr BP (marine isotope stage (MIS) 5 and the 5/4 transition). Site 1057 lies within Labrador Sea Water (LSW), but close to the present day boundary with Lower North Atlantic Deep Water (LNADW), while Site 1059 lies within LNADW. High resolution sortable silt mean ($\overline{SS}$) grain size and benthic $\delta^{13}C$ records were obtained and changes in the Deep Western Boundary Current (DWBC) intensity and spatial variability inferred. Comparisons are made with similar proxy records generated for the Holocene from equivalent depth cores on the BOR. During MIS 5e $\overline{SS}$ evidence at Site 1057 suggests slower relative flow speeds consistent with a weakening and a possible shoaling of the LSW sourced shallower limb of the DWBC that occupies these depths today. In contrast the palaeocurrent record from the deeper site suggests that the fast flowing deep core of the DWBC was located close to its modern depth below 3,500 m. During this interval the benthic $\delta^{13}C$ suggests little chemical stratification of the water column and the presence of a near uniform LNADW dominated water mass. After ~111 kyr BP the $\overline{SS}$ record at Site 1057 increases to reach values similar to Site 1059 for the rest of MIS 5. The strengthening of flow speeds at the shallow site may correspond to the initiation of Glacial North Atlantic Intermediate Water formation also suggested

by a divergence in the benthic $\delta^{13}C$ records with Site 1057 values increasing to ~1.2‰. Coupled suborbital oscillations in DWBC flow variability and palaeohydrography persisted throughout MIS 5. Comparison of these data with planktonic $\delta^{18}O$ records from the sites and alkenone-derived sea surface temperature (SST) estimates from the nearby Bermuda Rise suggest a hitherto unrecognised degree of linkage between oscillations in subtropical North Atlantic SST and DWBC flow.

[1]In press in *Paleoceanography* as
Evans H. K., I. R. Hall, G. G. Bianchi and D. W Oppo Intermediate Water links to Deep Western Boundary Current variability in the subtropical NW Atlantic during Marine Isotope Stages 5 and 4

6.1 Introduction

The Atlantic Meridional Overturning Circulation (MOC) is responsible for a substantial component of the meridional heat transport in the Atlantic Ocean (e.g. Ganachaud and Wunsch, 2000) and abrupt shifts of the MOC are considered to have played a key role in driving the dramatic and rapid climate variability during the last glacial period (Clark *et al.*, 2002 and references therein). Initiation of the MOC occurs through the production of North Atlantic Deep Water (NADW), which consists of two main components: cold and dense Lower North Atlantic Deep Water (LNADW) forming the deepest layer and Labrador Sea Water (LSW, also known as upper NADW) at an intermediate level. The renewal of LNADW is fed by the overflow of intermediate depth water formed following the convection of surface ocean waters in the Greenland, Iceland, and Norwegian (GIN) Seas (Aagaard *et al.*, 1985; Mauritzen, 1996). About 3.2 Sv (= 10^6 m^3 s^{-1}) of Northern Source Water (NSW) passes between Iceland and Scotland (Saunders, 1996). In addition, a nearly equal volume of slightly colder waters pass over the shallow sill in the Denmark Strait (Dickson and Brown, 1994). These waters form the Atlantic Deep Western Boundary Current (DWBC) along the continental slope east of Greenland. As the DWBC flows south, it encounters LSW formed by winter time convection of surface waters to an estimated depth of ~1,500 m in the central Labrador and Irminger Seas (Reid, 1994). Some LSW which is warmer, less saline, and less dense than LNADW (Dickson and Brown, 1994) is entrained by the DWBC, which transports about 13-14 Sv of NADW equatorward (Talley and McCartney, 1982; Schmitz and McCartney, 1993). Modern LSW is also present as far east as the Iceland Basin (Schmitz and McCartney, 1993) where it is already entrained by Iceland Scotland Overflow Water (ISOW) as it enters this basin and significantly augments the total flux of deepwater into the DWBC.

During its passage it is progressively undercut by northward flowing colder and denser Southern Source Water (SSW) from the Southern Ocean. The intensity and flow characteristics of the DWBC are known to have varied in space (depth) and time, which is believed to be a response to changes in source water production (Pickart, 1992; Bianchi *et al.*, 2001).

Palaeoceanographic reconstructions of past variability in the contribution of intermediate and deepwater masses in the North Atlantic are mainly based on the geochemical analyses of epifaunal benthic foraminifera. Such work is aimed at the proxy determination of the palaeohydrography or palaeo-biogeochemistry (e.g., nutrient content) of the waters inhabited by these organisms whose shell chemistry is believed to reflect the chemistry of the bottom waters they lived in. This method is particularly useful to detect the changing proportion of NADW and poorly ventilated SSW. The most widely employed nutrient proxy is the ratio of stable carbon isotopes of benthic foraminiferal calcite (e.g. Curry *et al.*, 1988; Duplessy *et al.*, 1988; Curry and Oppo, 2005). This approach is based on the observation that the $\delta^{13}C$ of ΣCO_2 dissolved in seawater displays a distribution in the world ocean that resembles the distribution of the main global water masses (Kroopnick, 1985). Biological nutrient cycling results in low $\delta^{13}C$ in nutrient rich waters like those derived from the Southern Ocean and high $\delta^{13}C$ in nutrient poor waters like those formed in the North Atlantic today. Carbon isotope gradients in the world's oceans reflect mixing between water masses and progressive oxidation of low-$\delta^{13}C$ organic matter. The application of $\delta^{13}C$ methods, in addition to other nutrient proxies such as Cd/Ca (e.g., Boyle, 1988; Boyle and Keigwin, 1982), have established that circulation patterns in the Atlantic were significantly different during glacial times. Northern source waters sank only to intermediate depths, forming the so-called Glacial North Atlantic Intermediate Water

(GNAIW), resulting in a shoaling of the Atlantic deepwater core layer to approximately 2,000 m, from 3,000 m during interglacials (Boyle and Keigwin, 1987; Duplessy *et al.*, 1988; Curry and Oppo, 2005). Dense southern waters filled the deep glacial Atlantic below GNAIW (Boyle and Keigwin, 1987; Duplessy *et al.*, 1988; Sarnthein *et al.*, 1994; Curry and Oppo 2005). However, occasional differences between estimated nutrient changes derived from benthic $\delta^{13}C$ measurements suggest that variations in isotope fractionation during air-sea exchange (Broecker and Maier-Reimer, 1992; Charles *et al.* 1993; Lynch-Stieglitz *et al.*, 1996, 1999; Oppo and Horowitz, 2000) and/or marine biological productivity (Mackensen *et al.*, 2001) may also have contributed to the changes in the benthic $\delta^{13}C$ signal. In addition to the complications in interpreting $\delta^{13}C$ mentioned above, neither benthic $\delta^{13}C$ nor Cd/Ca are conservative tracers, and therefore complementary methods (ideally not linked with the ocean's biogeochemical cycle) are required to reconstruct past changes in ocean circulation. One of these methods is sedimentological and quite distinct from geochemical proxies, as it provides physical evidence for relative changes in the intensity of the near-bottom water flow. The parameter used is the sortable silt ($\overline{SS}$), the mean grain size of the 10-63 μm terrigenous sediment sub-fraction (McCave *et al.*, 1995; McCave and Hall, 2006). From modern hydrographic investigations, it is clear that there is a link between the hydrographic location of NADW and vigorous deep water circulation (Stahr and Sanford, 1999). However, the hydrographic signal is more likely to be geographically widespread whereas the intensity of the DWBC will be more variable due to its interactions with local bathymetry (McCave and Hall, 2006).

Here, the focus is on reconstructing changes in the hydrography and near-bottom flow speeds of the DWBC bathing the Blake Outer Ridge (BOR) in the

western subtropical North Atlantic at intermediate water depths during marine isotope stage (MIS) 5 and into MIS 4 (~130-60 kyr) and compare this with the Holocene. The study sites are ideally located to monitor changes in the relative intensity of LNADW and LSW, a water mass whose contribution to the overall fluctuations in the MOC over the last glacial-interglacial period remains poorly understood (e.g. Hillaire-Marcel *et al.*, 2001; Rasmussen *et al.* 2003)

6.2 Material and methods

Data are reported from sediment cores recovered from sites located either side of the present day boundary between LNADW and LSW, and above the primary fast flowing core of the DWBC but below the shallower secondary core. The investigation of MIS 5 and the 5/4 transition utilises cores from Sites 1057 and 1059 of the ODP Leg 172. Site 1059 (31°40.5'N, 75°25.1'W; Figure 6.1) is located at a water depth of 2,985 m on a small sediment drift superimposed on the BOR (Keigwin *et al.*, 1998; Keigwin and Schlegel, 2002) and the shallower Site 1057 (32°01.8'N, 76°04.8'W; Figure 6.1) is at 2,584 m water depth. In addition, sediments recovered from *RV Knorr* cruise KNR 140/2, the site survey cruise for Leg 172 (Keigwin, 2004), are used to study the Holocene at corresponding water depths to Sites 1059 and 1057. The deeper of the sites is 39GGC (31°40.1'N, 75°24.9'W; Figure 6.1) at a water depth of 2,975 m, while 43GGC (32°01.2'N, 76°06.7'W; Figure 6.1) is situated at 2,590 m water depth. Sediments from Site 1059 and 39GGC are located within LNADW at a depth that is highly sensitive to changes in the composition of this water mass and particularly the degree of mixing with waters of southern origin from below.

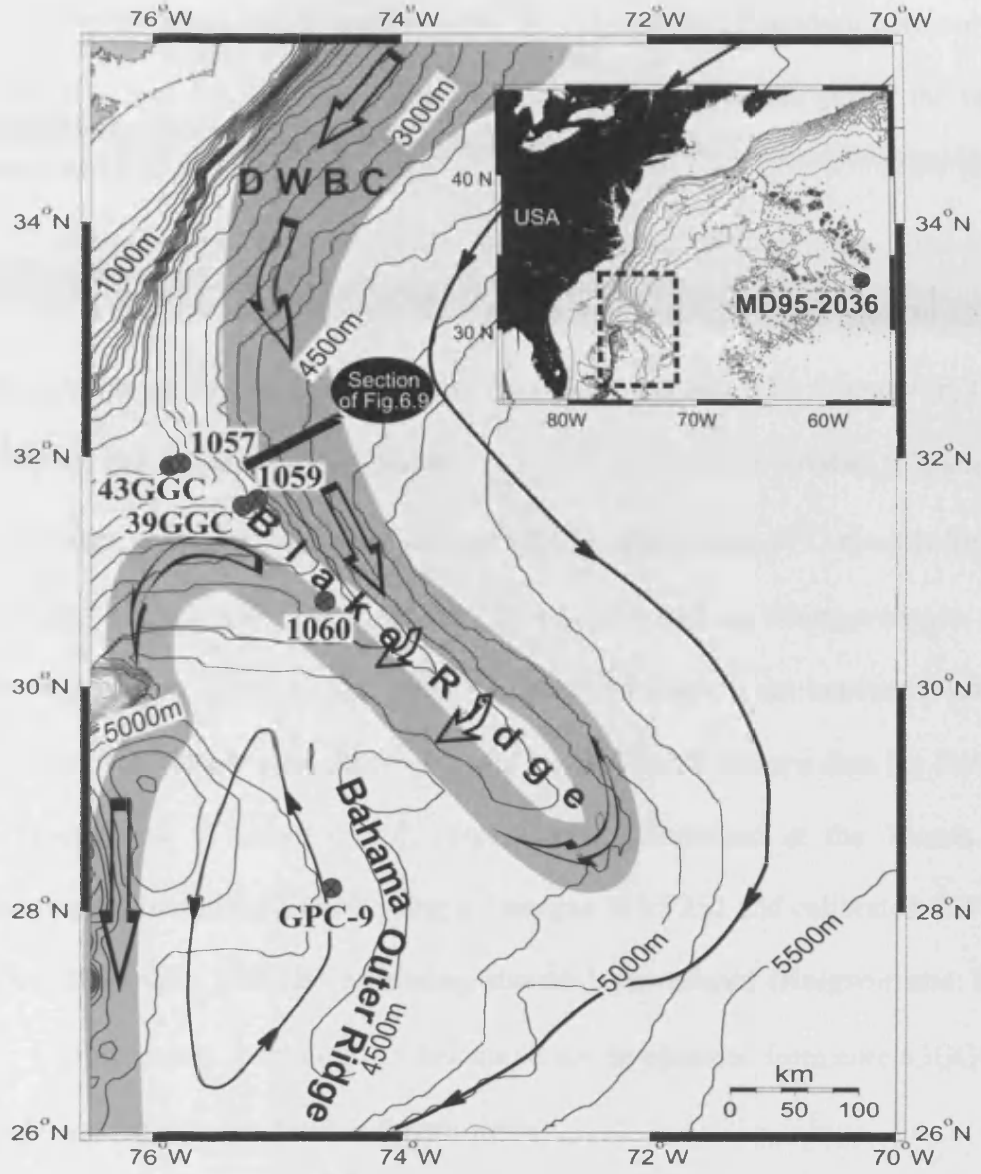

Figure 6.1: Bathymetric map of the study area showing the locations of sediment cores KNR 140/2 Sites 43GGC and 39GGC and the ODP Leg 172 Sites 1057 and 1059. The locations of KNR31-GPC-9 and MD95-2036 are also shown. The large arrows and the shaded area represent the fast flowing core of the DWBC (after Johns *et al.*, 1997; Stahr and Sanford, 1999; Bianchi *et al.*, 2001).

Sites 1057 and 43GGC are located in LSW, but close to the boundary between LSW and LNADW and are therefore ideally positioned to record changes in the relative influence of LSW and LNADW.

Stable isotope records based on the benthic foraminifera *Cibicidoides wuellerstorfi* for Site 1059 during the 145-65 kyr interval (27.96 and 39.12 mcd, average sample resolution of 5 cm) were previously published by Oppo *et al.* (2001) and Heusser and Oppo (2003), while benthic $\delta^{13}C$ data for core 39GGC (*Cibicidoides spp.*) are taken from Keigwin and Schlegel (2002). Planktonic $\delta^{18}O$ records for cores 39GGC and 43GGC are from Keigwin (2004) and based on *Globigerinoides ruber* (white variety). In addition, Site 1057 was sampled every 5 cm between 11.48 and 13.98 mcd. We present new planktonic and benthic stable isotope data for Site 1057 on *G. ruber* and *C. wuellerstorfi*, respectively, determined at the Woods Hole Oceanographic Institute (WHOI) using a Finnigan MAT252 and calibrated to Vienna Pee Dee Belemnite (VPDB) following standard procedures (Keigwin and Boyle, 1999). Unfortunately, benthic $\delta^{13}C$ data could not be obtained from core 43GGC due to the absence of suitable benthic foraminifera.

The biogenic calcium carbonate (% wt) contents for Sites 1059, 1057, 39GGC and 43GGC were indirectly estimated using a *Carlo Erba EA1106* elemental CHN analyzer to measure the inorganic carbon content. All $\overline{SS}$ grain size measurements were undertaken using a Coulter Multisizer III following the methods described in Bianchi *et al.* (1999). Measurements were made on the <63 μm terrigenous fraction following the removal of the biogenic carbonate by slow digestion in 1M acetic acid solution. Generally, the samples used in this study have an SS abundance of 8 to 10 % enabling the determination of the $\overline{SS}$ with an error ranging from 2.1% to 0.3% (Bianchi *et al.*, 1999). The $\overline{SS}$ values obtained from analyses on the Coulter Counter

can not be directly compared with previous palaeocurrent studies for MIS 5e based on Sedigraph measurements (e.g. Bianchi *et al.*, 2001) as these two techniques use different principles to calculate the $\overline{SS}$. The Coulter Counter measures the volume-equivalent spherical diameter inferred from electrical conductivity, while the Sedigraph provides a velocity-equivalent spherical diameter based on the settling principle (Stokes Law and assuming quartz densities) inferred from an X-ray scanning settling tube (McCave and Hall, 2006).

6.3 Chronology

The benthic and planktonic $\delta^{18}O$ stratigraphy for Sites 1059 and 1057 are shown in Figure 6.2. The temporal framework for Site 1059 is based on the previously published age model of Heusser and Oppo (2003), in which the benthic $\delta^{18}O$ record was correlated to the chronology of Martinson *et al.* (1987). This core provides the reference age model for all the other cores utilised in this study during MIS 5 and 4. The age model for Site 1057 was generated by graphic correlation to the chronology of Heusser and Oppo (2003; Figure 6.2). Initially, the benthic $\delta^{18}O$ isotopes were used to broadly correlate the two records (Figure 6.2A) and then the higher resolution planktonic $\delta^{18}O$ isotopes were used to fine tune the correlation (Figure 6.2B). Correlation between the planktonic $\delta^{18}O$ records was mainly focused during the youngest part of the record between 75-65 kyr BP where the benthic $\delta^{18}O$ record experiences some correlation difficulties. A notable period of light benthic $\delta^{18}O$ values between 74 and 68 kyr in Site 1057 is difficult to reconcile with Site 1059 as can be observed in Figure 6.2A. However, there is a close similarity between the planktonic $\delta^{18}O$ records during this interval allowing some confidence in our age assignment.

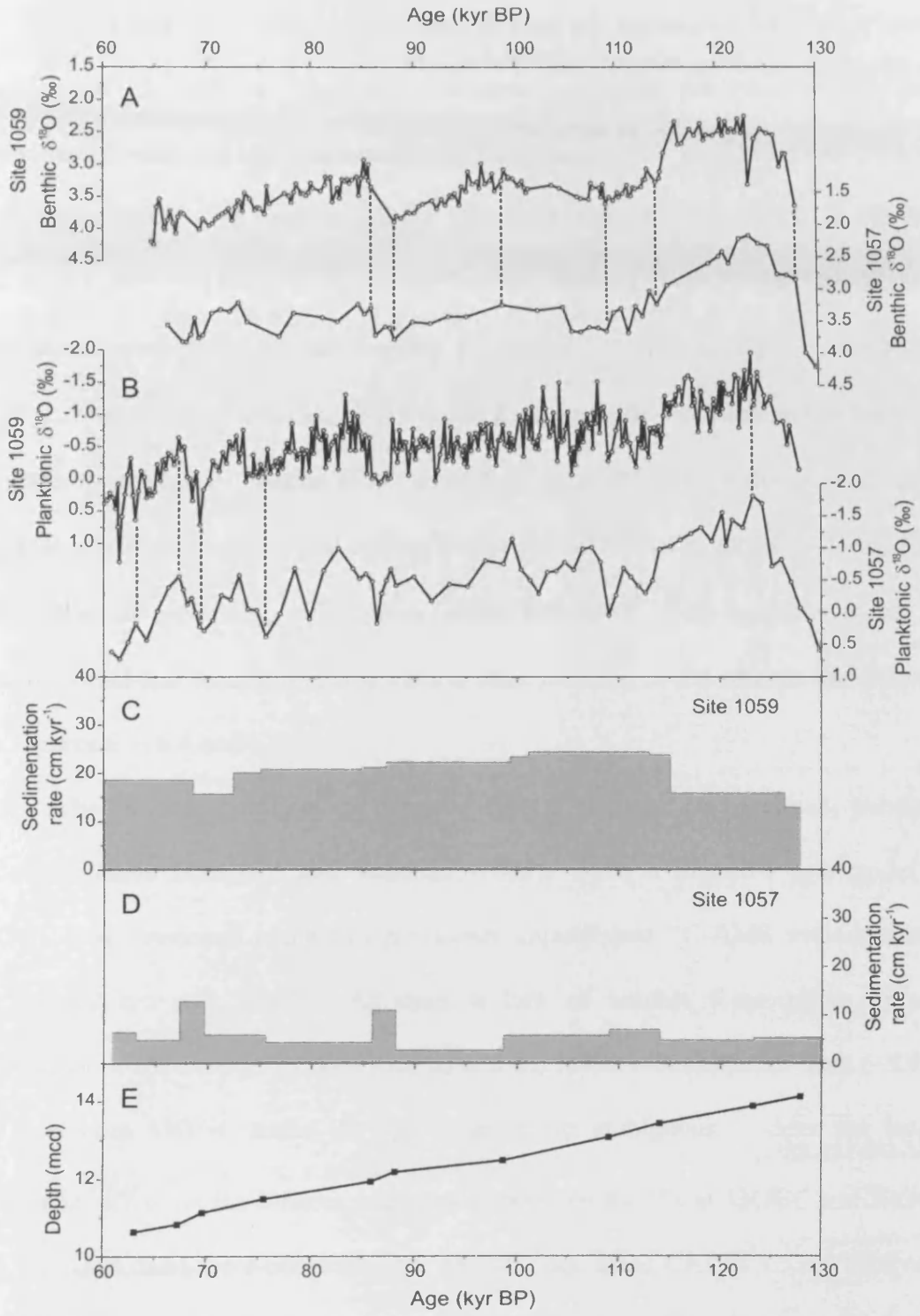

Figure 6.2: Chronology for Sites 1059 and 1057. (A) Benthic $\delta^{18}O$ data versus age (kyr BP) and (B) Planktonic $\delta^{18}O$ data versus age (kyr BP) for Site 1059 (2,997 m water depth) and Site 1057 (2,595 m water depth), respectively. (C) The sedimentation rates (cm kyr^{-1}) for Site 1059, and (D) the sedimentation rates (cm kyr^{-1}) for Site 1057. (E) The age-depth relationship for Site 1057. The Site 1059 chronology is based on Heusser and Oppo (2003). The age model for Site 1057 was generated by graphic correlation of the benthic and planktonic $\delta^{18}O$ with the Site 1059 records. Black lines show the correlation points used.

A number of previously published records are introduced for comparison in Section 6.4. In order to place each of these previously published records on a common timescale we have adjusted their chronologies to that of Site 1059 (Heusser and Oppo, 2003). The age models of Site 1060 (Bianchi *et al.*, 2001) at the BOR and KNR31-GPC-9 (Keigwin *et al.*, 1994) on the Bahama Outer Ridge (BahOR) were adjusted via correlation of their benthic $\delta^{18}O$ records with Site 1059. Core MD95-2036 (Lehman *et al.*, 2002) at the Bermuda Rise was also modified on the basis of a correlation between its benthic $\delta^{18}O$ record (Adkins *et al.*, 1997; Lehman *et al.*, 2002) and that of Site 1059, followed by fine tuning the MD95-2036 alkenone derived SST record and the planktonic $\delta^{18}O$ record from Site 1059. The locations of the age control points and resulting sedimentation rates for each of the records are shown in the Figures 6.3, 6.4 and 6.5.

The Holocene chronology for core 39GGC is based on previously published ^{14}C-AMS dates (Keigwin and Schlegel, 2002), while a tentative age model for 43GGC was developed using two previously unpublished ^{14}C-AMS dates located at 35 and 67 cm core depth. Although a lack of benthic foraminifera prevents correlation of the benthic oxygen records and the lower sedimentation rates (~5.9 cm kyr^{-1}) at core 43GGC make the age model more ambiguous, it does not have a substantial effect on the broader relationship between the $\overline{SS}$ at 43GGC and 39GGC. All ^{14}C-AMS dates were converted into calendar age using CALIB v.5.0.1 (Stuiver *et al.*, 2005), assuming a reservoir correction of 400 years. Ages between age control points were estimated by linear interpolation.

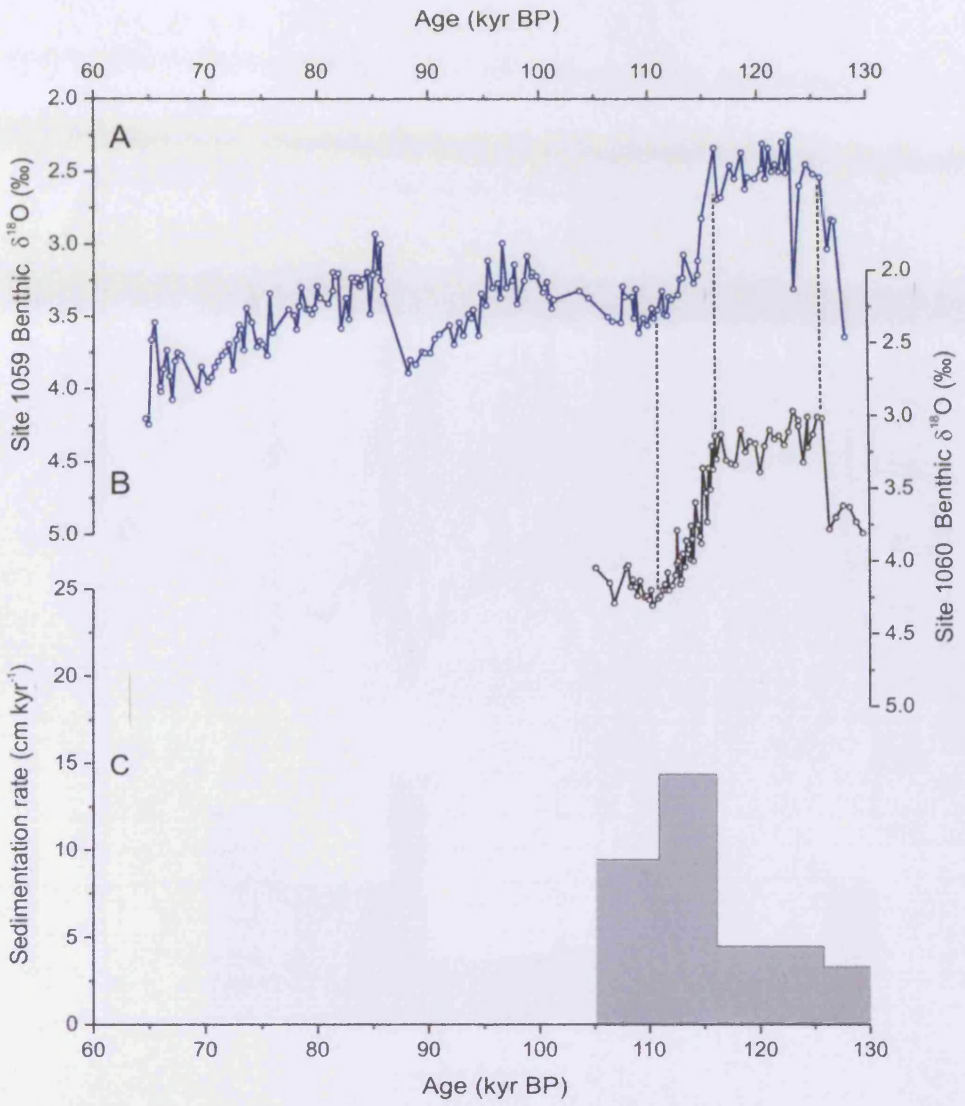

Figure 6.3: Adjusted chronology for Site 1060 (Bianchi *et al.,* 2001)] on the Blake Outer Ridge, derived by tying the benthic $\delta^{18}O$ record to the previously published benthic record from Site 1059 (Heusser and Oppo, 2003). (A) Benthic $\delta^{18}O$ data versus age (kyr BP) for Site 1059 (blue; 2,997 m water depth) and Site 1060 (black; 3,480 m water depth), respectively. (B) The resulting sedimentation rates (cm kyr^{-1}) for Site 1060. Black vertical lines show correlation points used.

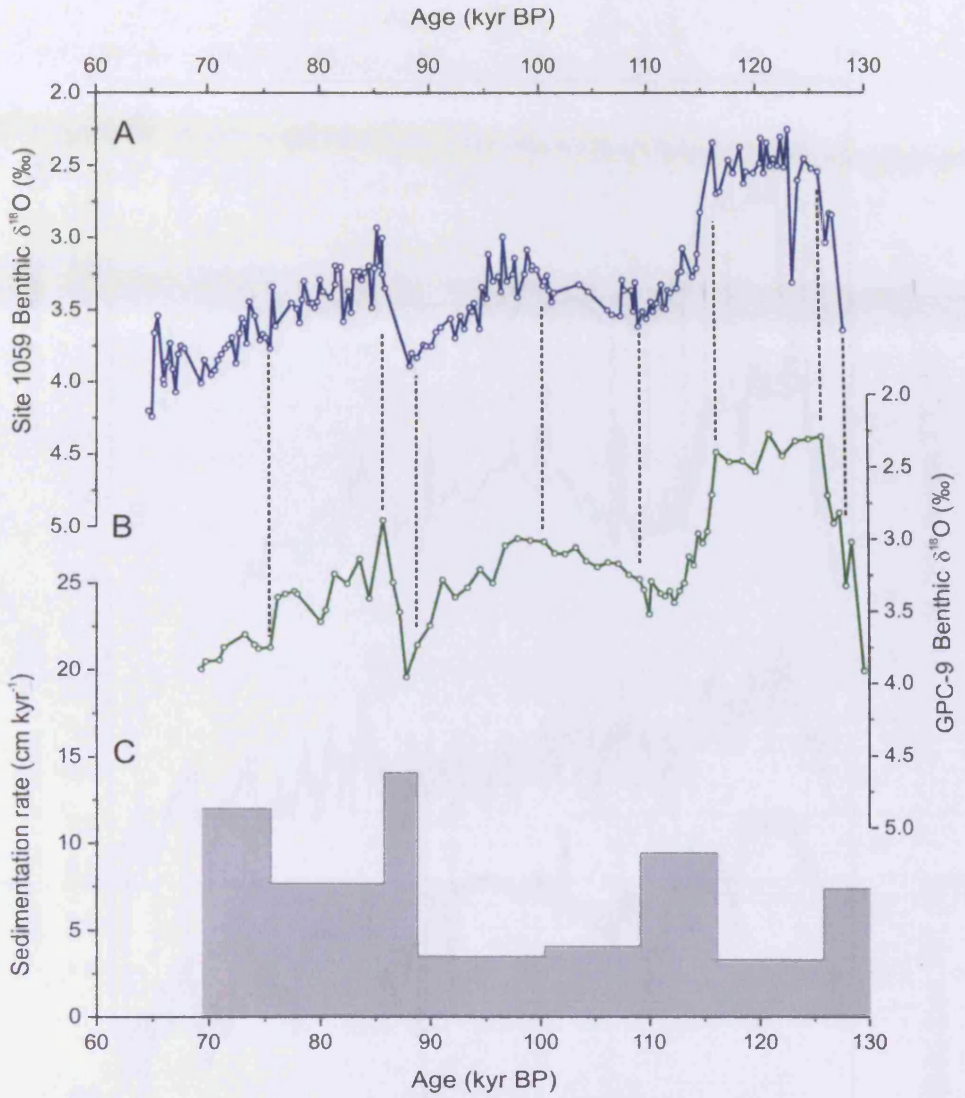

Figure 6.5: Adjusted chronology for Site GPC-9 (Keigwin *et al.,* 1994) on the Blake Outer Ridge, derived by tying the benthic $\delta^{18}O$ record to the previously published benthic record from Site 1059 (Heusser and Oppo, 2003). (A) Benthic $\delta^{18}O$ data versus age (kyr BP) for Site 1059 (blue; 2,997 m water depth) and Site GPC-9 (green; 4,760 m water depth), respectively. (B) The resulting sedimentation rate (cm kyr^{-1}) for Site GPC-9. Black vertical lines show correlation points used.

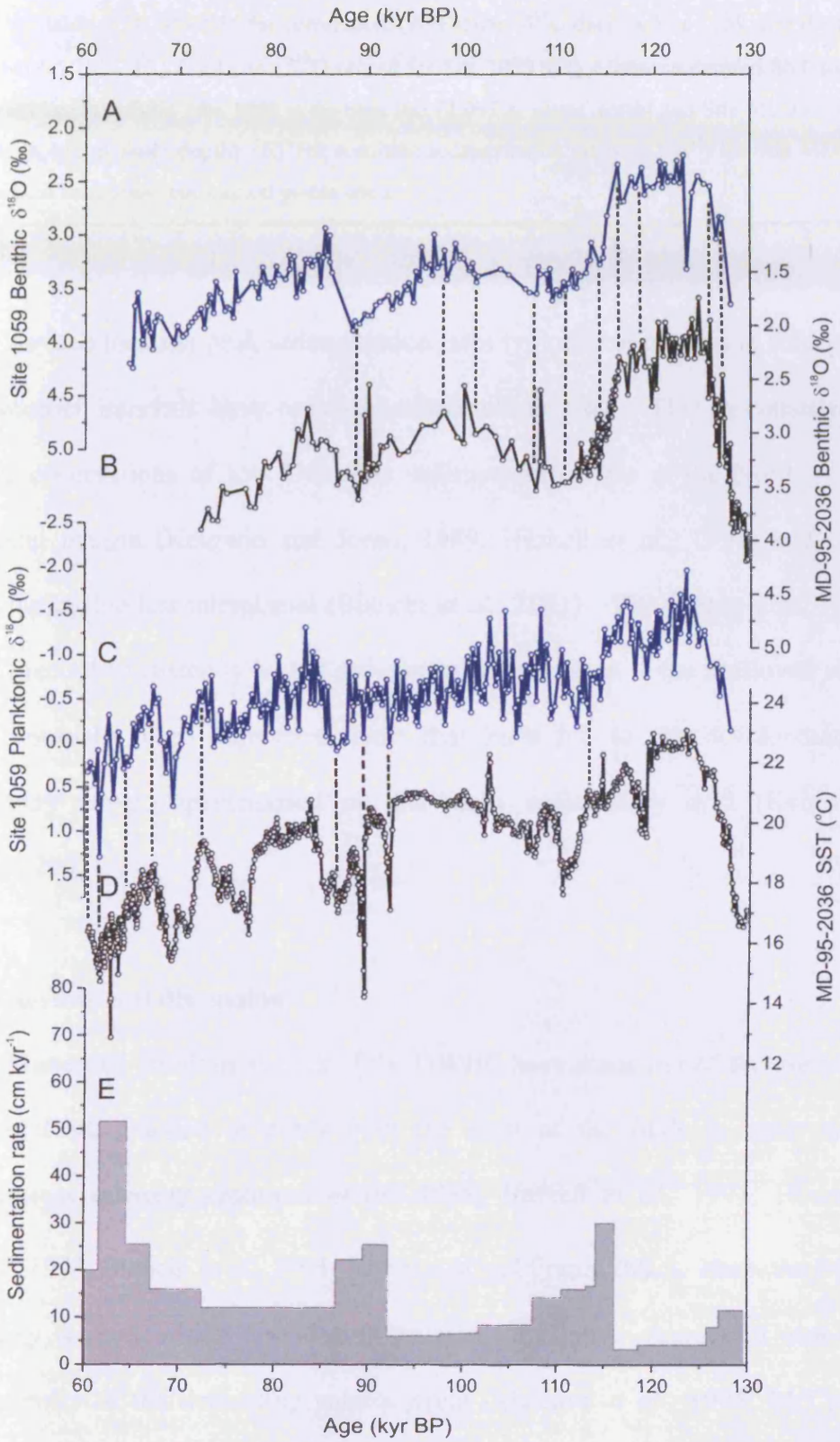

Figure 6.5: Adjusted chronology for Site MD-95-2036 (Lehman *et al.,* 2002) on the Blake Outer Ridge, derived by firstly tying the benthic $\delta^{18}O$ record to the previously published benthic record from Site 1059 (Heusser and Oppo, 2003) then fine tuning the correlation by tying the alkenone SST record of Site MD95-2036 to the planktonic $\delta^{18}O$ record from Site 1059 (Heusser and Oppo, 2003). This approach proved particularly useful in the younger part of the record where there were no benthic

isotopes available at MD95-2036 for correlation. (A) Benthic $\delta^{18}O$ data for Site 1059. (B) Benthic $\delta^{18}O$ data for MD95-2036. (C) Planktonic $\delta^{18}O$ record for Site 1059. (D) Alkenone derived SST for MD95-2036 versus age (kyr BP). Site 1059 is the blue line (2,997 m water depth) and Site MD95-2036 is the black line (4,462 m water depth). (E) The resulting sedimentation rate (cm kyr^{-1}) for Site MD95-2036. Black vertical lines show correlation points used.

At each location peak sedimentation rates typically occur during cold intervals while warmer intervals have reduced sedimentation rates. This is consistent with previous observations of low Holocene sedimentation rates at the North American continental margin (Keigwin and Jones, 1989; Haskell *et al.*, 1991) and previous studies during the last interglacial (Bianchi *et al.*, 2001). The deeper sites, 1059 and 39GGC, record consistently higher sedimentation rates than at the shallower sites due to the unusually high deposition rates that have led to the development of a sedimentary wave superimposed on the main sedimentary drift (Keigwin and Schlegel, 2002).

6.4 Results and discussion

Numerous previous studies of the DWBC have made use of the grain size of the detrital silt fraction of cores from the crest of the BOR in order to study palaeocurrent intensity (Johnson *et al.*, 1988; *Haskell et al.*, 1991; Haskell and Johnson, 1993; Bianchi *et al.*, 2001; Yokokawa and Franz, 2002). Here, the $\overline{SS}$ grain size proxy is used, which provides an estimate of relative changes in near-bottom flow intensity of the depositing palaeocurrent (McCave *et al.*, 1995; McCave and Hall, 2006), with near-bottom flow speeds decreasing with distance from the fast flowing core of the DWBC (Stahr and Sanford, 1999).

The $\overline{SS}$ proxy can be used where the source sediment is characterized by a broad range of grain sizes and the distance to the core site is sufficient for a sorted signal to develop (McCave *et al.*, 1995; Bianchi *et al.*, 2001, McCave and Hall, 2006). These conditions are met on the BOR as its supply of terrigenous sediment is principally transported by the DWBC (Heezen *et al.*, 1966) from the American continental margin. Bianchi *et al.* (2001) confirmed that at Sites 1060 and 1062 on the BOR there was no significant sediment input from ice rafted debris (IRD) or turbidity current influence during the MIS 5 interval. Likewise, visual inspection and core logs from Sites 1059 and 1057, which are both located on the ridge crest and so less likely to be affected by turbidites and debris flows, show no evidence of any major down-slope deposition events.

It has been shown that the DWBC changed position and migrated vertically in the water column during past climatic cycles (e.g. Ledbetter and Balsam, 1985; Johnson *et al.*, 1988; Haskell *et al.*, 1991; Bianchi *et al.*, 2001). As pointed out by Bianchi *et al.*, (2001), at any given point in time, no single value of the $\overline{SS}$ along the BOR is representative of the overall relative flow velocity of the DWBC. Therefore, any sedimentological palaeocurrent data from the BOR must be viewed in terms of both changing vigour at one or more given localities and position/depth of the DWBC. The records in this investigation (Figure 6.6) are interpreted using the same principles outlined in Bianchi *et al.* (2001), making the assumption that production rates of LNADW are a major control on the vertical movement of the DWBC. Therefore, as each of the core sites is located at water depths above the present day fast flowing primary DWBC core, a synchronous increase in $\overline{SS}$ at both depths is indicative of a shoaling of the DWBC core and a reduction in LNADW production.

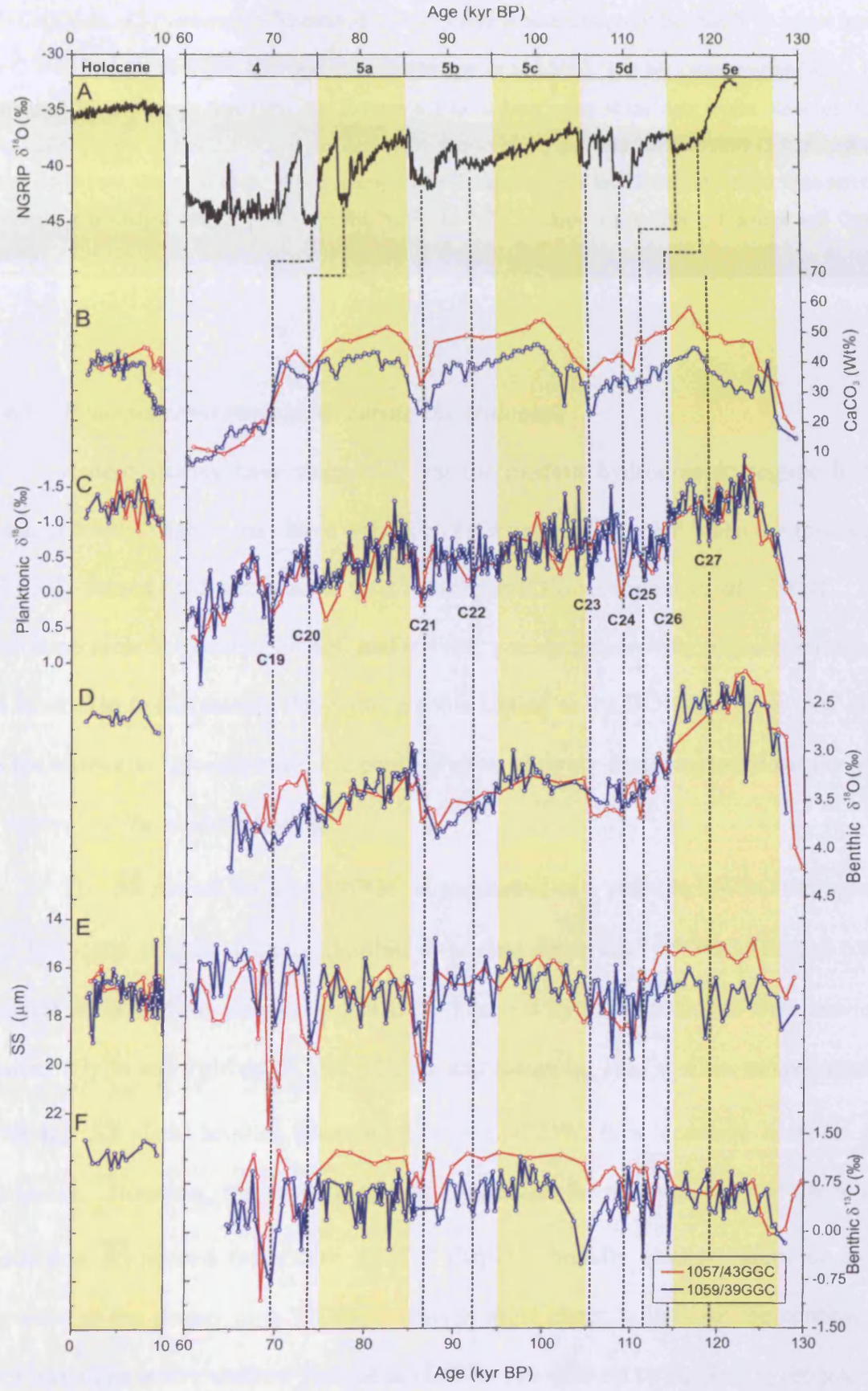

Figure 6.6: Holocene and MIS 5/4 proxy data for Sites 1059 and 1057. Note axis break between 10-60 kyr BP. From top to bottom: (A) NGRIP $\delta^{18}O$ (North Greenland Ice Core Project Members, 2004),

(B) CaCO3 %, (C) Planktonic $\delta^{18}O$ derived from *G. ruber* at both sites, (D) Benthic $\delta^{18}O$ where based on *C. wuellerstorfi* from Site 1059 and *Cibicidoides* spp. at Site 1057, (E) SS (note reversed axis), (F) Benthic $\delta^{13}C$ versus age (kyr BP). See Section 6.3 for a description of the data origin. Records from Site 43GGC/1057 (2,590/2,595 m water depth) are shown in red and Site 39GGC/1059 (2,975/2,985 m water depth) are shown in blue. Warm interglacial/substages are shaded. Vertical dashed lines refer to previously identified cold events (labelled "C19" to "C27"; Oppo *et al.*, 2001; Heusser and Oppo, 2003).

6.4.1 Palaeocurrent variability during the Holocene

Recent studies have suggested that the modern hydrographic regime in the western North Atlantic may have only been established ~7 kyr BP when the formation of LSW started (Hillaire-Marcel *et al.*, 2001 and Cottet-Puinel *et al.*, 2004). The Holocene records of cores 39GGC and 43GGC younger than ~7 kyr should, therefore, be most akin to the present day hydrographic setting at the BOR and these data offer us the chance to 'ground truth' the configuration of proxy data, employed for the MIS 5 interval, to the modern setting.

The $\overline{SS}$ record for core 39GGC is suggestive of a variable DWBC throughout the Holocene (Figure 6.6E). Benthic $\delta^{13}C$ data from core 39GGC (Figure 6.6F) suggest decreased ventilation of LNADW after ~8 kyr BP consistent with previous studies (Oppo and Fairbanks, 1987; Boyle and Keigwin, 1987). This, in conjunction with the $\overline{SS}$ data, implies greatest relative LNADW flow occurred early in the Holocene. However, the most important conclusion for this study is that the lower resolution $\overline{SS}$ record from core 43GGC displays broadly similar values to those recorded at the deeper core 39GGC. This is most likely to indicate the continuous presence of an active shallow limb of the DWBC, as detailed by modern hydrographic studies (Johns *et al.*, 1997; Stahr and Sanford, 1999) in the area, elevating the $\overline{SS}$

grain size at core 43GGC. A lack of benthic $\delta^{13}C$ data prevents the geochemical assessment of changes in ventilation at this site.

6.4.2 Palaeocurrent variability during the MIS 5 and 4

The boundaries of the MIS 5 sub-stages (Shackleton, 1969) discussed in this study are defined according to those set out in Heusser and Oppo (2003) and are represented by shaded panels in Figure 6.6. Comparing the $\overline{SS}$ for Sites 1057 and 1059 across the entire MIS 5 interval and into MIS 4 reveals the changing relationship of the relative flow speeds recorded at each site. Site 1057 shows a slight increasing trend in the $\overline{SS}$ throughout the record, a trend that is not present at Site 1059, although the $\overline{SS}$ increases in unison at both sites during the latter part of cold sub-stages 5d, 5b and during early stage 4 in conjunction with previously identified marine cold events (e.g. C19, C20, C21 and C23; McManus *et al.*, 1994; Oppo *et al.*, 2001; Heusser and Oppo, 2003). The $\delta^{13}C$ variations at Site 1057 also show a general increase to heavier values throughout the record, intersected by lighter excursions, indicating declining or reduced deep ocean ventilation during the larger cold events (C19-C24). Site 1059 records more pronounced excursions during these cold episodes, but the $\delta^{13}C$ values during the warm sub-stages (5c and 5a) remain similar to MIS 5e values.

During MIS 5e and early 5d (Figure 6.6E), the shallower Site 1057 records lower $\overline{SS}$ grain size values (mean = 15.4 μm) than Site 1059 (mean = 17.1 μm) and these are the lowest $\overline{SS}$ values throughout the record and are also lower than those observed in core 43GGC during the Holocene. The $\overline{SS}$ offset between the two sites is reasonably constant (1.7 μm ± 0.75 μm) and this observation strongly corroborates

one of the key assumptions in this work that sedimentation in the sortable silt range on the crest of the BOR is predominantly controlled by deepwater currents rather than simple down slope sediment movement where coarser grain sizes would always be found at shallower depths (Haskell *et al.*, 1991; Haskell and Johnson, 1993). Throughout the MIS 5e interval the benthic $\delta^{13}C$ (Figure 6.6E) at both sites are similar at around 0.7 ‰ and imply the presence of a well mixed water mass between the sites. To further investigate the extent of this water mass, benthic $\delta^{13}C$ data were incorporated from two deeper sites (Figure 6.7), ODP Site 1060 on the BOR (3,480 m; Bianchi *et al.*, 2001) and GPC-9 on the BahOR (4,758 m; Keigwin *et al.*, 1994). The $\delta^{13}C$ data from ODP Site 1060 (Bianchi *et al.*, 2001; Figure 6.7C) and GPC-9 (Keigwin *et al.*, 1994; Figure 6.7) also suggest the presence of a similar water mass at greater depths.

The benthic $\delta^{13}C$ records during MIS 5e are indicative of a water column that is dominated by NSW. However, the benthic $\delta^{13}C$ signature is slightly lighter than that experienced by core 39GGC in the Holocene (Figure 6.6F) and the $\delta^{13}C$ of ~1 ‰ (Kroopnick, 1985; Curry and Oppo, 2005) associated with contemporary LNADW. This suggests poorer ventilation during MIS 5e than the Holocene, with $\delta^{13}C$ values similar to those expected for the present day Bottom Water (BW) of Stahr and Sanford (1999; refer Chapter 2, section 2.1) where the influence of SSW is believed to slightly decrease the benthic $\delta^{13}C$ signature (Keigwin *et al.*, 1994). Today, BW on the BOR is restricted to water depths below 3,400 m and only contributes about 15% to the overall transport (Stahr and Sanford, 1999). However, it is suggested that during peak MIS 5e a NSW mass with a similar benthic $\delta^{13}C$ value to present day BW extended throughout the water column, at least up to ~2,600 m water depth, at the BOR.

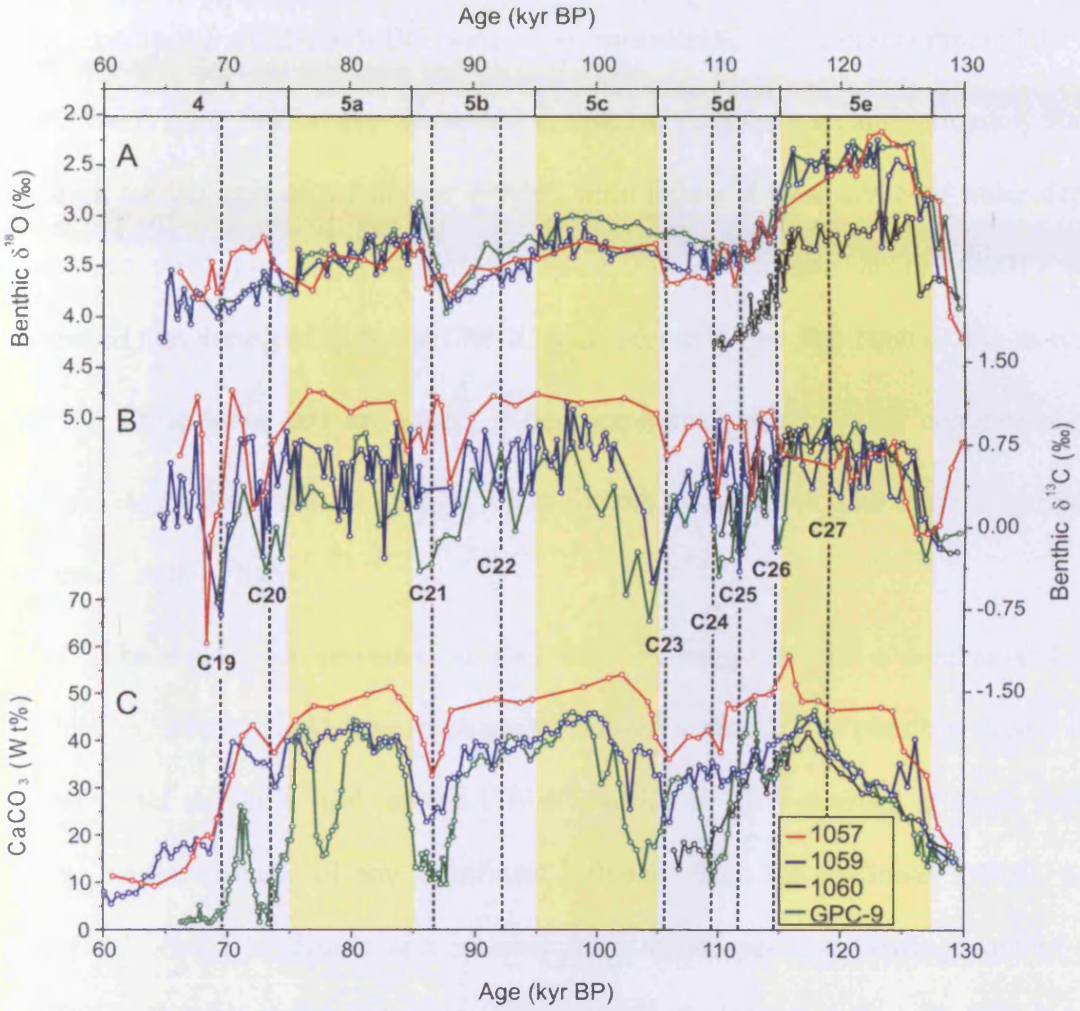

Figure 6.7: Extended depth range benthic isotope ($\delta^{18}O$ and $\delta^{13}C$) and $CaCO_3$ (wt%) data. From top to bottom: (A) Benthic $\delta^{18}O$, (B) Benthic $\delta^{13}C$, (C) $CaCO_3$ versus age (kyr BP). Records are shown in red (Site 1057, 2,584 m water depth), blue (Site 1059, 2,985 m water depth), black (Site 1060, 3,480 m water depth) and green (GPC-9, 4,758 m water depth). Data for Site 1060 are from Bianchi *et al.* (2001) and are based on *Cibicidoides wuellerstorfi*, *Cibicidoides* spp. and *Uvigerina* spp. The $\delta^{18}O$ results for *C. wuellerstorfi* and *Cibicidoides* spp. have been corrected by +0.64 ‰ to account for species dependent isotopic fractionation and a correction of +0.7 ‰ has been applied to the $\delta^{13}C$ data for *Uvigerina spp.* (see Bianchi *et al.*, 2001 for further details). The GPC-9 data from Keigwin *et al.* (1994) only show the *Cibicidoides* spp. record in this study. Warm interglacial/substages are shaded. Vertical dashed lines refer to previously identified cold events (labelled "C19" to "C27"; *Oppo et al.*, 2001; Heusser and Oppo, 2003).

The clear offset between the $\overline{SS}$ of Sites 1057 and 1059 demonstrates that flow conditions of the DWBC were also considerably different compared to the Holocene (Figure 6.6E). The $\overline{SS}$ record at Site 1059 suggests an approximately stable position for the axis of the deeper DWBC limb below at least 2,985 m water depth, consistent with the palaeocurrent reconstruction of Bianchi *et al.* (2001) who suggested that during MIS 5e the DWBC was located below Site 1060 (3,461 m water depth). These latter data are based on Sedigraph analysis of the $\overline{SS}$ component and the resulting grain sizes are therefore not directly comparable with the $\overline{SS}$ estimates presented in this study.

The lower $\overline{SS}$ recorded at Site 1057 is suggestive of a weakened LSW production, which would have presumably caused a shoaling or possibly even a loss of the upper dynamic limb of the DWBC, which is LSW-sourced at these depths today. In the absence of any significant influence from the shallower DWBC core Site 1057 would be distant and isolated from the deeper fast flowing core of the DWBC. The formation and properties of the North Atlantic intermediate and deep water over the last interglaciation are contentious. Hillaire-Marcel *et al.* (2001) suggest that LSW formation was absent during the last interglacial and advocate the presence of a single water mass originating from the Nordic Seas overlain by a thin buoyant surface layer. While Rasmussen *et al.* (2003) conclude that LSW, with a fairly similar composition as today, was generated throughout the peak of MIS 5e. They also suggest the presence of a benthic foraminiferal "Atlantic assemblage" that does not appear to be linked to overflow water from the Nordic Seas. The compiled benthic $\delta^{13}C$ record presented here strongly supports the presence of a uniform water mass, dominated by LNADW below ~2,500 m on the BOR, during peak MIS 5e, with evidence from the Site 1057 flow speed record of a weakened LSW. At 2,584 m

water depth Site 1057 is located at the base of LSW influence on the BOR and therefore highly sensitive to relative changes in LSW and LNADW production and DWBC flow. However, we need to be cautious as, clearly, on the basis of our $\overline{SS}$ data alone we cannot rule out continued vigorous production of SLSW ventilating shallower depths.

The benthic $\delta^{13}C$ records (Figure 6.7B) suggest an apparent reorganisation in the hydrography and flow of the DWBC starting close to the MIS 5e-5d boundary at ~117-110 kyr BP. At this time a significant lowering of $\delta^{13}C$ values was experienced at the two deeper sites (Sites 1060 and GPC-9) indicative of decreasing ventilation, while conditions at the two shallower sites (1057 and 1059) experience a smaller shift towards heavier values. In terms of the $\overline{SS}$ records this transition is much less obvious but is marked by the onset of gradually increasing $\overline{SS}$ at Site 1059 and 1057 (Figure 6.6E). These data support a shoaling of the water column structure in response to a decrease in LNADW production at that time (Adkins *et al.*, 1997; Hall *et al.*, 1998). Such a transition is consistent with the indication of a reduction in the depth of the deep core of the DWBC suggested in the Site 1060 $\overline{SS}$ record at ~118-117 kyr (Bianchi *et al.* 2001). Bianchi *et al.* (2001) suggest that it was only after ~113 kyr that the core of the DWBC shoaled above Site 1060. This study further suggests that the reduced LNADW between ~118-113 kyr is part of a longer transition. At ~111 kyr BP, a significant shift in the relationship between the $\overline{SS}$ and benthic $\delta^{13}C$ is observed at Sites 1057 and 1059 (Figure 6.6E, 6.6F): a $\overline{SS}$ increase at Site 1057 is responsible for the flow speed records at both sites converging and subsequently behaving more coherently through the remainder of MIS 5 and into MIS 4. It is suggested in this study that such behaviour is indicative of the re-

establishment of a stronger and possibly deeper secondary core of the DWBC after ~111 kyr. The strengthening and deepening of the shallower core would increase the flow speeds recorded at Site 1057 while possibly depressing the depth of the deeper flowing DWBC core. Coincident with this shift, the benthic $\delta^{13}C$ records diverge and Site 1057 benthic $\delta^{13}C$ values increase to typically >1 ‰ while the long-term values at Site 1059 remain unchanged. Immediately following this divergence the benthic $\delta^{13}C$ at GPC-9 reach minimum values (Figure 6.7B). The increased benthic $\delta^{13}C$ values at Site 1057 imply the development of a clear hydrographic boundary in the ~500 m of water column that separate the two sites. The shallower, more nutrient depleted water mass has benthic $\delta^{13}C$ values slightly higher than those experienced in the Holocene at 39GGC, implying that this water mass is of a northern origin and may represent the initiation of, or a similar water mass to Glacial North Atlantic Intermediate Water (GNAIW) formation. This is supported by Chapman and Shackleton (1998, 1999) and Chapman *et al.* (2000) who suggest that the gradual increase in $\delta^{13}C$ values in core SU90-03 (40°N, 32°W, 2,475 m water depth) in the North Atlantic during MIS 5, could signify a long-term change in the depth and/or production rate of NADW. This, in conjunction with the re-establishment of the shallower core of the DWBC, could also explain the long term increase in the $\overline{SS}$ evident at Site 1057 throughout the record (Figure 6.6E). However, it should be noted that Oppo and Lehman (1995) documented a similar rising trend in benthic $\delta^{13}C$ within MIS 5 in sub-polar North Atlantic core V29-202 (2,658 m water depth), and argued that it was driven by the changing composition of tropical surface feed waters, driven by either biological or thermodynamic processes. However, our grain size records demonstrate that a change in DWBC geometry occurred over MIS 5 and suggests that observed benthic $\delta^{13}C$ values can not be explained solely by changes in

the preformed composition of the surface waters, but must involve a physical change in deep ocean circulation.

Curry and Oppo (2005) demonstrate that the sharp boundary at ~2,000 m in the subpolar North Atlantic between northern and southern source water masses during the LGM is eroded as GNAIW flows southwards towards the BOR study sites and mixes with Southern Ocean waters. At comparable latitudes to the BOR the whole depth range from 2,000-4,000 m appears to be in a mixing zone. Although the precise geometry described by Curry and Oppo (2005) during the LGM may differ slightly from that experienced within MIS 5, our results suggest that once the $\delta^{13}C$ gradient was established it persisted throughout the subsequent glaciation and that at least 1059 lay in a water mass gradient most of the time. This is supported by data from GPC-9 (Keigwin *et al.*, 1994; Figure. 6.7C), which show a similar benthic $\delta^{13}C$ pattern to the shallower two sites but with a more pronounced influence of SSW.

The latter parts of cold substage 5b and, to a lesser extent, 5d are characterised by a transient interval of increased $\overline{SS}$ associated with significant positive excursions in the planktonic $\delta^{18}O$ records at each site indicative of sea surface cooling (cold events: C24, C23 and C21; Figure 6.6C, 6.6E). A lack of benthic foraminifera, possibly due to the increased influence of corrosive SSW, particularly during the MIS 5b event, precludes a clear observation of the deep hydrographic changes associated with these intervals but do hint at reduced water column ventilation. An increase in dissolution during these intervals is consistent with the reduced $CaCO_3$ observed (Figure 6.7C; Keigwin *et al.*, 1994). The maxima in DWBC flow speeds during these intervals are indicative of a rapid shoaling of the DWBC to a depth at which the fast flowing core is close to Sites 1059 and 1057 and most likely increased influence of SSW.

MIS 4 is only partly represented in our records. However, it is during this interval that the largest changes in DWBC flow speed and hydrography are recorded. Two $\delta^{13}C$ excursions centred at ~75 and ~69 kyr, consistent with surface cooling events C20 and C19, are associated with a substantial increase in the flow speed at Site 1057 and a smaller increase at the deeper Site 1059 (Figure 6.6C, 6.6E). This suggests a significant decrease in NADW/GNAIW production leading to a rapid shoaling of the deeper DWBC core more proximal to and possibly above Site 1057. These flow speed changes are accompanied by similarly abrupt excursions in the benthic $\delta^{13}C$ records at both sites, and have also been previously documented on the BahOR (Keigwin *et al.*, 1994). In the case of the younger C19 event benthic $\delta^{13}C$ values fall to below -0.5 ‰ at both Site 1057 and 1059, characteristic of a water mass similar to unmodified SSW during the LGM (Oppo and Fairbanks, 1987; Curry *et al.*, 1988). During the interstadial intervals surrounding these cold events the benthic $\delta^{13}C$ and $\overline{SS}$ values return to similar levels as those observed during MIS 5a. The correlation of these events in the deep ocean to other proxies such as the $\delta^{18}O$ NGRIP record which provides a temperature proxy record for the northern North Atlantic (Figure 6.6) highlights the potential global significance of these oscillations.

6.4.3 Surface-deep ocean links

Oppo *et al.* (2001) have previously made a detailed study comparing the planktonic $\delta^{18}O$ record at Site 1059 to its benthic $\delta^{13}C$ record, finding virtually synchronous oscillations between the two proxies suggestive of a persistent surface-deepwater linkage from early in MIS 5e. Oppo *et al.* (2001) argue that sea surface temperature (SST) variability provides the simplest explanation for the suborbital oscillations (4-10 kyr pacing) in planktonic $\delta^{18}O$ apparent during MIS 5, as they are

similar in magnitude and timing to the planktonic $\delta^{18}O$ variations in MIS 3, which have been previously attributed to SST (Keigwin and Boyle, 1999; Sachs and Lehman, 1999). In this study it is clear that planktonic $\delta^{18}O$ (Oppo *et al.*, 2001) evidence for surface cooling, particularly during cold events C24-C19, is not only associated with weak NADW (low benthic $\delta^{13}C$), but also corresponds to a shoaling DWBC as represented by increasing $\overline{SS}$ values (Figure 6.6).

No specific SST proxy measurements are available for MIS 5 from the BOR, so in Figure 6.8 we compare the Site 1057 and 1059 proxy records with the high resolution SST record derived from measurements of the unsaturated alkenone ratio in core MD95-2036 recovered from the nearby Bermuda Rise (33°41.4'N, 57°34.5'W, 4,462 m water depth; Lehman *et al.*, 2002). The correlation between the SST at MD95-2036 and the planktonic $\delta^{18}O$ at 1057 and 1059 (Figure 6.8A) confirms the presence of a series of synchronous abrupt cooling events at each site. Intriguingly, comparison of the alkenone derived SST record and the planktonic $\delta^{18}O$ record of Site 1059 also reveals a lack of shorter timescale structures in the alkenone record compared to the planktonic $\delta^{18}O$ record. This finer structure in the Site 1059 planktonic $\delta^{18}O$ data could be a function of changes in sea surface salinity (SSS), which is not recorded in the purely temperature-related alkenone record. Alternatively, the finer timescale structure may be lost in the alkenone record due to mixing of alkenones of different ages in any one sample (Ohkouchi *et al.*, 2002), or it could result from changes in seasonality, preservation or depth habitat between the two proxies (e.g. Popp *et al.*, 2006).

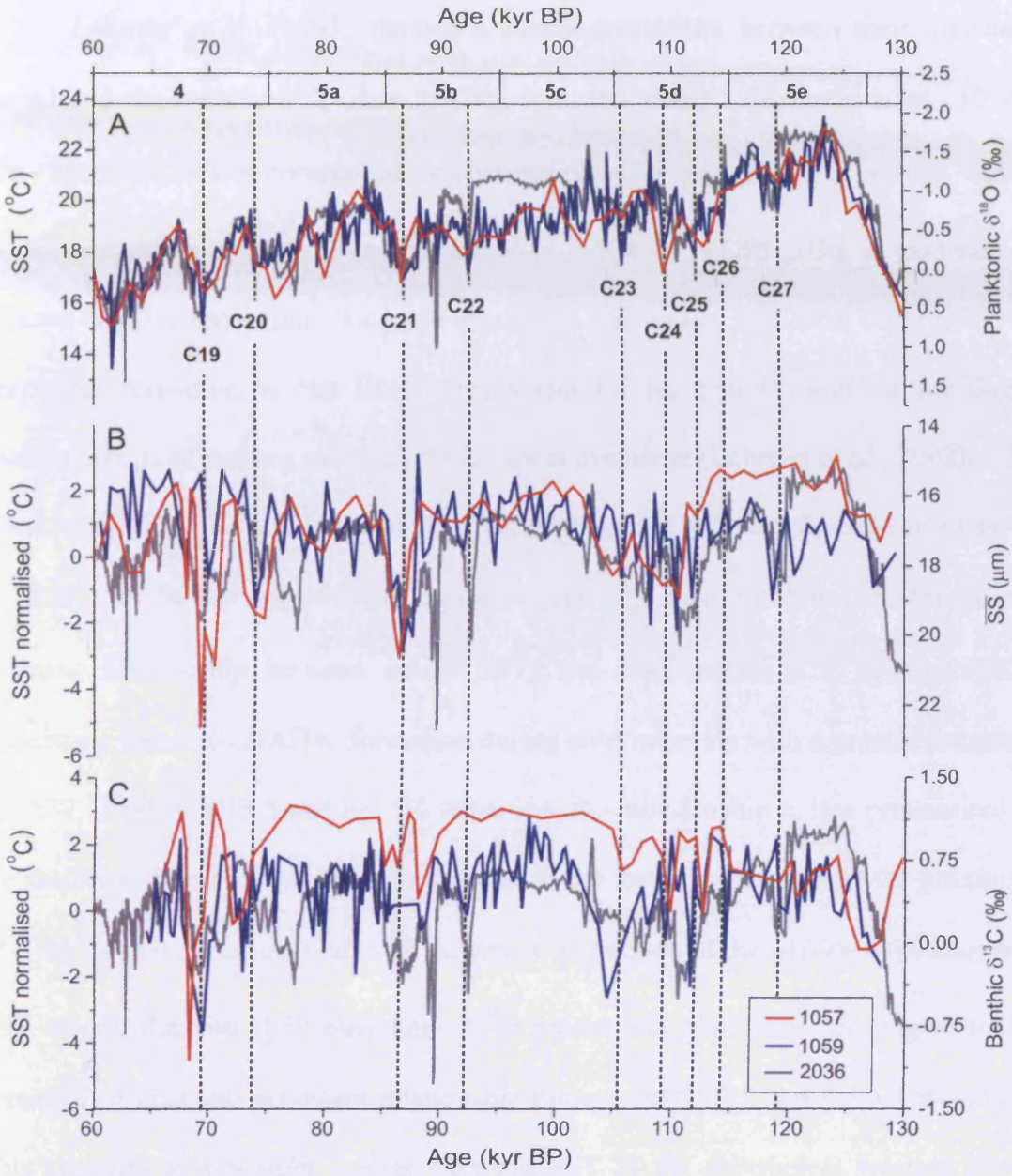

Figure 6.8: Comparison of the alkenone-derived SST from Bermuda Rise core MD95-2036 (Lehman *et al.*, 2002) and Site 1059 and 1057 proxy records. (A) MD95-2036 alkenone-derived SST along with planktonic $\delta^{18}O$ for Sites 1057 and 1059. (B) Sea surface temperature (SST) normalised using a simple 2nd order polynomial regression along with $\overline{SS}$ results for Sites 1057 and 1059. (C) Normalised SST along with the benthic $\delta^{13}C$ data for Sites 1057 and 1059. Vertical dashed lines refer to previously identified cold events (labelled "C19" to "C27"; Oppo *et al.*, 2001; Heusser and Oppo, 2003).

Lehman *et al.* (2002) showed a strong correlation between their alkenone record and the benthic $\delta^{13}C$ data of GPC-9 on the BahOR (Keigwin *et al.*, 1994). They observed a clear correspondence between low SST and low $\delta^{13}C$ values, which is also recorded in the $\overline{SS}$ record of Hall *et al.* (1998) in MD95-2036, as evidence of reduced NADW formation. This has resulted in speculation that local suppression of deepwater formation is one likely mechanism for the amplification of the direct cooling effects of iceberg melting and ice sheet discharge (Lehman *et al.*, 2002). The relationship described by Lehman *et al.* (2002) together with the findings of Oppo *et al.* (2001) are further substantiated by the benthic $\delta^{13}C$ record of Site 1059 that shows a strong relationship between colder SSTs and low benthic $\delta^{13}C$ (Figure 6.8C), suggesting reduced LNADW formation during cold intervals with a greater influence of SSW. During MIS 5 and the 5/4 transition, this relationship is less pronounced at the shallower Site 1057 probably in part due to the lower resolution and the proximity of GNAIW that maintains high $\delta^{13}C$ values. Comparison of the MD95-2036 alkenone SST record, the Site 1059 planktonic $\delta^{18}O$ record and Site 1059 $\overline{SS}$ (Figure 6.8B) reveals a striking and persistent relationship throughout MIS 5 and the 5/4 transition. This suggests a very tight linkage between SST in the subtropical western North Atlantic and DWBC activity which extends north to the Bermuda Rise. The link between these shallow and deep locations may lie in the Nordic Seas. During the last interglacial surface temperature variations in the Nordic Seas coincided with deepwater changes (Fronval and Jansen, 1996; Fronval *et al.*, 1998), with the majority of fluctuations being related to reductions in the MOC. Furthermore, Oppo *et al.* (2001) suggest that during deglacial and glacial periods ocean-ice interactions and deepwater variability may amplify suborbital variability. They suggest that during the penultimate deglaciation the NADW production varied between the Nordic Seas and

open North Atlantic positions, similar to the situation thought to occur during the LGM (Boyle and Keigwin, 1987), and this occurred in parallel with SST oscillations. It is suggested that this situation was not confined to the penultimate deglaciation but played an important role throughout MIS 5 and into MIS 4, with warm water penetrating into the Nordic Seas resulting in melting of ice and a weakening of NADW formation (Oppo *et al.* 2001). The effects of these intervals of weaker and shallower NADW formation are not confined to the marine environment. They can also be linked to cold events in the terrestrial pollen record of the south-eastern USA (see Heusser and Oppo, 2003) and the larger oscillations (C19-C24) have cold counterparts in the Greenland ice core records (Figure 6.6). Although the cause of such suborbital variability remains unknown, the observed variations in deepwater circulation and the associated northward transport of heat are likely to have played an important role communicating the climatic variation throughout the wider circum-North Atlantic region (Heusser and Oppo, 2003).

6.5 Summary and conclusions

This study presents the first comprehensive $\overline{SS}$ records and $\delta^{13}C$ gradients between sites on multiple cores for MIS 5 and early MIS 4. A schematic representation of the water column and high velocity core of the DWBC on the eastern flank of the BOR during the major intervals discussed above is presented in Figure 6.9. Palaeocurrent and hydrographic reconstructions suggest that the configuration of DWBC flow was substantially different during peak MIS 5e from the Holocene with strong evidence for a weakened LSW influence. Instead, a well mixed water mass, dominated by LNADW but less well ventilated than during the Holocene was present over a broad depth range from 2,584 to 4,758 m water depth.

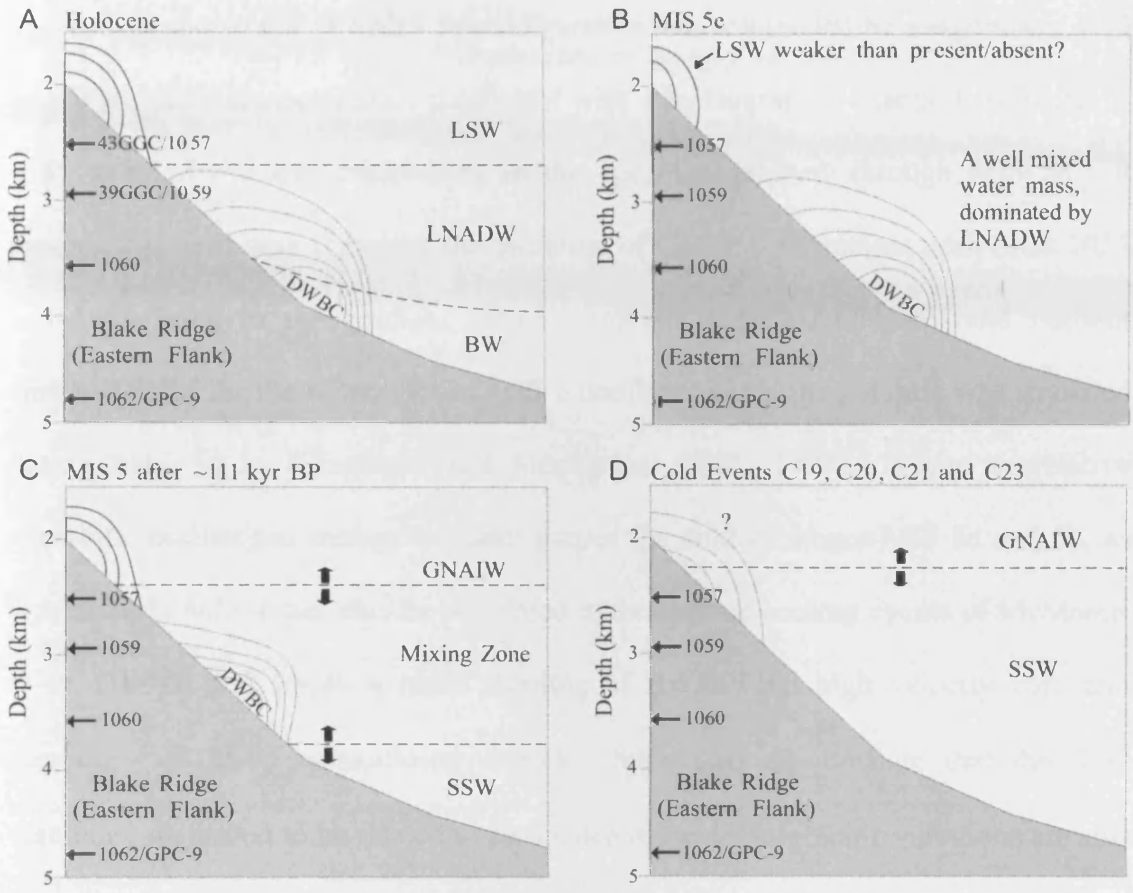

Figure 6.9: Schematic representation of the high velocity core of the DWBC on the eastern flank of the BOR for: (A) Present day after Stahr and Sanford (1999), and (B) peak MIS 5e, the influence of LSW and the shallow core have been reduced. The main axis of the current remains close to its present position but with the presence of a well mixed water mass. (C) MIS 5 after ~111 kyr BP, with the re-initiation of the shallower secondary core of the DWBC. LNADW has been replaced by a GNAIW like water mass. The sites sit in the gradient between these water masses. (D) Marine cold events C19 C20, C21 and C23 show an incursion of SSW to shallower depths and a shoaling of the high velocity core of the DWBC proximal to Sites 1059/1057. The boundaries of the various water masses defined within the text are shown by dashed lines, along with the depths not the positions of the sites under investigation. Arrows indicate the fluctuating behaviour of the water mass boundaries. The position of these idealised cross sections is shown in Figure 6.1.

It is shown that the MIS 5e configuration was terminated by a significant shift in DWBC flow characteristics coincident with a hydrographic change that began as early as ~118-117 kyr culminating in the transition midway through MIS 5d. It appears this shift may represent the initiation of GNAIW formation, with Sites 1057 and 1059 lying in the gradient between nutrient depleted GNAIW and nutrient enriched SSW for the remainder of MIS 5 confirming that the Atlantic was stratified during MIS 5d-5a (Chapman and Shackleton, 1998, 1999). Large correlative suborbital oscillations during the latter part of the cold substages MIS 5d and 5b, as well as early MIS 4 can also be correlated to the surface cooling events of McManus *et al.* (1994), and imply a rapid shoaling of the DWBC high velocity core and incursions of SSW to shallower depths. Such data demonstrate that the $\delta^{13}C$ variations suggested to be related to abrupt deepwater hydrographic variations are also associated with large scale dynamic changes in the DWBC flow. Furthermore, comparison with surface ocean oxygen isotope records and the alkenone derived SST estimates for core MD95-2036 on the Bermuda Rise (Lehman *et al.*, 2002) highlights a persistent link between subtropical North Atlantic surface ocean climate and the dynamics of the underlying DWBC. The results of this study demonstrate the importance of using multiple proxies related to both the hydrographic properties of deep ocean water masses and dynamical tracers of deep ocean flow in order to provide a better appreciation of past MOC variability.

Chapter 7: Summary and future work

7.1 Introduction

High resolution, multi-proxy analyses have been undertaken on a suite of sediment cores recovered from the BOR region in the western subtropical North Atlantic. These records have enabled a detailed reconstruction of the DWBC flow and its associated climatically important deepwater masses during various time intervals covering the past 130 kyr. The $\overline{SS}$ proxy, in conjunction with the SS% and silt/clay ratio, have been applied to sediment cores to produce depth transects at the BOR in order to provide insights into changes in DWBC intensity and to map its migration within the water column during selected climatic intervals. Changes in the intensity of the DWBC and/or changes in its position, observed in this study, have been linked back to changes in production rates in the deepwater source areas. The reconstruction of sea surface conditions at the BOR has been compared with changes in the circum-North Atlantic in order to assess the relative influence of changes in the MOC, hydrological cycle and meltwater events on the subtropical North Atlantic. Furthermore, an assessment was made of the consistency of the data presented in this investigation with suggestions of changes in the mode of the MOC during the climatic extremes of the past 130 kyr (Sarnthein *et al.,* 1994; Rahmstorf, 2002). The main results obtained in this dissertation are summarised below, followed by suggestions for further work.

7.2 Holocene, LGM and YD time slice reconstructions (Chapter 3)

Sedimentological proxies, stable isotopes and $CaCO_3$ records were used to assess the position and intensity of the DWBC during the Holocene, and the climatic

extremes of the LGM and the YD. A selection of core sites were carefully chosen to form detailed depth transects covering: (1) the mouth of the BOR; (2) part of the ridge crest, and; (3) the eastern flank of the ridge.

The initial purpose of this study was to ground truth the $\overline{SS}$ proxy against both physical and chemical hydrographic measurements (e.g. Stahr and Sanford, 1999; Curry and Oppo, 2005). The proxy and measured data are consistent, showing a vigorous core of the DWBC flow dominated by nutrient-depleted NADW between ~3,000-4,000 m water depth, which deepens to ~4,500 m water depth on the southeastern end of the ridge flanks. A shallower, secondary core of the DWBC is shown to be present along the transect over the crest of the ridge above 2,500 m. Although this cannot be confirmed by the other transects, such a feature has been observed in physical hydrographic measurements of the region (Johns *et al.*, 1997; Stahr and Sanford, 1999). The results of this study differ markedly from early attempts to reconstruct the modern flow regime at the BOR (Haskell and Johnson, 1993), highlighting the importance of using the 'sortable silt' fraction (10-63 μm) for grain size analyses aimed at reconstructing relative near-bottom current flow intensity, rather than the bulk silt fraction which includes coarse clays (in the 2-10 μm range) that behave cohesively and are therefore not sorted by currents individually (McCave *et al.*, 1995; McCave and Hall, 2006).

The LGM and YD reconstructions show that a similar hydrographic regime was present during both these intervals confirming the previous suggestions of Keigwin (2004). As expected, this regime was appreciably different to the previously described Holocene reconstruction. Nutrient-depleted, vigorously flowing water was confined to depths shallower than 2,500 m, consistent with GNAIW formation (Marchitto *et al.*, 1998; Curry and Oppo, 2005), while below 2,500 m the influence of

SSW increased with depth suggesting a highly stratified water column, with a large mixing zone between GNAIW and SSW. Below 4,000 m water depth, $\overline{SS}$ results hint at increased SSW flow vigour during both the LGM and YD with higher flow speeds than during the Holocene.

This study provides a framework for interpreting further proxy records in this region, particularly the $\overline{SS}$, in terms of changes in the intensity and depth of the DWBC and its component water masses.

7.3 Sea surface temperature and salinity reconstructions (Chapter 4)

Currently, there is considerable disagreement on the exact timing and spatial pattern of SST and salinity variability in the (sub)tropics during the last glacial-interglacial cycle, which could have important implications for our understanding of climate change induced variability in the MOC (Lea *et al.*, 2003; Flower *et al.*, 2004). High resolution SST and salinity records derived from Mg/Ca measurements on the foraminifera *G. ruber* (white), display evidence that rapid oscillations have occurred in the environmental conditions of the surface waters in the western subtropical North Atlantic during the last deglaciation. The SST record suggests the BOR is only partially influenced by the heat retention which generally dominates the tropical regions (Flower *et al.*, 2004; Schmidt *et al.*, 2004) during periods of reduced NSW export. Early in the deglaciation, prior to H1, the BOR is influenced by tropical heat retention, however, after the initiation of H1 the SST record at the BOR tracked Greenland air temperatures and tropical heat retention was likely to have been restricted to lower latitudes. The strength of the Gulf Stream also influences the SST record at the BOR.

Salinity reconstructions at the BOR reflect a combination of meltwater inputs, the evaporation-precipitation balance of the region and variations in the activity of the MOC. Heinrich event 1 is marked by a low salinity anomaly suggesting that meltwater from the eastern outlets of the Laurentide ice sheet reached as far south as the subtropics close to the continental margin. During the latter stages of H1 and the YD there is a salinity build up at the BOR consistent with tropical sites in the Gulf of Mexico and Caribbean Sea (e.g. Flower *et al.*, 2004; Schmidt *et al.*, 2004), due to a slowing down of the MOC (McManus *et al.*, 2004) and an increase in the evaporation-precipitation balance (Peterson *et al.*, 2000; Lea *et al.*, 2003; Wang *et al.*, 2004) caused by a southward migration of the ITCZ. During the latter stages of the B/A a meltwater signal routed via the Mississippi River into the Gulf of Mexico influences salinity at the BOR, consistent with a Northern Hemisphere origin for at least part of MWP-1a as proposed by Stanford *et al.* (2006). This meltwater pulse may have 'primed' the North Atlantic ready for the YD.

7.4 Divergent flow speeds in the deep North Atlantic (Chapter 5)

The search for the causes of rapid climate change has dominated previous research in the northern North Atlantic, with few studies concentrating on the role played by SSW. However, the production of cold, deep waters in the Southern Ocean is an important factor in the Earth's heat budget, and the involvement of deep SSW in deglacial climate change has yet to be fully understood. The $\overline{SS}$ data from two sediment cores retrieved from the western subtropical North Atlantic were used to reconstruct past changes in the speed of LNADW and SSW in the region. Evidence is presented for a broad-scale divergence in flow speed changes at the two sites, with the presence of a vigorous, but poorly ventilated SSW mass at ~4,200 m water depth

during the cold episodes of the last deglaciation when shallower (2,975 m water depth) $\overline{SS}$ and geochemical data suggest that NSW was suppressed. This is consistent with the operation of a bipolar see-saw (e.g. Broecker *et al.*, 1998).

7.5 Deep Western Boundary Current variability during MIS 5 and 4 (Chapter 6)

High resolution orbital and suborbital $\overline{SS}$ and benthic $\delta^{13}C$ records from ODP Sites 1057 (2584 m water depth) and 1059 (2985 m water depth) presently bathed by LSW and LNADW, respectively, were used to reconstruct the behaviour of the DWBC on the BOR from 130 to 60 kyr BP (MIS 5 and the 5/4 transition). The results are compared to two previously published records from deeper sites in the area investigated using similar methods in order to trace the vertical migration of the DWBC and the changes in water mass properties in time and space. During peak MIS 5e conditions palaeocurrent and hydrographic reconstructions suggest that the configuration of DWBC flow was substantially different from the Holocene with strong evidence for a weakened/shoaled LSW influence, while the fast flowing deep core of the DWBC was located close to its modern depth below 3,500 m. The benthic $\delta^{13}C$ suggests that during MIS 5e there was little chemical stratification of the water column with the presence of a water mass almost uniformly dominated by LNADW. It is shown that the MIS 5e configuration terminated by a significant shift in DWBC flow characteristics coincident with a hydrographic change midway through MIS 5d which may represent the initiation of GNAIW formation. Glacial North Atlantic Intermediate Water formation with nutrient-enriched SSW below led to a chemically stratified North Atlantic throughout MIS 5d-5a (Chapman and Shackleton, 1998, 1999), similar to the LGM reconstruction in **Chapter 3**. Coupled

suborbital oscillations in DWBC flow variability and palaeohydrography persisted throughout MIS 5. Comparison of these data with planktonic $\delta^{18}O$ records from the sites and alkenone-derived SST estimates from the nearby Bermuda Rise (Lehman *et al.*, 2002) suggest a hitherto unrecognised degree of linkage between oscillations in subtropical North Atlantic SST and DWBC flow.

The approach of combining geochemical proxies with physical parameters of the water masses at various water depths has led to a more comprehensive reconstruction of NADW strength in the past than previous reconstructions dealing with only one proxy. The results are important for our understanding of the relations between ocean circulation changes and climate.

7.6 Conclusions

In conclusion, this dissertation has highlighted the importance of acquiring depth transect records rather than basing interpretations on single core studies which may be prone to missing migrations of water masses and major currents within the water column. This depth transect approach has proved particularly useful at the BOR where the fast flowing core of the DWBC is shown to experience changes in both intensity and position within the water column which can be difficult to distinguish in a grain size record from a single depth. This work further establishes the importance of the SS proxy as a tracer providing a complement to the more widely used geochemical proxies.

This investigation provides evidence of two of the three proposed modes of operation of the MOC suggested by Stommel (1961), Rahmstorf (1994) and Sarnthein *et al.* (1994) and described in **section 1.2**. The hydrographic reconstructions presented in this study of the Holocene and the MIS 5e interglacial (130-120 kyr BP)

suggest that a deep overturning cell existed in the North Atlantic with vigorous flow speeds and a water column dominated by NSW. This is consistent with the 'warm' mode of the MOC with overturning in the Nordic Seas (Sarnthein *et al.*, 1994). However, considerable variation has been shown to exist within this 'warm' mode in the production of intermediate depth LSW. Labrador Sea Water was found to be significantly reduced/shallower in MIS 5e compared with the Holocene. The LGM and YD are shown in this dissertation to be hydrographically similar to one another with shallow, vigorous GNAIW formation above 2,500 m water depth at the expense of NADW formation. This is consistent with the glacial mode proposed for the MOC where overturning is restricted to shallower depths south of Iceland, with an incursion of oxygen-depleted SSW below. Previous investigations in the North Atlantic have also recorded GNAIW formation during these intervals (Oppo and Lehman, 1993; Came *et al.*, 2003; Keigwin, 2004; Robinson *et al.*, 2005; Curry and Oppo, 2005). The third suggested mode for the MOC is the 'off' or 'Heinrich' mode. Although this mode has found support in some past palaeo studies of H1 (e.g. McManus *et al.*, 2004), the $\overline{SS}$ results presented in **Chapter 5** suggest that while the reduction in flow speed at ~3,000 m water depth suggests shallower and/or weaker NSW production, the $\overline{SS}$ record shows small-scale variability within the H1 interval suggesting that the MOC was subdued at this time rather than totally absent. The $^{321}Pa/^{230}Th$ record of Hall *et al.* (2006) similarly suggests that H1 was represented by a slow down in intermediate depth waters but not a total cessation. Furthermore, the apparent shut down observed in the $^{231}Pa/^{230}Th$ record of McManus *et al.* (2004) may be the result of increased export from the Southern Ocean rather than a pure MOC average signature, which could also produce values close to the production ratio (Thomas *et al.*, 2006). This is not to suggest that transient shuts down in NSW did not occur

during H1 or other cold intervals in the last deglaciation, where the duration of the cessation was less than the resolution of palaeo records presented in this study. Transient changes in deepwater production have been shown to occur very rapidly in the modern ocean with evidence for a 15-day disappearance of the deep-ocean return leg of the Atlantic MOC recorded by the *NERC RAPID* array in November 2004 (Rapid Conference Summary, 2006). Although this brief event is unlikely to represent a complete shut down of the overturning circulation, it does suggest a previously unrecognised degree of variability in the ocean circulation system. Despite the suggestion that it is unlikely that a prolonged complete shut down of deepwater formation occurred in the North Atlantic during H1, it can not be speculated as to whether previous Heinrich events experienced such cessations.

This study has improved upon the understanding of low Southern Hemisphere involvement in episodes of abrupt climate change (e.g. Broecker, 1998; Knorr and Lohmann, 2003; Pahnke and Zahn, 2005), suggesting that at times of low NSW export there is an increase in the vigour of SSW circulation in the North Atlantic. The ultimate driver behind this rapid climate variability, in both the last deglaciation and the LGM however, remains elusive (e.g. Little *et al.,* 1997; Bond *et al.,* 2001; Rahmstorf and Alley, 2002). Evidence of significant palaeoceanographic and palaeoclimatic changes are also apparent during MIS 5 and the 5/4 transition. External solar forcing could provide an explanation for these changes. In isolation, the direct effects of solar forcing may be considered insufficient to cause the rapid changes observed in the climate (e.g. Frohlich, 2000). However, when coupled with natural amplifying mechanisms it provides a much more convincing argument. For example, increased cloud cover (Svenmark and FriisChristensen, 1997) can account for the reducing solar activity during the cold episodes of the last glacial cycle (Bond

et al., 2001). Additionally, the climate system is inherently non-linear and a weak solar forcing may be amplified by stochastic resonance within it (Rahmstorf and Alley, 2002). A significant causal link to solar forcing is also likely to be dependent on other factors such as the preconditioning of the North Atlantic by meltwater inputs. Although climatic variability at the BOR may be linked to solar activity, a direct link which may result from modulation by the ocean circulation is unclear.

Chapters 4, 5 and **6** clearly reveal a coherent surface-deep linkage during the last deglaciation, MIS 5 and the 5/4 transition. Such a linkage has been previously demonstrated between benthic $\delta^{13}C$ and planktonic $\delta^{18}O$ during MIS 5 (Oppo *et al.*, 2001) at the BOR, while Bianchi *et al.* (2001) correlated DWBC flow variability in the subtropics, cool SST events and reduced overturning in the Norwegian Sea during MIS 5e (Fronval and Jansen, 1996, Fronval *et al.*, 1998). This investigation further suggests that cool SST events in the northern North Atlantic and the Bermuda Rise are not only associated with weak NADW production but also correspond to a shoaling of the fast flowing core of the DWBC. Sea surface temperature records at the BOR are shown to be complex, demonstrating heat retention during the early deglaciation in response to a diminished MOC, similar to other more southerly (sub)tropical sites (e.g. Flower *et al.*, 2004; Schmidt *et al.*, 2004).

7.7 Future work

Below are some issues raised in this study and implications for further investigations, including some ideas of how these questions may be addressed in the future.

7.7.1 Multiple proxies

Present studies are generally performed using benthic carbon isotope records that can provide nutrient-related data when epibenthic species are used (Mackensen and Bickert, 1999; Curry and Oppo, 2005), in combination with the benthic Cd/Ca ratio (Boyle and Keigwin, 1987; Marchitto and Broecker, 2006). As these tracers are biologically mediated and therefore do not behave as conservative tracers they are unable to provide information based on water mass mixing. However, the recent application of the neodymium isotope water mass tracer, which is inorganic, used in conjunction with carbon isotopes (e.g. Piotrowski *et al.*, 2005) is taking the first steps towards solving this problem. To date however, neodymium isotopes have not been used in conjunction with any flow rate proxy. Generally, flow rate proxies, e.g grain size (McCave and Hall, 2006) and anisotropy of magnetic susceptibility (Hamilton and Rees, 1970), are compared with $\delta^{13}C$ records but rarely used together on the same cores. The challenge for future studies is to therefore use more than one flow rate proxy and more than two water mass markers from the same cores (McCave and Hall, 2006).

The use of the $^{231}Pa/^{230}Th$ tracer over a depth transect of cores from the BOR in conjunction with grain size measurements could help to establish whether the $^{231}Pa/^{230}Th$ proxy is indeed controlled by the whole water column giving an indication of average MOC conditions (e.g. McManus *et al.*, 2004) or whether in complex regions of hydrography such as the BOR it reflects the bottom 1,000 m of the water column (e.g. Thomas *et al.*, 2006).

7.7.2 Calibration of the grain size proxy

The $\overline{SS}$ proxy can currently only be interpreted in terms of relative changes in flow speed as it has yet to be calibrated. A major objective of future studies should therefore be to relate $\overline{SS}$ to flow speeds recorded by deep-sea, long-term current meters. Such a project is currently underway using a combination of core-top samples and current meter sites set to within 100 m of the sea bed giving the mean and variability of flow speeds from the geostrophic flow just above the boundary layer. It is hoped that relatively new initiatives such as the UK NERC *RAPID* array may help with this ongoing effort.

7.7.3 Palaeotemperature reconstructions

Climate models require accurate reconstructions of both SST and salinity to evaluate their simulations of past and future climates (e.g. Taylor *et al.*, 2004). Extensive core-top, sediment trap and culturing experiments at locations site specific to major palaeo sites may help to refine SST calibrations and allow a comprehensive review of the regional differences in same-species Mg/Ca-temperature relationship. Current Mg/Ca-derived SST and salinity reconstructions are largely restricted to low latitude (sub)tropical sites but further records are needed in the high latitude deepwater formation areas and around the northern and eastern outlets of the LIS in order to assess with confidence the origin of meltwater anomalies in the North Atlantic (Duplessy *et al.*, 1992; this study) and whether they are transported to and influence the regions of deepwater formation.

Currently Mg/Ca reconstructions are generally used in isolation, but additional palaeotemperature proxies such as alkenones, faunal diversity, transfer functions (e.g. MAT, RAM, SIMMAX) and dinocyst assemblages in the same cores would improve

reconstructions of the palaeo-environmental conditions at a site and lead to a better understanding of the climate signal recorded in each of these proxies.

7.7.4 Benthic isotope records

Although benthic foraminifera in the samples were scarce in the deglacial BOR sediment cores, detailed searching in larger sub-samples may enable detailed $\delta^{13}C$ records to be produced. These could complement other well-cited $\delta^{13}C$ and Cd/Ca records in the North Atlantic that demonstrate variability in water mass chemistry and structure during the last deglaciation (e.g. Boyle and Keigwin, 1987; McManus *et al.*, 1999) providing additional information that would help to further unravel the structure and origin of crucial climate-ocean perturbations such as H1 and the YD.

7.7.5 A comparison with other time periods

This thesis has provided a detailed reconstruction of both the surface and deep ocean at the BOR during the last deglaciation and may provide the ideal basis for a comparison study with high resolution records from Termination II. Currently, the sequence of events during Termination II is relatively still poorly understood (e.g. Adkins *et al.*, 1997; Oppo *et al.*, 1997; Oppo *et al.*, 2001). Recent evidence suggests a climatic pause in Termination II rather than a 'Younger Dryas style' climate reversal as recorded during Termination I (Lototskaya and Ganssen, 1999). It has also been suggested that the magnitude of oscillations recorded in Termination II may experience significant geographical variability (Oppo *et al.*, 2001) and therefore comparison studies should be made with both subpolar and subtropical cores.

It has been shown in **Chapters 3** and **5** that SSW vigour increased below ~4,000 m water depth at the BOR during the cold events of the last deglaciation i.e. Younger Dryas and H1, and the LGM. It is still unclear however, if this scenario is present during all the cold episodes of the Quaternary and indeed whether it is a common feature of all Heinrich events. Previous studies from the south Atlantic suggest increased SSW vigour during the cold intervals of the past 350 kyr (e.g. Masse *et al.*, 1994) however, these grain size measurements were made on the bulk silt fraction and therefore measurements on the current sorted sortable silt fraction and other flow vigour proxies are required to confirm these findings.

7.7.6 Interdisciplinary studies; data-model comparisons

This study highlights the potential application of proxy records in the pursuit of more accurate and realistic models of the ocean-atmospheric system.

1. Coupled atmospheric-ocean model reconstructions of the North Atlantic during both the LGM and last deglaciation (e.g. Ganopolski and Rahmstorf, 2001; Shin *et al.*, 2003) should consider the increased SSW flow speeds during the cold intervals of the LGM, H1 and the YD as revealed in the proxy records of **Chapters 3** and **5.** Shin *et al.* (2004) have previously attempted to simulate enhanced northwards flow of SSW during the LGM.
2. The influence and timing of the deglacial meltwater events highlighted in **Chapter 4** should be incorporated into climate models (e.g. Prange *et al.*, 2002) to better characterise the upper-ocean climate.
3. Reduced LSW production and a well mixed water column dominated by LNADW should be incorporated into models attempting to reconstruct MIS 5e.

4. As the DWBC is such an important component of the global climate system, models should attempt to realistically capture its flow characteristics so that future predictions of its strength and position within the water column can be accurately calculated.

References

A

Aagaard, K., J. H. Swift, and E. C. Carmack (1985), Thermohaline circulation in the Arctic/Mediterranean Seas, *J. Geophys. Res., 90,* 4833-4846.

Adkins, J. F. and D. P. Schrag (2003), Reconstructing Last Glacial Maximum bottom water salinities from deep-sea sediment pore fluid profiles, *Earth Planet. Sci. Lett., 216*, 109-123.

Adkins, J. F., E. A. Boyle, L. D. Keigwin, and E., Cortijo (1997), Variability of the North Atlantic thermohaline circulation during the last interglacial period, *Nature, 390,* 154-156.

Adkins, J. F., H. Cheng, E. A. Boyle, E. R. M. Druffel, and R. L. Edwards (1998), Deep-sea coral evidence for rapid change in ventilation of the deep North Atlantic 15,400 years ago, *Science, 280(5364)*, 725-728.

Adkins, J. F., K. McIntyre, and D. P. Schrag (2002), The salinity, temperature, and $\delta^{18}O$ of the glacial deep ocean, *Science*, 298, 1769–1773.

Aharon, P. (2003), Meltwater flooding events in the Gulf of Mexico revisited: implications for rapid climate changes during the last deglaciation, *Paleoceanography, 18,* doi:10.1029/2002PA000840.

Aharon, P. (2006), Entrainment of meltwaters in hyperpycnal flows during deglaciation superfloods in the Gulf of Mexico, *Earth Planet. Sci. Lett., 241*, 260-270.

Alley, R. B. (2000), The Younger Dryas cold interval as viewed from central Greenland, *Quat. Sci. Rev., 19 (1-5),* 213-226.

Alley, R. B., and P. U. Clark (1999), The deglaciation of the northern hemisphere: A global perspective, *Ann. Rev. Earth Planet. Sci., 27,* 149-182.

Alley, R. B., D. A. Meese, C. A. Shuman, A. J. Gow, K. C. Taylor, P. M. Grootes, J. W. C. White, M. Ram, E. D. Waddington, P. A. Mayewski, G. A. Zielinski. (1993), Abrupt increase in snow accumulation at the end of the Younger Dryas event, *Nature,* 362, 527–29.

Alley, R. B., S. Anandakrishnan, and P. Jung (2001), Stochastic resonance in the North Atlantic, *Paleoceanography, 16*, 190–198.

Allison, E. and M. T. Ledbetter (1982), Timing of bottom-water scour recorded by sedimentological parameters in the Southern Australian Basin, *Mar. Geol., 46*,131-147.

Amos, A. F., A. L. Gordon, and E. D. Schneider (1971), Water masses and circulation patterns in the region of the Blake-Bahama Outer Ridge, *Deep Sea Res.*, *18*, 145-165.

Anand, P., H. Elderfield, and M. H. Conte (2003), Calibration of Mg/Ca thermometry in planktonic foraminifera from a sediment trap time series, *Paleoceanography, 18(2),* 1050, doi:10.1029/2002PA000846.

Andersen, C., N. Koc¸ A. Jennings, and J. T. Andrews (2004), Nonuniform response of the major surface currents in the Nordic Seas to insolation forcing: Implications for the Holocene climate variability, *Paleoceanography, 19,* PA2003, doi:10.1029/2002PA000873.

Andrews, J. T., and K. Tedesco (1992), Detrital carbonate- rich sediments, northwestern Labrador Sea: implications for ice-sheet dynamics and iceberg rafting (Heinrich) events in the North Atlantic, *Geology, 20,* 1087–90.

Andrews, J. T., B. Maclean, M. Kerwin, W. Manley, A. E. Jennings, and F. Hall (1995), Final stages in the collapse of the Laurentide Ice Sheet, Hudson Strait, Canada, NWT: Based on ^{14}C AMS dates and magntic susceptibility logs, *Quat. Sci. Rev., 14,* 983-1004.

Andrews, J. T., L. M. Smith, R. Preston, T. Cooper, and A. E. Jennings (1997), Spatial and temporal patterns of iceberg rafting (IRD) along the East Greenland margin, ca. 68°N, over the last 14 cal ka, *J. Quat. Sci., 12,*1–13.

B

Balsam, W. L. (1983), Carbonate dissolution on the Muir Seamount (western North Atlantic): interglacial/glacial changes, *J. Sediment. Petrol., 53*, 719-731.

Bard, E., M. Arnold, P. Maurice, J. Duprat, J. Moyes, and J. –C.. Duplessy (1987), Retreat velocity of the North-Atlantic Polar Front during the last deglaciation determined by C-14 accelerator mass-spectrometry, *Nature, 328 (6133)*, 791-794.

Bard, E., B. Hamelin, and R. G. Fairbanks (1990), U-TH ages obtained by mass-spectrometry in corals from Barbados-sea-level during the past 130,000 years, *Nature, 346*, 456-458.

Bard, E., M. Arnold, J. Mangerud, M. Paterne, L. Labeyrie, J. Duprat, M. –A. Mélières, E. Sønstegaard, and J. -C Duplessy (1994), The North Atlantic atmosphere-sea surface ^{14}C gradient during the Younger Dryas climatic event, *Earth Planet. Lett., 126,* 275-287.

Bard, E., F. Rostek, J. L. Turon, and S. Gendreau (2000), Hydrological impact of Heinrich events in the subtropical northeast Atlantic, *Science, 289(5483),* 1321-1324.

Baringer, M. O., and J. C. Larsen (2001), Sixteen years of Florida Current transport at 27 degrees N, *Geophys. Res. Lett., 28(16),* 3179-3182.

Barker, S., M. Greaves, and H. Elderfield (2003), A study of cleaning procedures used for foraminiferal Mg/Ca paleothermometry, *Geochem. Geophys. Geosyst., 4,* doi:10.1029/2003GC000559.

Barker, S., I. Cacho, H. Benway, and K. Tachikawa (2005), Planktonic foraminiferal Mg/Ca as a proxy for past oceanic temperatures: a methodological overview and data compilation for the Last Glacial Maximum, *Quat. Sci. Rev., 24,* 821–834.

Barranco, F. T. Jr., W. L. Balsam, and B. C. Deaton (1989), Quantitative reassessment of brick red lutites: Evidence from reflective spectrophotometry, *Mar. Geol., 89,* 299-314.

Bé, A. W. H., G. Vilks, and L. Lott (1971), Winter distribution of planktonic foraminifera between the Grand Banks and the Caribbean, *Micropaleontology, 17,* 31–42.

Belanger, P. E., W. B. Curry, and R. K. Matthews (1981), Core-top evaluation of benthic formainiferal isotopic-ratios for paleo-oceanographic interpretations, *Palaeogeog. Palaeoclimat. Palaeoecol., 33(1-3),* 205-220.

Bemis, B. E., H. J. Spero, J. Bijma, and D. W Lea (1998), Reevaluation of the oxygen isotopic composition of planktonic foraminifera: Experimental results and revised paleotemperature equations, *Paleoceanography 13(2),* 150-160.

Berger, A. and M. F. Loutre (1991), Insolation values for the climate of the last 19 million years, *Quat. Sci. Rev., 10,* 297–317.

Bianchi, G. G., and I. N. McCave (1999), Holocene perodicity in North Atlantic climate and deep-ocean flow south of Iceland. *Nature, 397,* 515-517.

Bianchi, G. G., I. R. Hall, I. N. McCave, and L. Joseph (1999), Measurement of the sortable silt current speed proxy using the Sedigraph 5100 and Coulter Multisizer IIe: Precision and accuracy, *Sedimentology, 46,* 1001-1014.

Bianchi, G. G., M. Vautravers, and N. J. Shackleton (2001), Deep flow variability under apparently stable North Atlantic Deep Water production during the last inerglacial of the sub-tropical NW Atlantic, *Paleoceanography, 16,* 306-316.

Blunier, T. and E. J. Brook (2001), Timing of millennial-scale climate change in Antarctica and Greenland during the last glacial period, *Science, 291,* 109–112.

Blunier, T., J. Chappellaz, J. Schwander, A. Dallenbach, B. Stauffer, T. F. Stocker, D. Raynaud, J. Jouzel, H. B. Clausen, C. U. Hammer, and S. J. Johnsen (1998), Asynchrony of Antarctic and Greenland climate change during the last glacial period, *Nature, 394,* 739–743.

Bond, G. C., and R. Lotti (1995), Iceberg discharges into the North Atlantic on millennial time scales during the last glaciation, *Science, 267,* 1005– 1010.

Bond, G., H. Heinrich, W. Broecker, L. Labeyrie, J. McManus, J. Andrews, S. Huon, R. Jantschik, S. Clasen, C. Simet, K. Tedesco, M. Klas, G. Bonani, and S. Ivy (1992), Evidence for massive discharges of icebergs into the North-Atlantic ocean during the last glacial period, *Nature, 360(6401),* 245-249.

Bond, G., W. Broecker, S. Johnsen, J. McManus, L. Labeyrie, J. Jouzel, and G. Bonani (1993), Correlations between climate records from North Atlantic sediments and Greenland ice, *Nature, 365*, 143– 147.

Bond, G. C. W. Showers, M. Cheseby, R. Lotti, P. deMenocal, P. Priore, H. Cullen, I. Hajdas and G. Bonani (1997), A pervasive millennial-scale cycle in North Atlantic Holocene and glacial climates, *Science, 278,* 1257-1266.

Bond, G., B. Kromer, J. Beer, R. Muscheler, M. N. Evans, W. Showers, S. Hoffmann, R. Lotti-Bond, I. Hajdas, and G. Bonani, (2001), Persistent solar influence on North Atlantic climate during the Holocene, *Science, 294*, 2130–2136.

Boyle, E. A. (1983), Manganese carbonate overgrowths on foraminifera tests, *Geochim. Cosmochim. Acta,, 47,* 1815–1819.

Boyle, E. A. (1988), Vertical oceanic nutrient fractionation and glacial interglacial CO_2 cycles, *Nature, 331 (6151),* 55-56.

Boyle, E. A. (1991), Quaternary ocean paleochemistry, *Rev, Geophys., 29,* 634-638 Part 2 Suppl. S.

Boyle, E. A., and L. D. Keigwin (1982), Deep circulation of the North-Atlantic over the last 200,000 years - Geochemical evidence, *Science, 218(4574),* 784-787.

Boyle, E. A., and L. D. Keigwin (1985), Comparison of Atlantic and Pacific paleochemical records for the Last 215,000 years: Changes in deep ocean circulation and chemical inventories, *Earth Planet. Sci. Lett., 76*, 135–150.

Boyle, E. A., and L. D. Keigwin (1987), North Atlantic thermohaline circulation during thr past 20,000 years linked to hihg-latitude surface temperature, *Nature, 330*, 35-40.

Bradley, R. S. (1990), Holocene paleoclimatology of the Queen Elizabeth Islands, Canadian high Arctic, *Quat. Sci. Rev., 9,* 365–384.

Braiser, M. D. (1980), *Microfossils*. London: George Allen&Unwin Ltd, 193pp.

Broecker, W. S. (1991), The great ocean conveyor, *Oceanography, 4,* 79–89.

Broecker, W. S. (1997), Thermohaline circulation, the Achilles heel of our climate system: Will man-made CO_2 upset the current balance? *Science, 278,* 1582–1588.

Broecker, W. S. (1998), Paleocean circulation during the last deglaciation: A bipolar seesaw? *Paleoceanography, 13(2),* 119-121.

Broecker, W. S. (2000), Abrupt climate change: causal constraints provided by the paleoclimate record, *Earth-Science Reviews, 51(1-4),* 137-154.

Broecker, W. S., and G. H. Denton (1989), The role of ocean-atmosphere reorganizations in glacial cycles, *Geochemica et Cosmochima Acta, 53(10),* 2465-2501.

Broecker, W. S. and E. Maier-Reimer (1992), The influence of air and sea exchange on the carbon isotope distribution in the sea, *Global Biogeochemical Cycles, 6 (3)* 315-320.

Broecker, W. S., D. M. Peteet, and D. Rind (1985), Does the ocean-atmosphere system have more than one stable mode of operation? *Nature, 315,* 21-26.

Broecker, W. S., M. Andree, W. Wolfli, H. Oeschger, G. Bonani, J. P. Kennett, and D. Peteet (1988), The chronology of the last deglaciation: implications to the cause of the Younger Dryas event, *Paleoceanography, 3,* 1-19.

Broecker, W. S., J. P. Kennett, B. P. Flowers, J. T. Teller, S. Trumbore, G. Bonani, and W. Wolfli (1989), Routing of meltwater from the Laurentide Ice Sheet during the Younger Dryas cold episode, *Nature, 341,* 318– 321.

Broecker, W. S., T. -H. Peng, S. Trubore, G. Bonani, and W. Wolfli (1990), The distribution of radiocarbon in the glacial ocean, *Global Biogeochemical Cycles, 4,* 103–117.

Broecker, W. S., S. L. Peacock, S. Walker, R. Weiss, E. Fahrbach, M. Schroeder, U. Mikolajewicz, C. Heinze, R. Key, T. H. Peng, and S. Rubin (1998), How much deep water is formed in the Southern Ocean? *J. Geophys. Res.-Oceans, 103 (C8),* 15833-15843.

Brown, S. J., and H. Elderfield (1996), Variations in Mg/Ca and Sr/Ca ratios of planktonic foraminifera caused by post depositional dissolution: Evidence of shallow Mg- dependent dissolution, *Paleoceanography, 11,* 543–551.

Brown, E., A. Colling, D. Park, J. Phillips, D. Rothery, and J. Wright (2001), *Ocean circulation.* Oxford, Butterworth-Heinemann.

Bryan, G. M. (1970), Hydrodynamic model of the Blake Outer Ridge, *J. Geophys. Res.*, *75*, 4530-4537.

Bulfinch, D. L., M. T. Ledbetter, B. B.Ellwood, and W. L. Balsam (1982), The high-velocity core of the western boundary undercurrent at the base of the United States continental rise, *Science*, *215*, 970-73.

Cacho, I., J. O. Grimalt, C. Pelejero, M. Canals, F. J. Sierro, J. A. Flores, and N. Shackleton (1999), Dansgaard-Oeschger and Heinrich event imprints in Alboran Sea paleotemperatures, *Paleoceanography, 14,* 698–705.

Came, R. E., D. W. Oppo, and W. B. Curry (2003), Atlantic Ocean circulation during the Younger Dryas: Insights from a new Cd/Ca record from the western subtropical South Atlantic, *Paleoceanography, 18(4),* 1086, doi:10.1029/2003 PA000888.

Cane, M., and A. Clement (1999), A role for the tropical Pacific coupled ocean-atmosphere system on Milankovitch and millennial timescales: Part II, Global impacts, In: Clark, P., R. Webb, and L. Keigwin (ed.) *Mechanisms of Global Climate Change at Millennial Time Scales, Geophys. Monogr. Ser., vol. 112,* AGU, Washington, D. C, 373–383.

Caron, D. A., O. R. Anderson, J. L. Lindsey, W. W. Faber Jr., and E. L. Lim (1990), Effects of gametogenesis on test structure and dissolution of some spinose planktonic foraminifera and implications for test preservation, *Mar. Micropaleontol., 16,* 93–116.

Chaisson, W. P., M. –S. Poli and R. C. Thunell (2002), Gulf Stream and Western Boudary Undercurrent variations during MIS10-12 at Site 1056, Blake-Bahama Outer Ridge, *Mar. Geol., 189,* 79-105.

Chang, T. S., B.W. Flemming, and A. Bartholomä (2005), Distinction between sortable silts and aggregated particles in muddy intertidal sediments of the Southern North Sea, In, Flemming, B. W., D. Hartmann and M. T. Delafontaine (ed.), *From Particle Size to Sediment Dynamics*, Research Centre Terramare (Wilhelmshaven), *Report No. 13*, 117-119.

Chapman, M. R., and N. J. Shackleton (1998), Millennial-scale fluctuations in North Atlantic heat flux during the last 150,000 years, *Earth Planet. Sci. Lett., 159 (1-2),* 57-70.

Chapman, M. R., and N. J. Shackleton, (1999), Global ice-volume fluctuations, North Atlantic ice-rafting events, and deep-ocean circulation changes between 130 and 70 ka, *Geology, 27(9),* 795-798.

Chapman, M. R., N. J. Shackleton, and J. -C. Duplessy (2000), Sea surface temperature variability during the last glacial-interglacial cycle: assessing the magnitude and pattern of climate change in the North Atlantic, *Paleogeog., Paleoclim., Paleoecol., 157,* 1-25.

Chappellaz, J., T. Blunier, D. Raynaud, J. M. Barnola, J. Schwander, and B. Stauffer (1993), Synchronous changes in atmospheric CH_4 and Greenland climate between 40 and 8 kyr BP, *Nature*, 366, 443–445.

Charles, C. D., J. D. Wright, and R. G. Fairbanks (1993), Thermodynamic influences on the marine carbon isotope record, *Paleoceanography, 8(6),* 691-697.

Chave, K. E. (1954), Aspects of the biogeochemistry of magnesium 1. Calcareous marine organisms, *J. Geol., 62,* 266–283.

Chlachula, J. (2003), The Siberian loess record and its significance for reconstruction of Pleistocene climate change in north-central Asia, *Quat. Sci. Rev., 22(18-19),* 1879-1906.

Clark, P. U., S. J. Marshall, G. K. C. Clarke, S. W. Hostetler, J. M. Licciardi, and J. T. Teller, (2001), Freshwater forcing of abrupt climate change during the last deglaciation, *Science, 293,* 283–287.

Clark, P. U., J. X. Mitrovica, G. A. Milne, and M. E. Tamisiea (2002), Sea-level fingerprinting as a direct test for the source of global meltwater pulse 1a, *Science, 295,* 2438–2441.

Clark, P. U., N. G. Pisias, T. F. Stocker, and A. J. Weaver (2002), The role of the thermohaline circulation in abrupt climate change, *Nature, 415,* 863-869.

CLIMAP Project Members (1976), The surface of the ice-age earth, *Science, 191,* 1131-1137.

Coakley, J. P., and J. P. M. Syvitiski (1991), Sedigraph technique, In: Syvitski, J. P. M. (ed.), *Principles, Methods and Application of Particle Size Analysis,* Cambridge Univ. Press, New York, 129-142.

Corliss, B. H., D. G. Martinson, and T. Keffer (1986), Quaternary deep-ocean circulation, *Geol. Soc. Am. Bull., 97,* 1106-1121.

Cortijo, E., S. Lehman, L. Keigwin, M. Chapman, D. Paillard, and L. Labeyrie (1999), Changes in meridional temperature and salinity gradients in the North Atlantic Ocean (30°-72°N) during the last interglacial period, *Paleoceanography, 14,* 23-33.

Cottet-Puinel, M., A. J.Weaver, C. Hillaire-Marcel, A. de Vernal, P. U. Clark, and M. Eby (2004), Variation of Labrador Sea Water formation over the Last Glacial cycle in a climate model of intermediate complexity, *Quat. Sci. Rev., 23,* 449-465.

Crowley, T. J. (1992), North Atlantic deep water cools the southern hemisphere, *Paleoceanography, 7(4),* 489-497, doi:10.1029/92PA01058.

Crowley, T. J. (2000), CLIMAP SSTs re-revisited, *Climate Dynamics, 16,* 0241–0255.

Curry, W. B., and G. P. Lohmann (1982), Carbon isotope changes in benthic foraminifera from the western South-Atlantic – Reconstruction of glacial abyssal circulation patterns, *Quat. Res., 18(2),* 218-235.

Curry, W. B., and D. W. Oppo (2005), Glacial water mass geometry and the distribution of $\delta^{13}C$ of ΣCO_2 in the western Atlantic Ocean, *Paleoceanography, 20,* PA1017, doi:10.1029/2004PA001021.

Curry, W. B., J. -C. Duplessy, L. D. Labeyrie, and N. J. Shackleton (1988), Changes in the distribution of $\delta^{13}C$ of deep water ΣCO_2 between the last glaciation and the Holocene, *Paleoceanography, 3*, 317-341.

Curry, W. B., T. M. Marchitto, J. F. McManus, D. W. Oppo, and K. L. Laarkamp (1999), Millennial-scale changes in ventilation of the thermocline, intermediate and deep waters of the glacial North Atlantic, In: Clark, P. U., R. S. Webb, and L. D. Keigwin (ed.), *Mechanisms of Global Climate Change at Millennial Time Scales, Geophys. Monogr. Ser., vol. 112*, AGU, Washington, D. C, 59–76.

D

Dansgaard W., J. W. C White, and S. J. Johnson (1989), The abrupt termination of the Younger Dryas climate event, *Nature, 339*, 532-533.

Dansgaard, W., J. J. Johnson, B. H. Clausen, D. Dahl-Jensen, N. S. Gundestrup, C. U. Hammer, C. S. Hvidberg, J. P. Steffensen, A. E. Sveinbjörndottir, J. Jouzel, and G. Bond (1993), Evidence for general instability of past climate from a 250- kyr ice-core record, *Nature, 364,* 218-220.

de Vernal, A., and C. Hillaire-Marcel (2006), Provincialism in trends and high frequency changes in the northwest North Atlantic during the Holocene, *Global and Planetary Change, 54,* 263–290

de Villiers, S., M. Greaves, and H. Elderfield (2002), An intensity ratio calibration method for the accurate determination of Mg/Ca and Sr/Ca of marine carbonates by ICP-AES, *Geochem. Geophys. Geosyst., 3(1),* 1001, doi:10.1029/2001GC000169.

Deer, W. A., R. A. Howie, and J. Zussman (1992), *An Introduction to the Rock Forming Minerals*, 2 ed., Addison-Wesley-Longman, Reading, Mass.

Dekens, P. S., D. W. Lea, D. K. Pak, and H. J. Spero (2002), Core top calibration of Mg/Ca in tropical foraminifera: Refining paleotemperature estimation, *Geochem. Geophys. Geosyst., 3(4),* 1022, doi:10.1029/2001GC000200.

Deuser, W. G. (1987), Seasonal variations in isotopic composition and deep-water fluxes of the tests of perennially abundant planktonic foraminifera of the Sargasso Sea: Results from sediment trap collections and their paleoceanographic significance, *J. Foraminiferal Res., 17*, 14–27.

Deuser, W. G., and E. H. Ross (1989), Seasonally abundant planktonic foraminifera of the Sargasso Sea: Succession, deep-water fluxes, isotopic compositions, and paleoceanographic implications, *J. Foraminiferal Res., 19*, 268 – 293.

Dickson, R. R., and J. Brown (1994), The production of North Atlantic Deep Water: sources, rates, and pathways, *J. Geophys. Res., 99 (C6),* 12319-12341.

Driscoll, M. L., B. E. Tucholke, and I. N. McCave (1985), Seafloor zonation in sediment texture on the Nova Scotian Lower Continental Rise, *Mar. Geol., 66,* 25-41.

Duplessy, J. -C., N. J. Shackleton, R. K. Matthews, W. Prell, W. F. Ruddiman, M. Caralp, and C. H. Hendy (1984), ^{13}C Record of benthic foraminifera in the last interglacial ocean: Implications for the carbon cycle and the global deep water circulation, *Quat. Res., 21(3),* 225-243.

Duplessy, J. -C., M. Arnold, P. Maurice, E. Bard, J. Duprat, and J. Moyles (1986), Direct dating of the oxygen-isotope record of the last deglaciation by C-14 accelerated mass-spectrometry, *Nature, 320(6060),* 350-352.

Duplessy, J. -C., N. J. Shackleton, R. G. Fairbanks, L. Labeyrie, D. Oppo, and N. Kallel (1988), Deep-water source variations during the last climatic cycle and their impact on the global deep-water circulation. *Paleoceanography,* 3, 343-360.

Duplessy, J. -C., L. Labeyrie, M. Arnold, M. Paterne, J. Duprat, and D. C. E. van Weering (1992), Changes in surface salinity of the North Atlantic ocean during the last deglaciation, *Nature, 358,* 485– 87.

Dynesius, M., and R. Jansson (2000), Evolutionary consequences of changes in species' geographical distributions driven by Milankovitch climate oscillations, *Proceedings of the National Academy of Sciences of the United States of America, 97(16),* 9115-9120.

E

Eggins, S., P. DeDeckker, and A. T. Marshall (2003), Mg/Ca variation in planktonic foraminifera tests: implications for reconstructing palaeo-seawater temperature and habitat migration, *Earth Planet. Sci. Lett., 212,* 291–306.

Elderfield, H., and G. Ganssen (2000), Past temperature and delta-18O of surface ocean waters inferred from foraminiferal Mg/Ca ratios, *Nature, 405,* 442–445.

Elliot, M., L. Labeyrie, and J. -C. Duplessy (2002), Changes in North Atlantic deep-water formation associated with the Dansgaard–Oeschger temperature oscillations (60–10 ka), *Quat. Sci. Rev., 21,* 1153–1165.

Ellison, C. R. W., M. R. Chapman, and I. R. Hall (2006), Surface and Deep Ocean Interactions during the Cold Climate Event 8200 Years Ago, *Science, 312,* 1929-1932.

Ellwood, B. B. and M. T. Ledbetter (1977), Antarctic Bottom Water fluctuations in the Vema Channel: effects of velocity changes on particle alignment and size, *Earth Planet. Sci. Lett., 35,*189-198.

Embley, R. W., and R. D. Jacobi (1977), Distribution and morphology of large submarine slides and slumps on Atlantic continental margins, *Mar. Geotechnol., 2*, 205-228.

Emiliani, C. (1955), Mineralogical and chemical composition of the tests of certain pelagic foraminifera, *Micropaleontol., 1*, 377–380.

EPICA Community Members (2006), One-to-one coupling of glacial climate variability in Greenland and Antarctica, *Nature*, *444,* 195-198.

Ewing, J. I., and C. D. Hollister (1972), Regional aspects of deep sea drilling in the western North Atlantic, *Initial Rep. Deep Sea Drill. Proj., 11,* U. S. Govt. Print. Off., Washington, D.C, 951-973,

Ewing, J., M. Ewing, and R. Leyden (1966), Seismic profile survey of the Blake Plateau, *Am. Assoc. Petrol. Geologists Bull.*, *50*, 1948-1971.

F

Fairbanks, R. G. (1989), A 17,000-year glacio-eustatic sea level record: influence of glacial melting rates on the Younger Dryas event and deep-ocean circulation, *Nature*, *342,* 637–642.

Fehrenbacher, J., P. A. Martin, and G. Eshel (2006), Glacial deep water carbonate chemistry inferred from foraminiferal Mg/Ca: A case study from the western tropical Atlantic, *Geochem. Geophys. Geosyst., 7,* Art. No. Q09P16.

Fine, R. A. (1995), Tracers, time scales, and the thermohaline circulation: The lower limb in the North Atlantic Ocean, *Rev. Geophys., (Suppl.)*, 1353-1365.

Flood, R. D. (1979), Studies of deep-sea sedimentary microtopology in the North Atlantic Ocean, Doctoral thesis, WHOI/MIT, Joint program in Oceanogr., Mass. Inst. Of Technol./Woods Hole Oceanogr. Inst., Woods Hole, MA.

Flood, R. D. (1988), A lee-wave model for deep-sea mudwave activity, *Deep-Sea Res.*, *35*, 973-983.

Flower, B. P., D. W. Hastings, H. W. Hill, and T. M. Quinn (2004), Phasing of deglacial warming and Laurentide Ice Sheet meltwater in the Gulf of Mexico, *Geology, 32,* 597-600.

Frohlich, C. (2000), Observations of irradiance variations, *Space Science Reviews, 94,* 15-24.

Fronval, T., and E. Jansen (1996), Rapid changes in ocean circulation and heat flux in the Nordic seas during the last interglacial period, *Nature, 383*, 806-810.

Fronval, T., E. Jansen, H. Haflidason, H. P. Sejrup (1998), Variability in surface and deep water conditions in the Nordic seas during the last interglacial period, *Quat. Sci. Rev., 17,* 963-985.

G

Ganachaud, A., and C. Wunsch (2000), Improved estimates of global ocean circulation, heat transport and mixing from hydrographic data, *Nature, 408,* 453-456.

Ganopolski, A., and S. Rahmstorf (2001), Rapid changes of glacial climate simulated in a coupled climate model. *Nature , 409,* 153–158.

Ganopolski, A., S. Rahmstorf , V. Petoukhov , and M. Claussen (1998), Simulation of modern and glacial climates with a coupled global model of intermediate complexity, *Nature, 391 (6665),* 351-356.

Gherardi, J. M., L. Labeyrie, J. F. McManus, R. Francois, L. C. Skinner, and E. Cortijo (2005), Evidence from the Northeastern Atlantic basin for variability in the rate of the meridional overturning circulation through the last deglaciation, *Earth Planet. Sci. Lett., 240,* 710-723.

Goldstein, S. J., D. W. Lea, S. Chakraborty, M. Kashgarian, and M. T. Murrell (2001), Uranium-series and radiocarbon geochronology of deep-sea corals: implications for Southern Ocean ventilation rates and the oceanic carbon cycle, *Earth Planet. Sci. Lett., 193,* 167-182.

Graham, D. W., B. H. Corliss, M. L. Bender, and L. D. Keigwin (1981), Carbon and oxygen isotopic disequilibria of recent deep-sea benthic foraminifera, Marine *Micropaleontology, 6(5-6),* 483-497.

Grootes, P. M. and M. Stuiver (1997), Oxygen 18/16 variability in Greenland snow and ice with 10(-3)- to 10(5)-year time resolution, *J. Geophys. Res.-Oceans, 102(C12),* 26455-26470.

Grootes P. M., M. Stuiver, J. W. C. White, S. Johnsen, J. Jouzel (1993), Comparison of oxygen-isotope records from the GISP2 and GRIP Greenland ice cores, *Nature, 366(6455),* 552-554.

H

Haese, R. H. (2000), The reactivity of iron. In: Schulz, H. D., M. Zabel (ed.), *Marine geochemistry.* Springer, Berlin Heidelberg New York, 233-261.

Hagen S. and L. D. Keigwin (2002), Sea-surface temperature variability and deep water reorganisation in the subtropical North Atlantic during Isotope Stage 2-4, *Mar. Geol., 189,* 145-162.

Hall, M. M., and H. L. Bryden (1982), Direct estimates and mechanisms of ocean heat-transport, Deep-Sea Res., Part A, 29(3), 339-359.

Hall, I. R. and I. N. McCave (2000), Palaeocurrent reconstruction, sediment and thorium focussing on the Iberian margin over the last 140 ka, *Earth Planet. Sci. Lett., 178*, 151-164.

Hall, I. R., and J. Becker (2007), Deep Western Boundary Current variability in the subtropical Northwest Atlantic Ocean during Marine Isotope Stages 12-10, *Geochem. Geophys. Geosyst.*, 8, Q06013, DOI 10.1029/2006GC001518.

Hall, I. R., I. N. McCave, M. R. Chapman, and N. J. Shackleton (1998), Coherent deep flow variation in the Iceland and American Basins during the last interglacial, *Earth Planet. Sci. Lett., 164(1-2),* 15-21.

Hall, I. R., S. B. Moran, R. Zahn, P. C. Knutz, C. -C. Shen, and R. L. Edwards (2006) Accelerated draw-down of meridional overturning in the late-glacial Atlantic triggered by transient pre-H event freshwater perturbation, *Geophys. Res. Lett,. 33*, L16616, doi:10.1029/2006GL026239.

Hamilton, N., and A. F. Rees (1970), The use of magnetic fabric in paleocurrent estimation, In: Runcorn S. K. (ed.), *Paleogeophysics*, Academic Press, New York, 445-464.

Hanebuth, T., K. Stattegger, P. M. Grootes (2000), Rapid flooding of the Sunda Shelf: A late-glacial sea-level record, *Science, 288(5468),* 1033-1035.

Haskell, B. J., and T. C. Johnson (1993), Surface sediment response to deepwater circulation on the Blake Outer Ridge, western North Atlantic: paleoceanographic implications, *Sed. Geol., 82*, 133-144.

Haskell, B. J., T. C. Johnson, and W. J. Showers (1991), Fluctuations in deep western North Atlantic circulation on the Blake Outer Ridge during the last deglaciation, *Paleoceanography, 6*, 21-31.

Hastings, D. W., S. R. Emerson, J. Erez, and B. K. Nelson (1996), Vanadium in foraminiferal calcite: Evaluation of a method to determine paleo-seawater vanadium concentrations, *Geochim. Cosmochim. Acta, 60*, 3701–3715.

Hastings, D. W., A. D. Russell, and S. R. Emerson (1998), Foraminiferal magnesium in Globeriginoides sacculifer as a paleotemperature proxy, *Paleoceanography, 13(2),* 161–169.

Haug, G. H., K. A. Hughen, D. M. Sigman, L. C. Peterson, and U. Rohl (2001), Southward migration of the intertropical convergence zone through the Holocene, *Science, 293(5533),* 1304-1308.

Hays, J. D., J. Imbrie and N. J. Shackleton (1976), Variations in the Earth's orbit: pacemaker of the ice ages, *Science, 194,* 1121 -1132.

Healey, S., and R. Thunell (2004), Millennial-scale variability in western subtropical North Atlantic surface and deep water circulation during marine isotope stages 11 and 12, Paleoceanography, 19, PA1013, doi:10.1029/2003PA000925.

Heezen, B. C., C. D. Hollister, and W. F. Ruddiman (1966), Shaping of the continental rise by deep geostrophic contour currents, *Science*, *152*, 502-508.

Hemming, S. R. (2004), Heinrich events: Massive late Pleistocene detritus layers of the North Atlantic and their global climate imprint, *Rev. Geophys. 42,* doi:10.1029/2003RG000128.

Herbert, T. D. (2001), Review of alkenone calibrations (culture, water column, and sediments), *Geochem. Geophys. Geosyst., 2*, 2000GC000055.

Heusser, L., and D. W. Oppo (2003), Millennial- and orbital-scale climate variability in southeastern United States and in the subtropical Atlantic during Marine Isotope Stage 5: evidence from pollen and isotopes in ODP Site 1059, *Earth Planet. Sci. Lett., 214,* 483-490.

Hewitt, C. D. , R. J. Stouffer, A. J. Broccoli, J. F. B. Mitchell, and P. J. Valdes (2003), The effect of ocean dynamics in a coupled GCM simulation of the Last Glacial Maximum, *Climate Dynamics, 20*, 203-218.

Hillaire-Marcel, C., A. de Vernal, G. Bilodeau, and A. J. Weaver (2001), Absence of deep-water formation in the Labrador Sea during the last interglacial period, *Nature, 410*, 1073-1077.

Hogg, N. G. (1983), A note on the deep circulation of the western North Atlantic: Its nature and causes, *Deep Sea Res., Part A, 9,* 945 –961.

Hollister, C. D., and I. N. McCave (1984), Sedimentation under deep-sea storms, *Nature*, *309*, 220-225.

Hoogakker, B. A. A., I. N. McCave, and M. J. Vautravers, Antarctic link to deep flow speed variation during marine isotope stage 3 in the western North Atlantic, *EPSL*, (in press).

Hughen, K. A , J. T. Overpeck, S. J. Lehman, M. Kashgarian, J. Southon, L. C. Peterson, R. Alley, and D. M. Sigman (1998), Deglacial changes in ocean circulation from an extended radiocarbon calibration, *Nature, 391(6662),* 65-68.

Hüls, M., and R. Zahn (2000), Millennial-scale sea surface temperature variability in the western tropical North Atlantic from planktonic foraminiferal, *Paleoceangraphy, 15*, 659–678.

Imbrie, J., and K. P. Imbrie (1979), *Ice Ages: Solving the mystery*. London, Macmillan.

Imbrie, J., A. Berger, E. A. Boyle, S. C. Clemens, A. Duffy, W. R. Howard, G. Kukla, J., Kutzbach, D. G. Martinson, A. McIntyre, A. C. Mix, B. Molfino, J. J. Morley, L. C. Peterson, N. G. Pisias, W. L. Prell, M. E. Raymo, N. J. Shackleton, and J. R. Toggweiler (1993), On the structure and origin of major glaciation cycles 2. The 100,000-year cycle, *Paleoceaonography, 8(6)*,699-735.

Iselin, C. O. (1936), A study of the circulation of the Western North Atlantic, *Papers, Physics Oceanography Meteorology, 4(4)*, 1-101.

J

Jiang, H., N. O. Svenseeon, and S. Bjorck (1998), Meltwater discharge to the Skagerrak-Kattegat from the Baltic Ice Lake during the Younger Dryas interval, *Quat. Res., 49(3)*, 264-270.

Johns, E., R. A. Fine, and R. L. Molinari (1997), Deep flow along the western boundary of the Blake Bahama Outer Ridge, *J. Phys. Oceanogr., 27*, 2187-2208.

Johnsen, S. J., H. B. Clausen, W. Dansgaard, K. Fuhrer, N. Gundestrup, C. U. Hammer, P. Iversen, J. Jouzel, B. Stauffer, and J. P. Steffensen (1992), Irregular glacial interstadials recorded in a new Greenland ice core, *Nature, 359*, 311 –313.

Johnson, T. C., E. L. Lynch, W. J. Showers, and N. C. Placzuk (1988), Pleistocene fluctuations in the Western Boundary Undercurrent on the Blake Outer Ridge, *Paleoceanography, 3*, 191-207.

Jones, G. A., D. A. Johnson, and W. B. Curry (1984), High-resolution stratigraphy in Late Pleistocene/Holocene sediments of the Vema Channel, *Mar. Geol., 58*, 59–87.

K

Kaufman, D. K., T. A. Ager, N. J. Anderson, P. M. Anderson, J. T. Andrews, P. J. Bartlein, L. B. Brubaker, L. L. Coats, L. C. Cwynar, M. L. Duvall, A. S. Dyke, M. R. Edwards, W. R. Eisner, K. Gajewski, A. Geirsdottir, F. S. Hu, A. E. Jennings, M. R. Kaplan, M. W. Kerwin, A. V. Lozhkin, G. M. MacDonald, G. H. Miller, C. J. Mock, W. W. Oswald, B. L. Otto-Bliesner, D. F. Porinchu, K. Ruhland, J. P. Smol, E. J. Steig, and B. B. Wolfe (2004), Holocene thermal maximum in the western Arctic (0–180°W), *Quat. Sci. Rev., 23*, 529–560.

Keigwin, L. D. (1996), The Little Ice Age and Medieval Warm Period in the Sargasso Sea, *Science, 274*, 1504– 1508.

Keigwin, L. D. (2004), Radiocarbon and stable isotope constraints on Last Glacial Maximum and Younger Dryas ventilation in the western North Atlantic, *Paleoceanography, 19*, PA4012, doi:10.1029/2004PA001029.

Keigwin, L. D. and G. A. Jones (1989), Glacial-Holocene stratigraphy, chronology, and paleoceanographic observations on some North Atlantic sediment drifts. *Deep-Sea Res., 36(6),* 845-867.

Keigwin, L. D., and G. A. Jones (1994), Western North-Atlantic evidence for millennial-scale changes in ocean circulation and climate, *J. Geophys. Res. – Oceans, 99(C6),* 12397-12410.

Keigwin, L. D., and S. J. Lehman (1994), Deep circulation change linked to Heinrich event 1 and Younger Dryas in a middepth North Atlantic core, *Paleoceanography*, 9, 185–94.

Keigwin, L. D., and E. A. Boyle (1999), Surface and deep ocean variability in the northern Sargasso Sea during marine isotope stage 3, *Paleoceanography, 14 (2)*, 164-170.

Keigwin, L. D., and M. A. Schlegel (2002). Ocean ventilation and sedimentation since the glacial maximum at 3 km in the western North Atlantic, *Geochem. Geophys. Geosyst., 3(6),* 1034, doi:10.1029/2001GC000283.

Keigwin, L. D., G. A. Jones, S. J. Lehman, and E. A. Boyle (1991), Deglacial meltwater discharge, North-Atlantic deep circulation and abrupt climate change, *J. Geophys. Res.-Oceans, 96(C6),* 16811-16826.

Keigwin, L. D., G. A. Jones, and P. N. Froelich (1992), A 15,000 year paleoenvironmental record from Meiji Seamount, far northwestern Pacific, *Earth Planet. Sci. Lett., 111,* 425– 440.

Keigwin, L. D., W. B. Curry, S. J. Lehman, and S. Johnsen (1994), The role of the deep ocean in North Atlantic climate changes between 70 and 130 kyr ago, *Nature*, *371*, 323-325.

Keigwin, L. D., *et al.* (1998), *Proceedings of the ODP, Initial Reports*, vol. 172, Ocean Drilling Program, College Station, Tex.

King, P., H. Kennedy, P. P. Newton, T. D. Jickells, T. Brand, S. Calvert, G. Cauwet, H. Etcheber, B. Head, A. Khripounoff, B. Manighetti, and J. C. Miquel (1998), Analysis of total and organic carbon and total nitrogen in settling oceanic particles and a marine sediment: an interlaboratory comparison, *Mar. Chem.*, *60*, 203-216.

Kitoh, A., S. Murakami, H. Koide (2001), A simulation of the last glacial maximum with a coupled atmosphere-ocean GCM, *Geophys. Res. Lett., 28(11)*, 2221-2224.

Knorr, G., and G. Lohmann (2003), Southern Ocean origin for the resumption of Atlantic thermohaline circulation during deglaciation, *Nature, 424(6948),* 532-536.

Knutti, R., J. Fluckiger, T. F. Stocker, and A. Timmermann (2004), Strong hemispheric coupling of glacial climate through freshwater discharge and ocean circulation, *Nature, 430,* 851– 856.

Koç, N., and E. Jansen (1992), A high-resolution diatom record of the last deglaciation from the SE Norwegian Sea: Documentation of rapid climatic changes, *Paleoceanography, 7,* 499–520.

Koç,, N., and E. Jansen (1994), Response of the high-latitude Northern Hemisphere to orbital climate forcing: Evidence from the Nordic Seas, *Geology, 22,* 523–526.

Kranck, K. and T. Milligan (1979), The use of the Coulter Counter in studies of particle size-distribution in aquatic environments, Bedford Inst. *Oceanogr. Report Series, BI-R-79-7.* 48 pp.

Kroopnick, P. M. (1985), The distribution of C-13 of sigma-CO_2 in the world oceans, *Deep-sea Res., 32(1),* 57-84.

Kutzbach, J., G. Bonan, J. Foley, and S. P. Harrison (1996), Vegetation and soil feedbacks on the response of the African monsoon to orbital forcing in the early to middle Holocene, *Nature, 384 (6610),* 623-626.

L

Laine, E. P., W. D. Gardner, M. J. Richardson, and M. Kominz (1994), Currents and advection of resuspended sediment along the north eastern Bermuda Rise, *Mar. Geol., 119,* 159-171.

Lea, D. W., and E. A. Boyle (1991), Barium in planktonic foraminifera, *Geochim. Cosmochim. Acta, 55,* 3321–3331.

Lea, D. W., T. A. Mashiotta, H. J. Spero (1999), Controls on magnesium and strontium uptake in planktonic foraminifera determined by live culturing, *Geochim. Cosmochim. Acta, 63(16),* 2369-2379.

Lea, D. W., D. K. Pak, and H. J. Spero (2000), Climate impact of late quaternary equatorial Pacific sea surface temperature variations, *Science, 289,* 1719–1724.

Lea, D. W., P. A. Martin, D. K. Pak, and H. J. Spero (2002), Reconstructing a 350 ky history of sea level using planktonic Mg/ Ca and oxygen isotope records from Cocos Ridge core, *Quat. Sci. Rev., 21,* 283–293.

Lea, D. W., D. K. Pak, L. C. Peterson, and K. A. Hughen (2003), Synchroneity of tropical and high-latitude Atlantic temperatures over the last glacial termination, *Science, 301*, 1361– 1364.

Leaman, K. D., and P. S., Vertes (1996), Topographic influences on recirculation in the Deep Western Boundary Current: Results from RAFOS float trajectories between the Blake-Bahama Outer Ridge and the San Salvador 'Gate', J. Phys. Oceanogr., *26,* 941-961.

Ledbetter, M. T. (1979), Fluctuations of Antarctic Bottom Water in the Vema Channel during the last 160,000 years, *Mar. Geol., 33,* 71-89.

Ledbetter, M. T. (1986), Bottom-current pathways in the Argentine Basin revealed by mean silt particle size, *Nature, 321,* 423-425.

Ledbetter, M. T. and W. L Balsam (1985), Paleoceanography of the Deep Western Boundary Undercurrent on the North American continental margin for the past 25000 yr, *Geology, 13,* 181-184.

Ledbetter, M. T. and K. R. Bork (1993), Post-Miocene fluctuations of Antarctic Bottom Water paleospeed in the southwest Atlantic Ocean, *Deep-Sea Res., Part II, 40(415),* 1057-1071.

Lee, T. N., W. E. Johns, R. J. Zantopp, and E. R. Fillenbaum (1996), Moored observations of western boundary current variability and thermocline circulation at 26.5 'N in the subtropical North Atlantic, *J. Phys. Oceanogr., 26,* 962-983.

LeGrand, P., and C. Wunsch (1995), Constraints from paleotracer data on the Nrth-Atlantic circulation during the last glacial maximum, *Paleoceanography, 10 (6),* 1011-1045.

LeGrande A. N., and J. Lynch-Stieglitz (2007), Surface currents in the western North Atlantic during the Last Glacial Maximum, Geochem. Geophys. Geosyst., 8(1), Q01N0 doi:10.1029/2006GC001371.

Lehman, S. J., and L. D. Keigwin (1992), Sudden changes in North-Atlantic circulation during the last deglaciation, *Nature, 356 (6372),* 757-762.

Lehman, S. J., J. P. Sachs, A. M. Crotwell, L. D. Keigwin, and E. A. Boyle (2002), Relation of subtropical Atlantic temperature, high-latitude ice rafting, deep water formation, and European climate 130,000-60,000 years ago, *Quat. Sci. Rev., 21,* 1917-1924.

Levitus, S., and T. Boyer (1994) *World Ocean Atlas*, Volume 4: Temperature. NOAA Atlas NESDIS 4, U.S. Department of Commerce, Washington, D.C., www.cdc.noaa.gov/cdc/data.nodc.woa98.html.

Licciardi, J. M., J. T. Teller, P. U. Clark (1999), In: Clark, P. U., R. S.Webb, L. D. Keigwin (ed.), *Mechanisms of Global Climate Change at Millennial Time*

Scales, vol. 112, *Geophysical Monograph Series*, AGU, Washington, D.C, 177-201.

Lin, H. -L., L. C. Peterson, J. T. Overpeck, S. E. Trumbore, and D. W. Murray (1997), Late Quaternary climate change from $\delta^{18}O$ records of multiple species of planktonic foraminifera: High-resolution records from the anoxic basin of the Cariaco basin, Venezuela, *Paleoceanography, 12(3),* 415-427.

Lister, A. M. (2004), The impact of Quaternary Ice Ages on mammalian evolution, *Philosophical Transactions of the Royal Society of London Series B-Biological Sciences, 359(1442),* 221-241.

Little, M. G., R. R. Schneider, D. Kroon, B. Price, C. P. Summerhayes, and M. Segl (1997), Trade wind forcing of upwelling, seasonality, and Heinrich events as a response to sub-Milankovitch climate variability, *Paleoceanography, 12 (4),* 568-576.

Lohmann, G. (2003), Atmospheric and oceanic freshwater transport during weak Atlantic overturning circulation, *Tellus, 55A,* 438-449.

Lototskaya, A., and G. M. Ganssen (1999), The structure of Termination II (penultimate deglaciation and Eemian) in the North Atlantic, *Quat. Sci. Rev., 18(14)*, 1641-1654.

Loubere, P. (1991), Deep-sea benthic foraminiferal assemblage response to a surface ocean productivity gradient: A test, *Paleoceanography, 6,* 193– 204.

Loubere, P. (2000), Marine control of biological production in the eastern equatorial Pacific Ocean, *Nature, 406*, 497– 500.

Lowrie, W. and F. Hellier (1982), Magnetic properties of marine limestones, *Rev. Geophys. Space. Phys., 20,* 171-192.

Lund, D. A., J. Lynch-Stieglitz, and W. B Curry (2006), Gulf Stream density structure and transport during the past millennium, *Nature, 444,* 601-604.

Lynch-Stieglitz, J. (2003), In: H. Elderfield, (Ed.), *The Oceans and Marine Geochemistry,* 6, 433-451, Elsevier.

Lynch-Stieglitz, J., A. van Geen, and R. G. Fairbanks (1996), Interocean exchange of Glacial North Atlantic Intermediate Water: Evidence from Subantarctic Cd/Ca and $\delta^{13}C$ measurements, *Paleoceanography, 11*, 191–201.

Lynch-Stieglitz, J., W. B. Curry, and N. Slowey (1999), Weaker Gulf Stream in the Florida Straits during the Last Glacial Maximum, *Nature, 402*, 644– 648.

Lynch-Stieglitz, J., J. F. Adkins, W. B. Curry, T. Dokken, I. R. Hall, J. C. Herguera, J. J. M. Hirschi, E. V. Ivanova, C. Kissel, O. Marchal, T. M. Marchitto, I. N. McCave, J. F. McManus, S. Mulitza, U. Ninnemann, F. Peeters, E. F. Yu, R.

Zahn (2007), Atlantic Meridional Overturning Circulation during the Last Glacial Maximum, *Science, 316(5821),* 66-69.

M

McCartney, M. S. (1993), Crossing of the equator by the deep western boundary current in the Western Atlantic Ocean, *J. Phys. Oceanogr., 23,* 1953-1974.

McCave, I. N. (1985), Stratigraphy and sedimentology of box cores from the HEBBLE site on the Nova Scotian Continental Rise, *Mar. Geol., 66,* 59-89.

McCave, I. N., and B. E. Tucholke (1986), Deep current-controlled sedimentation in the western North Atlantic, In: Vogt, P.R., and B.E. Tucholke (Eds.), *The Geology of North America,* Volume M, Geol. Soc. America, Boulder, 451-468.

McCave, I. N., and I. R. Hall (2006), Size sorting in marine muds: processes, pitfalls and prospects for paleoflow-speed proxies, *Geochem., Geophys., Geosyst., 7,* 1-37.

McCave, I. N., B. Manighetti, and S. G. Robinson (1995a), Sortable silt and fine sediment size/composition slicing: parameters for palaeocurrent speed and palaeoceanography, *Paleoceanography, 10,* 593-610.

McCave, I. N., B. Manighetti, and N. A. S. Beveridge (1995b), Changes in circulation of the North Atlantic during the last 25,000 years inferred from grainsize measurements, *Nature, 374,* 149-152.

Mackensen, A., and T. Bickert (1999), *Stable carbon isotopes in benthic foraminifera: Proxies for deep and bottom water circulation and new production – Examples from the South Atlantic,* Springer, Berlin, Heidelberg, 229-254.

Mackensen, A., M. Rudolph, and G. Kuhn (2001), Late Pleistocene deep-water circulation in the subantarctic eastern Atlantic, *Global and Planetary Change 30, 3-4,* 197-229.

McManus, J. F., G. C. Bond, W. S. Broecker, S. Johnsen, L. Labeyrie, and S. Higgins (1994), High resolution climate records from the North Atlantic during the last interglacial, *Nature, 371,* 326-329.

McManus, J. F., D. W. Oppo, and J. L. Cullen (1999), A 0.5-Million-Year record of millennial-scale climate variability in the North Atlantic, *Science, 283,* 971-975.

McManus, J. F., R. Francois, J. -M. Gherardi, L. D. Keigwin, and S. Brown-Leger (2004), Collapse and rapid resumption of Atlantic meridional circulation linked to deglacial climate changes, *Nature,* 428, 834– 837.

Manabe, S. S., and A. J. Broccoli (1985), The influence of continental ice sheets on the climate of an ice-age, *J. Geophys. Res., Atmos., 90 (ND1)*, 2167-2190.

Manabe, S., and R. J. Stouffer (1988), Two stable equilibria of a coupled ocean-atmosphere model, *J. Climate, 1*, 841-863.

Manabe, S., and R. J. Stouffer (1993), Century scale effects of increased atmospheric CO2 on the ocean-atmosphere system, *Nature, 364,* 215– 218.

Manabe, S., and R. J. Stouffer (1994), Multiple-century response of a coupled ocean-atmosphere model to an increase of atmospheric carbon dioxide, *J. Climate 7(1),* 5-23.

Manabe, S., and R. Stouffer (1997), Coupled ocean-atmosphere model response to freshwater input: comparison to Younger Dryas event, *Paleoceanography, 12*, 321–336.

Mangerud, J., S. T. Andersen, B. E. Berglund, and J. J. Donner (1974), Quaternary stratigraphy of Norden, a proposal for terminology and classification, *Boreas, 3,* 179–181.

Marchal, O., R. Francois, T. F. Stocker, and F. Joos (2000), Ocean thermohaline circulation and sedimentary $^{231}Pa/^{230}Th$ ratio, *Paleoceanography, 15,* 625-641.

Marchal, O., I. Cacho, T. F. Stocker, J. O. Grimalt, E. Calvo, B. Martrat, N. Shackelton, M. Vautravers, E. Cortijo, S. Van Kreveld, C. Andersson, N. Koç, M. Chapman, L. Sbaffi, J. -C. Duplessy, M. Sarnthein, J. -L. Turon, J. Duprat, E. Jansen (2002), Apparent cooling of the sea surface in the northeastAtlantic andMediterranean during the Holocene, *Quat. Sci. Rev., 21,* 455–483.

Marchitto, T. M., and W. S. Broecker (2006), Deep water mass geometry in the glacial Atlantic Ocean: A review of constraints from the paleonutrient proxy Cd/Ca, *Geochem. Geophys. Geosyst., 7,* Q12003, doi:10.1029/2006GC001323

Marchitto, T. M., W. B. Curry, and D. W. Oppo (1998), Millennial-scale changes in North Atlantic circulation since the last glaciation, *Nature, 393(6685)*, 557-561.

Marchitto, T. M., Jr., W. B. Curry, and D. W. Oppo (2000), Zinc concentrations in benthic foraminifera reflect seawater chemistry, *Paleoceanography, 15,* 299–306.

Markl, R. G., G. M. Bryan, and J. I. Ewing (1970), Structure of the Blake-Bahama Outer Ridge. *J. Geophys. Res., 75,* 4539-4555.

Martinson, D. G., N. G. Pisias, J. D. Hays, J. Imbrie, T. C. Moore, and N. J. Shackleton (1987), Age dating and orbital theory of the ice ages: development of a high resolution 0-300,000-year chronostratigraphy, *Quat. Res., 27,* 1-29.

Maslin, M. A., N. J. Shackleton, U. Pflaumann (1995), Surface water temperature, salinity, and density changes in the northeast Atlantic during the last 45,000 years: Heinrich events, deepwater formation, and climatic rebounds, *Paleoceanography, 10,* 527–44.

Masse, L., J. C., Faugeres, M. Bernat, A. Pujos, and M. L. Mezerais (1994), A 600,000-year record of Antarctic Bottom Water activity inferred from sediment textures and structures in a sediment core from the Southern Brazilian Basin, *Paleoceanography, 9(6),* 1017-1026.

Masson, D. G., R. B. Wynn, and B. J. Bett (2004), Sedimentary environment of the Faroe- Shetland and Faroe Bank Channels, north-east Atlantic, and the use of bedforms as indicators of bottom current velocity in the deep ocean, *Sedimentology, 51,* 1207-1241.

Mauritzen, C. (1996), Production of dense overflow waters feeding the North Atlantic across the Greenland-Scotland Ridge. Part 1: Evidence for a revised circulation scheme, *Deep-Sea Res., 43(6),* 769-806.

Mauritzen, C., K. L. Polzin, M. S. McCartney, R. C. Millard, and D. E. West-Mack (2002), Evidence in hydrography and density fine structure for enhanced vertical mixing over the Mid-Atlantic Ridge in the western Atlantic, *J. Geophys. Res., 107(C10),* 3147, doi:10.1029/2001JC001114.

Mayewski, P. A., L. D. Meeker, M. S. Twickler, S. Whitlow, Q. Yang, W. B. Lyons, and M. Prentice (1997), Major features and forcing of high-latitude northern hemisphere atmospheric circulation using a 110,000-year-long glaciochemical series, *J. Geophys. Res., 102,* 26,345–26,366.

Meese, D. A. , A. J. Gow, R. B. Alley, G. A. Zielinski, P. M. Grootes, M. Ram, K. C. Taylor, P. A. Mayewski, J. F. Bolzan (1997), The Greenland Ice Sheet Project 2 depth-age scale: Methods and results, *J. Geophys. Res., -Oceans, 102(C12),* 26411-26423.

Milligan, T. G., and K. Kranck, (1991), Electroresistance particle size analysers. In: Syvitski, J. P. M. (ed.), *Principles, Methods and Application of Particle Size Analysis*, Cambridge Univ. Press, New York, 109-118.

Mix, A. C., and R. G. Fairbanks (1985), North Atlantic surface-ocean control of Pleistocene deep-ocean circulation, *Earth Planet. Sci. Lett., 73,* 231-243.

Mix, A., A. Morey, N. Pisias, and S. Hostetler (1999), Foraminiferal faunal estimates of paleotemperature: Circumventing the noanalog problem yields cool ice age tropics, *Paleoceanography, 14,* 350–359.

Moros, M., K. Emeis, B. Risebrobakken, I. Snowball, A. Kuijpers, J. McManus, and E. Jansen (2004), Sea surface temperatures and ice rafting in the Holocene North Atlantic: climate influences on northern Europe and Greenland, *Quat. Sci. Rev., 23*, 2113–2126.

N

North Greenland Ice Core Project Members (2004), High-resolution record of Northern Hemisphere climate extending into the last interglacial period, *Nature, 431*, 147-151.

Nürnberg, D. (1995), Magnesium in tests of Neogloboquadrina pachyderma (sinistral) from high northern and southern latitudes, *J. Foram. Res., 25,* 350–368.

Nurnberg, D., J. Bijma, and C. Hemleben (1996), Assessing the reliability of magnesium in foraminiferal calcite as a proxy for water mass temperatures *Geochim.Cosmochim. Acta, 60(5)*, 803-814.

O

O'Brien, S. R., P. A. Mayewski, L. D. Meeker, D. A. Meese, M. S. Twickler, and S. I. Whitlow (1995), Complexity of Holocene climate as reconstructed from a Greenland ice core, *Science, 270,* 1962–1964.

Ohkouchi, N., T. I. Eglinton, L. D. Keigwin, and J. M. Hayes (2002), Spatial and temporal offsets between proxy records in a sediment drift, *Science, 298*, 1224-1227.

Oppo, D. W., and R. G. Fairbanks (1987), Variability in the deep and intermediate water circulation of the Atlantic Ocean during the past 25,000 years: Northern Hemisphere modulation of the Southern Ocean, *Earth Planet. Sci. Lett., 86*, 1-15.

Oppo, D. W., and S. J. Lehman (1993), Mid-depth circulation of the subpolar North Atlantic during the Last Glacial Maximum, *Science, 259*, 1148–1152.

Oppo, D. W., and S. J. Lehman (1995), Suborbital timescale variability of North-Atlantic deep-water during the past 200,000 years, *Paleoceanography, 10(5),* 901-910.

Oppo, D. W., and M. Horowitz (2000), Glacial deep water geometry: South Atlantic benthic foraminiferal Cd/Ca and $\delta^{13}C$ evidence, *Paleoceanography, 15*, 147–160.

Oppo, D. W., M. Horowitz, and S. J. Lehman (1997), Marine core evidence for reduced deep water production during Termination II followed by a relatively stable substage 5e, *Paleoceanography, 12*, 51-63.

Oppo, D. W., J. F. McManus, and J. L. Cullen (1998), Abrupt climate events 500,000 to 340,000 years ago: Evidence from subpolar North Atlantic sediments, *Science, 279*, 1335– 1338.

Oppo, D. W., L. D. Keigwin, J. F. McManus and J. L. Cullen (2001), Persistent suborbital climate variability in marine isotope Stage 5 and Termination II, *Paleoceanography, 16,* 280–292.

Ostermann, D. R., and W. B. Curry (2000), Calibration of stable isotopic data: An enriched delta O-18 standard used for source gas mixing detection and correction, *Paleoceanography, 15(3),* 353-360.

Overpeck, J. T., L. C Peterson, N. Kipp, J. Imbrie, and D. Rind (1989), Climate change in the circum-North Atlantic region during the last deglaciation, *Nature, 338(6216),* 553-557.

P

Pahnke, K., and R. Zahn (2005), Southern hemisphere water mass conversion linked with North Atlantic climate variability, *Science, 307(5716),* 1741-1746.

Pahnke, K., R. Zahn, H. Elderfield, and M. Schulz (2003), 340,000-Year Centennial-Scale Marine Record of Southern Hemisphere Climatic Oscillation, *Science, 301,* 948–952.

Peltier, W. R. (2005), On the hemispheric origins of meltwater pulse 1a. *Quat. Sci. Rev., 24(14-15),* 1655-1671.

Peterson, L. C., G. H. Haug, K. A. Hughen, and U. Rohl (2000), Rapid changes in the hydrologic cycle of the tropical Atlantic during the last glacial, *Science, 290,* 1947– 1951.

Petit, J. R., J. Jouzel, D. Raynaud, N. I. Barkov, J. M. Barnola, I. Basile, M. Bender, J. Chappellaz, M. Davis, G. Delaygue, M. Delmotte, V. M. Kotlyakov, M. Legrand, V. Y. Lipenkov, C. Lorius, L. Pepin, C. Ritz, E. Saltzman, and M. Stievenard (1999), Climate and atmospheric history of the past 420,000 years from the Vostok ice core, Antarctica, *Nature, 399,* 429–436.

Pickart, R. S. (1992), Water mass components of the North-Atlantic Deep Western Boundary Current. *Deep-Sea Res., 39 (9A),* 1553-1572.

Pickart, R. S., and W. M. Smethie (1993), How does the Deep Western Boundary Current cross the Gulf-Stream, *J. Phys. Oceanogr., 23(12)*, 2602-2616.

Pickart, R. S., M. A. Spall, and J. R. N. Lazier (1997), Mid-depth ventilation in the western boundary current system of the sub-polar gyre, *Deep-Sea Res., 44(6),* 1025.

Piotrowski, A. M., S. L. Goldstein, S. R. Hemming, and R. G. Fairbanks (2005), Temporal relationships of carbon cycling and ocean circulation at glacial boundaries, *Science, 307(5717),* 1933-1938.

Popp, B. N., F. G. Prahl, R. J. Wallsgrove, and J. Tanimoto (2006), Seasonal patterns of alkenone production in the subtropical oligotrophic Pacific, *Paleoceanography, 21, 1, Art. No.* PA1004.

Prange, M., V. Romanova, and G. Lohmann (2002), The glacial thermohaline circulation: Stable or unstable?, Geophys. *Res. Lett., 29(21),* Art. No. 2028.

R

Rahmstorf, S. (1994), Rapid climate transitions in a coupled ocean-atmosphere model, *Nature, 372(6501),* 82-85.

Rahmstorf, S. (2002), Ocean circulation and climate during the past 120,000 years, *Nature, 419,* 207– 214.

Rahmstorf, S., and R. B. Alley (2002), Stochastic resonance in glacial climate, *EOS, 83,* 129-135.

Rapid Conference Summary (2006), http://www.noc.soton.ac.uk/rapid/kt/2006_ RAPID_conf _sum.pdf

Rasmussen,T. L., D. W. Oppo, E. Thomsen, and S. J. Lehman (2003), Deep sea records from the southeast Labrador Sea: Ocean circulation changes and ice-rafting events during the last 160,000 years, *Paleoceanography, 18,* 1018, doi:10.1029/2001PA000736.

Rathburn, A. E., and P. DeDeckker, (1997), Magnesium and strontium compositions of Recent benthic foraminifera from the Coral Sea, Australia and Prydz Bay, Antarctica, *Mar. Micropaleontol., 32,* 231–248.

Raymo, M. E.,W. F. Ruddiman, N. J. Shackleton, and D. Oppo (1990), Evolution of Atlantic- Pacific $\delta^{13}C$ gradients over the last 2.5 m.y., *Earth Planet. Sci. Lett., 97,* 353– 368.

Raymo, M. E., D. W. Oppo, B. P. Flower, D. A. Hodell, J. F.McManus, K. A. Venz, K. F. Kleiven, and K. McIntyre (2002), Stability of North Atlantic water masses in face of pronounced climate variability during the Pleistocene, *Paleoceanography, 19*(2), Art. No. PA2008.

Raymo, M. E., D. W. Oppo, B. P. Flower, D. A. Hodell, J. F. McManus, K. A. Venz, K. F. Kleiven, and K. McIntyre (2004), Stability of North Atlantic water

masses in face of pronounced climate variability during the Pleistocene, *Paleoceanography, 19,* PA2008, doi:10.1029/2003PA000921.

Reid, J. L. (1994), On the total geostrophic circulation of the North Atlantic Ocean: Flow patterns, tracers, and transports, *Prog. Oceanogr., 33,* 1-92.

Reimer, P. J., M. G. L. Baillie, E. Bard, et al. (2004), IntCal04 terrestrial radiocarbon age calibration, 0-26 cal kyr BP, *Radiocarbon, 46(3),* 1029-1058.

Renssen, H., H. Goosse, and T. Fichefet (2002), Modeling the effect of freshwater pulses on the early Holocene climate: The influence of high-frequency climate variability, P*aleoceanography, 17 (2),* Art. No.1020.

Rickaby, R. E. and M. H. Elderfield (2005), Evidence from the high-latitude North Atlantic for variations in Antarctic Intermediate water flow during the last deglaciation, *Geochem. Geophys. Geosyst. 6*, doi:10.1029/2004GC000858.

Rimbu, N., G. Lohmann, S. Lorenz, J. Kim, and J. -H Schneider, (2004), Holocene climate variability as derived from alkenone sea surface temperature and coupled ocean-atmosphere model experiments, *Climate Dynamics, 23,* 215–227.

Ridgewell, A. J., A. Watson, and M. E. Raymo (1999), Is the spectral signature of the 100 kyr glacial cycle consistent with Milankovitch origin? *Paleoceanography, 14(4),* 437-440.

Risebrobakken, B., E. Jansen, C. Andersson, E. Mjelde, and K. Hevrøy (2003), A high-resolution study of Holocene paleoclimatic and paleoceanographic changes in the Nordic Seas, *Paleoceanography, 18*, doi:10.1029/ 2002 PA 000764.

Robinson, L.F., Adkins, J.F., Keigwin, L.D., Southon, J., Fernandez, D.P., Wang, S.L. and D.S. Scheirer (2005), Radiocarbon variability in the western North Atlantic during the last deglaciation, *Science*, *310(5753),* 1469-1473.

Robinson, S. G. (1986), The late Pleistocene palaeoclimatic record of North Atlantic deep-sea sediment studies, *Geophys. J. R. Astron. Soc., 69*, 294.

Robinson, S. G. (1990), Applications for whole-core magnetic susceptibility measurements of deep-sea sediments:Leg 115 results. In: Duncan, R.A., J. Blackman, L. C. Peterson *et al.* (ed.), *Proceedings of the Ocean Drilling Program, Scientific Results, 115,* College Station, Texas (Ocean Drilling Program), 737-771.

Robinson, S. G., M. A. Maslin, I. N. McCave (1995), Magnetic susceptibility variations in he late Pleistocene deep-sea sediments of the NE Atlantic: Implications for ice-rafting and palaeocirculation at the last glacial maximum, *Paleoceanography, 10,* 221-250.

Rohling, E., and H. Pälike (2005), Centennial-scale climate cooling with a sudden cold event around 8,200 years ago, *Nature, 434*, 975–979.

Rosenthal, Y., E. A. Boyle, and N. Slowey (1997), Temperature control on the incorporation of magnesium, strontium, fluorine, and cadmium into benthic foraminiferal shells from Little Bahama Bank: prospects for thermocline paleoceanography, *Geochim. Cosmochim. Acta, 61,* 3633–3643.

Rosenthal, Y., G. P. Lohmann, K. C. Lohmann, and R. M. Sherrell (2000), Incorporation and preservation of Mg in *Globigerinoides sacculifer*: Implications for reconstructing the temperature and O-18/O-16 of seawater, *Paleoceanography, 15*, 135–145.

Rosenthal, Y., D. W. Oppo, and B. K. Linsley (2003), The amplitude and phasing of climate change during the last deglaciation in the Sulu Sea, western equatorial Pacific, *Geophys. Res. Lett., 30(8),* Art. No.1428.

Ruddiman, W. F. (1977), Late Quaternary deposition of ice rafted sand in the subpolar North Altantic (lat 40 degrees to 65 degrees N), *Bull. Geol. Soc. Am., 88,* 1813-1827.

Ruddiman, W. F., and A. McIntyre (1981), The North-Atlantic ocean during the last deglaciation, *Palaeogeog. Palaeoclim. Palaeoecol., 35(1-2),* 145-214.

Rühlemann C., S. Mulitza, P. J. Müller, G. Wefer, R. Zahn (1999), Warming of the tropical Atlantic Ocean and slowdown of thermohaline circulation during the last deglaciation, *Nature, 402,* 511 –514.

Russel, W. B. (1980), Review of the role of colloidal forces in the rheology of suspensions, *J. Rheol., 24,* 287-317.

S

Sachs, J. P., and S. J. Lehman (1999), Subtropical North Atlantic temperature 60,000 to 30,000 years ago, *Science, 286*, 756-759.

Sarnthein, M., K. Winn, S. J. A. Jung, J-. C. Duplessy, L. Labeyrie, H. Erlenkeuser, and G. Ganssen (1994), Changes in east Atlantic deepwater circulation over the last 30,000 years: eight time slice reconstructions, *Paleoceanography*, *9*, 209-267.

Saunders, P. M (1996), The flux of dense cold overflow water southeast of Iceland, *J. Phys. Oceanogr., 26(1),* 85-95.

Schiller, A., U. Mikolajewicz, and R. Voss (1997), The stability of the North Atlantic thermohaline circulation in a coupled ocean-atmosphere general circulation model, *Climate Dynamics, 13(5),* 325-347.

Schmidt, G. A., G. R. Bigg, and E. J. Rohling (1999), Global Seawater Oxygen-18 Database, Goddard Inst. for Space Studies, New York. (Available at http://www.giss.nasa.gov/cgi-bin/o18data/geto18.cgi.)

Schmidt, M. W., H. J. Spero, and D. W. Lea (2004), Links between salinity variation in the Caribbean and North Atlantic thermohaline circulation, *Nature, 428, (6979),* 160-163.

Schmidt, M. W., M. J. Vautravers, and H. J. Spero (2006), Rapid subtropical North Atlantic salinity oscillations across Dansgaard-Oeschger cycles, *Nature, 443 (7111),* 561-564.

Schmitz, W. J., and M. S. McCartney (1993), On the North Atlantic circulation, *Rev. Geophys., 31,* 29-49.

Seidov, D., M. Sarnthein, K. Stattegger, R. Prien, and M. Weinelt (1996), North Atlantic ocean circulation during the last glacial maximum and subsequent meltwater event: A numerical model, *J. Geophys. Res.-Oceans, 101(C7),* 16305-16332.

Shackleton, N. J. (1969), The last interglacial in the marine and terrestrial records, *Proceedings of the Royal Society, B174,* 135– 154.

Shackleton, N. J. (2000), The 100,000-year ice-age cycle identified and found to lag temperature, carbon dioxide, and orbital eccentricity, *Science, 289(5486),* 1897-1902.

Shackleton, N. J., and N. D. Opdyke (1973), Oxygen isotope and palaeomagnetic stratigraphy of equatorial pacific core V28- 238: Oxygen isotope temperature and ice volumes on a 105 year and 106 year scale, *Quat. Res., 3,* 39–55.

Shackleton, N. J., and J. P. Kennett (1975), Palaeo-temperature history of the Cenozoic and the initiation of Antarctic glaciation: Oxygen and carbon isotope analysis in DSDP sites 277, 279 and 281. In: Kennet, J. P. *et al.* (ed.), *Initail Report of the Deep Sea Drilling Project,* vol. 5, US Govt. Print. Office, Washington D.C, 743-755.

Shin, S. I., Z. Liu, B. Otto-Bliesner, E. C. Brad, J. E. Kutzbach, S. P. Harrison (2003), A simulation of the last glacial maximum climate using the NCAR-CCSM, *Climate. Dynamics, 20(2-3),* 127-151.

Shipboard Scientific Party (1998), *Proc. ODP, Init. Repts.,* 172: College Station, TX (Ocean Drilling Program), 321 pp.

Siddall, M., T. F. Stocker, G. M. Henderson, F. Joos, M. Frank, M. R. Edward, S. Ritz, and S. A. Müller (2007), Modelling the relationship between ^{231}Pa / ^{230}Th distribution in North Atlantic sediment and Atlantic Meridional Overturning Circulation, *Paleoceanography, 22,* doi:10.1029/2006PA001358.

Skinner L. C., and H. Elderfield, (2003) Constraining ecological and biological bias in planktonic foraminiferal Mg/Ca and $\delta^{18}O_{cc}$: A multispecies approach to proxy

calibration testing, *Paleoceanography, 20,* PA1015, doi:10.1029/2004PA 001058.

Slowey, N. C., and W. B. Curry (1995), Glacial-interglacial differences in circulation and carbon cycling within the upper western North Atlantic, *Paleoceanography, 10(4),* 715– 732.

Spero, H. J., and D. F. Williams (1991), Evidence for seasonal low-salinity surface waters in the Gulf of Mexico over the last 16,000 years, *Paleoceanography, 5,* 963–975.

Stahr, F. R., and T. B. Sanford (1999), Transport and bottom boundary layer observations of the North Atlantic Deep Western Boundary Current at the Blake Outer Ridge, *Deep Sea Res., 46,* 205-243.

Stanford, J. D., E. J. Rohling, S. E. Hunter, A. P. Roberts, S. O. Rasmussen, E. Bard, J. McManus, and R. G. Fairbanks (2006), Timing of meltwater pulse 1a and climate responses to meltwater injections, *Paleoceanography, 21(4),* Art. No. PA4103.

Stein, R. (1985) Rapid grain-size analysis of silt and clay fraction by Sedigraph 5000D: comparison with Coulter Counter and Atterberg methods. *J. Sedim. Petrol, 55,* 590-615.

Steinke, S., H. Y. Chiu, P. S. Yu, C. C. Shen, L. Lowemark, H. S. Mii, and M. T. Chen (2005), Mg/Ca ratios of two Globigerinoides ruber (white) morphotypes: Implications for reconstructing past tropical/ subtropical surface water conditions, *Geochem. Geophys. Geosyst., 6,* Art. No. Q11005.

Stocker, T. F., and D. G. Wright (1991), Rapid transitions of the oceans deep circulation induced by changes in surface-water fluxes, *Nature, 351(6329),* 729-732.

Stocker, T. F., and D. G. Wright (1998), The effect of a succession of ocean ventilation changes on ^{14}C, *Radiocarbon, 40,* 359–366.

Stocker, T. F. and O. Marchal (2000), Abrupt climate change in the computer: Is it real? *Proc. Natl Acad. Sci. USA, 97,* 1362–1365.

Stocker, T. F. and S. J. Johnsen (2003), A minimum thermodynamic model of the bipolar seesaw, *Paleoceanography, 18,* Art. No.PA1087.

Stommel, H. (1958), The abyssal circulation, *Deep-Sea Res., 5,* 80-82.

Stommel, H. (1961), Thermohaline convection with two stable regimes of flow, *Tellus, 13,* 224–230.

Street-Perrott, F. A., and R. A. Perrott (1990), Abrupt climate fluctuations in the tropics: The influence of Atlantic circulation. *Nature, 343,* 607-612.

Stuiver, M., P. J. Reimer, and R. W. Reimer (2005), CALIB 5.0 (www program and documentation) http://radiocarbon.pa.qub.ac.uk/calib/

Svenmark, H., and E. FriisChristensen (1997), Variation of cosmic ray flux and global cloud coverage – A missing link in solar-climate relationships, *Journal of atmospheric and solar-terrestrial physics, 59,* 1125-1232.

Swallow, J. C., and L. V. Worthington (1961), An observation of a deep counter current in the Western North Atlantic, *Deep-Sea Res., 8,* 1-19.

T

Talley, L., and M. McCartney (1982), Distribution and circulation of Labrador Sea Water, *J. Phys. Oceanogr., 12,* 1189-1205.

Taylor, S. P., A. M. Haywood, P. J. Valdes, and B. W. Sellwood (2004), An evaluation of two spatial interpolation techniques in global sea-surface temperature reconstructions: Last Glacial Maximum and Pliocene case studies, *Quat. Sci. Rev., 23 (9-10),* 1041-1051.

Tarasov, L., and W. R. Peltier (2005), Arctic freshwater forcing of the Younger Dryas cold reversal, *Nature, 435,* 662– 665.

Tedesco, K. A., and R. C. Thunell (2003), Seasonal and interannual variations in planktonic foraminiferal flux and assemblage composition in the Cariaco Basin, Venezuela, *J. Foram. Res., 33(3),* 192-210.

Thomas, A. L., M. Gideon G. M. Henderson, and L. F. Robinson (2006), Interpretation of the $^{231}Pa/^{230}Th$ paleocirculation proxy: New water-column measurements from the southwest Indian Ocean, *Earth Planet. Sci. Lett., 241,* 493– 504.

Thompson, R., and F. Oldfield (1986), *Environmental magnetism,* Allen and Unwin, London, 227pp.

Thunell, R. C., M. S. Poli, and D. Rio (2002), Changes in deep and intermediate water properties in the western North Atlantic during marine isotope stages 11-42: Evidence from ODP Leg 172, *Marine Geology 189(1-2),* 63-77.

Thunell, R., E. Tappa, C. Pride, and E. Kincaid (1999), Sea-surface temperature anomalies associated with the 1997–1998 El Niño recorded in the oxygen isotope composition of planktonic foraminifera, *Geology, 27(9),* 843–846.

Tolderlund, D. S., and A. W. H. Bé (1971), Seasonal distribution of planktonic foraminifera in the western North Atlantic, *Micropaleontology,17,*297–329.

Trenberth, K. E., and A. Solomon (1994), The global heat-balance - Heat transports in the atmosphere and ocean, *Climate Dynamics, 10(3),* 107-134.

U

Urey, H. C. (1947), The thermodynamic properties of isotopic substances, *J. Chem. Soc.*, 562-581.

V

van Kreveld, S., M. Sarnthein, H. Erlenkeuser, P. Grootes, S. Jung, M. J. Nadeau, U. Pflaumann, and A. Voelker (2000), Potential links between surging ice sheets, circulationchanges, and the Dansgaard-Oeschger cycles in the Irminger Sea, 60–18 kyr, *Paleoceanography, 15,* 425–442.

Vellinga, M., and R. Wood (2002), Global climatic impacts of a collapse of the Atlantic thermohaline circulation, *Climatic Change, 54,* 251-267.

Vidal, L., L., Labeyrie, E., Cortijo, M.,Arnold, J. -C., Duplessy, E., Michel, S. Becque, and T. C. E. van Weering (1997), Evidence for changes in the North Atlantic Deep Water linked to meltwater surges during the Heinrich events, *Earth Planet. Sci. Lett.*, *146(1-2),* 13-27.

Vidal, L., L. Labeyrie, and T. C. E van Weering (1998), Benthic delta O-18 records in the North Atlantic over the last glacial period (60-10 kyr): Evidence for brine formation, *Paleoceanography* , *13(3),* 245-251.

W

Waelbroeck, C., J. –C. Duplessy, E. Michel, L. Labeyrie, D. Paillard and J. Duprat (2001), The timing of the last deglaciation in North Atlantic climate records, *Nature, 412*, 724-727.

Wales, M. and J. N. Wilson (1961) Theory of coincidence in Coulter particle counters. *Rev. Scient. Instrum., 32,* 1132-1136.

Wales, M. and J. N. Wilson (1962) Coincidence in Coulter counters. *Rev. Scient. Instrum., 33,* 575-576.

Wang, L. (2000), Isotopic signals in two morphotypes of Globigerinoides ruber (white) from the South China Sea: Implications for monsoon climate change during the last glacial cycle, *Palaeogeogr. Palaeoclimatol. Palaeoecol., 161*, 381–394.

Wang, Y. J., H. Cheng, R. L. Edwards, Z. S. An, J. Y. Wu, C. C. Shen, and J. A. Dorale (2001), A high-resolution absolute-dated Late Pleistocene monsoon record from Hulu Cave, China, *Science, 294(5550)*, 2345-2348.

Wang, X., A. S. Auler, R. L. Edwards, H. Cheng, P. S. Cristalli, P. L. Smart, D. A. Richards, and C. -C. Shen (2004), Wet periods in northern Brazil over the past 210 kyr linked to distant climate anomalies, *Nature, 432,* 740– 743.

Weatherly, G. L., and E. A. Kelley (1984), Two views of the cold filament., *J. Phys. Oceanogr.*, *15*, 68-81.

Weaver, C. E. (1989), *Clays, Muds and Shales*, Elsevier, New York, 810 pp.

Weaver, P. P. E., and J. Thomson (1993), Calculating erosion by deep-sea turbidity currents during initiation and flow, *Nature*, *364*, 136-138.

Weaver, A. J., Oleg A. Saenko, P. U. Clark, and J. X. Mitrovica (2003), Meltwater Pulse 1A from Antarctica as a Trigger of the Bølling-Allerød Warm Interval, *Science, 299*, 1709-1713.

Weldeab, S., R. R. Schneider, and M. Kölling (2006), Deglacial sea surface temperature and salinity increase in the western tropical Atlantic in synchrony with high latitude climate instabilities, *Earth Planet. Sci. Lett., 241*, 699– 706.

Weyl, P. K. (1968), The role of the oceans in climatic change: A theory of the ice ages, *Meteorol. Monogr., 8,* 37–62.

Wiersma, A. P., and H. Renssen (2006), Model-data comparison for the 8.2 ka BP event: confirmation of a forcing mechanism by catastrophic drainage of Laurentide Lakes, *Quat. Sci. Rev., 25(1-2),* 63-88.

Willamowski, A., and R. Zahn (2000), Upper ocean circulation in the glacial North Atlantic from benthic foraminiferal isotope and trace element fingerprinting, *Paleoceanography*, *15,* 515–527.

Wood, R. A, A. B. Keen, J. F. B. Mitchell, and J. M. Gregory (1999), Changing spatial structure of the thermohaline circulation in response to atmospheric CO_2 forcing in a climate model, *Nature, 399(6736),* 572-575.

Wunsch, C. (2003), Determining paleoceanographic circulations, with emphasis on the Last Glacial Maximum, *Quat. Sci. Rev., 22*, 371–385.

Wunsch, C. (2004), Quantitative estimate of Milankovitch-forced contribution to observed Quaternary climate change. *Quat. Sci. Rev., 23,* 1001-1012.

Wüst, G. (1935), Schichtung und Zirkulation des Atlantischen Ozeans, Die Stratosphäre, *Wiss. Ergebn. Dtsch. Atl. Exped., 6,* 180.

Y

Yokokawa, M., and S. O. Franz (2002), Changes in grain size and magnetic fabric at Blake-Bahama Outer Ridge during the late Pleistocene (marine isotope stages 8-10), *Mar. Geol.*, *189*, 123-144.

Yu, E. -F., R. Francois, and M. P. Bacon (1996), Similar rates of modern and last-glacial ocean thermohaline circulation inferred from radiochemical data, *Nature, 379,* 689-694.

Z

Zahn R and A. Stüber (2002), Suborbital intermediate water variability inferred from paired benthic foraminiferal Cd/Ca and $\delta^{13}C$ in the tropical West Atlantic and linking with North Atlantic climates, *Earth Planet. Sci. Lett., 200,* 191-205.

Zahn, R., K. Winn, and M. Sarnthein (1986), Benthic foraminiferal $\delta^{13}C$ and accumulation rates of organic carbon: Uvigerina peregrina group and *Cibididoides wuellerstorfi*, *Paleoceanography, 1,* 27– 42.

Zahn, R., J. Schonfeld, H. –R. Kudrass, M. –H. Park, H. Erlenkeuser, and P. Grootes (1997), Thermohaline instability in the North Atlantic during meltwater events: Stable isotope and ice-rafted detritus records form core SO75-26KL, Portuguese margin, *Paleoceanography, 12,* 696-710.

Zhang, R., and T. L. Delworth (2005), Simulated Tropical Response to a Substantial Weakening of the Atlantic Thermohaline Circulation, *Journal of Climate, 18,* 1853-1860.

Appendix A

Depth transect database

VM3-5		RC7-2		VM30-7		AII-72-23PC		RC1-10	
Depth (cm)	Mag. Sus. (S.I.)	Depth (cm)	Mag. Sus. (S.I.)	Depth (cm)	Mag. Sus. (S.I.)	Depth (cm)	Mag. Sus. (S.I.)	Depth (cm)	Mag. Sus. (S.I.)
5	21.50	5	17.50	5	18.25	3	10.75	5	17.25
10	19.25	10	25.50	10	19.50	15	12.25	10	18.50
20	13.75	15	24.00	15	17.75	20.5	19.50	15	12.50
30	20.75	20	28.75	20	11.75	24.5	31.75	20	17.75
40	12.50	25	25.25	25	22.00	28.5	35.50	25	22.00
50	12.50	30	22.75	30	19.00	32.5	35.00	30	20.25
60	15.00	35	23.00	35	20.00	37	33.00	35	20.50
70	22.25	40	22.50	40	13.00	41	33.75	40	18.00
80	23.50	45	21.00	45	13.50	52.5	33.50	45	19.50
90	15.75	50	21.50	50	21.00	56.5	35.75	50	20.50
100	14.25	55	18.00	55	25.00	60.5	39.00	55	22.25
110	20.00	60	19.00	60	22.00	64.5	33.00	60	17.25
120	15.00	65	19.00	65	21.25	73.5	36.25	65	21.00
130	12.00	70	19.50	70	21.25	78	37.25	70	18.25
140	12.50	75	23.50	75	24.25	83	37.00	75	23.25
150	15.00	80	22.50	80	20.50	86.5	35.50	80	23.75
160	13.75	85	22.00	85	28.25	94.5	16.00	85	20.75
170	10.25	90	20.00	90	27.75	110	29.25	95	23.00
180	15.50	95	21.00	95	28.25	114	29.00	100	15.75
190	21.25	100	25.00	100	23.50	119	54.50	105	30.25
200	18.25	105	20.00	105	21.50	123	28.75	110	48.00
210	18.00	110	25.75	110	27.75	132	10.25	115	23.75
220	14.00	115	22.50	115	22.25	136	11.75	120	34.25
230	15.00	120	18.50	120	26.00	140	9.00	125	45.25
240	18.25	125	23.25	125	25.00	144	7.50	130	34.75
250	21.75	130	14.00	130	27.75	157	9.50	135	21.50
260	19.25	135	18.00	135	27.50	162	10.00	140	21.75
270	14.50	140	15.50	140	23.75	167	11.00	145	21.75
278	16.50	145	22.00	145	22.50	172	9.75	150	21.75
290	17.75	150	21.50	150	25.00	175.5	12.25	155	29.00
300	19.00	155	20.75	155	21.50	183.5	14.75	160	23.00
310	23.25	160	25.75	160	24.25	191.5	12.75	165	20.00
320	21.50	165	23.00	165	26.25	205	9.25	170	23.00
330	25.25	170	24.00	170	31.00	212	7.75	175	28.50
340	28.50	175	23.50	175	30.00	215.5	9.75	180	28.75
350	22.25	180	24.00	179	23.75	219	5.75	185	23.25
360	23.00	185	27.75	185	36.25	225	11.00	190	18.75
370	27.00	190	25.25	190	47.00	228	11.00	195	18.75
380	21.75	195	24.25	195	16.00	235.5	11.00	200	29.50
390	24.75	200	30.50	200	37.00	241.5	5.50	205	34.00
400	35.25	205	29.00	210	20.00	251.5	12.25	210	23.00
410	36.00	210	26.25	215	31.00	265.5	19.50	215	24.00
420	24.50	215	31.25	220	38.00	269	14.75	220	34.25
430	35.75	220	29.75	225	34.00	274	18.00	225	30.00
440	23.25	225	29.25	230	29.50	278	14.00	230	27.00
450	23.25	230	34.25	235	27.25	283.5	18.50	235	38.25
460	23.75	235	42.25	240	38.00	288	17.50	240	41.50
470	22.75	240	28.50	248	25.50	295	19.25	250	47.75
480	23.75	247	40.25	250	26.50	308	12.50	255	44.25
488	23.50	250	53.25	255	20.25	316	11.75	260	20.00
492	19.25	255	39.75	260	22.25	321.5	20.00	265	29.25
500	22.75	260	39.50	265	18.25	325	20.00	270	28.50

VM3-5		RC7-2		VM30-7		All-72-23PC		RC1-10	
Depth (cm)	Mag. Sus. (S.I.)	Depth (cm)	Mag. Sus. (S.I.)	Depth (cm)	Mag. Sus. (S.I.)	Depth (cm)	Mag. Sus. (S.I.)	Depth (cm)	Mag. Sus. (S.I.)
510	23.00	266	30.75	270	28.00	330	20.00	275	36.50
515	20.00	275	41.75	275	38.50	334	22.75	280	33.50
520	20.50	280	57.25	280	31.25	342	21.25	285	23.75
525	19.25	285	33.25	285	25.50	354	19.50	290	37.00
530	22.00	290	14.50	290	23.50	362	26.00	295	25.25
540	21.50	293	15.50	296	21.50	366	22.50	300	26.75
545	19.50	295	28.00	300	19.00	371.5	17.50	310	22.50
550	21.25	300	73.75	305	15.50	389	24.00	315	23.00
555	25.50	305	36.00	310	21.00	400	17.50	320	8.50
560	24.75	310	102.50	315	25.50	408	33.75	325	10.00
570	26.50	315	40.00	320	24.75	413	35.50	330	15.00
575	25.50	320	35.25	325	18.50	416	48.25	335	17.00
580	30.00	325	63.50	330	15.00	422	21.50	340	14.00
590	29.50	330	63.75	335	27.75	426	35.25	345	18.00
595	24.50	335	36.00	340	39.25	432	37.75	350	43.00
600	34.50	340	34.25	345	31.00	436	58.50	355	32.00
605	31.00	345	28.25	350	51.50	442	24.75	365	19.00
610	26.00	351	29.00	355	43.00	454	24.00	375	20.50
615	27.50	355	29.75	360	37.75	457	22.00	385	26.00
620	27.50	360	29.00	365	46.00	463	21.00	390	25.50
625	27.00	365	30.00	370	35.75	467	22.50	400	31.50
630	25.50	370	27.75	375	25.25	471	23.00	405	30.00
635	19.00	375	29.50	380	34.25	478	20.25	410	40.00
640	22.00	380	19.25	385	35.00	482	25.25	415	34.00
645	28.25	385	15.50	390	39.25	486	24.00	420	37.50
650	25.75	390	21.00	395	37.25	490	27.00	425	33.00
655	19.25	393	21.50	400	2.25	493	25.50	430	37.00
660	25.25	400	21.75	405	29.25	505.5	21.00	435	36.00
665	25.75	405	14.50	410	21.75	511	22.00	440	35.00
670	24.25	410	15.75	415	33.00	515	23.00	445	37.75
675	25.50	415	15.75	420	44.25	519	24.00	450	51.50
680	22.00	420	11.75	425	35.25	523	21.75	455	36.75
685	23.25	425	16.50	430	26.75	527	21.75	465	20.50
690	24.25	430	18.00	435	28.00	531	21.00	470	19.00
695	23.00	435	19.00	440	30.50	535	22.00	475	25.50
700	22.50	440	15.00	446	27.25	539	21.00	480	25.00
705	25.00	445	25.50	450	32.00	552	20.00		
710	23.00	450	27.75	455	35.00	556	18.00		
715	21.50	455	27.50	461	28.50				
720	19.50	460	30.00	465	29.00				
730	18.00	465	26.00	470	37.00				
735	8.00	470	28.25	475	23.50				
775	14.00	475	28.25	480	23.75				
780	12.50	481	17.50	485	18.50				
785	12.75	486	17.50						
795	14.25								
805	15.50								
814	8.75								
825	14.00								
835	11.00								

RC9-4		V22-6		VM26-175		RC9-13		RC9-10	
Depth	Mag. Sus. (S.I.)	Depth	Mag. Sus. (S.I.)	Depth	Mag. Sus. (S.I.)	Depth	Mag. Sus. (S.I.)	Depth	Mag. Sus. (S.I.)
5	10.50	5	14.00	5	16.00	6	14.75	2	18.00
10	12.50	10	18.50	10	15.00	9	17.75	7	20.00
15	14.50	15	19.00	15	15.50	11	15.00	12	24.25
20	10.50	20	18.00	20	20.50	15	16.50	17	25.25
25	11.00	25	17.00	25	27.00	17	15.25	22	17.75
30	11.00	30	23.00	31	20.25	22	16.25	27	17.50
35	12.00	35	22.50	36	16.75	25	16.50	32	21.00
40	11.00	40	22.00	40	22.00	30	20.00	37	22.00
45	11.50	45	23.50	49	23.75	35	17.00	42	27.00
50	11.50	50	22.50	60	22.25	40	20.00	47	20.50
55	12.50	55	23.50	66	18.50	45	23.00	52	20.00
60	12.00	60	22.50	71	22.50	50	23.50	57	21.50
65	12.50	70	20.50	78	25.00	55	25.50	62	20.00
70	12.00	75	21.50	83	23.00	60	19.00	67	22.00
75	12.00	80	17.50	88	24.00	65	17.00	72	19.50
80	12.00	90	16.00	92	23.25	70	19.50	77	19.50
85	12.50	95	19.50	97	25.00	75	21.00	82	20.50
90	18.50	100	18.50	102	23.00	80	23.00	87	20.00
95	17.00	105	20.00	108	28.00	85	24.50	92	19.50
100	16.00	110	19.00	112	30.75	90	28.50	97	19.00
105	15.50	115	20.00	117	32.50	95	29.00	102	18.00
110	19.00	120	20.50	122	30.75	100	25.25	107	20.75
115	20.00	125	22.00	127	35.25	105	23.25	112	25.25
120	18.50	130	23.50	132	31.50	110	24.00	117	21.50
125	20.00	138	20.75	137	33.00	115	17.00	122	19.50
130	20.50	140	19.00	142	43.00	120	16.50	127	19.75
135	23.00	145	19.25	147	32.25	125	14.00	132	19.75
140	23.00	150	19.00	152	31.00	130	21.25	137	20.00
145	22.00	155	21.00	157	33.00	135	22.25	142	16.75
151	17.50	160	18.50	162	28.75	140	17.00	147	20.25
155	19.50	165	21.25	167	28.75	145	20.00	152	19.50
162	24.50	170	20.25	172	21.00	150	20.00	157	18.75
168	38.50	175	18.50	177	30.50	155	20.00	162	17.50
170	22.00	180	20.00	184	26.25	160	17.75	167	19.00
175	24.50	185	17.50	188	29.25	165	21.25	172	19.75
180	15.00	190	22.50	192	31.00	170	20.50	177	19.25
185	15.00	195	20.50	198	30.75	175	21.00	182	17.50
190	14.00	200	18.50	202	31.00	180	20.50	187	18.25
195	14.50	205	19.50	208	31.00	185	17.50	192	19.00
200	13.50	210	20.50	214	23.00	190	21.00	197	20.00
205	15.00	215	20.50	219	32.00	195	22.00		
210	13.50	220	19.00	222	31.75	200	19.00		
215	87.00	225	22.50	227	32.00	205	20.00		
220	14.50	230	22.00	232	28.00	210	20.50		
225	15.00	235	19.50	237	30.75	215	19.00		
228	20.50	240	19.00	242	31.75	220	16.25		
235	14.00	245	18.50	248	30.00	225	18.25		
240	13.00	250	18.50	252	31.00	230	19.00		
245	17.50	255	20.50	258	30.00	235	24.00		
265	18.25	265	20.50	263	27.00	240	24.00		
270	19.00	270	20.00	268	31.00				
275	21.25	275	21.00	272	31.00				
280	21.50	280	20.50	279	26.75				
286	18.00	285	20.50	282	30.75				
290	19.50	290	19.50	288	26.00				
295	22.50	295	20.00	292	17.50				
300	20.50	300	17.50	295	19.50				

RC9-4		V22-6		VM26-175	
Mag. Sus. (S.I.)	Depth	Mag. Sus. (S.I.)	Depth	Mag. Sus. (S.I.)	Depth
305	22.25	305	18.50	305	32.75
315	12.25	310	18.50	315	27.75
322	19.50	315	19.25	318	33.50
327	14.00	320	14.25	328	28.50
330	13.00	325	19.50	335	30.50
335	13.25	330	20.00	342	38.00
340	11.75	335	18.50	348	32.00
345	15.50	340	20.50	355	21.00
350	12.00	345	19.50	365	27.75
355	18.50	350	19.00	370	26.25
360	19.00	355	18.50	375	29.00
365	20.50	365	16.50	380	33.00
370	22.50	370	19.50	385	39.00
375	20.50	375	18.50	395	19.50
385	24.50	380	15.00	400	33.00
390	24.00	385	20.00	405	27.50
395	25.00	390	17.50	412	25.00
400	19.50	395	21.00	419	32.75
405	22.50	400	19.00	425	28.75
410	19.50	405	18.50	431	24.00
415	17.50	412	17.50	435	31.00
420	19.00	418	17.50	441	29.25
425	17.50	425	19.00	445	25.25
430	18.50	430	17.50	451	41.50
435	17.25	445	19.00	455	42.50
440	17.75	450	16.75	465	42.00
445	14.75	455	16.25	470	30.25
450	18.25	465	19.50	475	33.25
455	19.00	470	18.00	480	26.00
460	18.25	485	19.50	485	32.75
465	17.75				
470	16.50				
475	16.00				
480	19.75				

Transect 1												
Core Name	Depth (m)	Av Holo PF $\delta^{18}O$ (‰)	Av LGM PF $\delta^{18}O$ (‰)	Av Holo SS mean (μm)	Av LGM SS mean (μm)	Holo-LGM	Av Holo BF $\delta^{13}C$ (‰)	Av Holo BF $\delta^{18}O$ (‰)	Av LGM BF $\delta^{13}C$ (‰)	Av LGM BF $\delta^{18}O$ (‰)	Av Holo $CaCO_3$ (wt%)	Av LGM $CaCO_3$ (wt%)
AII71-21PC	2202	-1.14	0.12	16.72	19.35	-2.63	1.07	2.66	-	-	4.54	3.81
AII71-22PC	2942	-1.60	0.38	18.52	17.42	1.10	-	-	-	-	3.99	3.52
VM30-5	3203	-1.30	-	18.33	-	-	-	-	-	-	4.31	-
AII71-23PC	3204	-1.50	0.44	17.72	16.45	1.27	-	-	-	-	4.03	3.12
RC9-4	3552	-1.30	0.50	18.49	16.48	2.01	-	-	-	-	4.01	3.01
AII71-24PC	3824	-1.20	0.46	17.52	16.48	1.04	-	-	-	-	3.72	2.86
VM26-175	3995	-1.01	0.42	18.58	17.51	1.07	1.02	2.65	-	-	3.90	2.90
RC7-2	4398	-0.70	0.55	15.50	16.57	-1.07	0.64	2.33	-	-	2.77	-
VM30-7	4702	-0.75	-	14.33	-	-	-	-	-	-	3.45	2.96
RC1-10	4892	-0.70	0.50	15.19	16.44	-1.26	-	-	-	-	-	2.68
AII71-16PC	5058	-	0.60	-	17.17	-	-	-	-	-	-	-

Transect 3												
Core Name	Depth (m)	Av Holo PF $\delta^{18}O$ (‰)	Av LGM PF $\delta^{18}O$ (‰)	Av Holo SS mean (μm)	Av LGM SS mean (μm)	Holo-LGM	Av Holo BF $\delta^{13}C$ (‰)	Av Holo BF $\delta^{18}O$ (‰)	Av LGM BF $\delta^{13}C$ (‰)	Av LGM BF $\delta^{18}O$ (‰)	Av Holo $CaCO_3$ (wt%)	Av LGM $CaCO_3$ (wt%)
KNR140/2-25PC	3865	-1.10	0.50	17.33	14.38	2.95	1.02	2.74	-	-	3.97	2.80
RC9-10	4277	-	-	17.45	15.50	1.95	0.77	2.74	-	-	3.90	2.67
VM22-6	4499	-0.91	-	16.69	15.32	1.37	0.51	2.89	-	-	3.62	2.67
RC9-13	4735	-0.78	-	15.24	16.53	-1.29	-	-	-	-	3.70	3.20
RC9-12	4958	-0.81	0.58	15.84	16.64	-0.80	-	-	-	-	3.12	2.75
RC9-11	5212	-	0.70	-	16.56	-	-	-	-	-	-	2.65

Transect 2																		
Core Name	Depth (m)	Av Holo PF $\delta^{18}O$ (‰)	Av LGM PF $\delta^{18}O$ (‰)	Av YD PF $\delta^{18}O$ (‰)	Av Holo SS mean (μm)	Av LGM SS mean (μm)	Av YD SS mean (μm)	Silt/Clay	Holo -LGM	Av Holo BF $\delta^{13}C$ (‰)	Av Holo BF $\delta^{18}O$ (‰)	Av LGM BF $\delta^{13}C$ (‰)	Av LGM BF $\delta^{18}O$ (‰)	Av YD BF $\delta^{13}C$ (‰)	Av YD BF $\delta^{18}O$ (‰)	Av Holo $CaCO_3$ (wt%)	Av LGM $CaCO_3$ (wt%)	Av YD $CaCO_3$ (wt%)
KNR140/2-50GGC	1903	-1.30	0.30	-0.42	17.84	19.13	18.79	0.815	-1.29	0.766	2.61	1.19	3.96	1.12	3.43	5.23	3.84	4.10
KNR140/2-66GGC	2155	-1.40	0.28	-0.50	17.75	20.29	18.99	0.703	-2.54	-	-	-	-	-	-	5.3	3.82	3.90
KNR140/2-1JPC	2243	-1.37	0.50	-0.37	18.14	18.57	18.26	0.813	-0.43	-	-	-	-	1.04	3.41	5.53	3.87	3.89
KNR140/2-46GGC	2320	-1.37	0.53	-	17.25	18.54	-	1.126	-1.29	1.032	2.606	-	-	-	-	5.60	3.35	-
KNR140/2-43GGC	2590	-1.00	0.90	-0.52	16.78	16.77	17.78	0.612	0.01	1.1	2.6	0.90	4.50	-	-	4.50	3.16	3.18
KNR140/2-42GGC	2710	-1.10	0.71	-	16.44	16.97	-	1.096	-0.53	1.196	2.43	0.65	4.25	-	-	5.10	2.85	-
KNR140/2-39GGC	2975	-1.10	0.74	-0.38	17.10	16.60	16.70	0.733	0.50	1.2	2.67	0.32	4.43	0.32	3.43	4.30	2.92	2.80
KNR140/2-36JPC	3007	-0.80	0.81	-	17.19	16.50	-	0.752	0.69	-	-	-	-	-	-	3.80	2.72	-
KNR140/2-33JPC	3315	-	0.78	-	-	15.39	-	0.815	-	-	-	0.40	4.21	-	-	-	2.96	-
KNR140/2-31GGC	3410	-1.15	0.68	-0.27	16.44	15.63	15.43	0.610	0.81	-	-	-	-	-	-	4.00	3.12	3.12
KNR140/2-26GGC	3845	-1.00	0.70	-	16.68	15.38	-	0.637	1.30	0.6	2.744	-0.10	4.15	-	-	4.20	2.77	-
KNR140/2-29GGC	3978	-0.90	0.74	-0.15	16.40	14.84	14.97	0.662	1.57	-	-	-	-	-	-	3.86	2.68	2.98
KNR140/2-28GGC	4211	-0.80	0.80	0.07	15.30	15.82	15.39	0.423	-0.52	-	-	-	-	-	-	3.85	2.65	3.02
KNR140/2-12JPC	4250	-	0.87	-0.16	-	16.37	15.87	-	-	-	-	-	-	0.08	3.31	-	2.74	3.00
RC16-7	4893	-	0.84	-	-	16.86	-	-	-	-	-	-	-	-	-	-	2.73	-
VM25-2	5409	-0.75	0.82	-	15.45	16.72	-	1.205	-1.27	-	-	-	-	-	-	2.77	2.70	-

Appendix B

Stable isotopes and Mg/Ca for core 39GGC

Depth (cm)	Age (kyr)	$\delta^{18}O$ (‰)	Mg/Ca	Sr/Ca	SST (°C)	$\delta^{18}O_{ivc-sw}$ (‰)	Salinity (‰)
9	1.74	-1.550	4.168	1.473	24.6	0.79	35.7
13	2.15	-1.486	4.055	1.471	24.3	0.79	35.7
15	2.35	-1.396	4.216	1.452	24.7	0.96	36.1
17	2.55	-1.362	4.153	1.470	24.5	0.95	36.1
19	2.75	-1.249	4.196	1.465	24.6	1.08	36.5
21	2.95	-1.337	4.355	1.466	25.0	1.06	36.4
23	3.15	-1.442	4.166	1.455	24.6	0.86	35.9
25	3.35	-1.198	4.104	1.455	24.4	1.07	36.4
27	3.55	-1.198	4.019	1.453	24.2	1.03	36.3
29	3.75	-1.376	4.464	1.473	25.2	1.06	36.4
31	3.95	-1.266	4.032	1.465	24.2	0.95	36.1
33	4.15	-1.484	4.202	1.446	24.6	0.82	35.8
35	4.35	-1.328	3.927	1.463	24.0	0.83	35.8
37	4.56	-1.442	4.275	1.456	24.8	0.88	36.0
39	4.76	-1.109	4.312	1.484	24.9	1.24	36.8
41	4.96	-1.403	4.144	1.460	24.5	0.87	35.9
43	5.16	-1.328	4.284	1.462	24.8	1.01	36.3
45	5.36	-1.455	4.169	1.461	24.6	0.83	35.8
47	5.56	-1.462	4.246	1.470	24.8	0.86	35.9
49	5.76	-1.467	4.251	1.465	24.8	0.87	35.9
51	5.96	-1.160	4.314	1.460	24.9	1.21	36.8
53	6.16	-1.375	4.152	1.476	24.5	0.89	36.0
55	6.36	-1.420	4.353	1.471	25.0	0.92	36.1
57	6.56	-1.464	4.310	1.478	24.9	0.84	35.8
59	6.76	-1.200	4.188	1.479	24.6	1.02	36.3
61	6.97	-1.455	4.258	1.469	24.8	0.78	35.7
65	7.26	-	4.670	1.462	25.7	-	-
66	7.38	-1.696	4.305	1.472	24.9	0.53	35.1
69	7.66	-1.079	4.061	1.459	24.3	1.01	36.3
71	7.82	-1.130	4.076	1.479	24.4	0.96	36.1
76	8.15	-	4.088	1.473	24.4	-	-
77	8.32	-0.976	4.255	1.486	24.8	1.16	36.6
78	8.40	-0.914	4.262	1.468	24.8	1.22	36.8
79	8.48	-1.089	4.320	1.475	24.9	1.06	36.4
80	8.57	-0.931	4.113	1.466	24.4	1.11	36.5
82	8.73	-1.187	4.316	1.478	24.9	0.94	36.1
83	8.81	-	4.202	1.476	24.7	-	-
84	8.89	-	4.358	1.479	25.0	-	-
85	8.98	-0.760	4.240	1.472	24.7	1.31	37.0
86	9.06	-0.960	4.202	1.473	24.7	1.09	36.5
87	9.14	-0.985	4.242	1.477	24.7	1.08	36.4
88	9.22	-0.960	4.376	1.471	25.0	1.16	36.6
89	9.31	-0.540	4.106	1.476	24.4	1.44	37.4
90	9.39	-1.040	4.246	1.478	24.8	0.99	36.2
91	9.47	-1.142	4.337	1.475	25.0	0.94	36.1

Depth (cm)	Age (kyr)	$\delta^{18}O$ (‰)	Mg/Ca	Sr/Ca	SST (°C)	$\delta^{18}O_{ivc-sw}$ (‰)	Salinity (‰)
92	9.55	-0.963	4.183	1.471	24.6	1.04	36.4
93	9.63	-1.200	4.365	1.469	25.0	0.89	36.0
94	9.72	-1.084	4.511	1.475	25.3	1.06	36.4
95	9.80	-1.121	4.414	1.474	25.1	0.97	36.2
96	9.88	-1.158	4.299	1.476	24.9	0.88	35.9
97	9.96	-1.288	4.316	1.480	24.9	0.76	35.6
98	10.05	-1.389	4.089	1.454	24.4	0.54	35.1
99	10.13	-1.027	4.206	1.476	24.7	0.96	36.2
100	10.21	-1.528	4.241	1.473	24.7	0.48	34.9
101	10.29	-1.109	4.202	1.477	24.7	0.88	35.9
102	10.37	-1.174	4.434	1.474	25.2	0.92	36.0
103	10.46	-0.851	4.178	1.481	24.6	1.11	36.5
104	10.54	-0.986	3.934	1.488	24.0	0.85	35.9
105	10.62	-1.215	4.139	1.475	24.5	0.72	35.6
106	10.70	-1.073	4.285	1.485	24.8	0.93	36.1
107	10.79	-0.962	4.178	1.465	24.6	0.99	36.2
108	11.03	-	4.215	1.471	24.7	-	-
110	11.12	-1.140	4.442	1.465	25.2	0.92	36.0
111	11.20	-1.226	4.185	1.486	24.6	0.68	35.5
112	11.28	-0.861	4.150	1.456	24.5	1.01	36.3
113	11.36	-0.738	4.187	1.493	24.6	1.14	36.6
114	11.44	-1.124	4.118	1.480	24.5	0.70	35.5
115	11.53	-0.990	4.534	1.478	25.4	1.02	36.3
117	11.61	-0.620	4.193	1.481	24.6	1.21	36.8
118	11.74	-0.605	3.900	1.456	23.9	1.04	36.4
119	11.87	-1.193	4.210	1.475	24.7	0.58	35.2
120	11.99	-0.716	3.954	1.472	24.1	0.89	36.0
121	12.12	-0.806	3.878	1.458	23.9	0.73	35.6
122	12.25	-0.463	3.910	1.458	23.9	1.05	36.4
123	12.38	-0.627	4.145	1.468	24.5	0.97	36.2
124	12.51	-0.318	3.871	1.469	23.8	1.11	36.5
128	12.92	-0.559	3.894	1.477	23.9	0.85	35.9
129	12.94	-0.601	3.961	1.475	24.1	0.75	35.6
130	12.97	-0.565	3.904	1.460	23.9	0.76	35.6
131	13.00	-	3.846	1.468	23.8	-	-
132	13.03	-	4.050	1.445	24.3	-	-
133	13.05	-	4.023	1.456	24.2	-	-
134	13.08	-	3.915	1.460	24.0	-	-
135	13.11	-0.632	3.995	1.451	24.2	0.72	35.6
136	13.13	-0.628	3.793	1.470	23.6	0.62	35.3
137	13.16	-0.627	3.980	1.458	24.1	0.72	35.5
138	13.19	-0.715	4.128	1.467	24.5	0.70	35.5
139	13.22	-0.483	4.148	1.475	24.5	0.94	36.1
140	13.24	-0.383	4.096	1.468	24.4	1.01	36.3
141	13.27	-0.027	3.989	1.450	24.1	1.31	37.0
142	13.30	-0.578	4.108	1.471	24.4	0.82	35.8
143	13.32	-0.438	3.720	1.462	23.5	0.75	35.6
144	13.35	-0.432	3.749	1.462	23.5	0.77	35.7
145	13.38	-0.702	3.894	1.470	23.9	0.58	35.2
146	13.41	-0.668	3.755	1.468	23.5	0.53	35.1

Depth (cm)	Age (kyr)	$\delta^{18}O$ (‰)	Mg/Ca	Sr/Ca	SST (°C)	$\delta^{18}O_{ivc-sw}$ (‰)	Salinity (‰)
147	13.43	-0.792	4.149	1.477	24.5	0.61	35.3
148	13.46	-1.058	5.118	1.478	26.6	0.77	35.7
149	13.49	-1.143	4.500	1.486	25.3	0.42	34.8
153	13.60	-0.429	3.786	1.470	23.6	0.77	35.7
154	13.62	-0.496	3.959	1.464	24.1	0.79	35.7
156	13.68	-0.608	4.181	1.469	24.6	0.79	35.7
159	13.76	-0.677	3.946	1.478	24.0	0.59	35.2
160	13.79	-0.977	4.388	1.477	25.1	0.51	35.0
162	13.84	-0.397	3.650	1.477	23.3	0.71	35.5
167	13.98	-0.040	3.814	1.474	23.7	1.16	36.6
169	14.03	-0.083	4.111	1.481	24.4	1.27	36.9
171	14.09	-0.616	3.901	1.473	23.9	0.63	35.3
173	14.14	0.048	4.125	1.478	24.5	1.41	37.3
175	14.20	0.099	4.252	1.474	24.8	1.52	37.6
177	14.25	0.052	4.273	1.475	24.8	1.49	37.5
179	14.30	0.173	3.687	1.474	23.4	1.31	37.0
181	14.36	0.003	3.825	1.467	23.7	1.21	36.8
183	14.41	-0.307	4.087	1.467	24.4	1.04	36.3
185	14.47	-0.262	4.137	1.480	24.5	1.11	36.5
187	14.52	-0.226	4.058	1.480	24.3	1.11	36.5
189	14.58	-0.093	3.937	1.495	24.0	1.18	36.7
191	14.63	-0.207	3.656	1.457	23.3	0.92	36.0
195	14.98	0.171	3.788	1.493	23.6	1.37	37.2
197	15.16	-0.018	3.473	1.489	22.8	1.00	36.3
199	15.33	0.118	3.476	1.498	22.8	1.14	36.6
201	15.51	-0.007	3.849	1.479	23.8	1.22	36.8
205	15.86	0.002	3.901	1.489	23.9	1.24	36.9
207	16.03	-0.172	3.692	1.493	23.4	0.95	36.1
209	16.09	-0.147	3.429	1.477	22.7	0.81	35.8
211	16.15	0.022	3.793	1.503	23.6	1.18	36.7
213	16.20	-0.060	3.681	1.470	23.4	1.03	36.3
215	16.26	0.095	3.823	1.471	23.7	1.25	36.9
217	16.31	0.232	3.637	1.484	23.2	1.28	36.9
219	16.37	0.015	3.751	1.483	23.5	1.12	36.5
221	16.42	-0.807	3.988	1.487	24.1	0.41	34.8
223	16.48	-0.482	3.919	1.491	24.0	0.69	35.5
225	16.53	0.060	3.523	1.492	22.9	1.01	36.3
227	16.59	-0.122	3.568	1.462	23.0	0.84	35.9
231	16.70	-0.086	3.499	1.468	22.9	0.83	35.8
235	16.81	-0.173	3.560	1.466	23.0	0.77	35.7
237	16.84	-0.131	3.640	1.460	23.2	0.85	35.9
239	16.87	0.017	3.587	1.478	23.1	0.96	36.1
241	16.90	-0.160	3.853	1.470	23.8	0.92	36.0
242	16.91	-0.063	3.692	1.468	23.4	0.91	36.0
243	16.93	0.078	3.525	1.487	22.9	0.95	36.1
244	16.94	0.012	3.639	1.474	23.2	0.94	36.1
245	16.95	-0.130	3.929	1.476	24.0	0.94	36.1
247	16.98	-0.028	3.814	1.482	23.7	0.97	36.2
249	17.01	0.026	3.824	1.490	23.7	1.03	36.3
251	17.04	0.167	3.597	1.481	23.1	1.04	36.3

Depth (cm)	Age (kyr)	$\delta^{18}O$ (‰)	Mg/Ca	Sr/Ca	SST (°C)	$\delta^{18}O_{ivc-sw}$ (‰)	Salinity (‰)
253	17.07	0.291	3.598	1.478	23.1	1.16	36.6
255	17.10	0.265	3.674	1.482	23.3	1.17	36.7
257	17.13	0.259	3.853	1.495	23.8	1.26	36.9
259	17.16	0.166	3.655	1.468	23.3	1.05	36.4
261	17.19	0.384	3.686	1.467	23.4	1.29	37.0
263	17.21	0.438	3.691	1.488	23.4	1.34	37.1
265	17.24	0.318	3.668	1.478	23.3	1.21	36.8
265	17.27	0.649	3.516	1.479	22.9	1.45	37.4
267	17.30	0.325	3.729	1.477	23.5	1.24	36.9
269	17.33	0.430	3.939	1.475	24.0	1.46	37.4
271	17.36	0.503	3.600	1.493	23.1	1.35	37.1
273	17.39	0.372	3.630	1.488	23.2	1.23	36.8
275	17.42	0.319	3.568	1.483	23.0	1.15	36.6
277	17.45	0.612	3.460	1.462	22.7	1.37	37.2
279	17.47	0.385	3.530	1.477	22.9	1.19	36.7
281	17.50	0.298	3.522	1.491	22.9	1.09	36.5
283	17.53	0.388	3.783	1.468	23.6	1.33	37.1
285	17.56	0.479	3.793	1.490	23.6	1.43	37.3
287	17.59	0.480	3.603	1.483	23.1	1.32	37.1
289	17.62	0.220	3.454	1.490	22.7	0.97	36.2
291	17.68	0.466	3.630	1.493	23.2	1.32	37.1
295	17.71	0.451	3.556	1.497	23.0	1.26	36.9
297	17.73	0.055	3.646	1.508	23.3	0.92	36.0
299	17.76	0.827	3.576	1.469	23.1	1.65	37.9
301	17.79	0.448	3.711	1.470	23.4	1.34	37.1
303	17.82	0.924	3.611	1.485	23.2	1.76	38.2
305	17.85	0.280	3.776	1.506	23.6	1.21	36.8
307	17.88	0.330	3.652	1.490	23.3	1.19	36.7
309	17.91	0.490	3.621	1.480	23.2	1.33	37.1
311	17.93	0.580	3.282	1.458	22.2	1.22	36.8
313	17.96	0.295	3.447	1.465	22.7	1.04	36.3
315	17.99	0.516	3.903	1.469	23.9	1.51	37.5
317	18.02	0.431	3.459	1.512	22.7	1.18	36.7
319	18.05	0.612	3.389	1.467	22.5	1.32	37.0
321	18.08	0.452	3.699	1.486	23.4	1.33	37.1
323	18.11	0.561	3.504	1.484	22.9	1.33	37.1
325	18.13	0.512	3.414	1.499	22.6	1.23	36.8
327	18.34	-	3.672	1.472	23.3	-	-
341	18.36	0.474	3.585	1.477	23.1	1.28	37.0
343	18.39	0.507	3.581	1.495	23.1	1.31	37.0
345	18.42	0.603	3.660	1.475	23.3	1.45	37.4
347	18.48	0.477	3.308	1.512	22.3	1.12	36.5
351	18.51	0.460	3.473	1.476	22.8	1.20	36.8
353	18.54	0.412	3.678	1.479	23.3	1.27	36.9
355	18.56	0.676	3.858	1.483	23.8	1.63	37.8
357	18.63	0.540	3.330	1.493	22.4	1.19	36.7
361	18.66	0.647	3.364	1.452	22.5	1.32	37.0
363	18.76	0.501	3.217	1.482	22.0	1.08	36.5
369	18.79	0.667	3.245	1.461	22.1	1.26	36.9
371	18.85	0.337	3.298	1.463	22.3	0.97	36.2

Depth (cm)	Age (kyr)	$\delta^{18}O$ (‰)	Mg/Ca	Sr/Ca	SST (°C)	$\delta^{18}O_{ivc-sw}$ (‰)	Salinity (‰)
375	18.89	0.454	3.327	1.457	22.4	1.10	36.5
377	18.92	0.495	3.401	1.459	22.6	1.18	36.7
379	18.95	0.447	3.410	1.481	22.6	1.14	36.6
381	18.98	0.376	3.278	1.470	22.2	0.99	36.2
383	19.02	0.517	3.481	1.466	22.8	1.25	36.9
385	19.11	0.434	3.591	1.476	23.1	1.23	36.8

Appendix C

Sedimentological database for cores KNR140/2-39GGC, 28GGC and 43GGC

Core KNR140/2-39GGC

Depth (cm)	Age (kyr)	>63 μm Dry Wt. (g)	<63μm Dry Wt. (g)	Inorg. C <63 μm (%)	$CaCO_3$ <63 μm (wt%)	SS Mean (μm)	SS Mean (St. dev Units)	SS %	Silt/clay
9	1.74	0.990	15.489	4.23	35.3	17.21	0.93	12.77	0.62
11	1.94	1.085	13.086	4.43	36.9	17.03	0.64	-	-
13	2.15	0.771	9.883	4.82	40.2	16.55	-0.11	13.64	0.84
15	2.35	1.144	8.924	4.74	39.5	17.94	2.08	12.31	0.97
17	2.55	0.909	12.535	4.65	38.8	16.64	0.03	12.25	0.91
19	2.75	1.089	10.645	5.17	43.1	17.36	1.16	11.71	0.91
21	2.95	0.561	9.844	5.02	41.8	16.26	-0.57	9.82	0.50
23	3.15	0.857	15.028	4.69	39.1	16.62	0.00	8.02	0.40
25	3.35	0.665	11.170	4.86	40.5	16.56	-0.10	8.02	0.53
27	3.55	0.635	10.150	4.91	40.9	16.54	-0.13	8.44	0.54
29	3.75	0.867	14.089	4.89	40.8	16.59	-0.05	8.32	0.49
31	3.95	0.802	14.354	4.81	40.1	16.65	0.04	9.07	0.50
33	4.15	0.599	10.493	5.04	42.0	16.05	-0.90	11.22	0.92
35	4.35	0.824	10.196	4.51	37.6	16.32	-0.48	9.90	0.82
37	4.56	0.598	10.767	4.24	35.3	16.66	0.06	8.83	0.56
39	4.76	0.708	12.611	4.46	37.2	16.58	-0.07	8.90	0.60
41	4.96	0.461	9.679	5.16	43.0	17.38	1.20	9.90	0.51
43	5.16	0.476	9.450	4.47	37.3	16.40	-0.35	12.18	1.17
45	5.36	0.848	13.026	4.58	38.2	17.04	0.66	8.68	0.72
47	5.56	0.607	12.173	4.10	34.2	17.21	0.93	10.42	0.44
49	5.76	0.653	11.554	5.01	41.8	16.87	0.39	10.10	0.47
51	5.96	0.761	11.882	4.50	37.5	16.66	0.06	9.34	0.37
53	6.16	1.000	15.271	4.59	38.3	18.13	2.38	8.04	0.38
55	6.36	0.659	9.415	4.61	38.4	16.69	0.11	11.80	0.84
57	6.56	0.576	12.908	4.60	39.2	17.00	0.60	9.37	0.46
59	6.76	0.605	11.422	4.64	38.7	17.74	1.76	11.12	0.62
61	6.97	0.258	6.206	4.60	38.3	16.90	0.44	12.76	0.82
65	7.30	0.918	15.991	4.72	39.3	17.51	1.40	10.16	0.46
67	7.43	0.752	9.703	4.72	39.3	17.20	0.91	9.52	0.45
69	7.56	1.486	6.790	4.67	38.9	17.18	0.88	10.73	0.61
71	7.70	0.665	11.968	3.97	33.1	17.38	1.20	10.73	0.55
73	7.83	0.441	14.324	3.53	29.4	17.70	1.70	7.38	0.37
75	7.96	0.402	13.231	3.82	31.8	17.57	1.50	8.53	0.45
77	8.09	0.669	15.039	3.42	28.5	17.10	0.75	10.08	0.44
79	8.23	0.430	8.760	3.44	28.7	18.01	2.19	7.05	0.39
80	8.29	0.300	12.395	3.21	26.8	17.53	1.43	7.30	0.35
81	8.36	0.323	10.474	2.92	24.3	16.39	-0.37	7.68	0.63
82	8.43	0.279	9.043	3.28	27.3	17.12	0.79	8.66	0.66
83	8.49	0.308	9.146	3.16	26.3	14.85	-2.80	7.10	0.52
84	8.56	0.404	10.250	2.68	22.3	17.10	0.75	9.32	0.73
85	8.63	0.323	11.120	2.76	23.0	18.07	2.29	8.04	0.44
86	8.69	0.267	13.045	2.93	24.4	17.52	1.42	6.78	0.36
87	8.76	0.193	8.653	2.86	23.8	16.49	-0.21	20.12	1.61

Core KNR140/2-39GGC cont.									
Depth (cm)	Age (kyr)	>63 μm Dry Wt. (g)	<63μm Dry Wt. (g)	Inorg. C <63 μm (%)	$CaCO_3$ <63 μm (wt%)	SS Mean (μm)	SS Mean (St. dev Units)	SS %	Silt/clay
88	8.82	0.340	14.830	2.72	22.7	17.60	1.54	14.69	1.08
89	8.89	0.241	10.817	2.94	24.5	16.78	0.25	8.22	0.44
90	8.96	0.127	5.472	2.88	24.0	17.03	0.64	13.02	1.06
91	9.02	0.233	9.946	2.89	24.1	18.74	3.34	7.78	0.46
92	9.09	0.184	9.549	2.75	22.9	16.84	0.34	8.58	0.69
93	9.16	0.188	9.663	2.86	23.8	16.93	0.49	17.34	1.36
94	9.22	0.218	10.425	2.91	24.3	17.29	1.05	7.66	0.43
95	9.29	0.230	15.583	2.78	23.2	16.33	-0.46	6.98	0.36
96	9.35	0.189	10.020	2.70	22.5	18.05	2.25	8.86	0.27
97	9.42	0.257	11.470	3.04	25.3	17.96	2.11	-	-
98	9.49	0.298	13.040	2.71	22.6	16.96	0.53	8.34	0.65
99	9.55	0.298	10.998	2.83	23.6	16.53	-0.15	14.55	1.26
100	9.62	0.257	11.609	2.71	22.6	17.26	1.01	8.49	0.64
101	9.72	0.208	10.194	2.71	22.6	17.35	1.15	7.94	0.41
102	9.82	0.202	10.105	2.53	21.1	17.04	0.66	6.69	0.38
103	9.92	0.250	12.680	2.63	21.9	17.05	0.68	8.51	0.55
104	10.02	0.171	7.421	2.59	21.6	17.52	1.42	7.09	0.50
105	10.12	0.224	9.722	2.47	20.6	16.93	0.49	8.16	0.43
106	10.22	0.199	9.237	2.49	20.8	17.08	0.72	8.52	0.58
107	10.32	0.173	9.087	2.50	20.8	17.88	1.99	9.26	0.48
108	10.42	0.255	12.750	2.65	22.1	17.14	0.82	8.64	0.73
110	10.61	0.214	10.600	2.64	22.0	17.36	1.16	13.75	0.98
111	10.71	0.199	8.742	2.56	21.3	16.98	0.57	9.39	0.69
112	10.81	0.228	10.339	2.61	21.8	17.58	1.51	8.43	0.60
113	10.91	0.209	9.035	2.61	21.8	17.68	1.67	7.27	0.41
114	11.01	0.322	12.277	2.70	22.5	16.92	0.47	8.02	0.39
115	11.11	0.229	10.327	2.79	23.3	17.43	1.28	9.54	0.69
116	11.21	0.338	11.000	2.78	23.2	16.60	-0.03	11.04	0.95
117	11.31	0.380	12.188	2.51	20.9	16.64	0.03	10.93	0.65
118	11.41	0.392	11.672	2.51	20.9	16.71	0.14	9.40	0.74
119	11.51	0.327	10.058	3.11	25.9	17.03	0.64	11.38	0.75
120	11.61	0.480	11.672	2.66	22.2	17.04	0.66	8.51	0.50
121	11.79	0.578	9.740	2.51	20.9	17.37	1.18	8.61	0.49
122	11.97	0.542	11.076	2.47	20.6	16.78	0.25	9.20	0.61
123	12.16	0.490	9.863	2.63	21.9	16.62	0.00	8.24	0.71
124	12.34	1.075	16.191	2.29	19.1	16.99	0.58	7.59	0.58
128	12.94	0.885	13.931	2.03	16.9	16.42	-0.32	8.18	0.40
129	12.98	0.397	8.617	2.34	19.5	17.10	0.75	6.62	0.39
130	13.03	0.335	5.983	2.08	17.3	17.86	1.95	6.21	0.35
131	13.08	0.505	11.694	1.99	16.6	16.94	0.50	6.71	0.44
132	13.12	0.157	5.843	2.40	20.0	17.57	1.50	6.59	0.54
133	13.17	0.201	8.072	2.52	21.0	16.84	0.34	6.19	0.42
134	13.22	0.320	14.225	2.16	18.0	16.66	0.06	6.14	0.39
135	13.27	0.414	8.715	2.31	19.3	17.39	1.21	9.67	0.98
136	13.31	0.328	14.750	2.24	18.7	17.19	0.90	7.12	0.48
137	13.36	0.309	12.251	2.01	16.8	16.15	-0.74	7.22	0.41
138	13.41	0.195	6.340	2.20	18.3	17.10	0.75	6.84	0.47

Core KNR140/2-39GGC cont.

Depth (cm)	Age (kyr)	>63 μm Dry Wt. (g)	<63μm Dry Wt. (g)	Inorg. C <63 μm (%)	$CaCO_3$ <63 μm (wt%)	SS Mean (μm)	SS Mean (St. dev Units)	SS %	Silt/clay
139	13.46	0.135	6.853	1.84	15.3	16.72	0.15	5.65	0.43
140	13.50	0.269	11.850	1.84	15.3	17.26	1.01	7.30	0.53
141	13.55	0.480	11.184	2.16	18.0	16.53	-0.15	5.98	0.41
142	13.60	0.240	11.750	1.78	14.8	16.66	0.06	5.94	0.39
143	13.64	0.205	13.151	1.55	12.9	16.76	0.22	5.63	0.39
144	13.69	0.183	12.650	1.52	12.7	17.14	0.82	7.15	0.43
145	13.74	0.187	10.230	1.69	14.1	16.28	-0.54	6.44	0.45
146	13.79	0.272	13.436	1.68	14.0	17.09	0.74	7.18	0.43
147	13.83	0.284	15.256	2.33	19.4	16.84	0.34	7.23	0.42
148	13.88	0.316	13.358	2.81	23.4	16.53	-0.15	6.90	0.60
149	13.93	0.272	14.030	1.92	16.0	16.55	-0.11	8.90	0.59
153	14.12	0.162	8.577	1.48	12.3	16.41	-0.33	6.78	0.46
154	14.16	0.235	10.611	1.59	13.3	16.52	-0.16	5.92	0.40
156	14.26	0.430	16.911	1.51	12.6	15.97	-1.03	5.44	0.46
159	14.40	0.215	9.786	1.81	15.1	16.64	0.03	7.50	0.50
160	14.45	0.205	7.580	2.22	18.5	16.92	0.47	6.99	0.71
162	14.54	0.218	9.717	1.60	13.3	17.30	1.07	6.24	0.43
163	14.59	0.293	11.648	1.35	11.3	17.33	1.12	6.92	0.44
167	14.78	0.465	13.926	1.26	10.5	16.71	0.14	6.77	0.43
169	14.87	0.585	10.306	2.01	16.8	17.20	0.91	8.73	0.50
171	14.97	0.897	9.186	1.46	12.2	17.11	0.77	7.64	0.49
173	15.06	1.584	7.495	1.37	11.4	15.78	-1.33	7.65	0.49
175	15.15	0.939	8.695	1.55	12.9	16.01	-0.97	7.98	0.50
177	15.21	1.509	12.530	1.46	12.2	16.92	0.47	8.86	0.50
179	15.26	1.199	11.731	1.40	11.7	16.08	-0.86	9.23	0.54
181	15.32	1.751	10.078	1.60	13.3	16.37	-0.40	9.80	0.58
183	15.37	0.864	11.968	1.62	13.5	16.30	-0.51	9.40	0.58
185	15.43	0.482	12.603	1.50	12.5	15.84	-1.23	7.83	0.55
187	15.48	0.331	11.715	1.51	12.6	16.28	-0.54	5.75	0.53
189	15.54	0.311	12.835	1.36	11.3	17.25	0.99	6.05	0.54
191	15.59	0.278	12.086	1.42	11.8	16.13	-0.78	7.33	0.53
195	15.70	0.234	11.210	1.45	12.1	15.73	-1.41	7.79	0.53
197	15.76	0.244	11.051	1.20	10.0	15.74	-1.39	6.18	0.53
199	15.81	0.209	11.173	1.33	11.1	16.50	-0.19	7.25	0.57
201	15.87	0.109	10.951	1.34	11.2	15.35	-2.01	6.32	0.57
203	15.92	0.099	9.130	1.28	10.7	16.23	-0.62	-	-
205	15.98	0.084	7.458	1.32	11.0	16.37	-0.40	7.58	0.57
207	16.03	0.124	10.618	1.36	11.3	15.87	-1.19	6.72	0.54
210	16.12	0.146	10.248	1.40	11.7	16.64	0.03	7.42	0.54
211	16.15	0.157	12.247	1.53	12.8	15.96	-1.04	6.34	0.55
213	16.20	0.204	13.510	1.47	12.3	16.43	-0.30	8.04	0.64
215	16.26	0.255	15.034	1.46	12.2	16.63	0.01	6.38	0.57
217	16.31	0.159	13.830	1.38	11.5	16.07	-0.87	7.75	0.56
219	16.37	0.196	13.829	1.40	11.7	16.19	-0.68	6.63	0.53
221	16.42	0.089	9.848	1.30	10.8	16.27	-0.56	5.43	0.51
223	16.48	0.131	15.524	1.49	12.4	15.72	-1.42	5.19	0.49
225	16.53	0.102	11.936	1.40	11.7	16.02	-0.95	6.37	0.55

Core KNR140/2-39GGC cont.

Depth (cm)	Age (kyr)	>63 μm Dry Wt. (g)	<63μm Dry Wt. (g)	Inorg. C <63 μm (%)	$CaCO_3$ <63 μm (wt%)	SS Mean (μm)	SS Mean (St. dev Units)	SS %	Silt/clay
229	16.64	0.070	8.607	1.43	11.9	16.42	-0.32	6.80	0.61
231	16.70	0.138	11.012	1.67	13.9	16.55	-0.11	5.63	0.48
233	16.75	0.166	9.475	1.63	13.6	16.08	-0.86	6.44	0.57
235	16.81	0.210	12.461	1.47	12.3	16.20	-0.67	7.18	0.58
237	16.84	0.211	11.842	1.55	12.9	15.87	-1.19	7.40	0.57
239	16.87	0.377	11.065	1.26	10.5	15.83	-1.25	6.83	0.51
241	16.90	0.197	13.005	1.38	11.5	16.21	-0.65	8.94	0.58
243	16.93	0.224	12.224	1.38	11.5	15.77	-1.34	8.16	0.59
245	16.95	0.187	9.558	1.55	12.9	15.84	-1.23	8.23	0.57
247	16.98	0.113	8.896	1.60	13.3	15.85	-1.22	7.07	0.53
249	17.01	0.136	10.802	1.77	14.8	16.39	-0.37	6.22	0.58
251	17.04	0.314	11.245	1.55	12.9	16.12	-0.79	7.33	0.57
253	17.07	0.115	7.898	1.31	10.9	15.98	-1.01	7.53	0.56
255	17.10	0.133	8.280	1.36	11.3	15.57	-1.66	6.85	0.61
257	17.13	0.089	6.193	1.46	12.2	16.15	-0.74	6.82	0.55
259	17.16	0.126	8.392	1.41	11.8	16.14	-0.76	6.74	0.59
261	17.19	0.163	12.878	1.25	10.4	16.21	-0.65	7.11	0.53
263	17.21	0.144	11.670	1.20	10.0	15.75	-1.38	7.47	0.61
265	17.24	0.243	15.295	1.41	11.8	15.78	-1.33	7.66	0.57
267	17.27	0.149	12.045	1.50	12.5	16.03	-0.93	5.71	0.50
269	17.30	0.172	15.412	1.72	14.3	15.82	-1.27	6.35	0.53
271	17.33	0.165	12.514	1.56	13.0	15.89	-1.15	6.83	0.53
273	17.36	0.154	9.988	1.51	12.6	16.32	-0.48	5.71	0.51
275	17.39	0.188	11.690	1.38	11.5	15.91	-1.12	7.38	0.55
277	17.42	0.203	12.643	1.34	11.2	16.34	-0.44	9.40	0.64
279	17.45	0.189	13.310	1.62	13.5	16.24	-0.60	8.14	0.60
282	17.49	0.202	14.285	1.31	10.9	16.38	-0.38	7.29	0.51
283	17.50	0.194	12.300	1.68	14.0	16.23	-0.62	7.35	0.54
285	17.53	0.093	11.380	1.24	10.3	15.99	-1.00	6.79	0.57
287	17.56	0.132	12.020	1.26	10.5	15.75	-1.38	5.52	0.53
289	17.59	0.120	12.711	1.22	10.2	15.54	-1.71	7.05	0.56
291	17.62	0.150	13.440	1.18	9.8	16.20	-0.67	7.53	0.56
295	17.68	0.166	11.210	1.36	11.3	16.87	0.39	8.63	0.56
297	17.71	0.166	12.119	1.37	11.4	16.06	-0.89	8.54	0.57
299	17.73	0.248	12.060	1.32	11.0	16.27	-0.56	9.47	0.57
301	17.76	0.256	11.680	1.46	12.2	16.39	-0.37	7.74	0.56
303	17.79	0.081	4.890	1.55	12.9	16.27	-0.56	-	-
305	17.82	0.177	12.485	1.54	12.8	16.35	-0.43	6.16	6.21
307	17.85	0.239	14.285	1.55	12.9	16.12	-0.79	7.18	0.59
309	17.88	0.271	11.185	1.40	11.7	17.04	0.66	9.70	0.67
311	17.91	0.384	14.306	1.58	13.2	16.22	-0.63	10.27	0.71
313	17.93	0.437	13.800	1.34	11.2	16.18	-0.70	12.38	0.75
315	17.96	0.259	7.298	1.55	12.9	16.37	-0.40	7.54	0.60
317	17.99	0.213	9.152	1.43	11.9	16.26	-0.57	-	-
319	18.02	0.454	19.213	1.47	12.3	16.67	0.08	8.84	0.58
321	18.05	0.163	12.023	1.35	11.3	16.35	-0.43	8.57	0.62
323	18.08	0.194	20.134	1.35	11.3	15.70	-1.45	6.99	0.57

Core KNR140/2-39GGC cont.									
Depth (cm)	Age (kyr)	>63 μm Dry Wt. (g)	<63μm Dry Wt. (g)	Inorg. C <63 μm (%)	$CaCO_3$ <63 μm (wt%)	SS Mean (μm)	SS Mean (St. dev Units)	SS %	Silt/clay
325	18.11	0.219	13.547	1.46	12.2	16.27	-0.56	10.65	0.67
327	18.13	0.248	14.681	1.48	12.3	14.88	-2.75	8.57	0.58
329	18.16	0.479	23.218	1.61	13.4	16.75	0.20	8.63	0.64
331	18.19	0.601	21.093	1.81	15.1	16.33	-0.46	8.58	0.62
333	18.22	0.503	17.652	1.75	14.6	16.47	-0.24	9.72	0.58
337	18.28	0.416	21.365	1.68	14.0	15.93	-1.09	9.54	0.66
339	18.31	0.293	14.036	1.57	13.1	15.86	-1.20	10.11	0.63
341	18.34	0.207	13.096	1.54	12.8	15.14	-2.34	8.48	0.63
343	18.36	0.282	17.236	1.54	12.8	15.41	-1.91	9.04	0.64
345	18.39	0.179	12.750	1.38	11.5	15.61	-1.60	7.61	0.65
347	18.42	0.177	13.982	1.52	12.7	16.10	-0.82	8.15	0.65
349	18.45	0.089	7.880	1.54	12.8	15.96	-1.04	8.36	0.71
351	18.48	0.243	15.851	1.59	13.3	15.96	-1.04	8.36	0.61
353	18.51	0.256	12.275	1.60	13.3	16.16	-0.73	9.08	0.65
355	18.54	0.413	16.894	1.62	13.5	16.36	-0.41	7.38	0.63
357	18.56	0.288	15.272	1.97	16.4	17.38	1.20	10.37	0.67
359	18.59	0.409	10.068	1.40	11.7	17.25	0.99	11.50	0.65
361	18.63	0.737	16.801	1.54	12.8	16.74	0.19	12.27	0.70
363	18.66	0.368	13.490	1.24	10.3	16.41	-0.33	13.02	0.76
367	18.72	0.101	5.140	1.37	11.4	16.55	-0.11	9.78	0.86
369	18.76	0.188	5.780	1.52	12.7	16.62	0.00	11.43	0.68
371	18.79	0.188	5.320	1.54	12.8	16.16	-0.73	12.29	0.72
373	18.82	0.163	5.235	1.65	13.8	17.25	0.99	10.11	0.68
375	18.85	0.676	5.670	1.47	12.3	16.55	-0.11	10.22	0.65
377	18.89	0.414	13.580	1.56	13.0	16.55	-0.11	10.69	0.65
379	18.92	0.161	14.323	1.56	13.0	16.30	-0.51	9.82	0.60
381	18.95	0.174	11.673	1.56	13.0	16.09	-0.84	9.15	0.56
382	18.97	0.056	5.236	1.50	12.5	16.69	0.11	-	-
383	18.98	0.070	6.660	1.46	12.2	16.90	0.44	7.87	0.52
385	19.02	0.168	6.458	1.69	15.2	17.61	1.56	8.27	0.53
391	19.11	0.248	8.632	1.82	13.0	16.43	-0.30	8.66	0.49
393	19.15	0.098	6.645	1.78	14.8	16.60	-0.03	10.62	0.67
406.5	19.36	0.159	5.395	1.83	15.3	16.13	-0.78	-	-
423	19.63	0.132	7.396	1.53	12.6	17.02	0.63	10.68	0.68

Core KNR10/2-28GGC									
Depth (cm)	Age (kyr)	>63 μm Dry Wt. (g)	<63μm Dry Wt. (g)	Inorg. C <63 μm (%)	$CaCO_3$ <63 μm (wt%)	SS Mean (μm)	SS Mean (St. dev Units)	SS %	Silt/clay
4	8.39	0.286	10.296	2.60	21.63	14.73	-1.55	5.53	1.03
5	8.49	0.132	12.653	2.79	23.21	14.88	-1.39	4.26	0.86
20	9.86	0.219	13.851	2.38	19.83	14.86	-1.41	4.27	1.26
24	10.23	0.398	13.673	2.35	19.58	14.22	-2.10	4.18	0.65
26	10.42	0.171	9.561	1.97	16.42	14.72	-1.56	5.56	1.20
28	10.60	0.130	9.933	2.22	18.50	15.39	-0.84	7.68	1.28
30	10.78	0.170	13.725	1.61	13.42	15.03	-1.23	11.08	1.62
31	10.88	0.116	9.099	1.54	12.83	14.76	-1.52	7.06	1.14
32	10.97	0.073	9.188	1.40	11.67	15.14	-1.11	6.95	1.12
33	11.06	0.163	10.141	1.24	10.33	16.36	0.21	9.51	1.44
34	11.15	0.119	9.480	1.16	9.67	15.89	-0.30	8.79	1.45
35	11.24	0.125	11.855	0.94	7.83	16.56	0.42	8.48	1.45
36	11.34	0.160	14.908	0.88	7.33	16.97	0.87	9.75	1.35
37	11.43	0.100	10.891	0.75	6.25	16.27	0.11	6.40	1.07
38	11.52	0.076	9.717	0.63	5.25	14.24	-2.08	5.18	0.89
39	11.61	0.056	11.835	0.50	4.17	15.83	-0.36	7.63	1.22
40	11.70	0.048	11.319	0.53	4.42	15.79	-0.41	6.86	1.06
41	11.80	0.708	16.316	0.68	5.67	16.45	0.31	6.16	0.47
42	11.89	0.664	12.535	0.81	6.75	14.42	-1.89	4.60	0.60
43	11.98	0.245	6.740	1.06	8.83	16.89	0.78	13.90	1.80
44	12.07	0.273	7.775	1.64	13.67	16.55	0.41	7.39	1.42
45	12.16	0.060	7.178	1.88	15.67	14.95	-1.32	4.51	1.12
46	12.26	0.079	6.613	2.05	17.08	15.26	-0.98	5.87	1.32
47	12.35	0.146	10.477	2.10	17.50	14.89	-1.38	4.49	0.85
48	12.44	0.153	11.159	2.11	17.58	16.13	-0.04	5.83	1.03
50	12.61	0.078	6.254	2.11	17.58	15.63	-0.58	7.33	1.54
51	12.70	0.119	8.334	2.19	18.25	16.11	-0.06	5.10	1.44
52	12.79	0.160	7.814	2.27	18.92	14.90	-1.37	3.39	0.87
53	12.88	0.160	9.308	2.32	19.33	16.30	0.14	5.85	1.22
54	12.96	0.215	11.693	2.37	19.75	15.29	-0.95	2.71	0.75
55	13.05	0.206	7.985	2.43	20.25	15.03	-1.23	3.22	0.84
56	13.14	0.301	6.129	2.69	22.42	15.28	-0.96	2.21	0.72
58	13.31	0.438	10.872	2.39	19.92	14.99	-1.27	4.19	0.91
60	13.49	0.414	10.694	2.50	20.83	15.26	-0.98	3.16	0.79
61	13.53	0.178	5.715	2.21	18.42	15.69	-0.52	5.03	0.92
62	13.57	0.283	10.688	1.93	16.08	15.92	-0.27	6.44	1.12
63	13.61	0.255	12.016	1.66	13.83	15.06	-1.20	5.49	1.16
64	13.65	0.204	10.931	1.47	12.25	15.23	-1.01	4.97	0.97
65	13.69	0.221	8.545	1.47	12.25	16.62	0.49	18.74	2.77
66	13.73	0.266	9.027	1.58	13.17	15.28	-0.96	3.46	0.51
67	13.76	0.196	11.029	1.41	11.75	15.06	-1.20	3.51	0.70
68	13.80	0.067	8.587	1.11	9.25	14.00	-2.34	2.85	0.41
69	13.84	0.166	14.087	1.15	9.58	16.01	-0.17	1.65	0.34
70	13.88	0.048	9.459	1.04	8.67	15.63	-0.58	1.21	0.53
71	13.92	0.028	9.325	1.00	8.33	15.67	-0.54	2.08	0.49
72	13.96	0.031	9.624	0.85	7.08	16.54	0.40	2.32	0.49
73	14.00	0.028	9.716	0.27	2.25	16.35	0.20	3.10	0.43

Core KNR10/2-28GGC cont.									
Depth (cm)	Age (kyr)	>63 μm Dry Wt. (g)	<63μm Dry Wt. (g)	Inorg. C <63 μm (%)	$CaCO_3$ <63 μm (wt%)	SS Mean (μm)	SS Mean (St. dev Units)	SS %	Silt/clay
74	14.04	0.048	10.297	0.44	3.67	16.89	0.78	9.82	1.51
75	14.08	0.123	8.020	0.41	3.42	18.27	2.27	13.95	1.82
76	14.12	0.158	12.398	0.33	2.75	16.70	0.58	3.22	0.45
77	14.16	0.230	8.483	0.38	3.17	20.58	4.77	13.16	1.49
78	14.20	0.016	10.891	0.53	4.42	18.34	2.35	4.98	0.92
79	14.24	0.017	9.466	0.71	5.92	16.30	0.14	7.00	0.97
80	14.28	0.010	5.954	0.89	7.42	16.56	0.42	4.69	0.51
81	14.32	0.014	5.341	0.90	7.50	16.29	0.13	4.01	0.73
82	14.36	0.049	14.608	0.96	8.00	16.03	-0.15	4.74	0.66
83	14.40	0.029	7.697	0.86	7.17	17.22	1.14	7.75	1.12
84	14.44	0.051	6.988	1.07	8.92	17.05	0.95	2.31	0.41
86	14.52	0.019	5.842	1.08	9.00	16.92	0.81	4.79	0.72
88	14.60	0.014	5.391	0.94	7.83	16.36	0.21	6.84	1.01
90	14.63	0.015	7.379	0.99	8.25	16.03	-0.15	8.94	1.10
92	14.66	0.015	5.759	1.01	8.42	18.17	2.16	12.23	1.62
94	14.69	0.019	7.050	1.01	8.42	16.62	0.49	8.92	1.22
96	14.73	0.015	6.805	0.92	7.67	16.33	0.18	7.12	0.92
98	14.76	0.021	7.881	1.02	8.50	17.77	1.73	15.02	1.98
101	14.81	0.013	6.842	1.10	9.17	17.16	1.07	12.73	1.72
102	14.82	0.012	6.495	0.97	8.08	17.02	0.92	9.82	1.30
104	14.85	0.012	6.286	0.96	8.00	18.80	2.85	14.15	1.86
106	14.89	0.010	5.471	0.97	8.08	16.00	-0.18	6.98	1.01
108	14.92	0.019	8.073	0.95	7.92	16.53	0.39	9.18	1.15
110	14.95	0.018	8.287	0.96	8.00	15.20	-1.05	5.03	0.60
112	14.98	0.019	6.296	1.00	8.33	16.00	-0.18	8.17	1.08
114	15.02	0.009	5.489	1.01	8.42	17.72	1.68	11.00	1.44
116	15.05	0.022	8.954	1.07	8.92	15.91	-0.28	6.39	0.88
118	15.08	0.019	7.115	1.06	8.83	18.27	2.27	10.47	1.19
120	15.11	0.011	6.209	1.10	9.17	15.97	-0.21	0.76	0.88
122	15.15	0.021	10.427	0.96	8.00	15.43	-0.80	7.29	0.77
124	15.18	0.013	6.252	1.01	8.42	16.27	0.11	10.43	1.37
126	15.21	0.013	5.514	1.03	8.58	16.17	0.00	7.69	1.05
128	15.24	0.025	9.730	0.99	8.25	16.40	0.25	9.08	1.38
130	15.28	0.014	5.235	1.08	9.00	15.33	-0.90	-	-
132	15.31	0.018	5.764	1.05	8.75	15.03	-1.23	12.31	1.76
134	15.34	0.016	5.438	0.97	8.08	16.02	-0.16	9.57	1.65
136	15.37	0.018	9.377	1.02	8.50	17.34	1.27	12.17	1.83
138	15.41	0.017	5.864	1.44	12.00	16.22	0.06	6.60	0.94
140	15.44	0.017	5.943	1.06	8.83	16.30	0.14	5.42	1.04
142	15.47	0.023	6.923	1.05	8.75	15.70	-0.50	5.05	0.96
144	15.50	0.035	9.859	1.17	9.75	16.21	0.05	7.18	1.38
146	15.54	0.020	7.573	1.00	8.33	16.16	-0.01	5.73	0.94
148	15.57	0.026	8.979	0.92	7.67	15.77	-0.43	9.36	1.38
150	15.60	0.021	9.257	1.09	9.08	16.56	0.42	12.76	1.67
152	15.63	0.029	10.079	1.01	8.42	15.23	-1.01	4.71	0.90
154	15.67	0.026	9.142	1.02	8.50	15.54	-0.68	7.20	1.12
156	15.70	0.023	8.227	1.03	8.58	16.92	0.81	10.64	1.38

Core KNR10/2-28GGC cont.

Depth (cm)	Age (kyr)	>63 μm Dry Wt. (g)	<63μm Dry Wt. (g)	Inorg. C <63 μm (%)	$CaCO_3$ <63 μm (wt%)	SS Mean (μm)	SS Mean (St. dev Units)	SS %	Silt/clay
160	15.76	0.022	7.768	1.14	9.50	15.76	-0.44	5.32	0.93
162	15.80	0.025	8.779	1.11	9.25	16.98	0.88	-	-
164	15.83	0.025	11.561	1.03	8.58	16.74	0.62	3.17	0.68
166	15.86	0.018	7.784	1.11	9.25	16.49	0.35	5.14	0.90
168	15.90	0.023	8.195	1.12	9.33	16.14	-0.03	6.47	1.03
170	15.93	0.027	6.960	1.18	9.83	16.66	0.53	7.54	1.06
172	15.96	0.051	8.082	1.17	9.75	15.41	-0.82	2.96	0.52
174	16.00	0.020	5.964	1.16	9.67	15.77	-0.43	4.16	0.72
176	16.03	0.039	7.656	1.29	10.75	16.88	0.77	-	-
178	16.06	0.053	9.635	1.24	10.33	17.11	1.02	13.04	1.69
180	16.10	0.032	7.992	1.17	9.75	16.59	0.46	7.51	1.17
184	16.16	0.105	10.881	0.82	6.83	16.67	0.54	-	-
186	16.19	0.020	7.266	0.91	7.58	17.43	1.36	8.69	1.49
188	16.23	0.018	6.630	0.96	8.00	16.32	0.17	4.35	0.93
190	16.26	0.039	11.427	1.02	8.50	16.90	0.79	6.13	1.00
192	16.29	0.018	5.476	0.85	7.08	16.86	0.75	7.36	1.05
196	16.36	0.040	8.606	1.07	8.92	18.19	2.19	18.38	1.84
198	16.39	0.065	10.662	1.04	8.67	15.94	-0.25	6.10	1.13
200	16.43	0.018	7.678	0.88	7.33	16.80	0.68	5.13	0.94
202	16.46	0.016	6.817	0.97	8.08	16.88	0.77	5.14	0.87
204	16.49	0.035	10.615	1.08	9.00	17.13	1.04	7.32	1.23
206	16.52	0.031	9.578	1.08	9.00	15.86	-0.33	10.78	1.32
208	16.56	0.040	10.297	1.07	8.92	15.77	-0.43	5.02	0.56
210	16.58	0.016	7.495	0.98	8.17	16.34	0.19	6.42	1.09
212	16.59	0.018	6.824	1.00	8.33	15.48	-0.74	6.55	1.02
214	16.61	0.019	6.607	0.94	7.83	15.77	-0.43	5.42	0.88
216	16.63	0.024	7.442	1.07	8.92	15.92	-0.27	4.81	0.56
218	16.65	0.029	8.647	1.08	9.00	16.19	0.02	4.64	0.72
220	16.67	0.024	7.407	0.74	6.17	15.37	-0.86	4.36	0.52
222	16.68	0.035	11.026	0.96	8.00	16.72	0.60	9.38	1.43
224	16.70	0.053	9.302	1.08	9.00	17.51	1.45	9.96	1.29
226	16.72	0.031	7.631	1.02	8.50	16.73	0.61	7.50	1.10
228	16.74	0.036	10.059	0.87	7.25	16.58	0.45	8.50	1.17
232	16.77	0.025	8.363	1.04	8.67	15.94	-0.25	5.77	0.92
234	16.79	0.042	9.408	1.00	8.33	16.77	0.65	9.74	1.45
236	16.81	0.029	10.717	0.83	6.92	16.52	0.38	7.42	1.09
238	16.83	0.015	9.235	0.91	7.58	15.54	-0.68	5.13	0.91
240	16.85	0.025	6.366	0.90	7.50	16.71	0.59	7.79	1.23
242	16.87	0.037	8.246	0.96	8.00	16.69	0.57	8.44	1.19
244	16.88	0.066	11.282	0.88	7.33	16.57	0.44	9.01	1.00
246	16.90	0.051	10.060	0.91	7.58	15.91	-0.28	4.71	0.46
248	16.92	0.026	7.300	0.92	7.67	16.36	0.21	5.84	0.87
250	16.94	0.062	10.687	0.88	7.33	15.09	-1.16	3.41	0.42
252	16.96	0.051	9.417	0.95	7.92	16.47	0.33	9.45	11.28
256	16.99	0.065	8.533	0.90	7.50	16.23	0.07	5.44	0.62
258	17.01	0.065	9.625	0.91	7.58	15.57	-0.65	5.76	0.65
260	17.03	0.068	8.262	0.92	7.67	16.14	-0.03	6.37	0.81

Core KNR10/2-28GGC cont.									
Depth (cm)	Age (kyr)	>63 μm Dry Wt. (g)	<63μm Dry Wt. (g)	Inorg. C <63 μm (%)	$CaCO_3$ <63 μm (wt%)	SS Mean (μm)	SS Mean (St. dev Units)	SS %	Silt/clay
262	17.05	0.054	10.363	0.88	7.33	16.13	-0.04	4.63	0.51
264	17.06	0.038	11.237	0.95	7.92	16.47	0.33	5.76	0.65
268	17.10	0.046	12.635	0.90	7.50	16.23	0.07	5.26	0.66
285	17.25	0.023	9.375	0.92	7.67	16.24	0.08	-	-
323	17.60	0.043	9.584	0.86	7.17	16.16	-0.01	-	-
341	17.76	0.068	9.317	0.89	7.42	15.92	-0.27	5.63	0.63
359	17.92	0.084	10.562	0.84	7.00	15.88	-0.31	-	-
377	18.09	0.035	9.348	0.86	7.17	16.34	0.19	-	-
395	18.25	0.057	8.135	0.90	7.50	15.69	-0.52	4.27	0.60
395	18.25	0.041	9.375	0.84	7.00	15.51	-0.71	-	-
416	18.44	0.025	8.765	0.82	6.83	15.78	-0.42	5.43	0.63

Core KNR10/2-43GGC									
Depth (cm)	Age (kyr)	>63 μm Dry Wt. (g)	<63μm Dry Wt. (g)	Inorg. C <63 μm (%)	$CaCO_3$ <63 μm (wt%)	SS Mean (μm)	SS Mean (St. dev Units)	SS %	Silt/clay
1	2.08	0.693	8.953	5.36	44.67	16.54	-2.77	-	-
6	2.93	0.726	9.685	5.43	45.25	16.24	-1.19	-	-
8	3.26	0.789	9.651	5.84	48.67	15.94	-1.62	-	-
8.5	3.60	0.689	9.298	5.68	47.33	16.92	-0.23	-	-
18	4.95	0.834	10.713	5.23	43.58	16.80	-0.40	-	-
30	6.30	0.513	8.161	5.89	49.08	16.84	-0.35	-	-
35	7.81	0.934	10.750	5.32	44.33	16.43	-0.92	6.73	0.48
37	8.15	0.781	11.926	5.28	44.00	18.11	1.45	4.43	0.26
39	8.49	0.729	9.879	5.06	42.17	16.70	-0.54	6.06	0.35
41	8.83	0.849	11.264	4.52	37.67	16.63	-0.64	6.36	0.41
43	9.16	0.851	11.993	4.64	38.67	16.43	-0.92	5.25	0.30
44	9.33	0.684	10.860	4.78	39.83	16.55	-0.75	5.46	0.31
45	9.50	0.556	9.483	4.88	40.67	16.34	-1.05	6.42	0.55
46	9.67	0.389	6.296	4.37	36.42	16.76	-0.46	6.72	0.33
47	9.84	0.653	11.633	4.32	36.00	16.96	-0.18	4.97	0.33
48	10.00	0.968	16.123	4.57	38.08	17.95	1.22	5.92	0.45
49	10.17	0.663	10.926	3.69	30.75	16.34	-1.05	-	-
50	10.34	0.402	7.725	3.29	27.42	18.01	1.31	7.30	0.48
51	10.51	0.588	9.670	3.48	29.00	18.28	1.69	6.01	0.43
52	10.68	1.403	15.885	3.29	27.42	16.85	-0.33	-	-
53	10.85	0.521	9.479	3.26	27.17	16.41	-0.95	3.66	0.31
54	11.02	0.382	8.198	3.51	29.25	17.54	0.64	5.75	0.33
55	11.18	0.688	14.740	3.59	29.92	17.17	0.12	5.06	0.41
56	11.35	0.708	13.039	3.25	27.08	16.94	-0.20	7.73	0.46
57	11.52	0.614	11.140	3.23	26.92	16.77	-0.44	6.12	0.36
58	11.69	0.672	10.990	1.84	25.33	17.13	0.06	7.05	0.59
59	11.86	0.509	8.196	3.01	25.08	18.49	1.98	8.88	0.60
60	12.03	0.587	7.908	3.02	25.17	17.45	0.52	8.66	0.59
61	12.20	1.380	16.335	2.68	22.33	18.60	2.14	7.56	0.43
62	12.36	1.219	12.271	3.12	26.00	18.62	2.17	10.57	0.56
63	12.53	1.018	7.446	2.93	24.42	16.46	-0.88	6.59	0.39
65	12.70	1.585	9.909	2.94	24.50	17.86	0.46	6.24	0.63

Appendix D

MIS 5/4 Database

Site 1059A													
mcd (m)	Age (kyr)	Wt. <63 μm (g)	Wt. >63 μm (g)	C %	Ca CO_3	PF $\delta^{13}C$	PF $\delta^{18}O$	BF	BF $\delta^{13}C$	BF $\delta^{18}O$	SS Mean (μm)	SS % (μm)	S/C
25.23	60.09	10.20	0.13	0.967	8.06	0.45	0.38	-	-	-	17.21	-	-
25.28	60.36	-	-	-	-	0.02	0.33	-	-	-	-	-	-
25.33	60.63	9.63	0.11	0.648	5.40	-0.36	0.22	-	-	-	16.75	-	-
25.38	60.90	-	-	-	-	0.07	0.29	-	-	-	-	-	-
25.43	61.16	9.07	0.08	0.887	7.39	-0.13	0.46	-	-	-	17.81	-	-
25.48	61.43	-	-	-	-	0.36	0.08	-	-	-	-	-	-
25.48	61.43	-	-	-	-	0.10	0.74	-	-	-	-	-	-
25.50	61.54	9.46	0.10	0.839	6.99	0.16	1.29	-	-	-	15.77	17.67	0.888
25.55	61.81	-	-	-	-	0.38	0.58	-	-	-	-	-	-
25.60	62.08	9.72	0.13	0.936	7.80	0.31	0.24	-	-	-	15.87	-	-
25.65	62.34	-	-	-	-	-0.13	-0.06	-	-	-	-	-	-
25.70	62.61	9.34	0.08	0.911	7.59	-0.16	-0.32	-	-	-	15.84	12.77	0.728
25.75	62.88	-	-	-	-	0.29	0.25	-	-	-	-	-	-
25.79	63.09	9.36	0.25	1.115	9.29	0.15	0.63	-	-	-	17.23	-	-
25.84	63.36	6.58	0.08	1.358	11.3	-0.15	0.19	-	-	-	15.07	17.08	0.747
25.89	63.63	-	-	-	-	-0.04	-0.12	-	-	-	-	-	-
25.94	63.90	10.02	0.09	1.355	11.2	0.02	-0.03	-	-	-	17.17	-	-
25.99	64.17	-	-	-	-	0.31	0.29	-	-	-	-	-	-
26.04	64.43	11.65	0.10	1.832	15.2	0.16	0.16	-	-	-	15.29	14.87	0.734
26.08	64.65	-	-	-	-	0.28	0.26	C. wue	0.11	4.20	-	-	-
26.13	64.92	10.68	0.12	2.139	17.8	0.32	0.20	C. sp	0.00	4.24	15.66	-	-
26.18	65.18	-	-	-	-	0.17	-0.22	C. wue	0.13	3.66	-	-	-
26.23	65.45	8.93	0.18	1.823	15.1	0.06	0.03	C. sp	0.58	3.54	15.87	9.58	0.577
26.28	65.72	-	-	-	-	-0.16	-0.29	-	-	-	-	-	-
26.32	65.93	-	-	-	-	0.16	-0.31	C. wue	0.16	3.98	15.69	-	-
26.33	65.99	9.79	0.22	2.018	16.8	0.27	-0.15	C. sp	0.01	4.02	-	-	-
26.38	66.26	-	-	-	-	0.20	-0.40	C. wue	0.46	3.86	-	-	-
26.43	66.52	9.66	0.14	2.189	18.2	0.06	-0.36	C. sp	0.44	3.73	15.28	9.96	0.514
26.48	66.79	-	-	-	-	-0.33	-0.22	C. wue	0.10	3.91	-	-	-
26.53	67.06	9.70	0.14	2.028	16.9	0.26	-0.33	C. sp	0.06	4.07	16.06	-	-
26.57	67.27	-	-	-	-	-0.14	-0.64	C. wue	0.32	3.81	-	-	-
26.62	67.54	8.78	0.26	2.288	19.0	0.46	-0.45	C. sp	0.94	3.75	17.32	13.39	0.575
26.67	67.81	-	-	-	-	0.28	-0.50	C. wue	0.19	3.77	-	-	-
26.72	68.08	8.36	0.87	2.133	17.7	0.35	-0.03	-	-	-	17.92	-	-
26.77	68.35	-	-	-	-	0.28	0.00	-	-	-	-	-	-
26.81	68.59	-	-	-	-	0.07	0.34	-	-	-	15.89	-	-
26.82	68.66	8.42	1.54	1.941	16.1	0.22	0.08	-	-	-	-	27.07	0.966
26.87	68.97	-	-	-	-	0.27	-0.11	-	-	-	-	-	-
26.92	69.29	9.42	1.57	2.856	23.8	0.29	0.71	C. sp	-0.69	4.01	15.38	-	-
26.97	69.61	-	-	-	-	0.35	0.16	C. wue	-0.80	3.85	-	-	-
27.02	69.93	8.20	0.32	3.916	32.6	-	-	-	-	-	18.38	16.82	0.762
-27.06	70.19	-	-	-	-	0.02	0.01	C. wue	0.02	3.95	-	-	-
27.11	70.50	8.28	0.22	4.759	39.6	0.33	-0.28	C. sp	0.03	3.92	17.37	-	-
27.16	70.82	-	-	-	-	-0.13	-0.20	C. wue	0.42	3.85	-	-	-
27.21	71.14	7.27	0.23	4.658	38.8	0.22	-0.12	C. sp	0.80	3.81	15.26	11.53	0.632
27.26	71.46	-	-	-	-	0.13	-0.41	C. wue	0.76	3.77	-	-	-
27.31	71.78	6.72	0.20	4.46	37.1	0.13	-0.24	C. wue	0.81	3.74	15.87	-	-
27.36	72.10	-	-	-	-	0.02	-0.58	C. wue	0.82	3.69	-	-	-
27.41	72.42	10.21	0.23	4.231	35.2	-0.01	-0.47	C. sp	0.22	3.87	16.23	14.61	0.765
27.46	72.74	-	-	-	-	0.39	-0.67	C. wue	0.41	3.66	-	-	-
27.51	72.99	8.98	0.23	4.23	35.2	-0.04	-0.26	C. sp	-0.27	3.56	15.54	-	-

Site 1059A cont.

mcd (m)	Age (kyr)	Wt. <63 μm (g)	Wt. >63 μm (g)	C %	Ca CO_3	PF $\delta^{13}C$	PF $\delta^{18}O$	BF	BF $\delta^{13}C$	BF $\delta^{18}O$	SS Mean (μm)	SS % (μm)	S/C
27.55	73.18	-	-	-	-	0.03	-0.40	C. wue	0.32	3.59	-	-	-
27.60	73.42	8.88	0.43	4.179	34.8	0.20	-0.76	C. sp	-0.01	3.73	17.02	13.64	0.613
27.65	73.66	-	-	-	-	0.43	0.04	C. wue	0.76	3.44	-	-	-
27.70	73.90	8.82	2.12	3.625	30.2	0.47	-0.08	-	-	-	19.14	-	-
27.75	74.14	-	-	-	-	0.08	-0.07	C. wue	0.38	3.54	-	-	-
27.79	74.33	-	-	-	-	0.13	-0.05	-	-	-	-	-	-
27.80	74.38	10.28	1.08	3.93	32.7	0.08	-0.37	-	-	-	18.28	22.09	0.939
27.85	74.62	-	-	-	-	-0.07	-0.11	C. wue	0.67	3.71	-	-	-
27.90	74.86	8.81	0.3-2	4.78	39.8	0.03	-0.03	C. sp	0.87	3.67	16.83	-	-
27.95	75.10	-	-	-	-	-0.14	-0.22	C. wue	0.51	3.69	-	-	-
27.99	75.29	8.74	0.22	4.817	40.1	0.35	-0.09	-	-	-	15.95	12.14	0.579
28.04	75.53	-	-	-	-	0.18	-0.15	C. wue	0.76	3.77	-	-	-
28.09	75.77	9.58	0.30	4.906	40.8	0.33	-0.46	C. sp	0.18	3.34	16.70	-	-
28.14	76.01	-	-	-	-	0.14	-0.09	C. wue	0.79	3.61	-	-	-
28.19	76.25	9.86	0.25	4.455	37.1	0.16	-0.20	-	-	-	17.64	17.20	0.755
28.24	76.49	-	-	-	-	0.18	-0.28	-	-	-	-	-	-
28.28	76.68	-	-	-	-	-0.08	-0.19	-	-	-	-	-	-
28.29	76.73	8.98	0.22	4.161	34.6	0.34	-0.08	-	-	-	15.98	-	-
28.34	76.97	-	-	-	-	-0.06	-0.32	-	-	-	-	-	-
28.39	77.21	8.19	0.21	4.684	39.0	0.06	-0.17	-	-	-	17.19	12.35	0.569
28.44	77.45	-	-	-	-	0.22	-0.42	C. wue	0.70	3.45	-	-	-
28.48	77.64	8.00	0.20	4.89	40.7	-0.46	-0.55	-	-	-	16.87	-	-
28.53	77.88	-	-	-	-	0.08	-0.42	C. wue	0.46	3.49	-	-	-
28.58	78.12	10.89	0.28	5.026	41.8	-0.18	-0.86	C. sp	0.73	3.59	17.78	14.63	35.02
28.63	78.36	-	-	-	-	-0.10	-0.43	C. wue	0.72	3.43	-	-	-
28.68	78.59	9.23	0.33	4.858	40.4	0.09	-0.30	C. sp	0.44	3.30	16.87	-	-
28.73	78.83	-	-	-	-	0.09	-0.39	-	-	-	-	-	-
28.78	79.07	9.63	0.23	5.022	41.8	-0.31	-0.47	C. wue	0.07	3.45	17.51	14.42	0.600
28.78	79.07	-	-	-	-	0.31	-0.02	-	-	-	-	-	-
28.83	79.31	-	-	-	-	-0.09	-0.39	C. wue	0.58	3.45	-	-	-
28.87	79.50	10.26	0.20	5.013	41.7	-	-	-	-	-	18.46	-	-
28.88	79.55	-	-	-	-	0.52	-0.44	C. sp	0.15	3.48	-	-	-
28.93	79.79	-	-	-	-	-0.12	-0.12	C. wue	0.55	3.44	-	-	-
28.97	79.98	9.05	0.26	5.133	42.7	0.00	-0.78	C. wue	-0.08	3.29	15.63	13.94	0.583
29.02	80.22	-	-	-	-	-0.17	-0.40	C. wue	0.60	3.37	-	-	-
29.07	80.46	9.68	0.21	5.097	42.4	0.10	-0.98	-	-	-	16.59	-	-
29.12	80.70	-	-	-	-	0.18	-0.65	-	-	-	-	-	-
29.17	80.94	10.40	0.33	5.191	43.2	0.35	-0.61	C. sp	0.71	3.41	17.27	17.16	0.781
29.22	81.18	-	-	-	-	-0.46	-0.75	-	-	-	-	-	-
29.26	81.37	-	-	-	-	0.07	-0.18	C. wue	0.63	3.32	-	-	-
29.27	81.42	11.14	0.27	5.177	43.1	-0.29	-0.67	C. sp	0.45	3.19	16.93	-	-
29.32	81.66	-	-	-	-	0.46	-0.30	C. wue	0.72	3.22	-	-	-
29.37	81.90	9.57	0.20	4.509	37.5	-0.19	-0.53	C. sp	0.42	3.20	16.64	14.25	0.69
29.41	82.09	-	-	-	-	0.28	-0.58	C. wue	0.72	3.58	-	-	-
29.46	82.33	11.74	0.19	4.84	40.3	0.04	-0.67	-	-	-	18.31	-	-
29.51	82.57	-	-	-	-	0.29	-0.15	C. wue	0.59	3.37	-	-	-
29.56	82.81	10.10	0.26	4.776	39.8	0.04	-0.83	C. sp	-0.28	3.52	16.65	14.08	0.654
29.61	83.05	-	-	-	-	-0.18	-0.65	C. wue	0.59	3.23	-	-	-
29.66	83.29	9.09	0.27	4.771	39.7	-0.50	-1.31	C. sp	0.35	3.26	16.52	-	-
29.71	83.53	-	-	-	-	-0.80	-0.74	C. wue	0.78	3.23	-	-	-
29.75	83.72	-	-	-	-	-0.04	-0.86	C. wue	0.47	3.28	-	-	-
29.76	83.77	10.10	0.42	4.918	40.9	0.24	-0.45	C. sp	0.95	3.29	17.23	16.17	0.783
29.81	84.01	-	-	-	-	-0.16	-1.03	C. wue	0.78	3.24	-	-	-
29.86	84.25	8.69	0.31	4.6	38.3	-0.04	-0.44	-	-	-	17.72	-	-
29.90	84.44	-	-	-	-	-0.04	-0.97	C. wue	0.30	3.19	-	-	-
29.95	84.68	9.44	0.37	4.247	35.3	0.07	-0.74	C. sp	0.17	3.48	16.41	16.95	0.813

Site 1059A cont.

mcd (m)	Age (kyr)	Wt. <63 μm (g)	Wt. >63 μm (g)	C %	Ca CO_3	PF $\delta^{13}C$	PF $\delta^{18}O$	BF	BF $\delta^{13}C$	BF $\delta^{18}O$	SS Mean (μm)	SS % (μm)	S/C
30.00	84.92	-	-	-	-	0.21	-0.46	C. wue	0.89	3.21	-	-	-
30.05	85.16	8.49	1.34	3.449	28.7	0.40	-0.68	C. wue	0.40	2.93	16.68	-	-
30.10	85.39	-	-	-	-	0.10	-0.08	C. wue	0.19	3.19	-	-	-
30.15	85.63	9.41	2.02	3.24	27.0	0.51	-0.64	C. wue	0.55	3.00	18.76	30.50	1.270
30.15	85.63	-	-	-	-	-	-	C. wue	0.25	3.25	-	-	-
30.20	85.87	-	-	-	-	0.36	-0.01	C. wue	0.34	3.35	-	-	-
30.25	86.11	10.94	2.55	2.745	22.8	0.48	-0.06	-	-	-	18.30	-	-
30.30	86.35	-	-	-	-	-	-	-	-	-	-	-	-
30.35	86.58	9.87	1.51	2.848	23.7	0.32	0.08	-	-	-	20.47	13.90	0.588
30.39	86.76	-	-	-	-	0.30	0.04	-	-	-	-	-	-
30.44	86.98	10.29	1.29	3.094	25.7	-	-	-	-	-	19.53	-	-
30.49	87.21	-	-	-	-	0.07	-0.09	-	-	-	-	-	-
30.54	87.43	10.02	1.19	2.981	24.8	0.60	0.00	-	-	-	20.04	25.25	0.938
30.59	87.66	-	-	-	-	0.42	-0.02	-	-	-	-	-	-
30.64	87.88	10.40	0.26	3.82	31.8	0.27	-0.92	-	-	-	14.82	-	-
30.69	88.11	-	-	-	-	0.16	-0.46	C. wue	0.36	3.89	-	-	-
30.73	88.29	-	-	-	-	-0.09	-0.42	-	-	-	-	-	-
30.74	88.33	9.67	0.30	3.851	32.0	0.02	-0.26	C. sp	0.12	3.80	17.76	16.18	0.861
30.79	88.55	-	-	-	-	0.31	-0.76	-	-	-	-	-	-
30.84	88.78	9.77	0.26	3.963	33.0	0.38	-0.46	C. sp	0.21	3.83	17.51	-	-
30.88	88.96	-	-	-	-	-0.27	-0.58	-	-	-	-	-	-
30.93	89.18	7.76	0.23	4.638	38.6	0.04	-0.57	-	-	-	16.87	11.65	0.644
30.98	89.41	-	-	-	-	0.28	-0.06	C. wue	0.78	3.74	-	-	-
31.03	89.63	9.79	0.24	4.369	36.4	0.88	-0.43	C. sp	0.77	3.75	16.27	-	-
31.08	89.86	-	-	-	-	0.03	-0.78	-	-	-	-	-	-
31.08	89.86	-	-	-	-	0.15	-0.60	-	-	-	-	-	-
31.13	90.08	8.57	0.27	4.773	39.7	-0.07	-0.31	C. sp	0.70	3.75	16.90	13.55	0.604
31.18	90.31	-	-	-	-	0.32	-0.49	-	-	-	-	-	-
31.22	90.48	-	-	-	-	0.33	-0.50	-	-	-	-	-	-
31.23	90.53	8.82	0.21	4.672	38.9	0.06	-0.61	C. sp	0.40	3.65	16.41	-	-
31.28	90.75	-	-	-	-	-0.21	-0.67	-	-	-	-	-	-
31.32	90.93	9.29	0.42	4.654	38.7	0.16	-0.51	C. wue	0.88	3.62	15.87	17.32	0.731
31.37	91.16	-	-	-	-	0.23	-0.62	-	-	-	-	-	-
31.42	91.38	9.54	0.22	4.08	34.0	0.55	-0.44	-	-	-	17.29	-	-
31.47	91.61	-	-	-	-	-0.37	-0.52	-	-	-	-	-	-
31.52	91.83	8.95	0.26	4.778	39.8	-0.18	-0.72	C. sp	0.39	3.56	17.54	16.74	0.761
31.57	92.06	-	-	-	-	-0.03	0.03	-	-	-	-	-	-
31.62	92.28	8.57	0.50	4.703	39.1	-0.02	-0.13	C. sp	0.25	3.69	16.41	-	-
31.67	92.50	-	-	-	-	-0.10	-0.38	-	-	-	-	-	-
31.72	92.73	6.87	0.21	4.523	37.6	0.32	-0.53	C. wue	0.61	3.54	16.46	16.16	0.693
31.77	92.95	-	-	-	-	-0.37	-0.93	-	-	-	-	-	-
31.81	93.13	9.83	0.39	4.569	38.0	-0.56	-0.28	C. sp	0.76	3.63	16.63	-	-
31.86	93.36	-	-	-	-	0.12	-0.35	-	-	-	-	-	-
31.91	93.58	9.81	0.39	4.727	39.3	-0.89	-0.80	C. sp	0.80	3.48	15.58	15.6	0.856
31.96	93.81	-	-	-	-	-0.25	-0.28	C. wue	0.31	3.51	-	-	-
32.01	94.03	8.90	0.37	4.872	40.6	0.13	-0.55	C. sp	0.71	3.45	16.44	-	-
32.06	94.26	-	-	-	-	0.00	-0.64	-	-	-	-	-	-
32.11	94.48	8.80	0.30	4.653	38.7	0.16	-0.47	C. sp	0.91	3.63	17.97	15.87	0.708
32.16	94.70	-	-	-	-	-0.43	-0.37	C. wue	0.31	3.34	-	-	-
32.20	94.88	-	-	-	-	0.00	-0.24	-	-	-	-	-	-
32.21	94.93	9.11	0.29	4.848	40.4	-0.53	-0.52	-	-	-	15.99	-	-
32.26	95.15	-	-	-	-	0.28	-0.19	C. wue	0.73	3.42	-	-	-
32.30	95.33	9.79	0.27	4.858	40.4	-0.73	-0.70	C. wue	0.93	3.11	16.21	16.47	0.639
32.35	95.56	-	-	-	-	-0.09	-0.44	-	-	-	-	-	-
32.40	95.78	9.28	0.27	5.097	42.4	0.21	-0.64	C. sp	0.69	3.30	16.14	-	-
32.45	96.01	-	-	-	-	-0.70	-0.71	-	-	-	-	-	-

Site 1059A cont.

mcd (m)	Age (kyr)	Wt. <63 μm (g)	Wt. >63 μm (g)	C %	Ca CO_3	PF $\delta^{13}C$	PF $\delta^{18}O$	BF	BF $\delta^{13}C$	BF $\delta^{18}O$	SS Mean (μm)	SS % (μm)	S/C
32.50	96.23	7.74	0.23	4.981	41.5	-0.15	-0.46	C. sp	0.56	3.27	15.45	14.41	0.595
32.55	96.45	-	-	-	-	-0.30	-0.84	C. wue	0.64	3.37	-	-	-
32.60	96.68	10.85	0.36	5.056	42.1	-0.27	-0.71	C. sp	0.80	2.99	16.44	-	-
32.65	96.90	-	-	-	-	-0.12	-0.77	-	-	-	-	-	-
32.68	97.04	10.02	0.32	5.248	43.7	-0.86	-0.86	C. sp	0.32	3.30	16.72	15.69	0.822
32.70	97.13	-	-	-	-	0.04	-0.58	-	-	-	-	-	-
32.74	97.31	-	-	-	-	0.05	-0.36	-	-	-	-	-	-
32.79	97.53	8.87	0.38	5.255	43.7	-0.04	-0.85	C. wue	1.14	3.25	15.74	-	-
32.84	97.76	-	-	-	-	-0.03	-0.47	C. wue	0.72	3.14	-	-	-
32.89	97.98	8.92	0.34	5.22	43.5	-0.39	-0.21	C. sp	1.07	3.41	16.85	14.15	0.594
32.94	98.21	-	-	-	-	0.21	-0.60	-	-	-	-	-	-
32.99	98.43	8.52	0.30	5.382	44.8	0.04	-0.60	-	-	-	15.92	-	-
33.04	98.65	-	-	-	-	-0.40	-0.84	C. wue	0.74	3.25	-	-	-
33.09	98.88	9.17	0.32	5.347	44.5	-0.72	-0.54	C. wue	1.01	3.08	17.20	15.05	0.666
33.14	99.10	-	-	-	-	-0.43	-0.51	-	-	-	-	-	-
33.18	99.28	-	-	-	-	0.23	-0.71	C. wue	0.93	3.22	-	-	-
33.19	99.33	8.09	0.39	5.494	45.7	-0.35	-0.44	C. sp	0.76	3.19	16.55	-	-
33.23	99.51	-	-	-	-	-0.57	-0.63	-	-	-	-	-	-
33.28	99.73	10.85	0.40	5.507	45.8	-0.45	-0.46	C. sp	0.63	3.22	16.29	15.67	0.679
33.40	100.25	9.20	0.24	5.371	44.7	-	-	-	-	-	16.28	-	-
33.41	100.29	-	-	-	-	-0.20	-0.98	C. wue	0.74	3.33	-	-	-
33.45	100.45	-	-	-	-	-0.32	-0.91	C. wue	0.84	3.30	-	-	-
33.50	100.66	9.27	0.35	5.227	43.5	-0.10	-0.35	C. sp	0.86	3.26	15.95	17.12	0.732
33.55	100.86	-	-	-	-	-0.43	-1.07	C. wue	0.72	3.36	-	-	-
33.60	101.07	8.61	0.22	4.785	39.8	-0.65	-0.96	C. sp	0.53	3.44	17.06	-	-
33.65	101.27	-	-	-	-	-0.79	-0.63	C. sp	0.76	3.38	-	-	-
33.70	101.48	9.59	0.23	4.622	38.5	-0.20	-1.12	-	-	-	16.93	14.15	0.689
33.74	101.64	-	-	-	-	-0.08	-0.57	-	-	-	-	-	-
33.79	101.84	9.20	0.21	4.477	37.3	-0.46	-0.48	-	-	-	17.39	-	-
33.84	102.05	-	-	-	-	-0.31	-0.60	-	-	-	-	-	-
33.88	102.21	-	-	-	-	-0.04	-0.46	-	-	-	-	-	-
33.89	102.25	8.78	0.29	4.272	35.6	-0.33	-0.68	-	-	-	16.89	15.32	0.655
33.94	102.46	-	-	-	-	-0.02	-0.90	-	-	-	-	-	-
33.99	102.66	10.14	0.26	3.068	25.5	-0.72	-1.42	-	-	-	15.94	-	-
34.04	102.87	-	-	-	-	-0.39	-1.09	-	-	-	-	-	-
34.09	103.07	7.55	0.21	4.548	37.9	0.15	-0.90	-	-	-	16.76	15.77	0.700
34.14	103.28	-	-	-	-	-0.42	-0.66	-	-	-	-	-	-
34.18	103.44	7.17	0.22	4.658	38.8	-0.20	-0.74	-	-	-	17.30	-	-
34.23	103.65	-	-	-	-	-1.26	-1.03	C. wue	0.15	3.32	-	-	-
34.28	103.85	9.95	0.29	4.472	37.2	-	-	-	-	-	16.62	15.49	0.674
34.33	104.06	-	-	-	-	-0.26	-0.28	-	-	-	-	-	-
34.37	104.22	-	-	-	-	-0.24	-0.61	-	-	-	-	-	-
34.38	104.26	10.20	0.32	4.517	37.6	-0.45	-1.50	-	-	-	16.25	-	-
34.43	104.47	-	-	-	-	-0.27	-0.58	C. wue	-0.50	3.37	-	-	-
34.48	104.67	10.51	0.33	3.924	32.7	0.06	-0.61	-	-	-	16.43	14.85	0.696
34.53	104.88	-	-	-	-	-0.76	-0.78	-	-	-	-	-	-
34.58	105.08	10.49	0.55	3.939	32.8	-0.48	-1.04	-	-	-	17.15	-	-
34.63	105.29	-	-	-	-	-0.35	-0.40	-	-	-	-	-	-
34.67	105.45	9.04	1.10	2.822	23.5	0.04	-0.07	-	-	-	18.34	31.58	1.202
34.71	105.61	-	-	-	-	0.37	-0.49	-	-	-	-	-	-
34.75	105.78	-	-	-	-	0.17	-0.22	-	-	-	-	-	-
34.80	105.98	9.57	0.94	2.733	22.7	0.18	-0.74	-	-	-	16.60	-	-
34.85	106.19	-	-	-	-	-0.32	-0.47	C. sp	0.16	3.50	-	-	-
34.90	106.39	9.90	0.23	3.455	28.7	-0.30	-0.88	-	-	-	16.56	17.44	0.754
34.95	106.60	-	-	-	-	-0.55	-0.58	C. sp	0.28	3.53	-	-	-
35.00	106.80	10.63	0.30	3.634	30.2	-0.13	-0.85	-	-	-	17.90	-	-

Site 1059A cont.

mcd (m)	Age (kyr)	Wt. <63 μm (g)	Wt. >63 μm (g)	C %	Ca CO_3	PF $\delta^{13}C$	PF $\delta^{18}O$	BF	BF $\delta^{13}C$	BF $\delta^{18}O$	SS Mean (μm)	SS % (μm)	S/C
35.05	107.01	-	-	-	-	-0.83	-1.01	-	-	-	-	-	-
35.10	107.21	9.51	0.22	3.788	31.5	-0.28	-0.79	-	-	-	17.24	16.56	0.730
35.14	107.38	-	-	-	-	-0.52	-0.87	C. wue	0.51	3.54	-	-	-
35.18	107.54	-	-	-	-	-0.11	-0.48	-	-	-	-	-	-
35.19	107.58	9.54	0.26	4.031	33.5	0.20	-1.03	C. sp	0.31	3.29	16.67	-	-
35.24	107.79	-	-	-	-	-0.41	-0.87	C. wue	0.16	3.36	-	-	-
35.29	107.99	8.43	0.21	3.657	30.4	-1.11	-1.52	-	-	-	19.70	14.79	0.656
35.34	108.20	-	-	-	-	-0.38	-0.72	-	-	-	-	-	-
35.39	108.40	8.79	0.26	4.172	34.7	-0.38	-1.10	C. wue	0.40	3.36	15.92	-	-
35.44	108.61	-	-	-	-	-0.75	-1.12	C. wue	0.49	3.51	-	-	-
35.49	108.81	10.11	0.37	4.096	34.1	-1.13	-0.96	C. wue	0.75	3.31	17.90	18.83	0.716
35.54	109.02	-	-	-	-	-0.38	-0.40	-	-	-	-	-	-
35.55	109.06	8.98	0.24	3.85	32.0	-0.15	-0.28	C. wue	0.36	3.61	16.80	-	-
35.64	109.43	8.34	0.58	4.261	35.5	-0.21	-0.42	C. wue	0.02	3.51	17.25	18.38	0.692
35.74	109.84	7.90	0.90	4.137	34.4	0.14	-0.76	C. wue	0.97	3.56	17.25	-	-
35.84	110.25	7.06	1.69	3.649	30.4	0.36	-1.06	C. wue	0.49	3.44	19.82	19.46	0.678
35.87	110.37	6.30	0.28	3.785	31.5						17.18		
35.88	110.41	-	-	-	-	-0.51	-0.52	C. wue	0.48	3.51	-	-	-
35.92	110.57	-	-	-	-	-0.29	-0.60	-	-	-	-	-	-
35.97	110.78	8.91	0.23	3.804	31.7	-0.09	-0.91	C. wue	0.73	3.45	18.07	14.16	0.683
36.02	110.98	-	-	-	-	-0.35	-0.58	-	-	-	-	-	-
36.07	111.19	10.15	0.34	4.097	34.1	-0.52	-0.56	C. wue	0.38	3.32	16.56	-	-
36.12	111.39	-	-	-	-	-0.06	-0.40	C. wue	0.17	3.48	-	-	-
36.17	111.60	8.35	0.22	3.953	32.9	-	-	C. wue	-0.40	3.49	18.91	14.44	0.729
36.22	111.80	-	-	-	-	-0.05	-0.19	C. wue	0.75	3.36	-	-	-
36.27	112.01	9.83	0.26	4.028	33.5	-0.38	-0.63	C. wue	0.45	3.38	17.08	-	-
36.32	112.21	-	-	-	-	0.12	-0.54	-	-	-	-	-	-
36.36	112.38	-	-	-	-	-0.62	-0.95	-	-	-	-	-	-
36.37	112.42	6.84	0.32	4.047	33.7	-0.18	-0.49	-	-	-	17.13	14.81	0.714
36.42	112.62	-	-	-	-	-0.84	-0.87	C. wue	0.26	3.35	-	-	-
36.47	112.83	8.28	0.44	4.555	37.9	-0.50	-0.46	C. wue	0.67	3.24	16.34	-	-
36.52	113.03	-	-	-	-	-0.46	-0.34	C. wue	0.82	3.23	-	-	-
36.55	113.16	7.87	0.38	4.547	37.8	-0.53	-0.79	C. wue	0.98	3.07	17.40	15.74	0.722
36.62	113.44	-	-	-	-	-0.42	-0.72	-	-	-	-	-	-
36.65	113.57	4.78	0.26	4.132	34.4	-0.24	-0.80	-	-	-	17.17	-	-
36.72	113.85	-	-	-	-	-0.24	-0.69	-	-	-	-	-	-
36.77	114.06	6.59	0.28	4.696	39.1	-0.60	-0.82	C. wue	0.90	3.27	17.03	14.50	0.612
36.82	114.26	-	-	-	-	-0.44	-0.50	-	-	-	-	-	-
36.86	114.43	-	-	-	-	-0.55	-0.69	C. wue	0.57	3.21	-	-	-
36.88	114.51	5.69	0.54	4.704	39.2	0.44	-0.98	C. wue	-0.18	3.11	16.27	-	-
36.92	114.67	-	-	-	-	-0.63	-1.29	-	-	-	-	-	-
36.97	114.88	6.2-2	0.37	4.820	40.1	-0.73	-1.08	C. wue	0.65	2.82	17.01	13.00	0.660
37.02	115.12	-	-		-	-0.48	-1.19	-	-	-	-	-	-
37.02	115.12	-	-		-	-0.64	-1.01	-	-	-	-	-	-
37.07	115.44	5.41	0.44	4.9.00	40.8	-0.47	-1.19	-	-	-	16.76	-	-
37.12	115.75	-	-	-	-	-0.06	-1.31	-	-	-	-	-	-
37.12	115.75	-	-	-	-	-0.78	-1.15	-	-	-	-	-	-
37.17	116.06	6.25	0.69	4.967	41.3	-0.75	-1.43	C. wue	0.64	2.34	16.70	10.14	0.470
37.22	116.38	-	-	-	-	-0.39	-1.16	C. wue	0.89	2.69	-	-	-
37.22	116.38	-	-	-	-	-0.36	-1.36	-	-	-	-	-	-
37.27	116.69	6.65	0.46	5.062	42.1	-0.59	-1.56	C. kull	0.57	2.68	16.06	-	-
37.32	117.00	-	-	-	-	-0.09	-1.61	-	-	-	-	-	-
37.32	117.00	-	-	-	-	-0.34	-1.61	-	-	-	-	-	-
37.38	117.38	-	-	-	-	-1.45	-1.14	-	-	-	-	-	-
37.38	117.38	-	-	-	-	-0.40	-1.54	-	-	-	-	-	-
37.40	117.50	7.40	0.61	5.381	44.8	-0.43	-1.39	C. wue	0.36	2.46	16.73	12.30	0.516

Site 1059A cont.

mcd (m)	Age (kyr)	Wt. <63 μm (g)	Wt. >63 μm (g)	C %	Ca CO_3	PF $\delta^{13}C$	PF $\delta^{18}O$	BF	BF $\delta^{13}C$	BF $\delta^{18}O$	SS Mean (μm)	SS % (μm)	S/C
37.42	117.62	-	-	-	-	-0.54	-1.19	-	-	-	-	-	-
37.42	117.62	-	-	-	-	-1.18	-1.24	-	-	-	-	-	-
37.47	117.94	7.61	0.62	5.339	44.4	-0.30	-0.74	C. kull	0.62	2.55	16.63	-	-
37.52	118.25	-	-	-	-	-1.07	-1.35	-	-	-	-	-	-
37.52	118.25	-	-	-	-	-0.86	-1.37	-	-	-	-	-	-
37.57	118.56	8.76	0.63	4.958	41.3	0.05	-1.11	C. wue	0.79	2.37	18.95	15.80	0.586
37.62	118.87	-	-	-	-	-0.64	-1.09	C. wue	0.94	2.62	-	-	-
37.62	118.87	-	-	-	-	-0.77	-1.07	-	-	-	-	-	-
37.66	119.13	8.03	0.46	4.491	37.4	-0.25	-0.75	C. kull	0.35	2.54	17.47	-	-
37.72	119.50	-	-	-	-	-0.76	-1.25	-	-	-	-	-	-
37.72	119.50	-	-	-	-	-0.84	-1.17	-	-	-	-	-	-
37.77	119.81	9.05	0.51	4.371	36.4	-0.12	-1.05	C. kull	0.28	2.55	16.46	17.15	0.692
37.82	120.13	-	-	-	-	-0.36	-1.00	-	-	-	-	-	-
37.82	120.13	-	-	-	-	-0.82	-1.49	-	-	-	-	-	-
37.86	120.37	-	-	-	-	-0.74	-1.50	C. wue	0.75	2.48	-	-	-
37.86	120.37	-	-	-	-	-0.78	-1.09	-	-	-	-	-	-
37.88	120.50	8.37	0.50	4.183	34.8	-0.36	-1.47	C. wue	0.54	2.31	18.25	-	-
37.92	120.75	-	-	-	-	-0.57	-1.33	C. wue	0.19	2.55	-	-	-
37.97	121.06	9.88	0.38	3.887	32.3	-0.35	-1.32	C. wue	0.63	2.34	17.80	16.03	0.619
38.02	121.37	-	-	-	-	-0.86	-1.17	C. wue	0.37	2.50	-	-	-
38.02	121.37	-	-	-	-	-1.05	-1.34	-	-	-	-	-	-
38.06	121.63	6.59	0.22	4.016	33.4	-0.81	-1.62	C. wue	0.91	2.45	16.80	-	-
38.12	122.00	-	-	-	-	-0.91	-0.80	C. wue	0.37	2.50	-	-	-
38.12	122.00	-	-	-	-	-0.92	-1.56	-	-	-	-	-	-
38.17	122.31	9.63	0.27	3.59	29.9	-0.40	-1.36	C. wue	0.64	2.30	17.05	16.63	0.625
38.22	122.63	-	-	-	-	-1.15	-1.69	C. wue	0.72	2.51	-	-	-
38.22	122.63	-	-	-	-	-0.72	-1.25	-	-	-	-	-	-
38.27	122.94	10.51	0.33	3.759	31.3	-1.09	-1.49	C. wue	0.62	2.25	16.65	-	-
38.32	123.25	-	-	-	-	-0.38	-1.96	C. wue	0.79	3.31	-	-	-
38.32	123.25	-	-	-	-	-0.87	-1.60	-	-	-	-	-	-
38.36	123.50	-	-	-	-	-0.55	-1.15	-	-	-	-	-	-
38.36	123.50	-	-	-	-	-0.86	-1.23	-	-	-	-	-	-
38.38	123.63	7.78	0.20	3.623	30.1	-	-	-	-	-	17.67	16.88	0.633
38.42	123.87	-	-	-	-	-1.28	-1.59	C. wue	0.29	2.60	-	-	-
38.42	123.87	-	-	-	-	-1.08	-1.66	-	-	-	-	-	-
38.47	124.19	8.63	0.24	3.429	28.5	-	-	-	-	-	17.16	-	-
38.52	124.50	-	-	-	-	-0.72	-1.30	C. wue	0.25	2.45	-	-	-
38.52	124.50	-	-	-	-	-0.35	-1.11	-	-	-	-	-	-
38.57	124.81	9.99	0.58	4.223	35.1	-	-	-	-	-	16.41	9.34	0.508
38.62	125.12	-	-	-	-	-0.68	-1.28	C. wue	0.55	2.52	-	-	-
38.62	125.12	-	-	-	-	-0.59	-1.23	-	-	-	-	-	-
38.67	125.44	7.55	0.34	3.649	30.4	-	-	-	-	-	16.71	-	-
38.72	125.75	-	-	-	-	-0.42	-0.88	C. wue	0.64	2.54	-	-	-
38.77	126.06	10.24	0.35	4.840	40.3	-	-	-	-	-	17.12	11.16	0.469
38.82	126.38	-	-	-	-	0.00	-0.90	C. wue	0.07	3.03	-	-	-
38.88	126.75	-	-	-	-	0.04	-0.54	C. wue	0.09	2.83	-	-	-
38.90	126.88	9.15	1.54	2.632	21.9	-	-	-	-	-	17.28	-	-
38.92	127.00	-	-	-	-	-0.07	-0.83	C. wue	-0.04	2.84	-	-	-
38.97	127.31	9.08	1.99	2.181	18.1	-	-	-	-	-	18.61	20.98	0.823
39.02	127.92	-	-	-	-	-0.06	-0.15	C. wue	-0.19	3.64	-	-	-
39.08	129.19	7.40	2.07	1.740	14.5	-	-	-	-	-	17.65	-	-
39.12	130.03	-	-	-	-	-0.28	0.40	C. wue	-0.08	4.39	-	-	-

Site 1057B

mcd (m)	Age (kyr)	Wt. <63 μm (g)	Wt. >63 μm (g)	C %	Ca CO_3	PF $\delta^{13}C$	PF $\delta^{18}O$	BF	BF $\delta^{13}C$	BF $\delta^{18}O$	SS Mean (μm)	SS % (μm)	S/C
10.58	59.968	7.60	0.12	1.242	10.4	0.20	0.47	-	-	-	17.01	27.15	2.048
10.63	62.94	8.81	0.11	1.166	9.7	0.09	0.18	-	-	-	18.18	-	-
10.68	65.915	9.91	0.06	1.096	9.1	0.35	0.44	-	-	-	18.19	23.86	1.65
10.73	69.17	9.92	0.12	-	-	0.32	-0.01	-	-	-	-	-	-
10.73	69.17	10.88	0.14	-	-	-	-	-	-	-	16.83	-	-
10.78	69.67	8.98	0.13	1.503	12.5	0.02	-0.38	C.wue	0.65	3.57	16.08	13.22	1.119
10.83	70.75	8.62	0.19	1.856	15.5	-0.14	-0.54	-	-	-	15.64	-	-
10.88	71.047	9.49	0.30	2.258	18.8	-0.01	-0.35	C.wue	1.18	3.82	16.12	8.79	1.737
10.93	71.345	8.81	0.32	-	-	0.28	-0.11	C.wue	0.85	3.83	-	-	-
10.93	71.345	10.13	0.37	-	-	-	-	-	-	-	18.94	-	-
10.98	71.643	8.73	0.31	2.392	19.9	0.01	-0.21	C.wue	-1.06	3.72	15.80	16.85	1.462
11.03	71.94	9.76	0.43	2.323	19.4	0.31	0.02	C.wue	-0.07	3.46	16.28	-	-
11.08	72.174	8.92	1.05	2.809	23.4	0.37	0.23	C.wue	0.11	3.77	22.63	42.37	2.257
11.13	72.407	7.84	0.66	-	-	0.19	0.29	C.wue	0.20	3.72	-	-	-
11.13	72.407	10.44	1.53	-	-	-	-	-	-	-	19.88	-	-
11.18	72.642	8.55	0.98	3.905	32.5	0.33	0.13	C.wue	1.24	3.38	20.90	49.07	4.473
11.23	72.875	5.58	0.47	4.913	40.9	0.00	-0.26	C.wue	0.98	3.32	16.28	-	-
11.28	73.109	7.60	0.72	5.182	43.2	0.02	-0.19	C.wue	0.17	3.36	16.10	16.89	1.334
11.33	73.999	8.14	0.99	-	-	0.19	-0.56	C.wue	0.29	3.22	-	-	-
11.33	73.999	9.17	1.08	-	-	-	-	-	-	-	18.83	-	-
11.38	74.888	7.69	1.41	4.486	37.4	0.49	-0.04	C.wue	0.79	3.51	19.34	37.46	2.677
11.43	75.089	7.60	0.41	-	-	0.21	-0.02	-	-	-	-	-	-
11.43	75.089	10.42	0.60	-	-	-	-	-	-	-	19.52	-	-
11.48	75.29	5.41	0.33	5.306	44.2	-0.35	0.38	-	-	-	17.18	20.82	1.777
11.53	76.287	6.28	0.35	5.676	47.3	0.06	0.03	C.wue	1.24	3.74	16.07	-	-
11.58	81.6	8.64	0.42	5.627	46.9	-0.43	-0.67	C.wue	1.22	3.38	17.21	25.01	2.182
11.63	82.59	7.61	0.31	-	-	0.04	0.11	-	-	-	-	-	-
11.63	82.59	9.50	0.49	-	-	-	-	-	-	-	17.62	-	-
11.68	83.18	8.18	0.50	5.972	49.8	0.61	-0.64	C.wue	1.05	3.45	16.49	19.15	1.498
11.73	83.77	8.75	0.60	6.167	51.4	-0.69	-0.99	C.wue	1.12	3.51	15.99	-	-
11.78	84.384	8.41	0.71	5.907	49.2	-0.40	-0.68	-	-	-	16.91	20.58	1.528
11.83	84.998	8.31	1.03	-	-	0.26	-0.52	C.rug	1.14	3.24	-	-	-
11.83	84.998	10.10	1.14	-	-	-	-	-	-	-	16.67	-	-
11.88	85.613	8.27	1.34	5.362	44.7	0.27	-0.59	C.wue	0.70	3.39	17.82	25.54	1.688
11.93	86.222	7.18	1.69	4.701	39.2	0.12	-0.48	C.wue	0.89	3.30	19.67	-	-
11.98	86.83	8.59	1.44	3.905	32.5	0.50	0.17	C.wue	0.69	3.72	20.66	37.92	2.425
12.03	87.715	7.04	0.50	-	-	0.43	-0.29	-	-	-	-	-	-
12.03	87.715	9.72	0.76	-	-	-	-	-	-	-	19.47	-	-
12.08	88.6	7.43	0.43	4.470	37.3	0.51	-0.49	C.wue	1.18	3.59	17.50	23.5	1.91
12.13	89.485	7.44	0.47	5.052	42.1	-0.10	-0.66	C.wue	1.11	3.61	17.02	-	-
12.18	90.37	7.50	0.66	5.563	46.4	-0.28	-0.41	C.wue	0.41	3.78	16.16	15.03	1.576
12.23	91.349	7.16	0.55	-	-	-0.39	-0.55	C.wue	0.99	3.52	-	-	-
12.23	91.349	9.03	0.71	-	-	-	-	-	-	-	16.71	-	-
12.28	92.33	7.27	0.64	5.860	48.8	0.30	-0.17	C.wue	1.19	3.54	16.73	18.07	1.636
12.33	93.727	6.98	0.46	5.765	48.0	0.04	-0.43	C.wue	1.11	3.43	16.06	-	-
12.38	95.126	6.26	0.38	5.841	48.7	0.02	-0.40	C.wue	1.21	3.43	16.92	15.56	1.232
12.43	96.524	6.79	0.47	-	-	-0.27	-0.80	-	-	-	-	-	-
12.43	96.524	9.42	0.73	-	-	-	-	-	-	-	16.01	-	-
12.48	97.921	7.99	0.61	6.170	51.4	-0.09	-0.75	C.wue	1.13	3.25	15.87	13.01	1.069
12.53	99.32	8.58	0.71	6.414	53.5	-0.55	-1.14	-	-	-	15.58	-	-
12.58	99.848	7.11	0.58	6.493	54.1	-0.29	-0.66	-	-	-	16.03	14.07	1.111
12.63	100.39	7.33	0.52	-	-	-0.62	-0.50	-	-	-	-	-	-
12.63	100.39	9.49	0.74	-	-	-	-	-	-	-	15.74	-	-
12.68	100.94	9.37	0.61	5.791	48.3	-0.55	-0.29	C.wue	1.18	3.33	16.05	15.44	1.198
12.73	101.02	6.99	0.58	5.457	45.5	-0.39	-0.62	-	-	-	17.05	-	-
12.78	101.12	8.21	0.68	4.896	40.8	-0.74	-0.64	-	-	-	17.75	28.11	2.019

Site 1057B cont.													
mcd (m)	Age (kyr)	Wt. <63 μm (g)	Wt. >63 μm (g)	C %	Ca CO_3	PF $\delta^{13}C$	PF $\delta^{18}O$	BF	BF $\delta^{13}C$	BF $\delta^{18}O$	SS Mean (μm)	SS % (μm)	S/C
12.83	101.23	8.50	0.85	-	-	0.22	-0.77	C.wue	1.03	3.28	-	-	-
12.83	101.23	9.23	1.22	-	-	-	-	-	-	-	18.28	-	-
12.88	103.1	7.74	0.78	4.333	36.1	0.18	-0.65	C.wue	0.66	3.66	17.90	27.14	1.614
12.93	104.97	8.85	0.58	-	-	-0.05	-0.98	C.wue	0.72	3.67	-	-	-
12.93	104.97	9.26	0.53	-	-	-	-	-	-	-	17.09	-	-
12.98	106.63	7.98	0.65	4.901	40.8	-0.10	-1.01	C.wue	0.91	3.60	17.92	24.26	1.852
13.03	107.95	8.38	1.17	4.865	40.5	0.29	-0.77	C.wue	0.96	3.61	18.16	-	-
13.08	109.27	9.07	0.68	5.075	42.3	-0.26	0.05	C.wue	0.79	3.66	18.57	29.05	1.841
13.13	110.58	8.68	0.90	-	-	-0.33	-0.27	C.wue	0.29	3.37	-	-	-
13.13	110.58	9.83	1.23	-	-	-	-	-	-	-	18.42	-	-
13.18	111.9	6.85	0.68	4.505	37.5	-0.12	-0.68	C.wue	1.00	3.31	18.93	32.63	2.515
13.23	114.07	7.46	0.90	5.730	47.8	-0.22	-0.55	C.wue	0.92	3.68	16.22	-	-
13.28	115.13	8.17	1.11	5.613	46.8	-0.07	-0.41	C.wue	0.96	3.27	16.56	13.53	0.958
13.33	116.19	8.56	1.03	-	-	-0.12	-0.29	C.wue	0.27	3.42	-	-	-
13.33	116.19	9.02	1.06	-	-	-	-	-	-	-	16.20	-	-
13.38	116.87	9.14	1.01	5.941	49.5	-0.27	-0.49	C.rug	1.04	3.03	15.48	13.88	1.257
13.43	117.55	9.76	1.13	5.968	49.7	-0.55	-0.98	C.wue	1.05	3.24	15.25	-	-
13.48	118.5	7.54	0.88	6.175	51.5	0.20	-1.03	C.kull	0.67	2.94	15.46	10.89	1.118
13.53	119.01	8.16	0.98	-	-	-0.69	-1.13	-	-	-	-	-	-
13.53	119.01	9.90	1.28	-	-	-	-	-	-	-	15.28	-	-
13.58	119.51	8.40	1.16	6.976	58.1	-1.11	-1.22	-	-	-	15.45	8.64	1.073
13.63	119.93	8.82	0.80	6.465	52.0	-0.37	-1.32	-	-	-	-	-	-
13.68	121.97	8.89	0.72	5.809	48.4	-0.25	-1.10	C.kull	0.56	2.60	-	10.42	1.849
13.73	124.01	6.28	0.71	-	-	-0.95	-1.55	C.wue	0.75	2.49	-	-	-
13.75	125	9.32	0.64	5.814	48.5	-0.26	-1.04	C.kull	0.43	2.42	15.06	14.08	1.269
13.78	125.31	8.30	0.61	5.576	46.5	-0.50	-1.44	C.kull	0.48	2.60	15.53	12.38	1.219
13.83	125.82	7.42	0.63	-	-	-0.90	-1.32	C.wue	0.68	2.22	-	-	-
13.83	125.82	9.23	0.79	-	-	-	-	-	-	-	15.80	-	-
13.88	126.33	9.56	0.65	5.650	47.1	-0.54	-1.81	C.wue	0.67	2.17	15.53	9.58	0.909
13.93	128.24	11.03	0.79	5.569	46.4	-0.96	-1.69	C.wue	0.79	2.29	14.85	-	-
13.98	130.14	9.58	0.74	4.549	37.9	-0.15	-0.71	C.wue	0.24	2.33	16.42	10.39	1.038